Supplementary Document of "Integration of Preferences in Decomposition Multi-Objective Optimization"
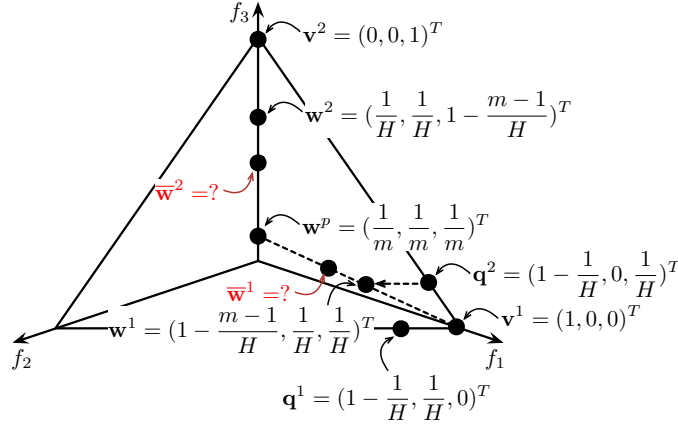
Fig. 1: Illustrative example for η computation.

Proof: Let us use a specific example shown in Fig. 1 to prove this theorem. Suppose the reference points are originally generated by the Das and Dennis's method [1]. Therefore, reference points are distributed on an unit m-simplex. Let the centroid of this simplex, i.e., $\mathbf{w}^p = (\frac{1}{m}, \cdots, \frac{1}{m})^T$, be the pivot point. Let us consider $\mathbf{v}^1 = (1,0,0)^T$ and $\mathbf{v}^2 = (0,0,1)^T$ as two vertices of an edge of this simplex. Obviously, the length of each edge of this simplex is the same, i.e., $\|\mathbf{v}^1 - \mathbf{v}^2\| = \sqrt{2}$. Suppose $\mathbf{w}^1$ and $\mathbf{w}^2$ are two reference points inside this simplex and closest to $\mathbf{v}^1$ and $\mathbf{v}^2$. Since reference points are generated in a structured manner, we can use a geometric method to find the coordinates of $\mathbf{w}^1$ and $\mathbf{w}^2$. As shown in Fig. 1, $\mathbf{q}^1$ and $\mathbf{q}^2$ are two reference points lying on the two edges and closest to $\mathbf{v}^1$. Obviously, $\mathbf{w}^1$ is a linear combination of $\mathbf{v}^1$, $\mathbf{q}^1$ and $\mathbf{q}^2$ as:

$$w_i^1 = (q_i^2 - v_i^1) + q_i^1 \tag{1}$$

where $i \in \{1, \cdots, m\}$. In summary, we can have $\mathbf{w}^1 = (1 - \frac{m-1}{H}, \cdots, \frac{1}{H})^T$ and $\mathbf{w}^2 = (\frac{1}{H}, \cdots, 1 - \frac{m-1}{H})^T$. Based on our non-uniform mapping scheme, we have the new locations of $\mathbf{w}^1$ and $\mathbf{w}^2$ can be calculated as:

$$\overline{\mathbf{w}}^i = \mathbf{w}^p + t \times \mathbf{u}^i \tag{2}$$

where $i \in \{1,2\}$, $\mathbf{u}^i = \frac{\mathbf{v}^i - \mathbf{w}^p}{\|\mathbf{v}^i - \mathbf{w}^p\|}$ and

$$t = d - d(\frac{d - D}{d})^{\frac{1}{\eta+1}} \tag{3}$$

where $d = \|\mathbf{v^i} - \mathbf{w^p}\|$ and $D = \|\mathbf{w}^i - \mathbf{w}^p\|$. Let $q = \frac{d-D}{d}$, we have:

$$t = d(1 - q^{\frac{1}{\eta+1}}) \tag{4}$$

In order to have the extent of ROI become size of τ of the EF, we have the following equation:

$$\frac{\|\overline{\mathbf{w}}^1 - \overline{\mathbf{w}}^2\|}{\|\mathbf{v}^1 - \mathbf{v}^2\|} = \tau \tag{5}$$

Since $\|\mathbf{v}^1 - \mathbf{v}^2\| = \sqrt{2}$, we have:

$$\|\overline{\mathbf{w}}^1 - \overline{\mathbf{w}}^2\| = \sqrt{2}\tau \tag{6}$$

Using equation (2) to substitute $\overline{\mathbf{w}}^1$ and $\overline{\mathbf{w}}^2$ in equation (6), we have:

$$\|t \times (\mathbf{u}^1 - \mathbf{u}^2)\| = \sqrt{2}\tau \tag{7}$$

Using equation (4) to substitute t in equation (7), we have:

$$d(1 - q^{\frac{1}{\eta+1}}) \times \|\mathbf{u}^1 - \mathbf{u}^2\| = \sqrt{2}\tau \tag{8}$$

By substitution, we have:

$$(1 - q^{\frac{1}{\eta+1}}) \times \|\mathbf{v}^1 - \mathbf{v}^2\| = \sqrt{2}\tau$$
$$\implies q^{\frac{1}{\eta+1}} = 1 - \tau \tag{9}$$
$$\implies \eta = \frac{\log q}{\log(1 - \tau)} - 1$$

Since the coordinates of $\mathbf{v}^1$, $\mathbf{w}^1$ and $\mathbf{w}^p$ are known, we have:

$$d = \sqrt{(1 - \frac{1}{m})^2 + (m - 1)\frac{1}{m^2}}$$
$$= \sqrt{1 - \frac{1}{m}} \tag{10}$$

and

$$D = \sqrt{(1 - \frac{m-1}{H} - \frac{1}{m})^2 + (m - 1)(\frac{1}{m} - \frac{1}{H})^2}$$
$$= \sqrt{1 - \frac{1}{m}}(1 - \frac{m}{H}) \tag{11}$$
$$= (1 - \frac{m}{H})d$$

Based on equation (10) and equation (11), we have:

$$q = \frac{d - D}{d}$$
$$= \frac{d - (1 - \frac{m}{H})d}{d} \tag{12}$$
$$= \frac{m}{H}$$

∎

APPENDIX B
PROOF OF COROLLARY 1

Proof: As discussed in Section III-D, we should set $\eta > 0$ in the NUMS. Thus, based on Theorem 1, we have:

$$\frac{\log \frac{m}{H}}{\log(1 - \tau)} > 1 \tag{13}$$

Since $\frac{m}{H} < 1$ and $1 - \tau < 1$, we have:

$$\log \frac{m}{H} \leq \log(1 - \tau) \implies 0 < \tau < 1 - \frac{m}{H} \tag{14}$$

∎

APPENDIX C
PROOF OF COROLLARY 2

Proof: The proof of this corollary is similar to the Theorem 1. Let us use Fig. 1 for illustration again. As for the reference points $\mathbf{w}^1$ and $\mathbf{w}^2$, we should have the following relationship after the non-uniform mapping:

$$\frac{\|\overline{\mathbf{w}}^1 - \overline{\mathbf{w}}^2\|}{\|\mathbf{w}^1 - \mathbf{w}^2\|} = \tau \tag{15}$$

Since $\|\mathbf{w}^1 - \mathbf{w}^2\| = \sqrt{2}(1 - \frac{m}{H})$, we have:

$$\|\overline{\mathbf{w}}^1 - \overline{\mathbf{w}}^2\| = \sqrt{2}(1 - \frac{m}{H})\tau \tag{16}$$

Using equation (2) to substitute $\overline{\mathbf{w}}^1$ and $\overline{\mathbf{w}}^2$ in equation (16), we have:

$$\|t \times (\mathbf{u}^1 - \mathbf{u}^2)\| = \sqrt{2}(1 - \frac{m}{H})\tau \tag{17}$$

Using equation (4) to substitute t in equation (17), we have:

$$d(1 - q^{\frac{1}{n+1}}) \times \|\mathbf{u}^1 - \mathbf{u}^2\| = \sqrt{2}(1 - \frac{m}{H})\tau \tag{18}$$

Since $\|\mathbf{v}^1 - \mathbf{v}^2\| = \sqrt{2}$, by substitution, we have:

$$1 - q^{\frac{1}{n+1}} = (1 - \frac{m}{H})\tau$$
$$\implies \eta = \frac{\log q}{\log[1 - (1 - \frac{m}{H})\tau]} - 1 \tag{19}$$

where $q = \frac{m}{H}$ according to equation (12). ∎

APPENDIX D
PROOF OF COROLLARY 3

Proof: Since $\eta > 0$, according to equation (19), we have:

$$\frac{\log q}{\log[1 - (1 - \frac{m}{H})\tau]} > 1 \tag{20}$$

Since $\frac{m}{H} < 1$ and $1 - (1 - \frac{m}{H})\tau < 1$, we have:

$$\log \frac{m}{H} < \log[1 - (1 - \frac{m}{H})\tau] \implies 0 < \tau < 1 \tag{21}$$

∎

APPENDIX E
PARAMETER SETTINGS

TABLE I: Settings of Aspiration Level Vector

Problem	m	Unattainable	Attainable
DTLZ1	2	$(0.3,0.5)^T$	$(0.5,0.6)^T$
	3	$(0.05,0.05,0.2)^T$	$(0.3,0.3,0.2)^T$
	5	$(0.05,0.05,0.1,0.08,0.03)^T$	$(0.2,0.1,0.1,0.3,0.4)^T$
	8	$(0.01,0.02,0.07,0.02,0.06,0.2,0.1,0.01)^T$	$(0.1,0.2,0.1,0.4,0.4,0.1,0.3,0.1)^T$
	10	$(0.02,0.01,0.06,0.04,0.04,0.01,0.02,0.03,0.05,0.08)^T$	$(0.05,0.1,0.1,0.05,0.1,0.2,0.08,0.03,0.3,0.1)^T$
DTLZ2-4	2	$(0.65,0.7)^T$	$(0.75,0.75)^T$
	3	$(0.2,0.5,0.6)^T$	$(0.7,0.8,0.5)^T$
	5	$(0.3,0.1,0.4,0.2,0.3)^T$	$(0.7,0.6,0.3,0.8,0.5)^T$
	8	$(0.3,0.1,0.4,0.25,0.1,0.15,0.4,0.25)^T$	$(0.6,0.5,0.75,0.2,0.3,0.55,0.7,0.6)^T$
	10	$(0.1,0.1,0.3,0.4,0.2,0.5,0.25,0.15,0.1,0.4)^T$	$(0.3,0.3,0.3,0.1,0.3,0.55,0.35,0.35,0.25,0.45)^T$
WFG41	2	$(0.65,0.7)^T$	$(0.75,0.75)^T$
	3	$(0.2,0.5,0.6)^T$	$(0.7,0.8,0.5)^T$
	5	$(0.3,0.1,0.4,0.2,0.3)^T$	$(0.7,0.6,0.3,0.8,0.5)^T$
	8	$(0.3,0.1,0.4,0.25,0.1,0.15,0.4,0.25)^T$	$(0.6,0.5,0.75,0.2,0.3,0.55,0.7,0.6)^T$
	10	$(0.1,0.1,0.3,0.4,0.2,0.5,0.25,0.15,0.1,0.4)^T$	$(0.3,0.3,0.3,0.1,0.3,0.55,0.35,0.35,0.25,0.45)^T$
WFG42	2	$(0.5,0.1)^T$	$(0.6,0.15)^T$
	3	$(0.05,0.05,0.2)^T$	$(0.15,0.15,0.25)^T$
	5	$(0.03,0.04,0.08,0.04,0.04)^T$	$(0.1,0.05,0.1,0.05,0.05)^T$
	8	$(0.01,0.02,0.03,0.01,0.01,0.05,0.01,0.01)^T$	$(0.2,0.2,0.1,0.3,0.05,0.15,0.2,0.15)^T$
	10	$(0.005,0.002,0.005,0.005,0.008,0.005,0.002,0.002,0.001,0.005)^T$	$(0.3,0.3,0.5,0.3,0.5,0.45,0.25,0.35,0.25,0.4)^T$
WFG43	2	$(0.9,0.8)^T$	$(0.95,0.93)^T$
	3	$(0.6,0.8,0.8)^T$	$(0.95,0.95,0.85)^T$
	5	$(0.4,0.4,0.5,0.4,0.4)^T$	$(0.5,0.7,1,0.9,0.6)^T$
	8	$(0.4,0.4,0.5,0.4,0.4,0.5,0.6,0.5)^T$	$(0.95,1,1,0.95,0.8,0.95,0.95,1)^T$
	10	$(0.5,0.2,0.4,0.3,0.4,0.5,0.6,0.7,0.6,0.7)^T$	$(1,0.85,1,0.95,0.85,0.95,0.95,1,0.8,0.9)^T$
WFG44	2	$(0.008,0.006)^T$	$(0.009,0.008)^T$
	3	$(0.0004,0.0004,0.0003)^T$	$(0.001,0.0001,0.0005)^T$
	5	$(5e-06,1e-05,1e-05,1e-05,5e-06)^T$	$(0.0005,0.001,0.0003,0.0006,0.0008)^T$
	8	$(5e-06,1e-06,1e-06,1.5e-06,5e-07,1e-06,5e-07,2e-07)^T$	$(0.001,0.0015,0.002,0.002,0.003,0.003,0.002,0.001)^T$
	10	$(2e-06,8e-07,3e-07,3e-07,7e-07,1e-07,2e-08,2e-07,5e-07,2e-07)^T$	$(0.0015,0.002,0.002,0.001,0.0015,0.002,0.002,0.003,0.003,0.002)^T$
WFG45	2	$(0.7,0.45)^T$	$(0.75,0.5)^T$
	3	$(0.3,0.7,0.3)^T$	$(0.5,0.8,0.5)^T$
	5	$(0.6,0.3,0.3,0.3,0.3)^T$	$(0.8,0.5,0.4,0.5,0.5)^T$
	8	$(0.2,0.3,0.3,0.3,0.3,0.2,0.1,0.2)^T$	$(0.8,0.5,0.4,0.5,0.5,0.7,0.7,0.9)^T$
	10	$(0.2,0.15,0.15,0.2,0.1,0.15,0.05,0.1,0.1,0.2)^T$	$(0.9,0.65,0.6,0.5,0.55,0.8,0.8,0.9,0.5,0.55)^T$
WFG46	2	$(0.55,0.4)^T$	$(0.65,0.5)^T$
	3	$(0.3,0.25,0.3)^T$	$(0.35,0.35,0.4)^T$
	5	$(0.1,0.1,0.2,0.1,0.15)^T$	$(0.2,0.3,0.4,0.2,0.3)^T$
	8	$(0.1,0.08,0.05,0.1,0.05,0.1,0.05,0.2)^T$	$(0.2,0.5,0.3,0.2,0.3,0.1,0.1,0.2)^T$
	10	$(0.05,0.08,0.05,0.02,0.05,0.04,0.05,0.08,0.1,0.05)^T$	$(0.25,0.5,0.35,0.5,0.35,0.6,0.5,0.5,0.4,0.35)^T$
WFG47	2	$(0.4,0.45)^T$	$(0.5,0.5)^T$
	3	$(0.7,0.4,0.4)^T$	$(0.9,0.5,0.6)^T$
	5	$(0.5,0.3,0.3,0.3,0.2)^T$	$(0.8,0.4,0.5,0.4,0.6)^T$
	8	$(0.08,0.15,0.1,0.1,0.12,0.1,0.1,0.1)^T$	$(0.5,0.4,0.7,0.4,0.8,0.8,0.75,0.7)^T$
	10	$(0.05,0.05,0.1,0.1,0.05,0.08,0.05,0.05,0.03,0.05)^T$	$(0.6,0.35,0.75,0.6,0.85,0.8,0.75,0.7,0.7,0.8)^T$
WFG48	2	$(0.6,0.4)^T$	$(0.7,0.5)^T$
	3	$(0.25,0.2,0.1)^T$	$(0.35,0.3,0.2)^T$
	5	$(0.05,0.08,0.05,0.06,0.05)^T$	$(0.1,0.2,0.08,0.15,0.1)^T$
	8	$(0.02,0.03,0.02,0.01,0.02,0.03,0.04,0.03)^T$	$(0.15,0.25,0.35,0.45,0.15,0.45,0.35,0.25)^T$
	10	$(0.005,0.008,0.01,0.01,0.02,0.03,0.04,0.03,0.02,0.01)^T$	$(0.25,0.45,0.3,0.6,0.2,0.5,0.35,0.5,0.6,0.7)^T$

TABLE II: Settings of Number of Function Evaluations (FEs), N is the population size

Problem	m	# of FEs	Problem	m	# of FEs
DTLZ1	3	$400 \times N$	DTLZ3	3	$1000 \times N$
	5	$1000 \times N$		5	$1200 \times N$
	8	$1200 \times N$		8	$1500 \times N$
	10	$1500 \times N$		10	$1800 \times N$
DTLZ2	3	$250 \times N$	DTLZ4	3	$600 \times N$
	5	$800 \times N$		5	$1200 \times N$
	8	$1000 \times N$		8	$1500 \times N$
	10	$1360 \times N$		10	$1800 \times N$
WFG41-WFG48	2	$400 \times N$			
	3	$400 \times N$			
	5	$1000 \times N$			
	8	$1200 \times N$			
	10	$1500 \times N$			

APPENDIX F
DESCRIPTION OF STATISTICAL ANALYSIS FRAMEWORK

In this work, we employ the statistical analysis suggested in [2] to validate the statistical significance of the results obtained by different algorithms. Specifically, as shown in Fig. 2, we at first carry out a Kolmogorov-Smirnov test to check whether the results follow a normal distribution or not. If so, we use Levene test to check the homogeneity of the variances. Afterwards, we use ANOVA test to validate the significance if samples are with equal variance; otherwise we use Welch test instead. On the other hand, if the results do not follow a normal distribution, we use Kruskal-Wallis test to compare the median metric values obtained by different algorithms. Note that we set the confidence level as 95% (i.e., significance level of 5% or p-value under 0.05) in the statistical tests.
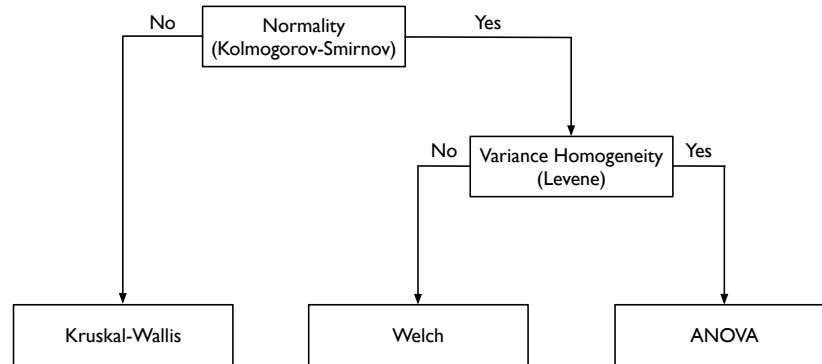
Fig. 2: Statistical analysis framework [2].

APPENDIX G
PROOF-OF-PRINCIPLE RESULTS

In this section, we empirically validate the effectiveness of the NUMS for assisting the decomposition-based EMO algorithms seek the DM's preferred solutions on problem instances with 2 to 10 objectives. Our recently proposed MOEA/D variant based on stable matching model, named MOEA/D-STM [3] is used as the baseline algorithm. Different from the canonical MOEA/D, where the selection of the next parents is merely determined by the aggregation function value of a solution, MOEA/D-STM treats subproblems and solutions as two sets of agents and considers their mutual preferences simultaneously. In particular, the preference of a subproblem over a solution measures the convergence issue, while the preference of a solution over a subproblem measures the diversity issue. Since the stable matching achieves an equilibrium of the mutual preferences between subproblems and solutions, MOEA/D-STM strikes a balance between convergence and diversity of the search process. Here we use the simulated binary crossover (SBX) [4] and the polynomial mutation [5] as the reproduction operators. For the SBX, the crossover probability is set as $p_c = 1.0$ and its distribution index is set as $\eta_c = 10$; for the polynomial mutation, the mutation probability is set as $p_m = \frac{1}{n}$ and its distribution index is set as $\eta_m = 20$. ZDT [6] and DTLZ [7] problem suites are chosen to form the benchmark.

Generally speaking, the proof-of-principle studies consist of two parts. First of all, we validate the effectiveness of the NUMS on the problem instances with two and three objectives. Afterwards, we empirically demonstrate some interesting extensions of the NUMS for handling various other scenarios, i.e. problems with many objectives, multiple ROIs and an interactive preference incorporation.

A. Problems with Two and Three Objectives

Let us start from the two-objective ZDT1 problem instance that has a convex PF [6]. The population size of MOEA/D-STM is set to 100 and it performs 300 generations. Fig. 3 shows a comparative results of solutions obtained by MOEA/D-STM with different τ settings. From this figure, we clearly see that the NUMS adapts the originally evenly distributed reference points to a biased distribution according to the required extent. In the meanwhile, MOEA/D-STM provides a well approximation of the partial PF with respect to those biased reference points. Note that, in order to approximate the whole PF without preference on any particular region, we need to set $\tau = 1 - \frac{2}{99}$ rather than 1.0 according to Theorem 1.

Next, we assess the performance of MOEA/D-STM with the NUMS on the three-objective DTLZ1 and DTLZ2 problem instances respectively. Here we set $\tau = 0.2$ in the NUMS, and MOEA/D-STM performs 300 generations for DTLZ2 and 1,000 generations for DTLZ1 due to its multi-modality. As shown in Fig. 4 and Fig. 5, with either an infeasible ($\mathbf{z}^r = (0.3, 0.3, 0.2)^T$ for DTLZ1) or feasible ($\mathbf{z}^r = (0.3, 0.5, 0.6)^T$ for DTLZ2) aspiration level vector, MOEA/D-STM has no difficulty in finding the preferred solutions in the ROI. Furthermore, MOEA/D-STM also well approximates the boundaries for both cases.
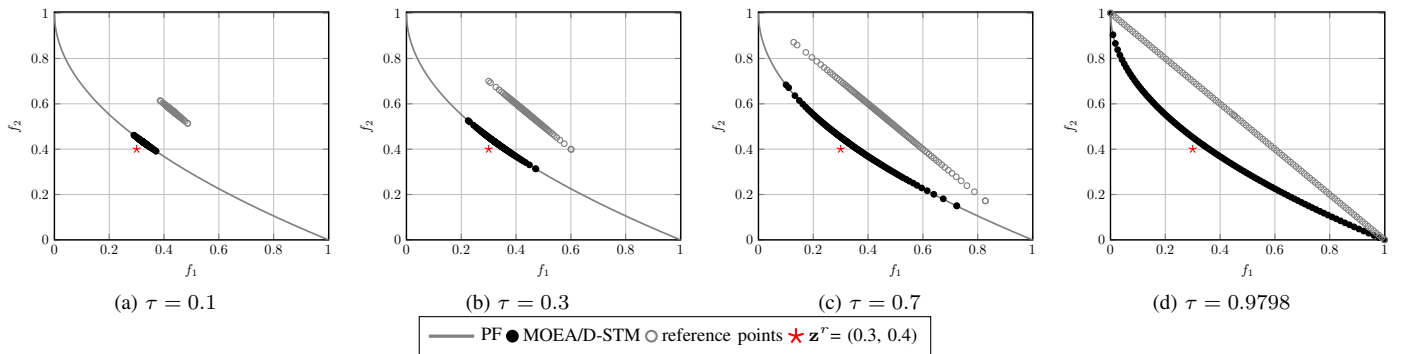

(a) $\tau = 0.1$ (b) $\tau = 0.3$ (c) $\tau = 0.7$ (d) $\tau = 0.9798$

—— PF ● MOEA/D-STM ○ reference points ★ $\mathbf{z}^r$ = (0.3, 0.4)

Fig. 3: Comparisons of solutions obtained by MOEA/D-STM with different τ settings for NUMS on ZDT1 problem.

B. Problems with Many Objectives

Now let us consider the five-objective DTLZ2 problem instance where $\mathbf{z}^r = (0.3, 0.1, 0.4, 0.2, 0.3)^T$. Now, we set $H = 7$ in the Das and Dennis's method which generates 330 uniformly distributed reference points, and τ is set to 0.1 in the NUMS. Fig. 6(c) gives the corresponding Pareto-optimal points, with respect to the biased reference points given in Fig. 6(b), according to the method developed in [8]. Comparing Fig. 6(a) with Fig. 6(c), we can see that MOEA/D-STM, after performing 1,000 generations, has a well approximation to both the ROI and the boundary points.

As discussed in [8] and [9], in order to have intermediate reference points within the simplex, we should set $H \geq m$ in the Das and Dennis's method. Otherwise, all reference points should lie on the boundary of the simplex. However, in a large-dimensional space, we can have a huge amount of reference points even when $H = m$. For example, when $m = 10$,
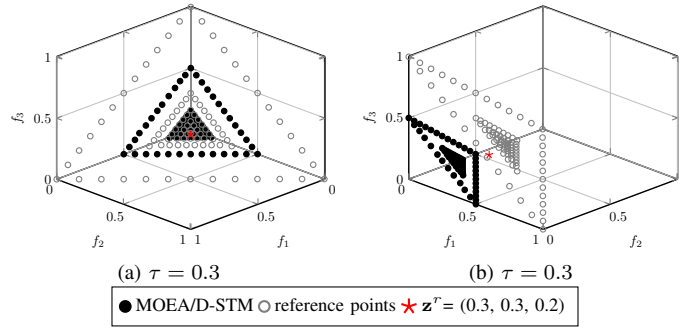
(a) $\tau = 0.3$ (b) $\tau = 0.3$

● MOEA/D-STM ○ reference points ★ $\mathbf{z}^r$ = (0.3, 0.3, 0.2)

Fig. 4: Solutions obtained by MOEA/D-STM on DTLZ1 problem where $\mathbf{z}^r = (0.3, 0.3, 0.2)^T$.

(a) $\tau = 0.3$ (b) $\tau = 0.3$

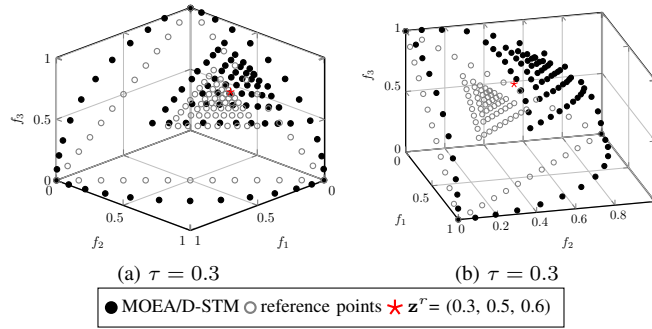● MOEA/D-STM ○ reference points ★ $\mathbf{z}^r$ = (0.3, 0.5, 0.6)

Fig. 5: Solutions obtained by MOEA/D-STM on DTLZ2 problem where $\mathbf{z}^r = (0.2, 0.5, 0.6)^T$.

the Das and Dennis's method can generate $\binom{10+10-1}{10-1} = 92378$ uniformly distributed reference points if $H = 10$. Obviously, current EMO algorithms cannot hold such huge number of solutions in a population. Even worse, when $H = m$, there is only one intermediate reference point which lies in the center of the simplex. Thus, the original NUMS might not be directly applicable when facing a large number of objectives. Inspired by the multi-layer weight vector generation method developed in [8] and [9], we make a slight modification to adapt the NUMS to the many-objective scenario. First of all, we use the Das and Dennis's method, where $H < m$, more than one time, to generate $(l > 1)$ layers of reference points. Afterwards, we use the method developed in Section III-E of our paper to shift these reference points, which lie on the boundary of the simplex, onto the ROI layer by layer. Fig. 7(b) shows an example of 661 reference points generated by the multi-layer NUMS where $\mathbf{z}^r = (0.3, 0.3, 0.3, 0.1, 0.3, 0.55, 0.35, 0.35, 0.25, 0.45)^T$. In particular, we first use the Das and Dennis's method to generate $l = 3$ layers of reference points. Since we set $H = 3$, each layer contains 220 reference points. Then two layers of them are shifted onto the ROI, where the shrinkage factor τ is set to 0.4 and 0.2 respectively. Fig. 7(a) shows the final solutions obtained by MOEA/D-STM after 1,000 generations. Comparing to the corresponding Pareto-optimal points shown in Fig. 7(c), we can see that MOEA/D-STM still has a satisfactory approximation to the ROI in a 10-objective space.

(a) MOEA/D-STM.   (b) Reference points.   (c) Corresponding Pareto-optimal points.
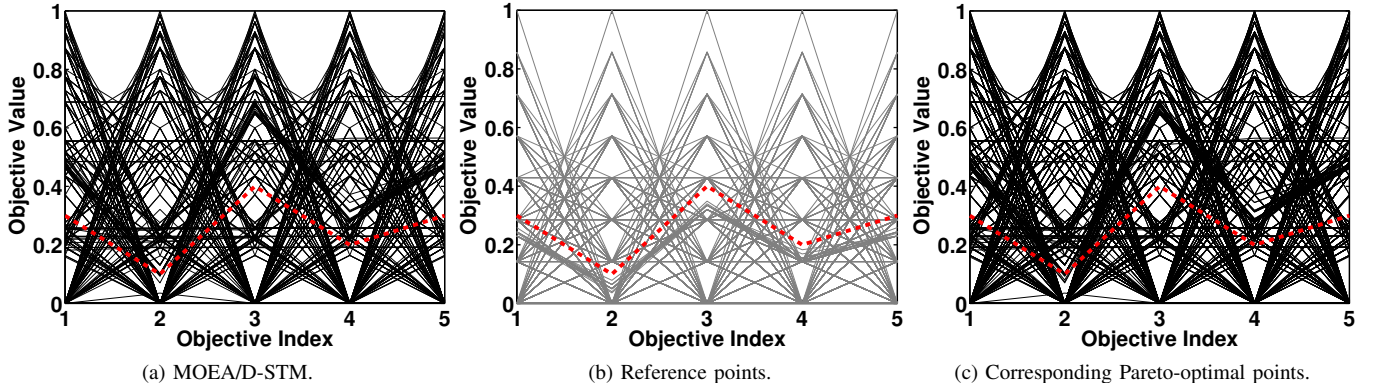
Fig. 6: Solutions obtained by MOEA/D-STM on 5-objective DTLZ2 problem where $\mathbf{z}^r = (0.3, 0.1, 0.4, 0.2, 0.3)^T$ is represented as the red dotted line.

(a) MOEA/D-STM.

(b) Reference points.

(c) Corresponding Pareto-optimal points.
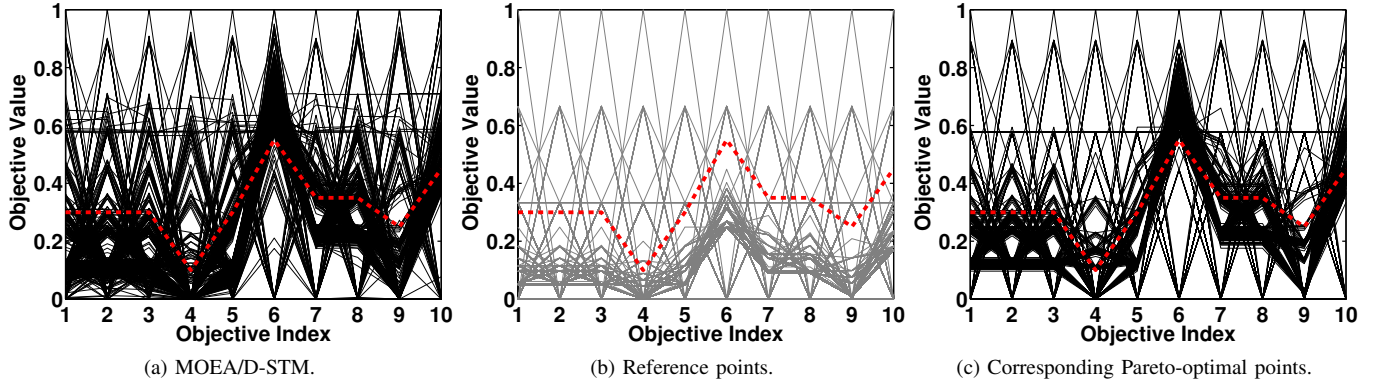
Fig. 7: Solutions obtained by MOEA/D-STM on 10-objective DTLZ2 problem where $\mathbf{z}^r = (0.3, 0.3, 0.3, 0.1, 0.3, 0.55, 0.35, 0.35, 0.25, 0.45)^T$ is represented as the red dotted line.

C. Investigations on multiple ROIs

In practice, the DM might not be sure about his/her exact preferences and he/she would like to simultaneously explore several ROIs. In this case, the DM would like to supply more than one, say $T > 1$, aspiration level vectors at a time. To accommodate multiple ROIs, we only need to apply the NUMS T times with respect to each aspiration level vector. Note that each time the NUMS can preserve the boundary reference points, but we only need to keep these boundary reference points once. In other words, the duplicated boundary reference points are exempted from the final reference point set. Fig. 8 shows an example of two aspiration level vectors. In particular, the gray points are the adapted reference points for each ROI; while the black points are the final solutions obtained by MOEA/D-STM with respect to the corresponding reference points. From the experimental results, we can clearly see that MOEA/D-STM with the NUMS is also able to approximate multiple ROIs simultaneously.

(a) $\tau = 0.3$

(b) $\tau = 0.3$

● MOEA/D-STM ○ reference points ★ $\mathbf{z}^{r1} = (0.3, 0.5, 0.7)$ ⊥ $\mathbf{z}^{r2} = (0.9, 0.3, 0.3)$
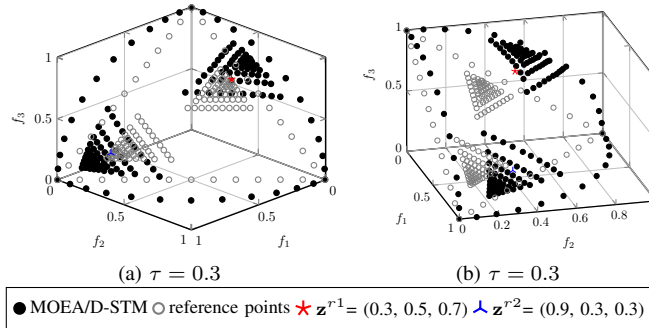
Fig. 8: Solutions obtained by MOEA/D-STM with two different reference points on DTLZ2 problem.

D. Interactive Scenario

In practice, it is not uncommon that the DM is not fully confident about his/her elicited preference information due to the black box property of the problem itself. Therefore, an interactive decision-making procedure where the DM can progressively adapt his/her preference information during the optimisation process is attractive in the preference-based EMO. Since the NUMS can easily adapt the distribution of reference points to be biased toward the ROI, it facilitates the interactive scenario. Moreover, also due to the lack of the knowledge of the PF, the DM can easily specify an aspiration level vector which is beyond the boundary of the PF. Since the NUMS is able to preserve the boundary reference points, it finally helps the DM better understand the PF (e.g. its general shape, boundary, ideal and nadir points) and further adjusts his/her preference information. In Fig. 9, we describe an interactive run, which includes three cycles, of MOEA/D-STM on the DTLZ2 problem. We call a run of MOEA/D-STM for a certain number of generations specified by the DM as a cycle. First, as shown in Fig. 9(a), the DM specifies an aspiration level vector $\mathbf{z}_1^r = (1.4, 1.9, 1.5)^T$ beyond the PF. After 200 generations, MOEA/D-STM finds the solutions not only crowd in the ROI, but also distribute along the boundary. Thereafter, the DM realises that $\mathbf{z}_1^r$ is a bad choice, and then he/she resets another aspiration level vector, say $\mathbf{z}_2^r = (0.7, 0.6, 0.3)^T$. In addition, since the DM already knows the boundary of the PF, he/she might not be interested in the boundary any longer. Thus, he/she sets the NUMS to adapt all reference points to the ROI. By using the final population of the first interaction as the initial population, MOEA/D-STM finally finds the solutions in the ROI after 200 generations. However, we assume that the DM still does not satisfy them and he/she

sets another aspiration level vector, say $\mathbf{z}_3^r = (0.3, 0.4, 0.8)^T$. After 200 generations, as shown in Fig. 9(c), MOEA/D-STM finds the solutions in the vicinity of the ROI. This time, the DM is comfortable with the obtained solutions and this interactive EMO process terminates.
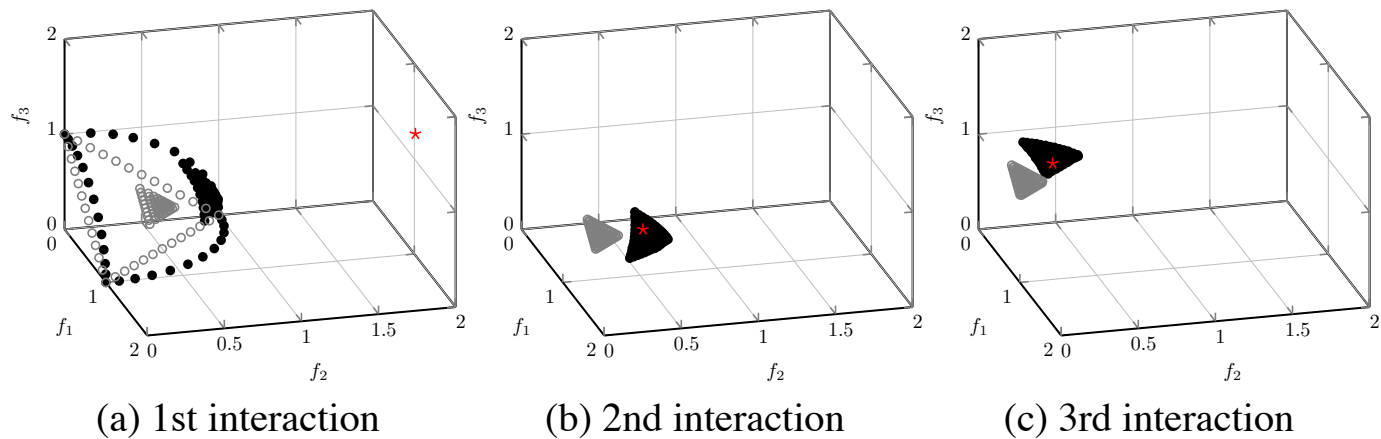

(a) 1st interaction   (b) 2nd interaction   (c) 3rd interaction

Fig. 9: Interactive scenario on DTLZ2 problem.

APPENDIX H
EXPERIMENTAL RESULTS ON WFG PROBLEMS

WFG41 to WFG48 problems are constructed by applying different shape functions provided in the WFG toolkit to the standard WFG4 problem [10]. Specifically, WFG41 and WFG42 problems have regular concave and convex shapes respectively. From the results shown in Table III and Table IV, and Fig. 42 to Fig. 61 in the supplementary document, we can see that three decomposition-based EMO algorithms obtain the best ROI approximation, in terms of convergence toward the PF and the diversity within the ROI. In addition, the spread of the ROI approximation is also satisfactory according to the DM's expectation. In contrast, the other three preference-based EMO algorithms are not quite comparable. In particular, for WFG42, the solutions obtained by R-NSGA-II and r-NSGA-II stray away from the ROI. Moreover, the performance of g-NSGA-II deteriorates significantly with the increase of the number of objectives.

Different from the previous two problems, WFG43 and WFG44 have strong concave and convex shapes respectively. In particular, they are built by scaling the corresponding shape function with a power $\frac{1}{4}$. As shown in Fig. 62 and Fig. 81 of the supplementary document, all three decomposition-based EMO algorithms find an appropriate ROI approximation with respect to the DM supplied aspiration level vector on WFG43. Although the solutions obtained by g-NSGA-II cover the ROI, their spread is too wide. In contrast, solutions obtained by r-NSGA-II and R-NSGA-II are away from the ROI. However, the performance of g-NSGA-II deteriorate significantly with the increase of the number of objectives. As for WFG44, due to its sharp convex property, all solutions crowded in the knee region. In this case, the extent of the ROI approximated by the three decomposition-based EMO algorithms does not meet the DM's expectation.

WFG45 has a mixed PF shape, which has both concave and convex parts simultaneously. Similar to the observations on WFG43 and WFG44, three decomposition-based EMO algorithms show the most promising performance while the solutions obtained by g-NSGA-II are acceptable when $m = 2$ whereas its performance deteriorate significantly with the increase of dimensionality.

WFG46 has a relatively simple PF shape, which is a hyperplane. All algorithms do not have difficulty in converging toward the PF when the number of objectives is small. However, g-NSGA-II cannot find well converged solutions for the attainable aspiration level vector setting when the number of objectives becomes large. In addition, we also notice that the spread of the ROI approximation obtained by g-NSGA-II is excessively wider than the other peers. Note that g-NSGA-II do not have any control on the extent of the ROI.

Both WFG47 and WFG48 have disconnected concave and convex PF shapes respectively. For the 2-objective WFG47, as shown in Fig. 102 and Fig. 103 of the supplementary document, g-NSGA-II find solutions on the PF segment which is far away from the DM supplied aspiration level vector. For the 2-objective WFG48, as shown in Fig. 112 and Fig. 113 of the supplementary document, solutions obtained by g-NSGA-II do not fully converge to the PF segment. The performance of three decomposition-based EMO algorithms is robust across different aspiration level vector settings. It is interesting to note that r-NSGA-II obtains the best R-HV value on the 2-objective WFG48 with an attainable aspiration level vector setting. As shown in Fig. 113 of the supplementary document, solutions obtained by r-NSGA-II has a slightly wider spread comparing to those obtained by the three decomposition-based EMO algorithms. However, its performance deteriorates with the increase of the number of objectives.

In summary, the experimental results fully demonstrate the effectiveness of the NUMS for assisting the decomposition-based EMO algorithms, where we use MOEA/D-STM, MOEA/D and NSGA-III as the baseline, to approximate the ROIs. In addition, we find that R-NSGA-II is also good at searching for the ROIs for DTLZ problems. However, it cannot find satisfied ROI approximation when tackling WFG problems. In addition, the spread of the preferred solutions of R-NSGA-II and r-NSGA-II is controlled in an ad-hoc manner.

TABLE III: Comparison results of median R-HV values and the IQR obtained by six preference-based EMO algorithms on WFG41 to WFG44 problems with unattainable and attainable aspiration level vectors.

Problem	m	ref	MOEA/D-STM	MOEA/D	NSGA-III	g-NSGA-II	r-NSGA-II	R-NSGA-II
WFG41	2	1	**2.4298(5.07E-5)**	2.4296(1.27E-6)	2.4296(6.98E-5)	4.2215(5.69E-3)†	4.2117(1.32E-1)†	4.0174(5.12E-1)†
		2	**4.5631(2.17E-4)**	4.5630(2.55E-6)	4.5630(1.67-2)	4.5628(2.66E-3)†	4.5271(8.27E-2)†	4.3848(3.33E-1)†
	3	1	**7.6199(1.66E-2)**	7.6124(0.00E+0)	7.6171(5.79E-3)	7.0242(2.20E-1)†	7.2876(3.08E-1)†	7.0602(5.12E-1)†
		2	**10.4009(1.37E-2)**	10.4005(0.00E+0)	10.3871(1.02E-2)	10.1891(1.71E-1)†	10.1288(1.02E+0)†	9.9453(3.33E-1)†
	5	1	**23.8070(1.52E-1)**	23.7453(0.00E+0)†	23.7291(2.46E-1)†	13.6383(1.17E+0)†	18.1798(5.23E+0)†	19.7685E(1.99E+0)†
		2	50.9815(2.50E+0)	**52.4696(0.00E+0)**	48.9575(2.78E-1)	24.0680(3.76E+0)†	33.7121(6.92E+0)†	42.4963(3.19E+0)†
	8	1	211.5465(1.21E+1)†	214.8829(9.02E+0)†	**226.3126(2.64E+0)**	77.3684(2.39E+1)†	146.1190(3.38E+1)†	50.8910(5.12E+0)†
		2	555.5724(3.81E+1)†	**561.8469(2.98E+1)**	432.7265(1.34E+1)†	–	325.4018(3.95E+1)†	121.6208(1.25E+1)†
	10	1	**1040.2589(3.56E+1)**	1013.6855(5.07E+1)†	923.8265(1.42E+1)†	304.7739(5.76E+1)†	704.5660(1.66E+2)†	–
		2	**1570.5781(4.67E+1)**	1357.7199(5.51E+1)†	1275.3521(3.24E+1)†	397.6032(8.63E+1)†	1182.4211(2.93E+2)†	–
WFG42	2	1	4.1574(4.96E-5)	**4.1577(2.44E-6)**	4.1574(1.85E-6)	4.1063(1.88E-3)†	3.1070(3.77E-2)†	4.0109(3.20E-1)†
		2	**4.3817(1.81E-4)**	4.3813(7.92E-7)	4.3811(1.23E-5)†	4.3431(1.99E-3)†	4.1510(1.19E+0)†	3.3759(5.56E-2)†
	3	1	7.7250(4.34E-3)†	**7.7283(1.24E-3)**	7.7238(1.41E-3)†	7.0382(2.21E-1)†	6.7867(1.67E-1)†	5.5130(3.20E-1)†
		2	**8.8508(5.77E-3)**	8.8504(1.03E-3)	8.8483(1.70E-3)†	8.7219(6.06E-1)†	7.7817(1.95E-1)†	8.9615(1.19E+0)†
	5	1	31.5611(7.61E-2)	31.5879(2.31E-2)	**32.1921(6.26E-1)**	28.6955(2.54E+0)†	30.4173(9.88E-1)†	25.2410(2.14E+0)†
		2	33.7777(6.64E-2)	33.9092(8.76E-2)	**34.4050(2.15E-1)**	25.6623(1.52E+0)†	31.9766(6.78E-1)†	30.4631(5.12E-1)†
	8	1	253.1978(1.31E+0)	**254.1460(1.12E+0)**	251.1147(2.80E-1)	200.0911(1.83E+1)†	215.1664(8.45E+0)†	181.5920(1.11E+1)†
		2	318.1471(8.21E-1)	**318.9400(8.27E-1)**	313.5087(3.82E-1)	–	304.6694(7.32E+0)†	125.2891(1.52E+0)†
	10	1	**5012.3321(1.07E+2)**	4958.7847(3.19E+1)	4911.8221(5.14E+1)	755.5785(1.19E+2)†	907.1323(3.58E+1)†	–
		2	**3122.4221(1.14E+2)**	3021.1282(8.12E+1)	2912.7725(9.34E+1)	2697.5424(5.80E+1)†	2455.2939(3.97E+2)†	–
WFG43	2	1	4.1409(1.02E-2)	**4.1411(6.96E-6)**	4.1409(2.52E-5)	4.1348(5.82E-3)†	4.0203(6.24E-3)†	3.7845(4.32E-3)†
		2	4.4693(6.18E-5)	**4.4693(1.17E-5)**	4.4692(6.85E-5)	4.3842(2.71E-3)†	3.9950(8.52E-2)†	4.0001(5.98E-2)†
	3	1	**7.6676(2.92E-2)**	7.6618(3.01E-3)†	7.6574(3.93E-3)†	7.6264(8.46E-2)†	6.6693(5.97E-1)†	5.8659(1.87E-1)†
		2	9.7480(5.34E-2)†	9.6992(4.32E-3)†	**9.7876(3.83E-3)**	9.7212(5.15E-2)†	8.5460(6.18E-1)†	8.6911(5.12E-1)†
	5	1	9.0901(2.29E-2)†	10.3782(3.91E-2)†	**10.5747(1.29E-1)**	7.9014(3.90E-1)†	8.6955(5.89E-1)†	7.6087(2.19E-2)†
		2	34.3411(3.09E+0)†	**36.0054(3.79E+0)**	34.3394(1.52E-1)†	15.3444(3.70E+0)†	34.0859(2.99E+0)†	33.4689(5.12E+0)†
	8	1	**60.6142(2.21E+0)**	60.5416(3.64E-1)†	60.5910(5.62E+0)†	12.6672(4.17E+0)†	50.8572(6.04E+0)†	15.7898(5.19E+0)†
		2	443.5193(5.25E+0)†	**598.8932(3.74E+1)**	497.9952(1.43E+1)†		382.9223(5.78E+1)†	370.8867(2.15E+1)†
	10	1	389.5884(9.04E+1)†	391.9223(7.21E+1)†	**418.3354(1.16E+1)**	20.9774(3.54E+1)†	283.0227(4.04E+1)†	–
		2	**2981.7520(1.89E+1)**	2268.6651(8.72E+1)†	2382.3351(9.01E+1)†	–	1637.4484(2.91E+2)†	–
WFG44	2	1	4.0040(3.21E-5)	**4.0040(3.98E-6)**	4.0039(3.60E-5)	4.0034(4.50E-5)†	4.0031(6.24E-3)†	4.0028(5.24E-5)†
		2	4.0096(4.60E-4)	**4.0100(5.33E-7)**	4.0099(4.60E-4)	4.0070(4.02E-5)†	4.0093(3.79E-3)	4.0098(6.31E-5)
	3	1	8.0004(1.70E-5)	**8.0004(1.10E-5)**	8.0004(1.50E-5)	–	7.9805(2.15E-4)†	8.0000(2.78E-4)†
		2	8.0022(9.20E-5)	**8.0022(1.13E-8)**	8.0022(1.36E-4)	–	7.9940(5.36E-4)†	–
	5	1	31.9997(2.00E-5)	31.9997(1.60E-5)	**31.9999(1.36E-4)**	31.9304(2.23E-1)†	31.9579(1.98E-3)†	31.0422(2.41E-5)†
		2	**32.0239(1.46E-6)**	32.0239(1.60E-5)	32.0243(1.60E-5)	–	32.0057(6.18E-3)†	32.0192(1.82E-4)†
	8	1	**255.9988(3.41E-5)**	255.9988(4.12E-4)	255.9988(2.15E-4)	–	245.9537(4.14E-2)†	–
		2	**257.0258(5.12E-5)**	257.0258(4.52E-4)	257.0258(4.01E-4)	–	–	–
	10	1	**1023.9980(5.12E-5)**	1023.9980(6.15E-5)	1023.9980(6.12E-5)	–	–	–
		2	1029.1315(4.52E-5)	1029.1315(5.17E-4)	1029.1315(6.20E-5)	–	–	–

† denotes the best median metric value is significantly better than the other peers according to the statistical analysis described in Appendix F of the supplementary document. ref $= 1$ means the unattainable aspiration level vector while ref $= 2$ means the attainable aspiration level vector. – means all solutions obtained by the corresponding algorithm are dominated by the other counterparts, thus no solution can be used for R-HV computation.

TABLE IV: Comparison results of median R-HV values and the IQR obtained by six preference-based EMO algorithms on WFG45 to WFG48 problems with unattainable and attainable aspiration level vectors.

Problem	m	ref	MOEA/D-STM	MOEA/D	NSGA-III	g-NSGA-II	r-NSGA-II	R-NSGA-II
WFG45	2	1	4.1226(1.84E-5)	**4.1227(2.14E-6)**	4.1224(1.81E-2)	4.1184(6.24E-3)†	3.9696(1.09E-1)†	3.9797(1.20E-2)†
		2	4.3076(9.20E-5)	**4.3076(6.72E-6)**	4.3075(2.51E-5)	4.3058(6.95E-3)†	4.1388(1.31E-1)†	4.1935(4.12E-2)†
	3	1	7.9929(4.09E-2)†	**8.0422(1.05E-7)**	8.0091(5.65E-2)†	7.6983(1.86E-1)†	6.3118(2.27E-1)†	6.3916(4.12E-1)†
		2	10.0080(2.65E-2)†	**10.0167(1.08E-8)**	10.0049(1.61E-2)†	9.8311(1.33E-1)†	8.6045(2.03E-1)†	8.6955(1.92E-1)†
	5	1	**32.9969(1.57E-1)**	32.5638(4.44E-1)†	32.4787(1.18E-1)†	13.9932(1.61E+0)†	21.4709(1.38E+0)†	19.0242(2.19E+0)†
		2	**50.1882(5.22E-1)**	50.0938(6.77E-1)†	50.1626(2.95E-1)†	15.1340(3.48E+0)†	36.7563(9.49E-1)†	32.8139(4.19E+0)†
	8	1	206.9412(7.04E+0)†	**215.0497(9.00E+0)**	208.4627(5.53E+0)†	55.1598(1.14E+1)†	85.4227(2.07E+1)†	65.1287(3.00E+1)†
		2	881.3934(1.09E+2)†	**885.3012(9.41E+1)**	762.7465(1.24E+1)†	–	679.4919(7.59E+1)†	565.8972(1.11E+1)†
	10	1	504.2658(2.17E+1)†	**510.6926(3.81E+1)**	502.7624(7.64E+0)†	136.4298(4.30E+1)†	229.8957(4.77E+1)†	–
		2	**5166.8933(1.29E+2)**	5127.3900(4.12E+2)†	5165.4071(8.31E+1)†	–	3862.8323(4.54E+2)†	–
WFG46	2	1	4.2529(1.07E-4)	4.2525(1.01E-6)	**4.2529(6.04E-5)**	4.2390(3.56E-3)†	4.2424(4.07E-2)†	4.1165(4.12E-2)†
		2	4.6540(1.77E-5)	**4.6540(1.05E-6)**	4.6539(1.07E-4)	4.6058(3.70E-3)†	4.5891(1.53E-2)†	4.5535(1.23E-2)†
	3	1	8.1923(7.69E-3) †	**8.1943(0.00E+0)**	8.1895(3.61E-3)†	7.9882(2.60E-1)†	8.0084(3.37E-1)†	8.0927(3.15E-1)†
		2	9.2414(6.06E-3)†	**9.2460(0.00E+0)**	9.2339(2.66E-3)†	9.0906(2.26E-1)†	9.1799(1.41E-1)†	8.3755(1.52E-1)†
	5	1	28.6674(1.29E-1)†	28.9272(3.50E-1)†	**29.1393(8.20E-1)**	20.4895(1.56E+0)†	25.5624(2.15E+0)†	19.4437(1.52E+0)†
		2	41.5600(1.69E-1)†	**41.7071(3.12E-1)**	41.3900(7.96E-1)†	20.7724(2.39E+0)†	35.3240(1.26E+0)†	33.1124(2.11E+0)†
	8	1	245.8676(1.82E+0)†	**250.8208(2.91E+0)**	238.0273(1.07E+0)†	114.1802(1.47E+1)†	195.0574(4.26E+1)†	131.5928(3.19E+1)†
		2	359.3627(1.64E+1)†	**380.4842(3.16E+1)**	349.0137(7.11E+0)†	–	333.9457(1.02E+1)†	285.2951(5.21E+0)†
	10	1	**953.4312(6.86E+0)**	947.1682(6.30E+0)†	854.2753(1.38E+0)†	367.5474(1.09E+2)†	332.0280(1.80E+2)†	–
		2	3565.0137(1.45E+2)†	**3766.2139(2.36E+2)**	3078.1682(1.02E+1)†	–	2591.9254(4.67E+2)†	–
WFG47	2	1	4.0063(2.81E-3)†	4.0091(2.84E-3)†	**4.0114(6.01-5)**	3.9420(2.12E-3)†	4.0043(6.36E-3)†	3.9781(5.82E-3)†
		2	4.1728(2.09E-5)†	4.1729(6.03E-3)†	**4.1794(3.82E-2)**	4.0455(1.64E-3)†	4.1703(6.96E-3)†	4.1655(6.12E-3)†
	3	1	**7.3908(1.56E-1)**	7.0188(0.00E+0)	7.2178(1.89E-1)	7.0741(6.86E-1)†	7.1013(1.16E-1)†	7.0603(2.10E-1)
		2	9.7758(2.13E-1)	9.4688(0.00E+0)	**9.9818(2.44E-1)**	9.7088(4.74E-2)†	9.7477(2.04E-1)†	9.5621(5.12E-1)†
	5	1	24.8848(5.48E-1)†	**25.3266(7.69E-1)**	24.6731(3.49E-1)†	16.5077(1.57E+0)†	17.3956(1.51E+0)†	15.0582(1.51E+0)†
		2	**46.6839(2.46E+0)**	45.2913(1.81E+0)†	44.9970(1.52E+0)†	23.6424(3.04E+0)†	39.0747(8.82E-1)†	44.0194(6.12E-1)†
	8	1	92.5835(4.01E+0)†	92.2396(7.45E+0)†	**92.7802(7.61E-1)**	30.9631(5.45E+0)†	54.4934(5.33E+0)†	40.5829(3.15E+0)†
		2	**690.1867(3.61E+1)**	687.1738(9.76E+1)†	667.5491(2.24E+1)†	–	620.2782(5.00E+1)†	420.1125(4.19E+1)†
	10	1	179.1392(4.42E+1)†	169.1904(3.01E+1)†	**207.1498(3.10E+1)**	34.0169(9.29E+0)†	98.6983(9.57E+0)†	–
		2	**5742.8695(5.60E+2)**	5570.3522(5.82E+2)†	4070.0848(1.40E+2)†	–	3038.5789(4.47E+2)†	–
WFG48	2	1	3.8883(1.52E-4)†	**3.8887(1.51E-6)**	3.8884(2.97E-5)†	3.7947(2.99E-3)†	3.6997(5.75E-2)†	3.7239(4.23E-3)†
		2	4.2779(2.30E-4)†	4.2779(9.27E-7)†	4.2784(3.97E-3)†	4.2397(2.66E-3)†	**4.3005(6.16E-3)**	4.2501(2.12E-3)†
	3	1	8.2294(3.77E-3)	**8.2305(3.01E-7)**	8.2250(2.49E-3)†	8.2039(3.24E-1)†	8.2285(1.66E-1)†	7.0455(1.11E-1)†
		2	**9.4073(4.17E-3)**	9.4054(1.23E-6)†	9.4071(3.83E-3)	9.1336(7.11E-1)†	9.4050(1.03E-1)†	8.8295(3.02E-1)†
	5	1	31.3466(8.79E-2)†	31.3978(1.48E-1)†	**32.2048(5.75E-1)**	26.3694(2.17E+0)†	29.7800(8.01E-1)†	21.5212(7.91E-1)†
		2	37.2188(9.57E-2)†	37.1747(3.80E-1)†	**37.9064(5.32E-1)**	–	35.4740(3.96E-1)†	35.7858(5.12E-1)†
	8	1	**261.2983(1.90E+0)**	259.1756(1.11E+0)†	255.7826(2.60E-1)†	181.4143(4.03E+1)†	255.4237(9.22E+0)†	–
		2	**459.8634(2.05E+0)**	456.9066(3.10E+0)†	451.0410(4.22E-1)†	447.4523(1.79E+1)†	442.6764(2.25E+1)†	–
	10	1	**422.4212(4.21E+1)**	403.7712(8.224E+0)†	400.2181(1.28E+1)†	–	320.1247(6.64E+1)†	–
		2	**1422.7213(8.21E+2)**	1399.2381(9.72E+2)†	1391.5048(1.04E+3)†	–	911.9634(1.69E+2)†	–

† denotes the best median metric value is significantly better than the other peers according to the statistical analysis described in Appendix F of the supplementary document. ref = 1 means the unattainable aspiration level vector while ref = 2 means the attainable aspiration level vector. – means all solutions obtained by the corresponding algorithm are dominated by the other counterparts, thus no solution can be used for R-HV computation.

APPENDIX I
COMPARISON OF CPU TIME COSTS

In Table V, we compare the average CPU time cost by the three decomposition-based EMO algorithms assisted by the NUMS and their corresponding baseline algorithms. From the comparison results, we can see that the NUMS does not incur additional computational costs to the baseline algorithm.

TABLE V: Comparison results of the average CPU time costs (in second) of three decomposition-based EMO algorithms assisted by the NUMS and their corresponding baseline algorithms.

Problem	m	NUMS Assisted			Baseline Algorithm		
		MOEAD/STM	MOEAD	NSGA-III	MOEAD/STM	MOEAD	NSGA-III
DTLZ1	3	1	1	2	1	1	2
	5	2	2	3	2	1	3
	8	4	4	7	3	3	7
	10	14	14	122	15	14	120
DTLZ2	3	1	1	1	1	1	1
	5	2	2	2	2	1	1
	8	4	5	8	3	4	7
	10	15	14	132	16	14	136
DTLZ3	3	2	3	3	2	3	2
	5	3	4	4	2	3	3
	8	7	8	11	6	8	11
	10	18	22	272	16	23	244
DTLZ4	3	1	1	2	1	1	2
	5	5	3	7	5	3	6
	8	6	7	11	6	6	10
	10	14	11	125	15	10	136
WFG41	3	1	1	0	1	1	1
	5	3	3	5	3	3	4
	8	5	11	12	4	10	12
	10	18	16	164	19	16	151
WFG42	3	2	2	2	1	1	1
	5	3	3	3	3	2	2
	8	6	10	12	5	9	11
	10	18	20	346	18	19	355
WFG43	3	1	1	1	1	1	1
	5	6	3	9	5	3	8
	8	8	8	11	7	8	11
	10	16	10	101	14	9	93
WFG44	3	1	1	2	1	1	1
	5	3	3	5	2	3	4
	8	5	5	7	5	5	7
	10	17	15	146	17	13	135
WFG45	3	2	2	1	1	2	1
	5	2	3	3	1	3	3
	8	5	9	12	4	8	11
	10	19	17	382	17	18	358
WFG46	3	1	1	1	1	1	1
	5	3	2	11	2	2	11
	8	5	8	13	5	8	12
	10	15	10	100	14	10	108
WFG47	3	1	1	1	1	1	1
	5	2	3	3	1	2	3
	8	2	4	7	1	4	6
	10	20	17	161	21	18	163
WFG48	3	2	2	1	1	2	1
	5	2	2	3	2	1	3
	8	4	11	11	4	10	12
	10	20	21	313	18	21	300

Moreover, in Table VI, we also show the comparisons of the average CPU time cost by the three decomposition-based EMO algorithms assisted by the NUMS with the other three preference-based EMO algorithms. From the comparison results, we can clearly see that the three decomposition-based EMO algorithms are faster.

TABLE VI: Comparison results of the average CPU time costs (in second) of three decomposition-based EMO algorithms assisted by the NUMS and the other three preference-based EMO algorithms.

Problem	m	MOEAD/STM	MOEAD	NSGA-III	g-NSGA-II	r-NSGA-II	R-NSGA-II
DTLZ1	3	1	1	2	6	8	23
	5	2	2	3	18	22	371
	8	4	4	7	43	58	1822
	10	14	14	122	323	352	10122
DTLZ2	3	1	1	1	6	7	21
	5	2	2	2	16	21	366
	8	4	5	8	51	54	2245
	10	15	14	132	347	346	11212
DTLZ3	3	2	3	3	11	13	43
	5	3	4	4	23	32	366
	8	7	8	11	51	53	2245
	10	18	22	272	421	432	15282
DTLZ4	3	1	1	2	7	6	18
	5	5	3	7	16	21	437
	8	6	7	11	37	66	1481
	10	14	11	125	382	291	9131
WFG41	3	1	1	0	6	5	19
	5	3	3	5	13	26	395
	8	5	11	12	42	69	2371
	10	18	16	164	333	406	13124
WFG42	3	2	2	2	10	11	37
	5	3	3	3	25	36	459
	8	6	10	12	58	58	1808
	10	18	20	346	369	461	10848
WFG43	3	1	1	1	8	5	17
	5	6	3	9	15	24	465
	8	8	8	11	40	59	1225
	10	16	10	101	432	310	11073
WFG44	3	1	1	2	7	5	15
	5	3	3	5	15	28	475
	8	5	5	7	41	60	2659
	10	17	15	146	412	483	14463
WFG45	3	2	2	1	11	11	36
	5	2	3	3	22	44	466
	8	5	9	12	63	74	2119
	10	19	17	382	417	376	12714
WFG46	3	1	1	1	7	5	14
	5	3	2	11	16	21	535
	8	5	8	13	35	54	1325
	10	15	10	100	367	396	15850
WFG47	3	1	1	1	8	5	12
	5	2	3	3	18	29	416
	8	2	4	7	53	69	2664
	10	20	17	161	429	536	16671
WFG48	3	2	2	1	13	10	39
	5	2	2	3	25	43	519
	8	4	11	11	65	79	1864
	10	20	21	313	462	381	11184

APPENDIX J
PLOTS OF FINAL POPULATIONS

This section provides the visual comparisons of different preference-based EMO algorithms. In particular, we plot the final solutions obtained by different algorithms that achieve the best R-HV value.
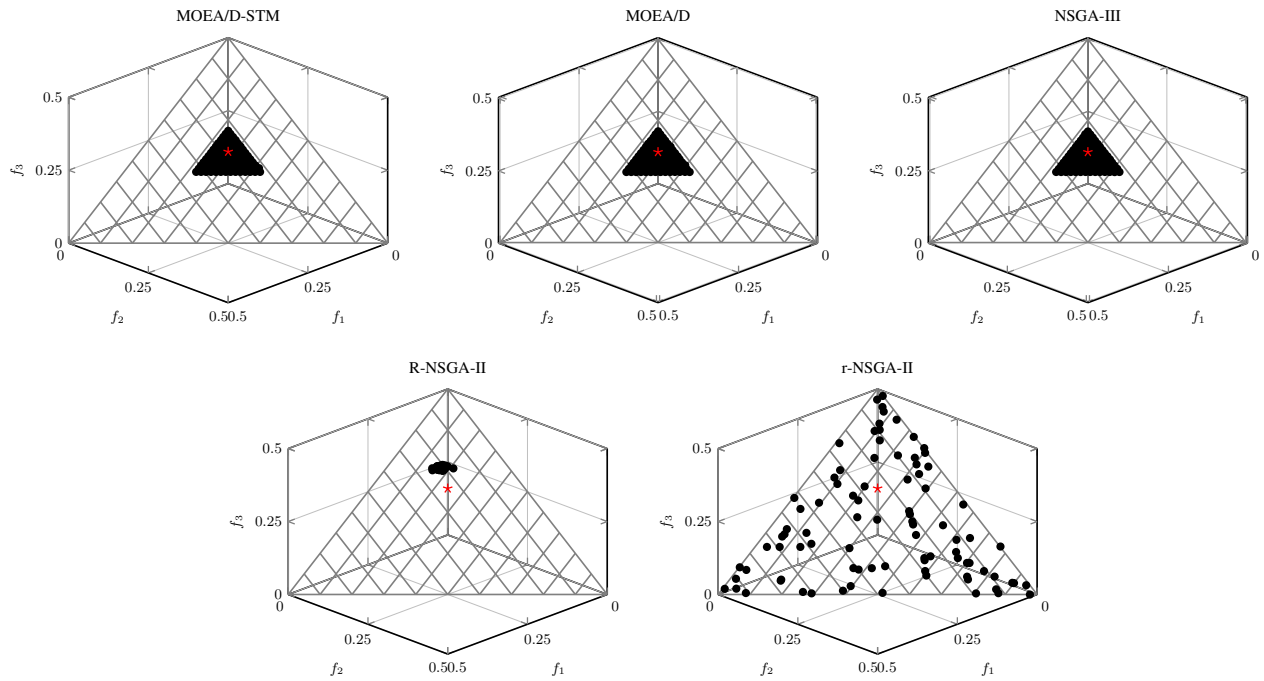
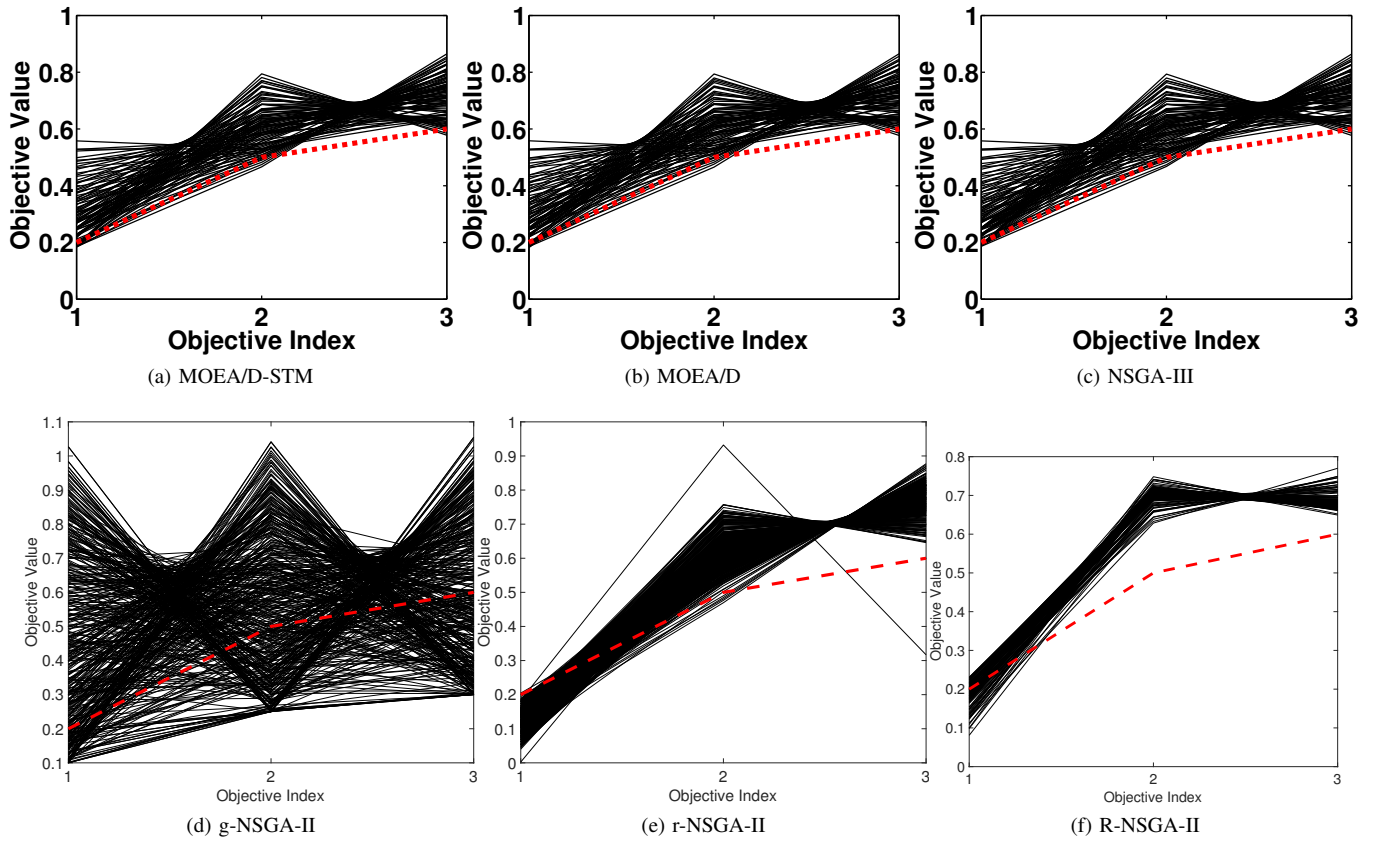

Fig. 10: Comparisons on 3-objective DTLZ1 where $\mathbf{z}^r = (0.05, 0.05, 0.2)$.
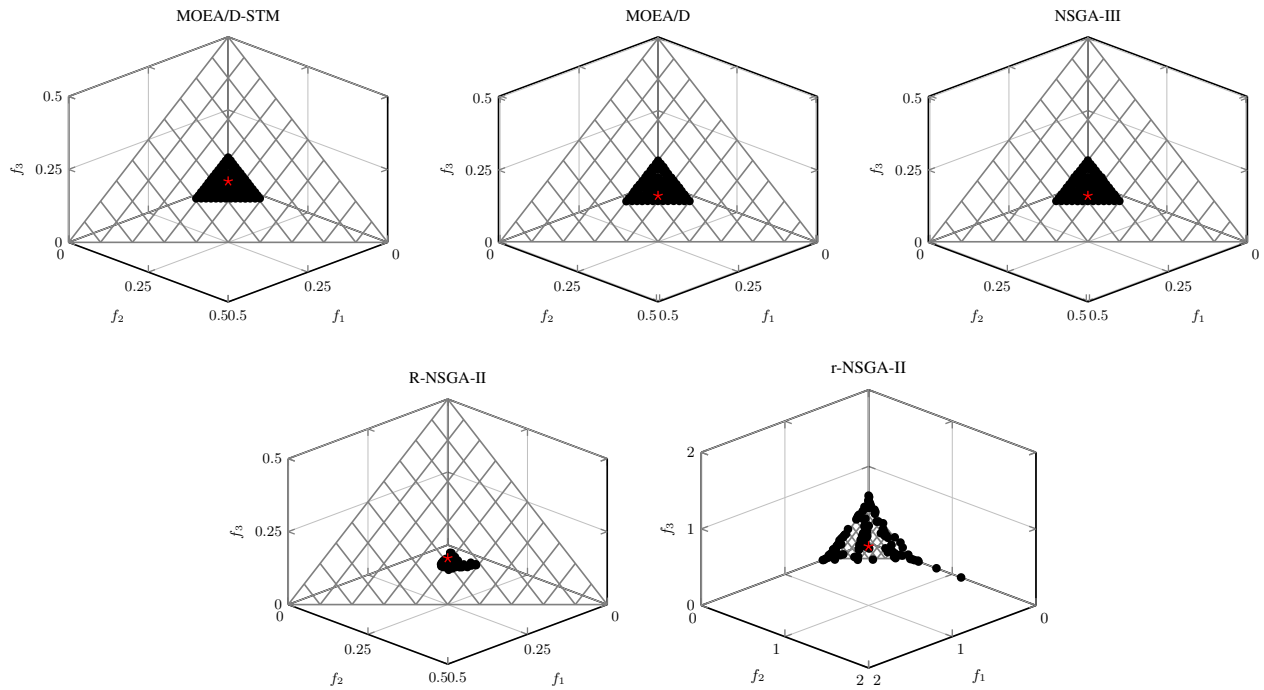
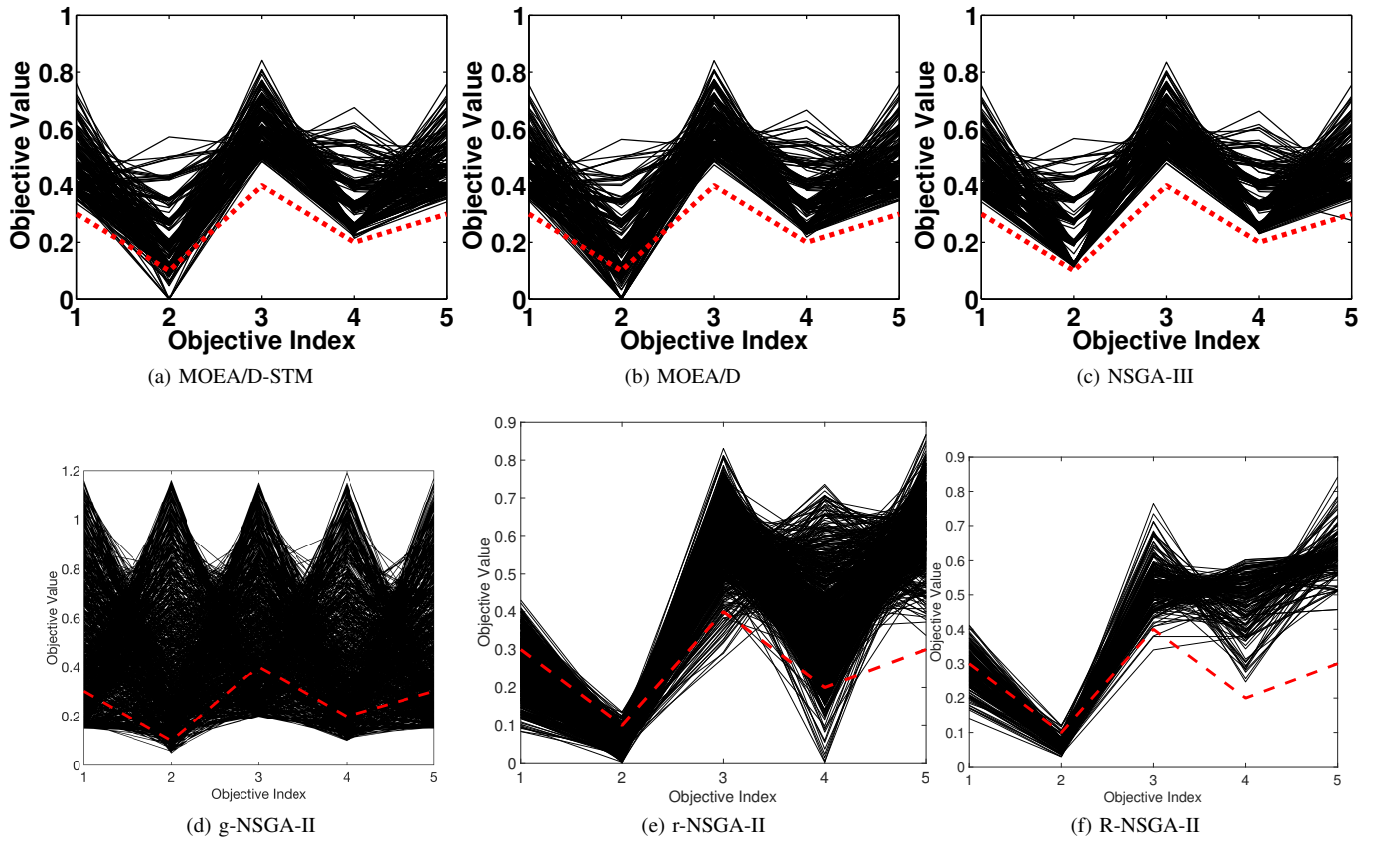Fig. 11: Comparisons on 3-objective DTLZ1 where $\mathbf{z}^r = (0.3, 0.3, 0.2)$.
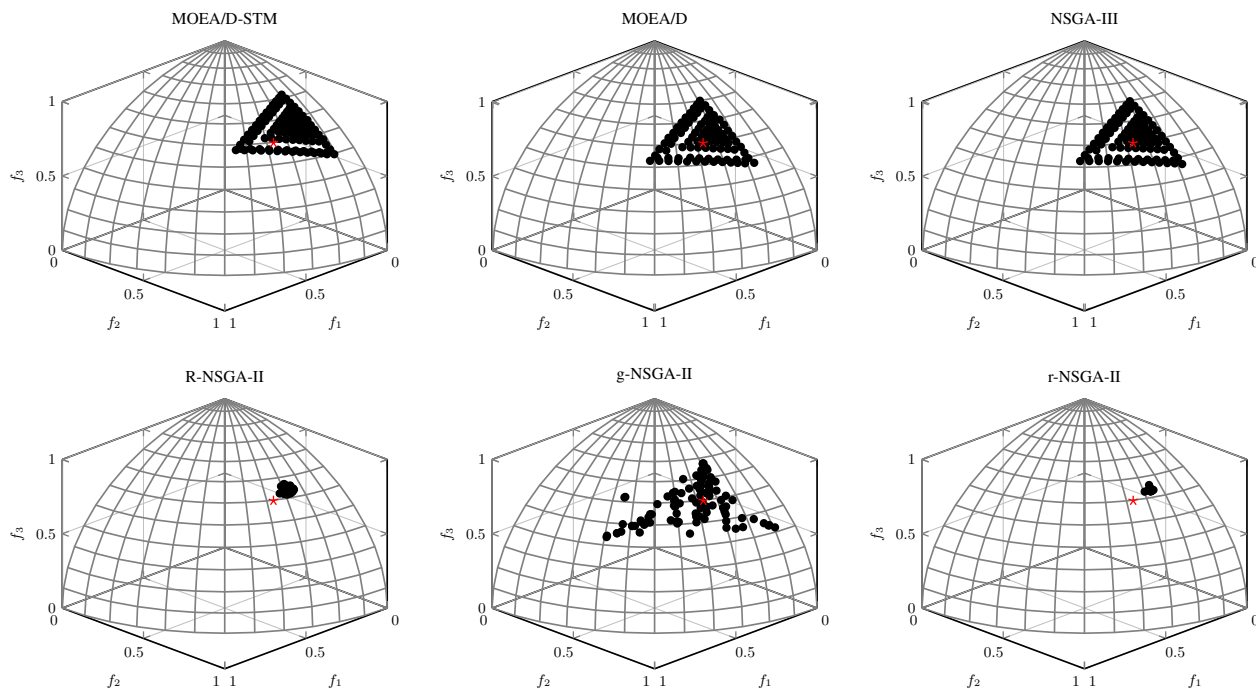
Fig. 12: Comparisons on 3-objective DTLZ2 where $\mathbf{z}^r = (0.2, 0.5, 0.6)$.
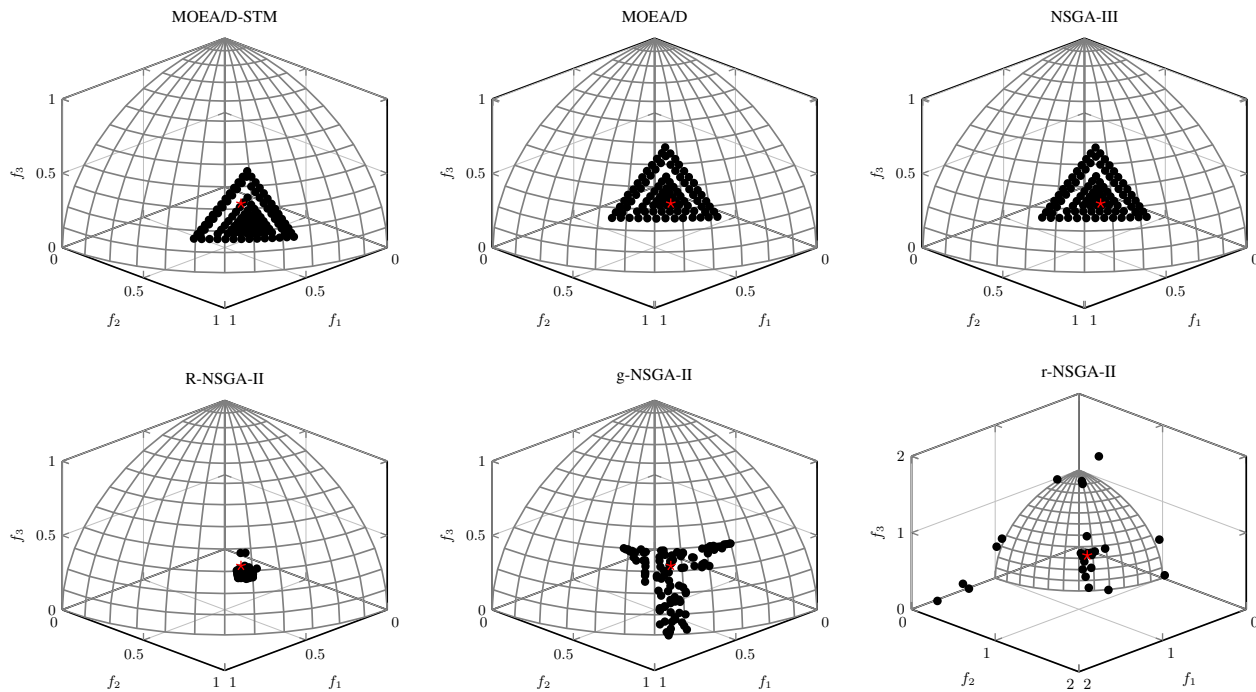
Fig. 13: Comparisons on 3-objective DTLZ2 where $\mathbf{z}^r = (0.7, 0.8, 0.5)$.
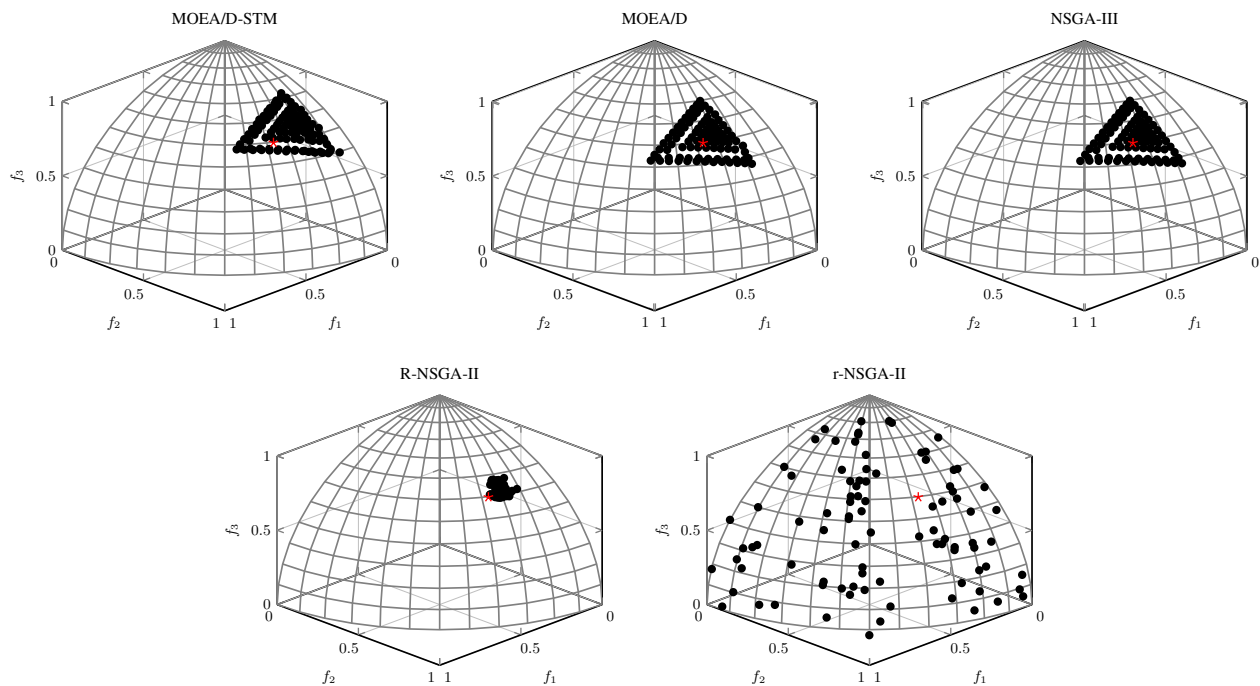
Fig. 14: Comparisons on 3-objective DTLZ3 where $\mathbf{z}^r = (0.2, 0.5, 0.6)$.
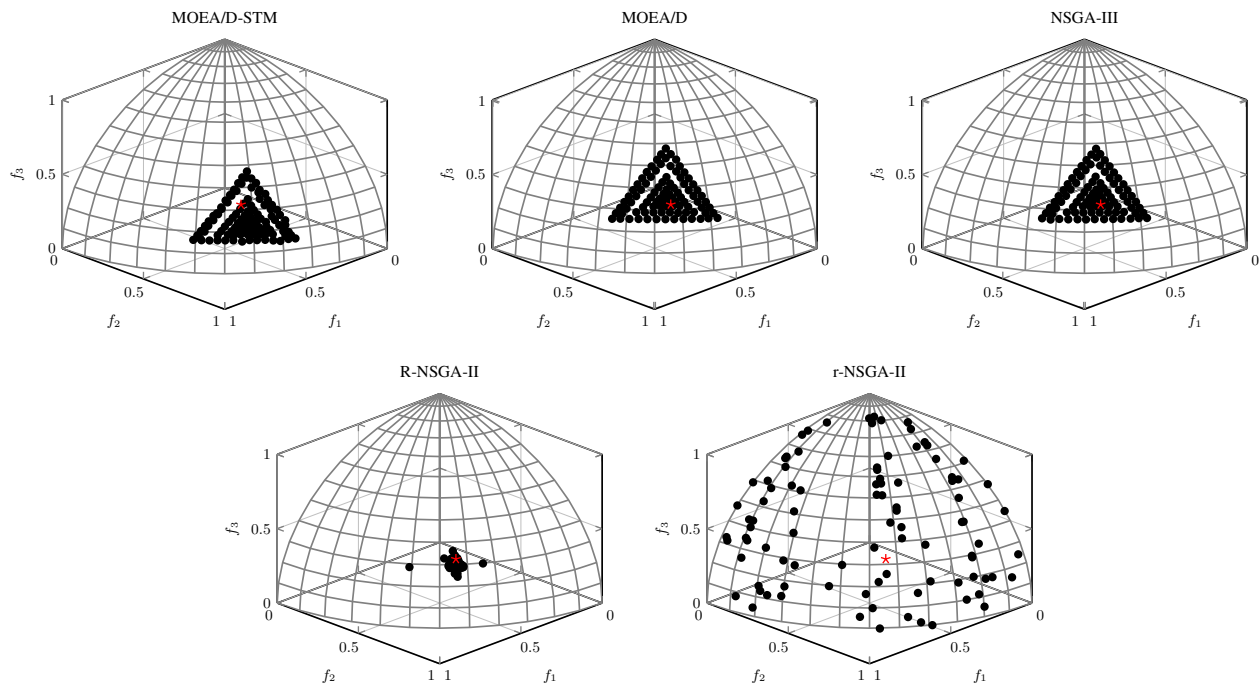
Fig. 15: Comparisons on 3-objective DTLZ3 where $\mathbf{z}^r = (0.7, 0.8, 0.5)$.
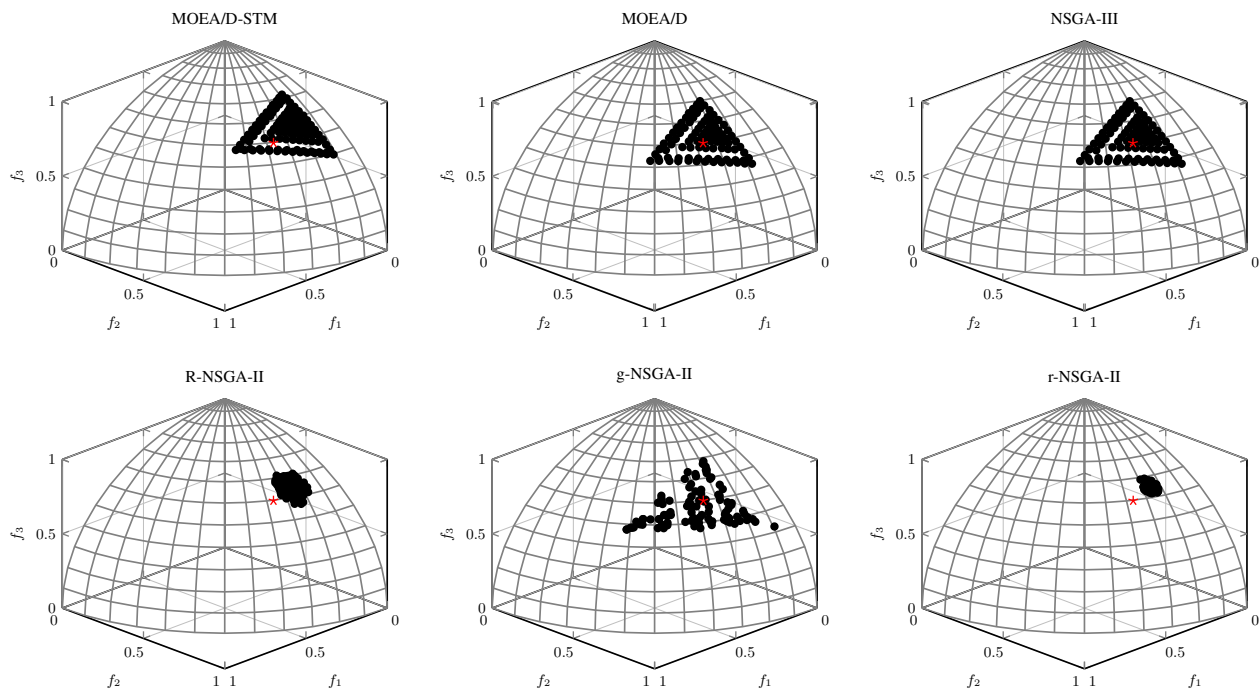
Fig. 16: Comparisons on 3-objective DTLZ4 where $\mathbf{z}^r = (0.2, 0.5, 0.6)$.
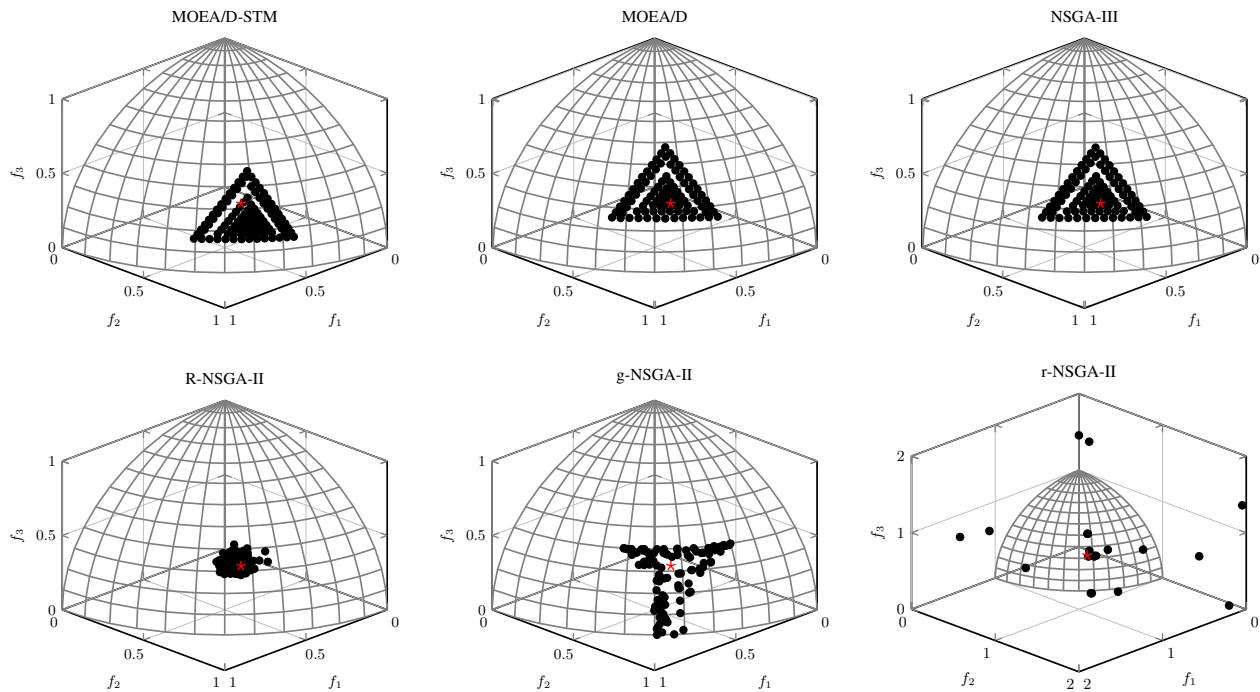
Fig. 17: Comparisons on 3-objective DTLZ4 where $\mathbf{z}^r = (0.7, 0.8, 0.5)$.
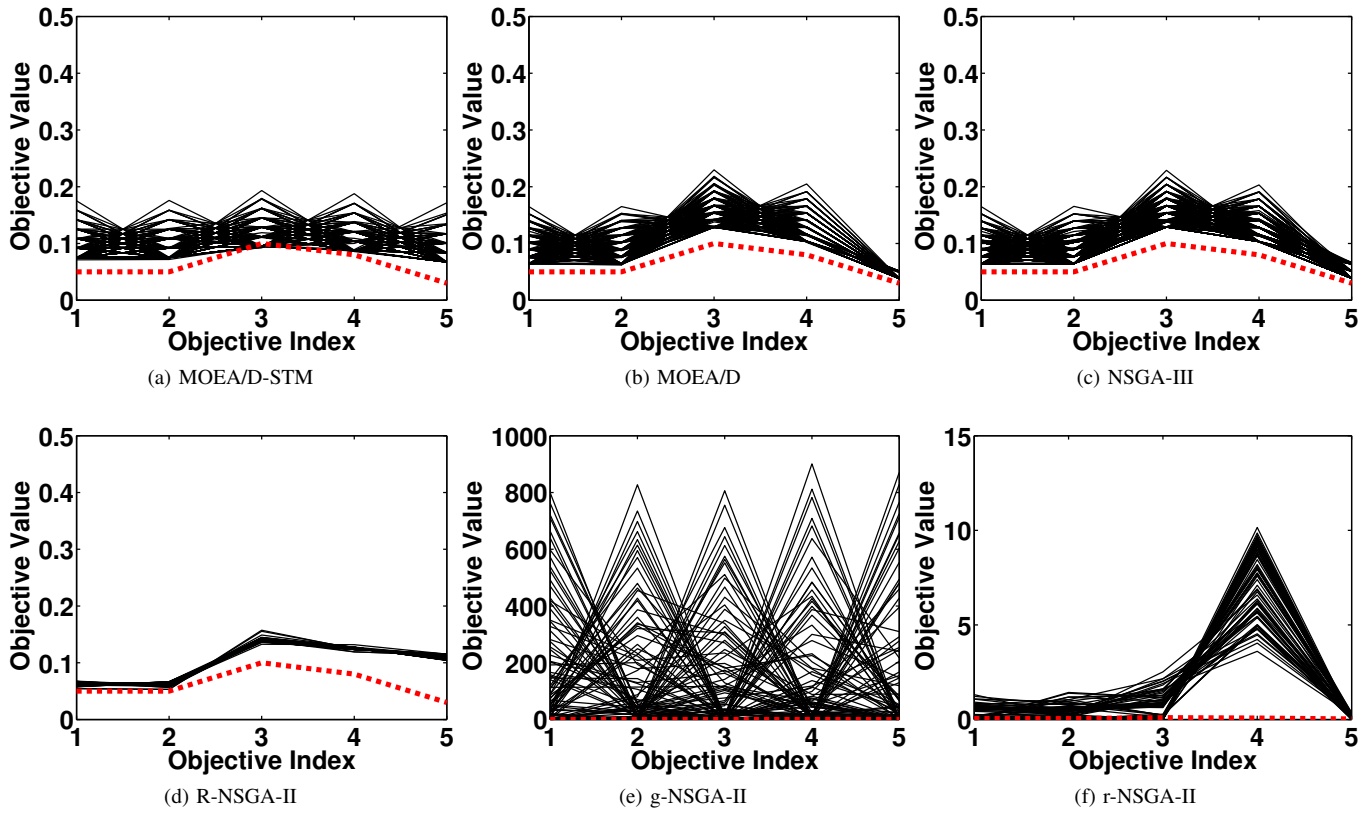
Fig. 18: Comparisons on 5-objective DTLZ1 where $\mathbf{z}^r = (0.05, 0.05, 0.1, 0.08, 0.03)^T$.
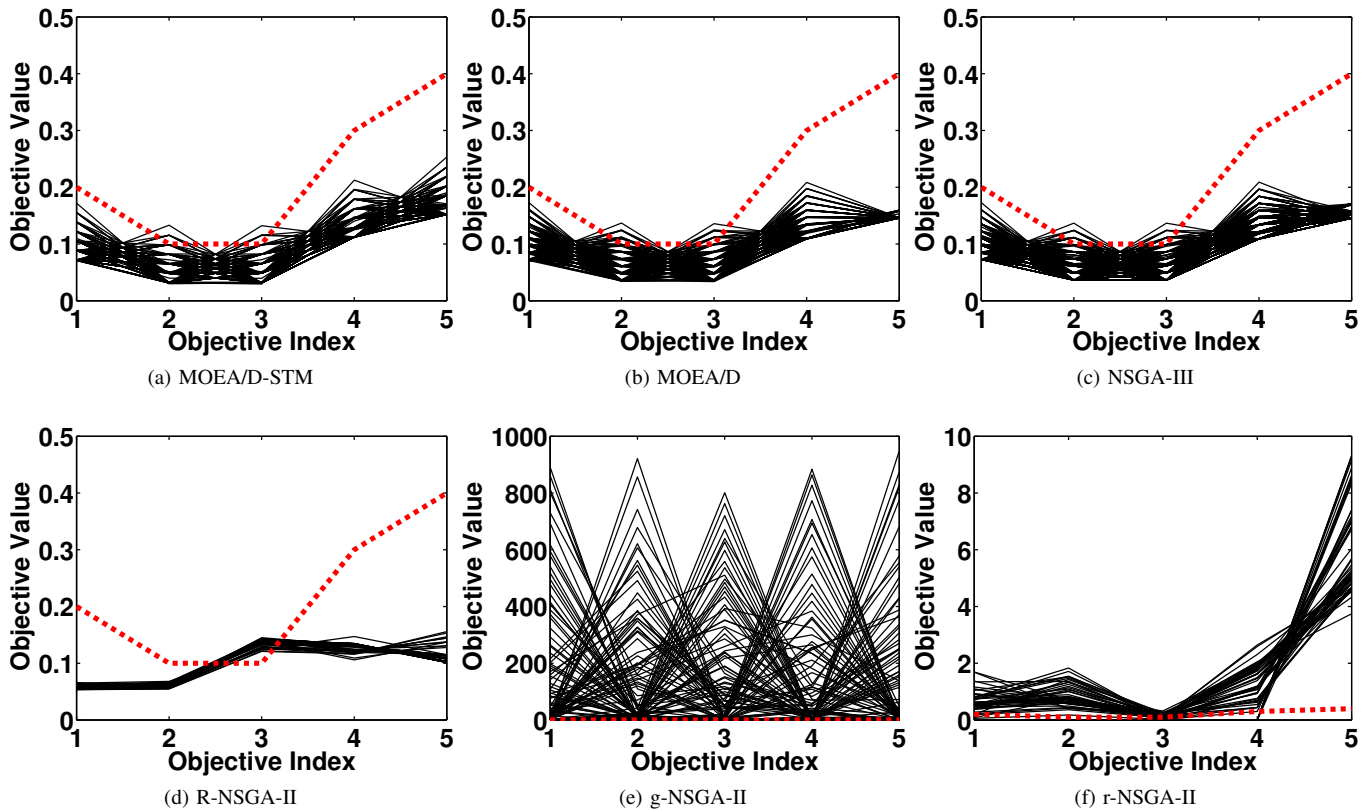
Fig. 19: Comparisons on 5-objective DTLZ1 where $\mathbf{z}^r = (0.2, 0.1, 0.1, 0.3, 0.4)^T$.
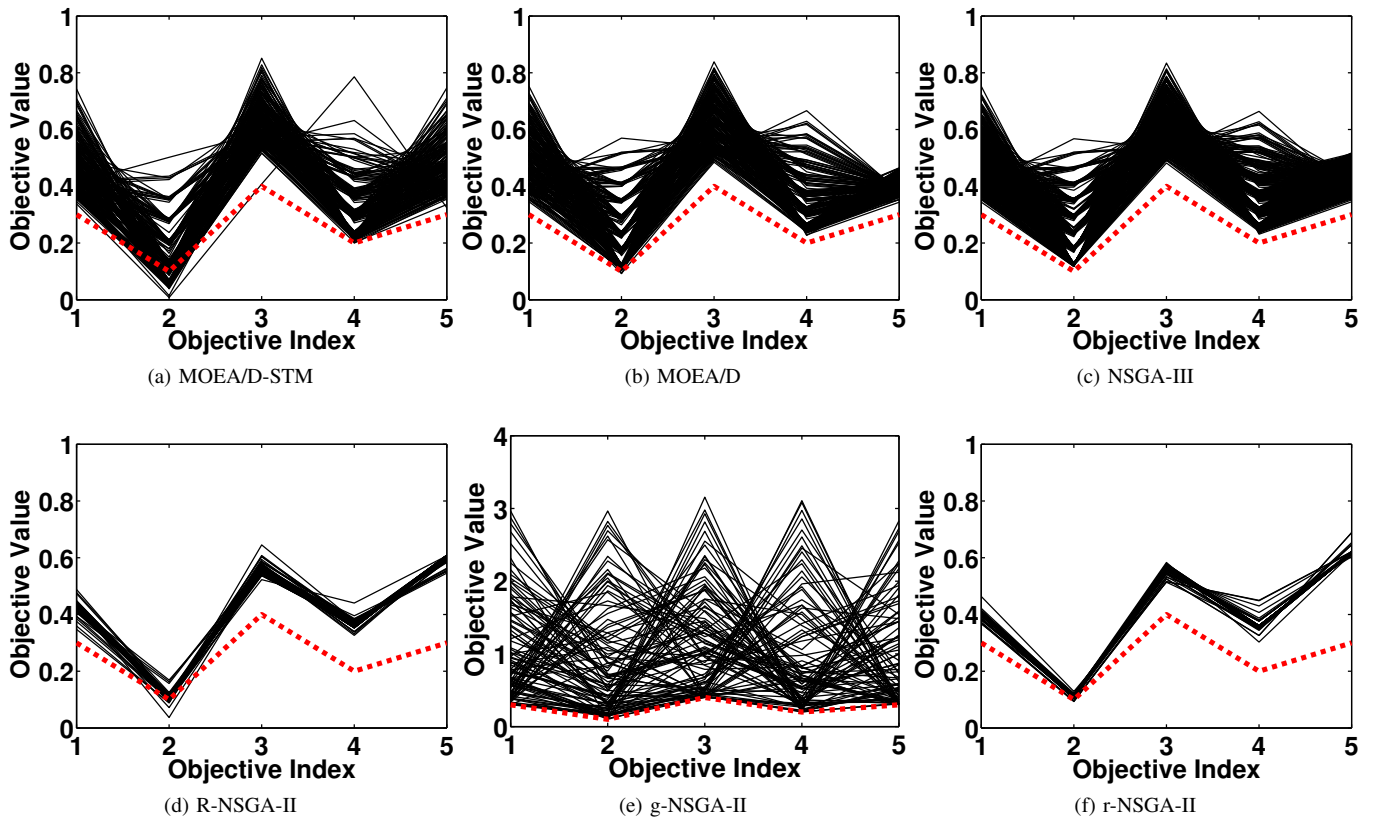
Fig. 20: Comparisons on 5-objective DTLZ2 where $\mathbf{z}^r = (0.3, 0.1, 0.4, 0.2, 0.3)^T$.
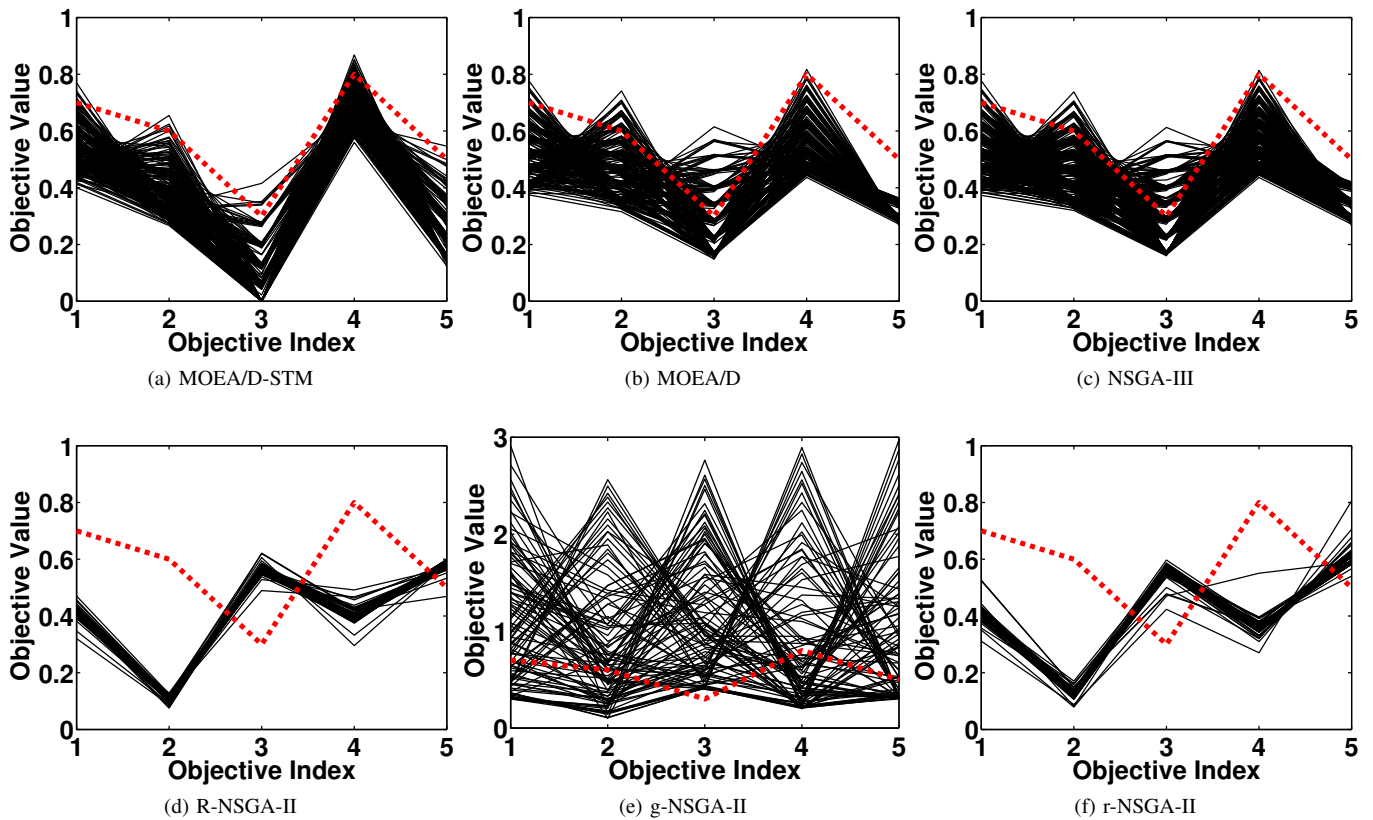
Fig. 21: Comparisons on 5-objective DTLZ2 where $\mathbf{z}^r = (0.7, 0.6, 0.3, 0.8, 0.5)^T$.

(a) MOEA/D-STM

(b) MOEA/D

(c) NSGA-III

(d) R-NSGA-II

(e) g-NSGA-II

(f) r-NSGA-II

Fig. 22: Comparisons on 5-objective DTLZ3 where $\mathbf{z}^r = (0.3, 0.1, 0.4, 0.2, 0.3)^T$.

(a) MOEA/D-STM

(b) MOEA/D

(c) NSGA-III

(d) R-NSGA-II

(e) g-NSGA-II

(f) r-NSGA-II
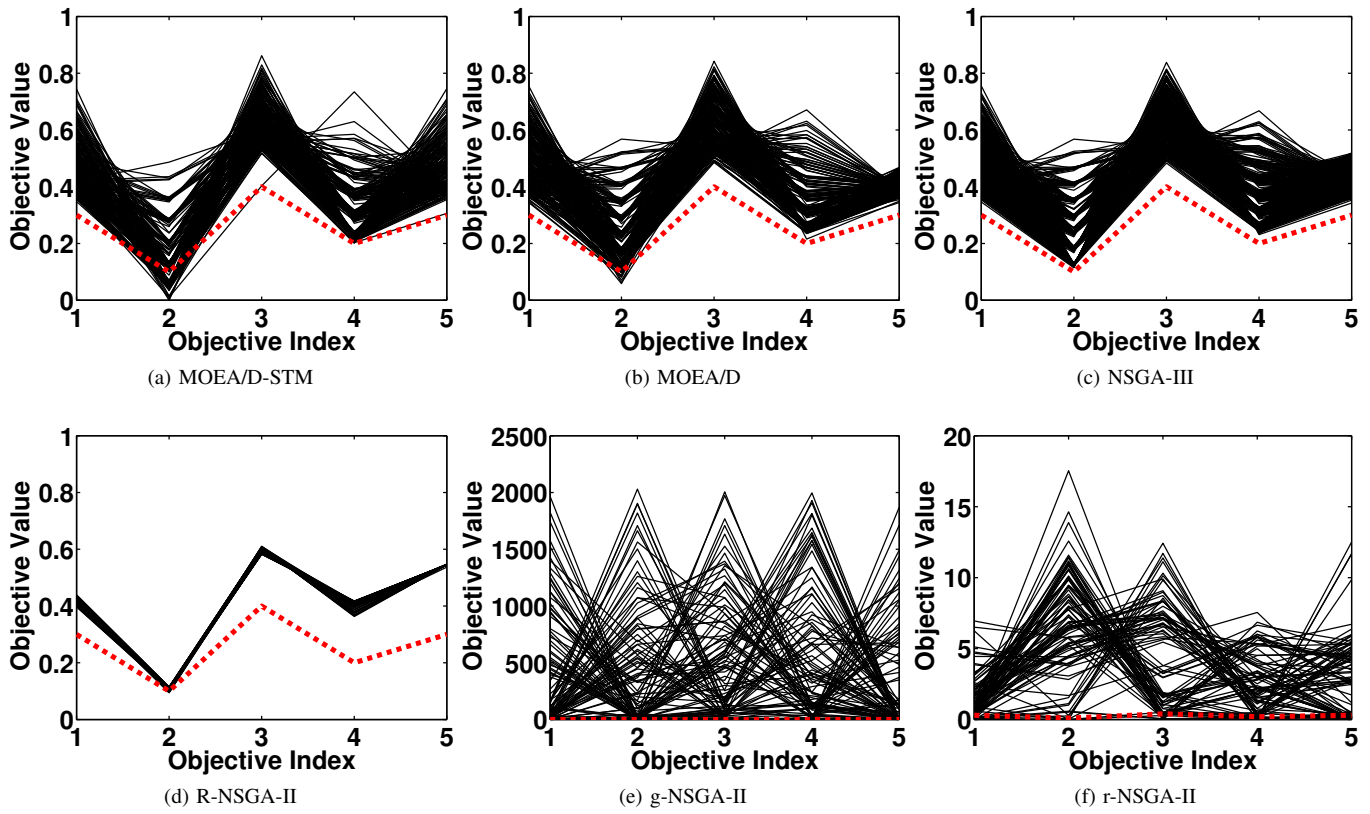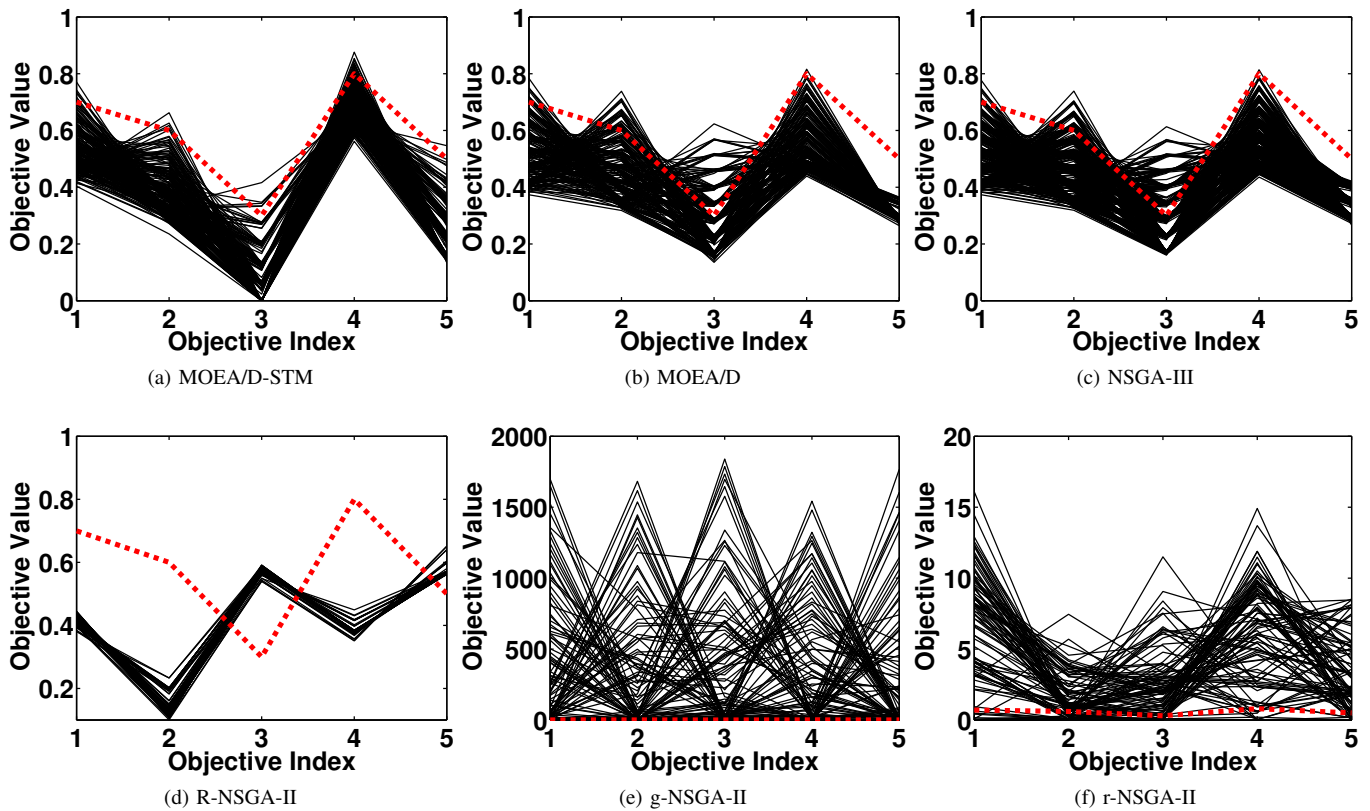
Fig. 23: Comparisons on 5-objective DTLZ3 where $\mathbf{z}^r = (0.7, 0.6, 0.3, 0.8, 0.5)^T$.
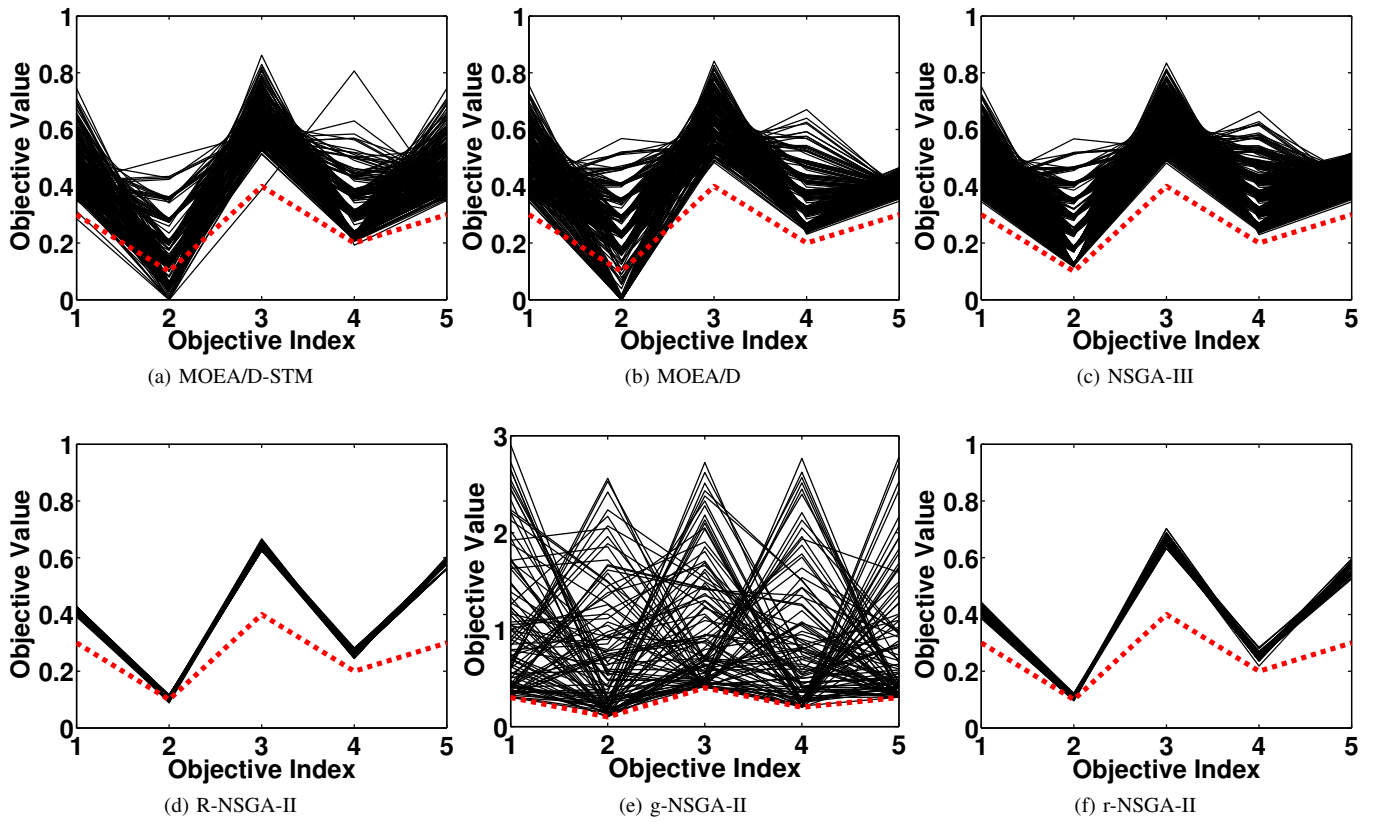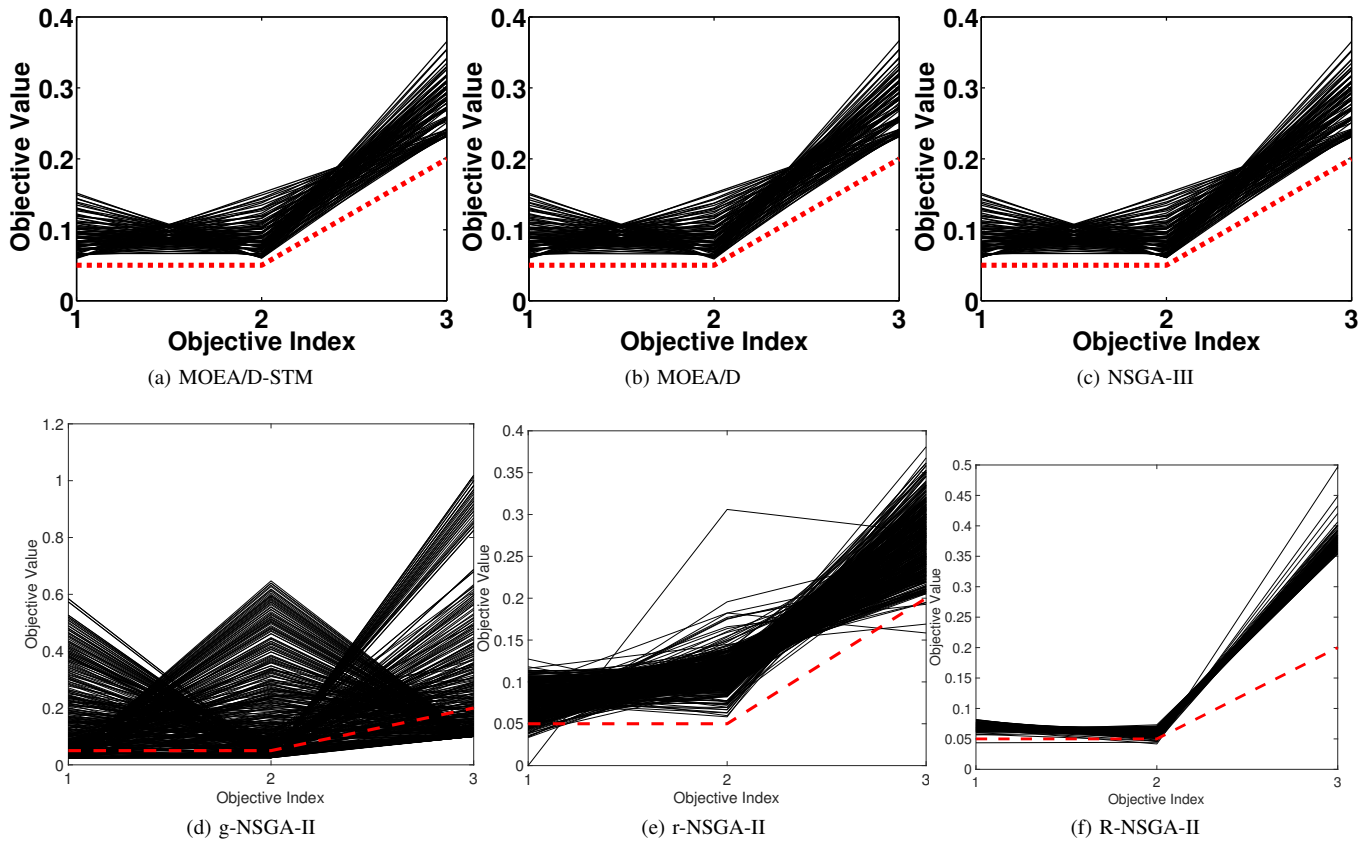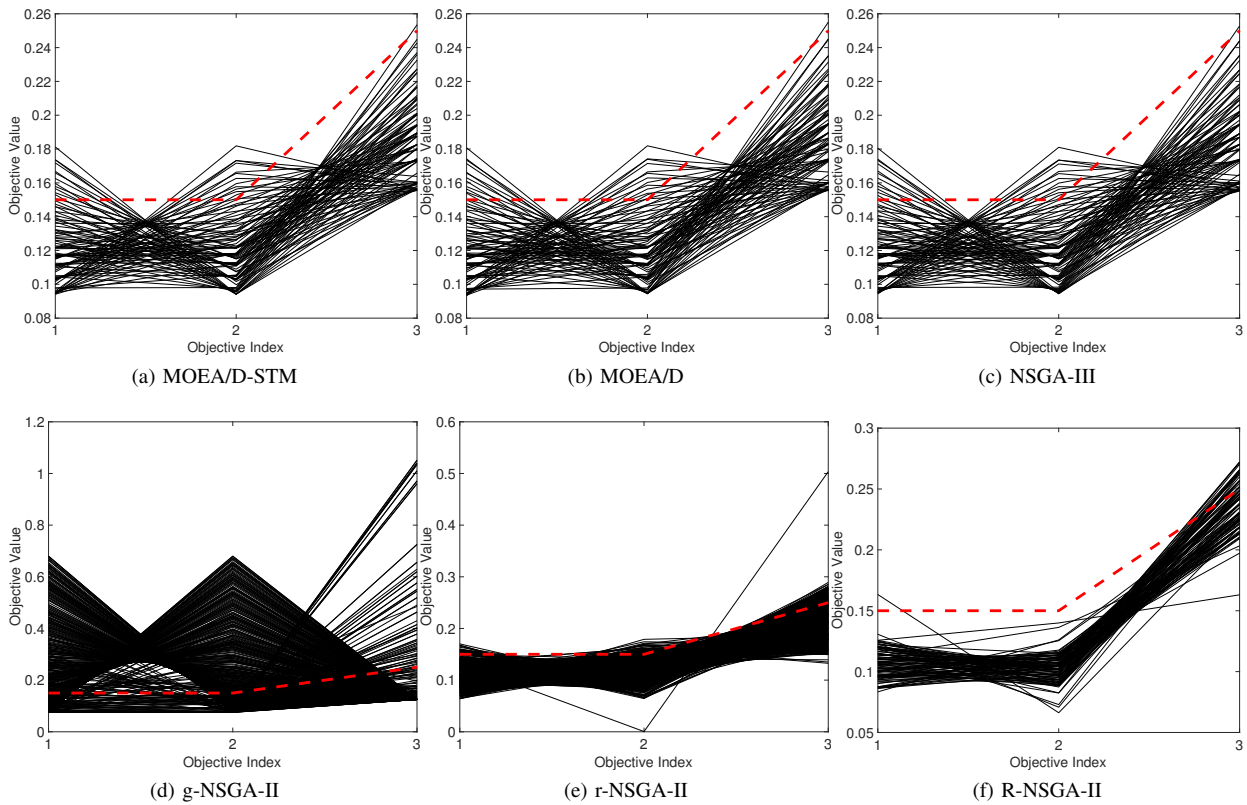
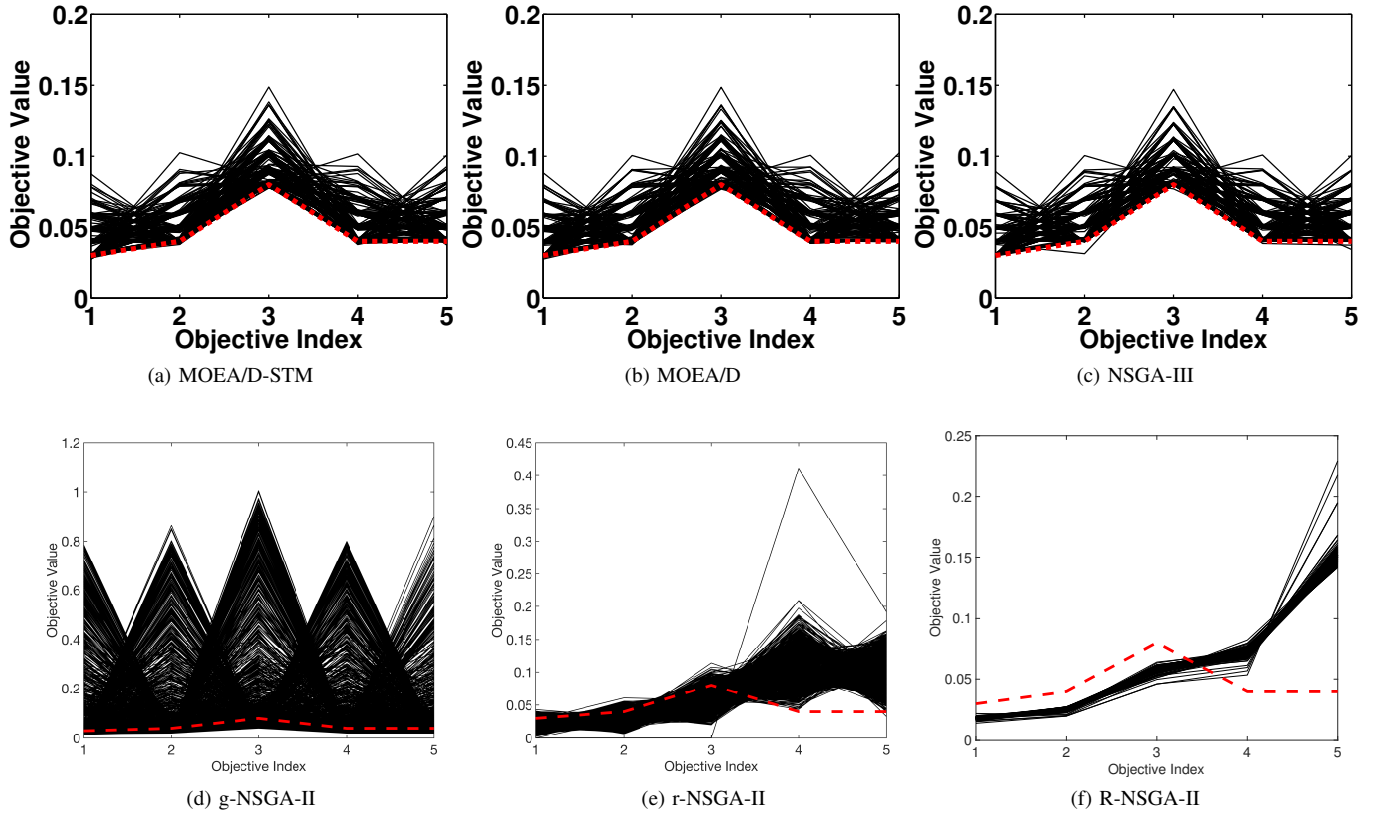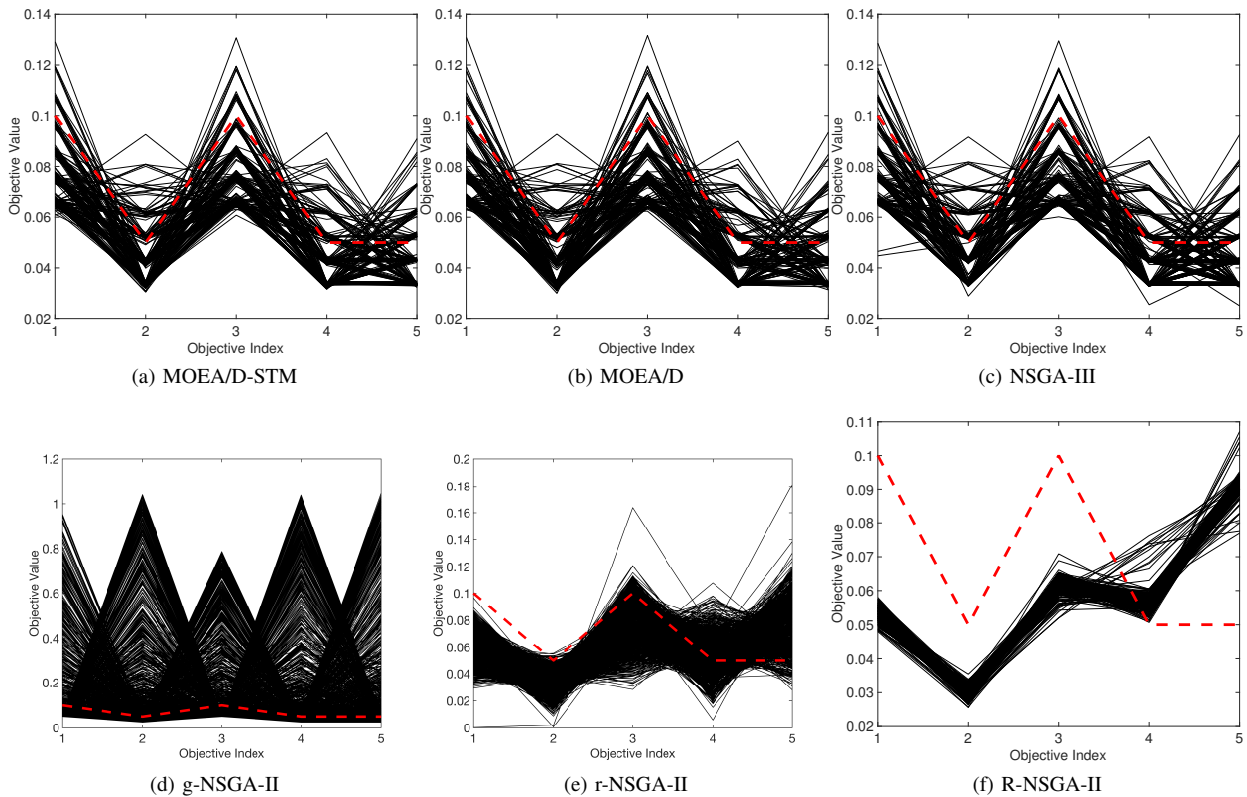Fig. 24: Comparisons on 5-objective DTLZ4 where $\mathbf{z}^r = (0.3, 0.1, 0.4, 0.2, 0.3)^T$.
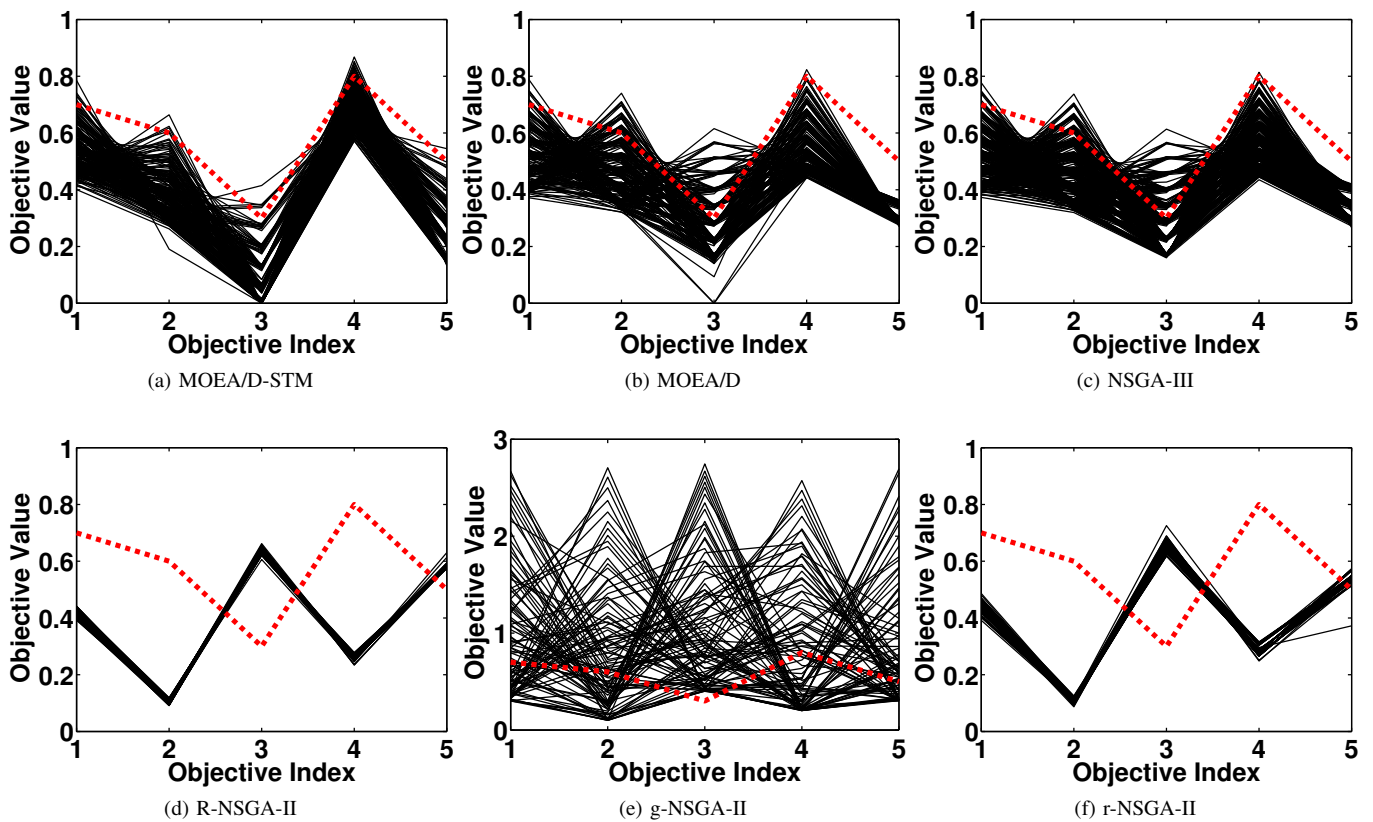
Fig. 25: Comparisons on 5-objective DTLZ4 where $\mathbf{z}^r = (0.7, 0.6, 0.3, 0.8, 0.5)^T$.
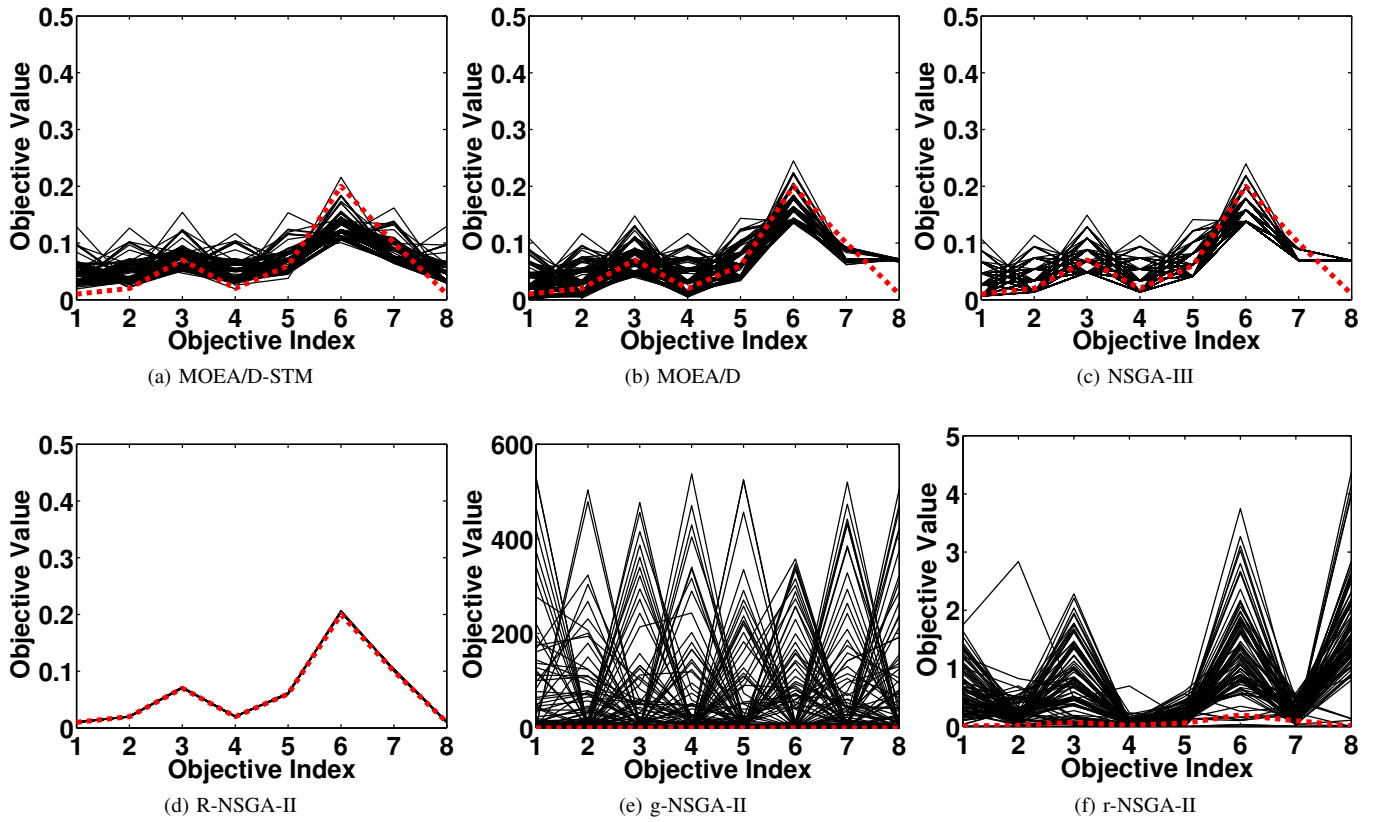
Fig. 26: Comparisons on 8-objective DTLZ1 where $\mathbf{z}^r = (0.01, 0.02, 0.07, 0.02, 0.06, 0.2, 0.1, 0.01)^T$.
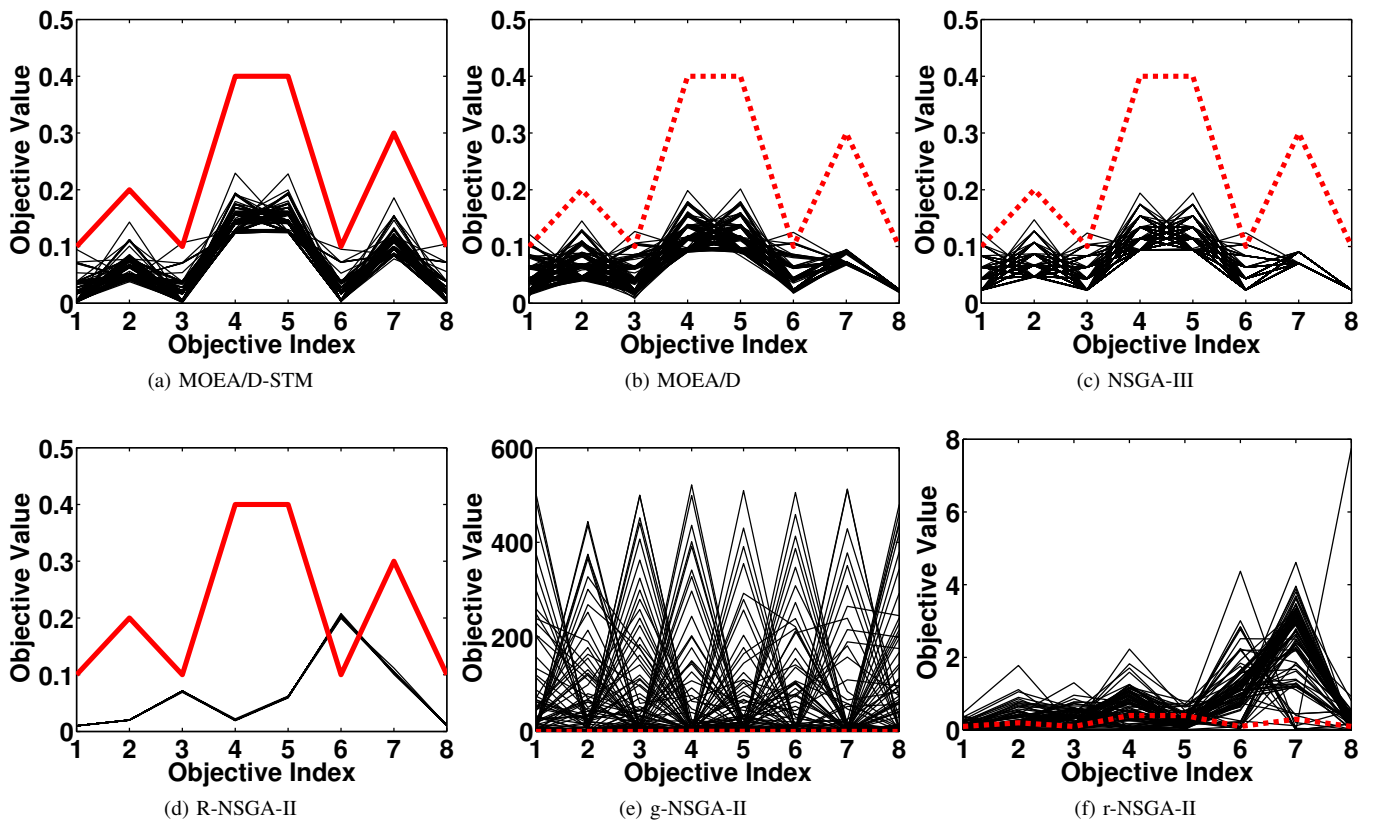
Fig. 27: Comparisons on 8-objective DTLZ1 where $\mathbf{z}^r = (0.1, 0.2, 0.1, 0.4, 0.4, 0.1, 0.3, 0.1)^T$.

(a) MOEA/D-STM

(b) MOEA/D

(c) NSGA-III

(d) R-NSGA-II

(e) g-NSGA-II

(f) r-NSGA-II

Fig. 28: Comparisons on 8-objective DTLZ2 where $\mathbf{z}^r = (0.3, 0.1, 0.4, 0.25, 0.1, 0.15, 0.4, 0.25)^T$.

(a) MOEA/D-STM

(b) MOEA/D

(c) NSGA-III

(d) R-NSGA-II

(e) g-NSGA-II

(f) r-NSGA-II
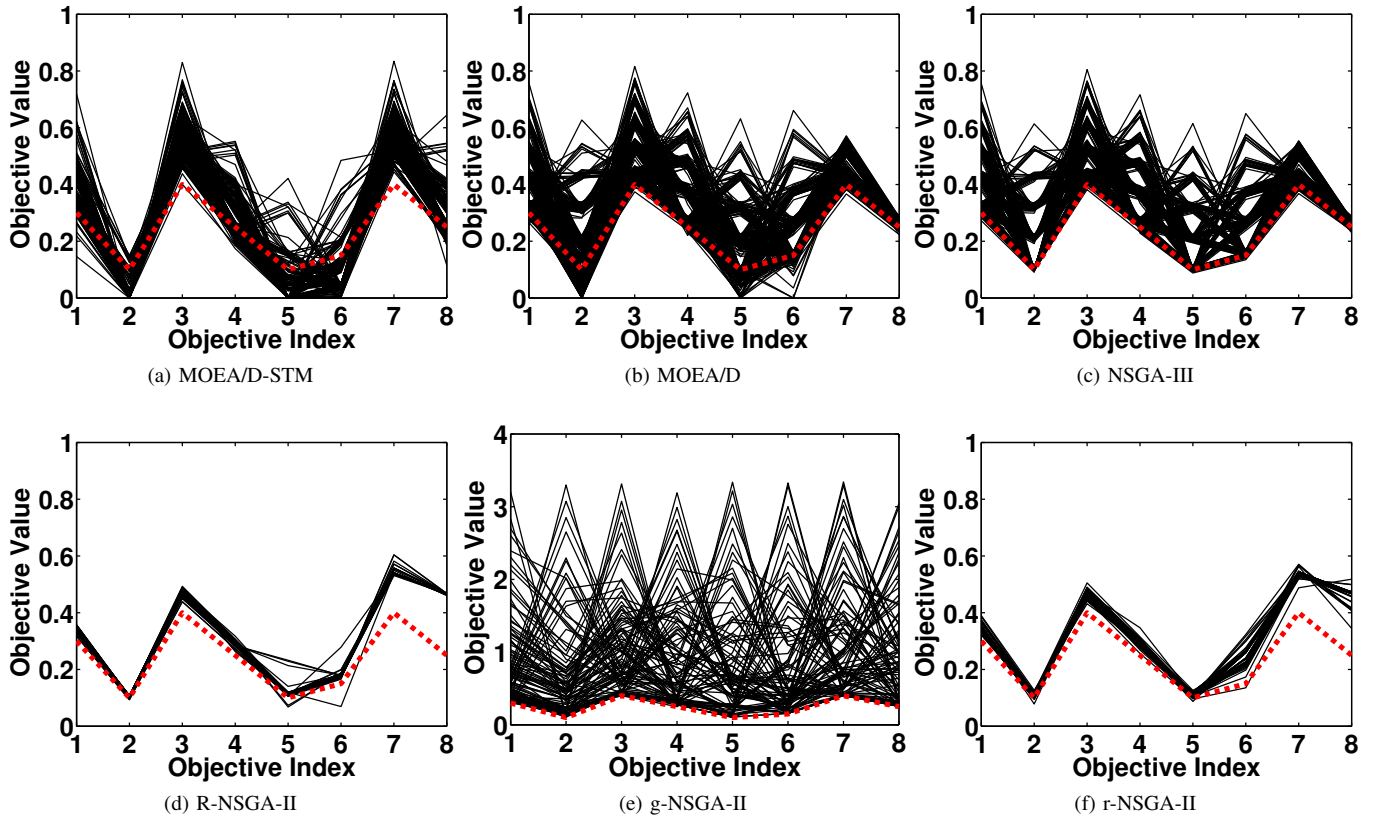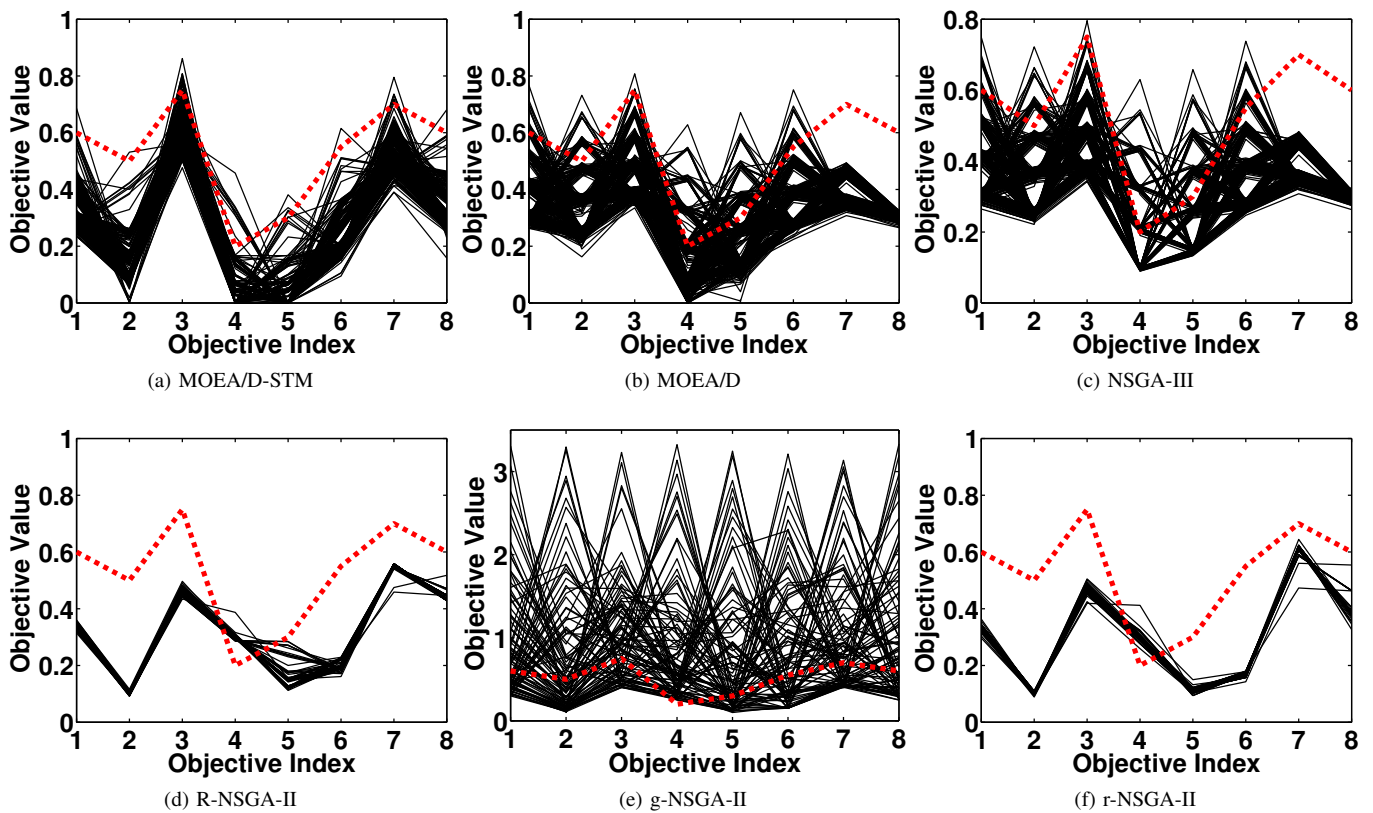
Fig. 29: Comparisons on 8-objective DTLZ2 where $\mathbf{z}^r = (0.6, 0.5, 0.75, 0.2, 0.3, 0.55, 0.7, 0.6)^T$.
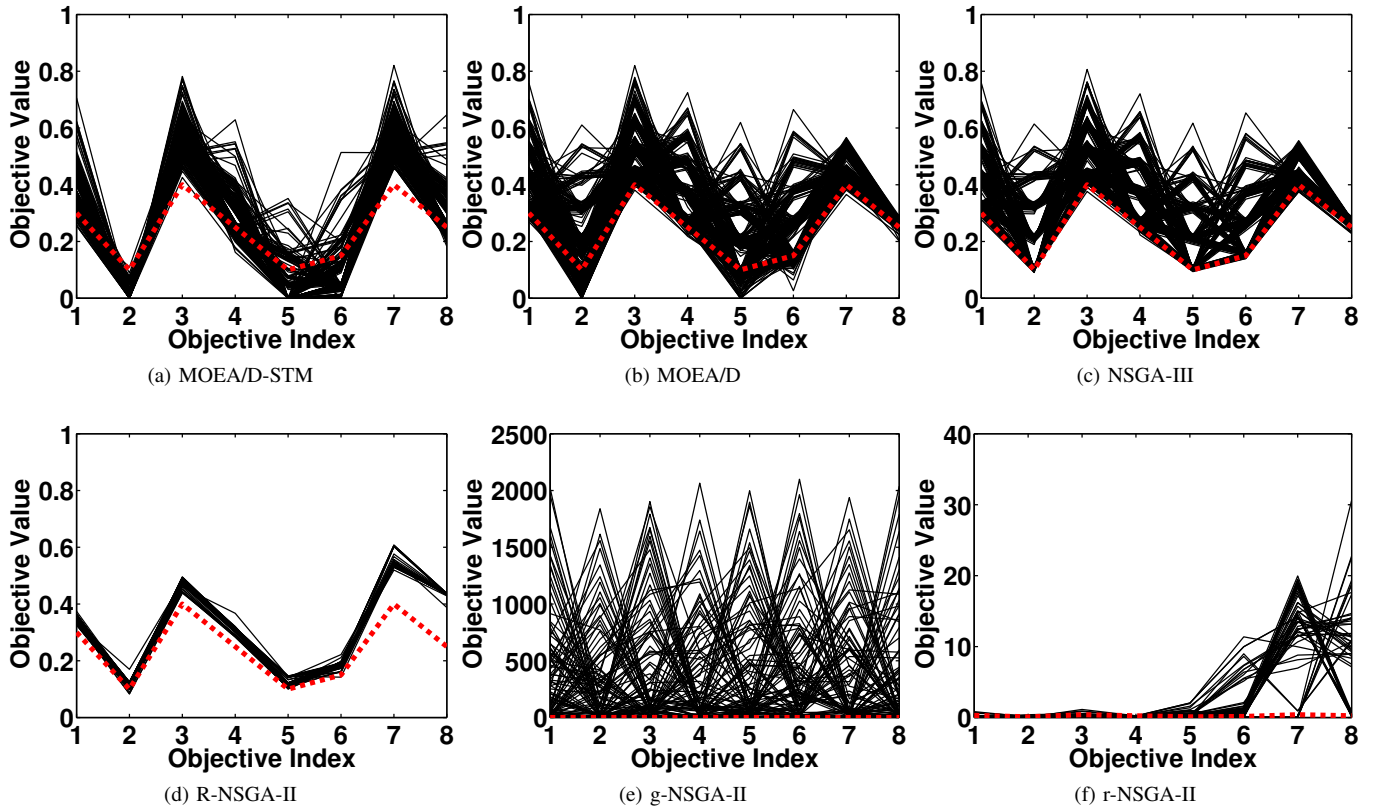
Fig. 30: Comparisons on 8-objective DTLZ3 where $\mathbf{z}^r = (0.3, 0.1, 0.4, 0.25, 0.1, 0.15, 0.4, 0.25)^T$.
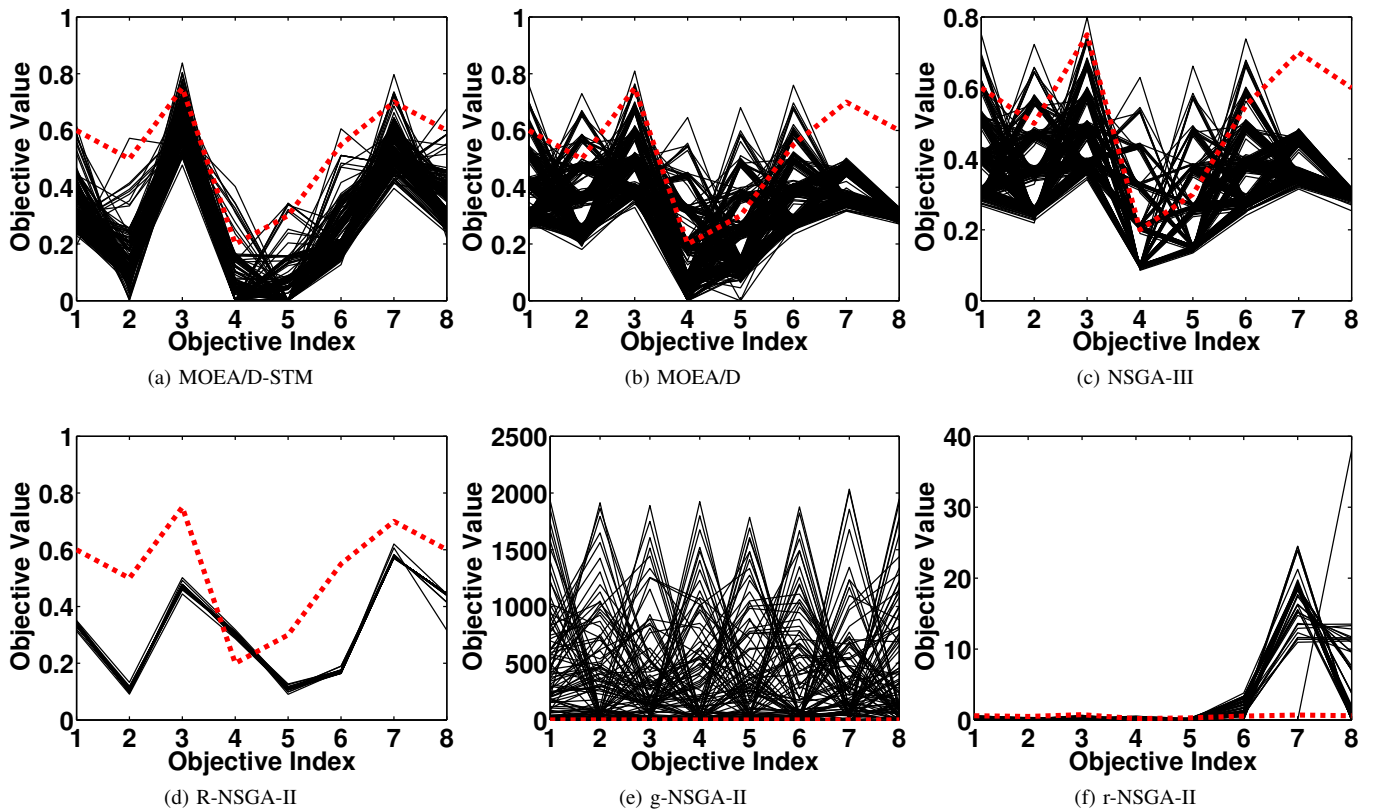
Fig. 31: Comparisons on 8-objective DTLZ3 where $\mathbf{z}^r = (0.6, 0.5, 0.75, 0.2, 0.3, 0.55, 0.7, 0.6)^T$.

(a) MOEA/D-STM

(b) MOEA/D

(c) NSGA-III

(d) R-NSGA-II

(e) g-NSGA-II

(f) r-NSGA-II

Fig. 32: Comparisons on 8-objective DTLZ4 where $\mathbf{z}^r = (0.3, 0.1, 0.4, 0.25, 0.1, 0.15, 0.4, 0.25)^T$.

(a) MOEA/D-STM

(b) MOEA/D

(c) NSGA-III

(d) R-NSGA-II

(e) g-NSGA-II

(f) r-NSGA-II
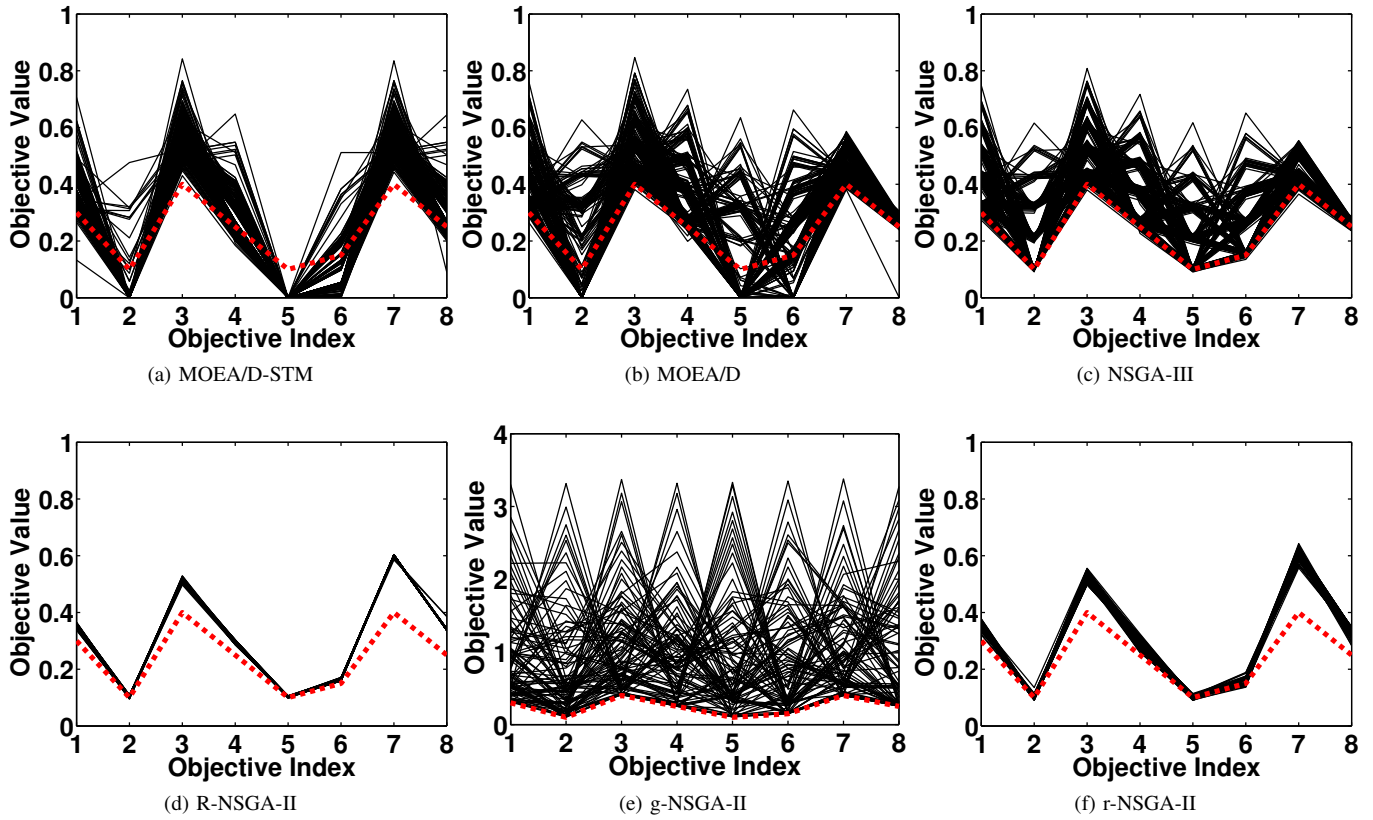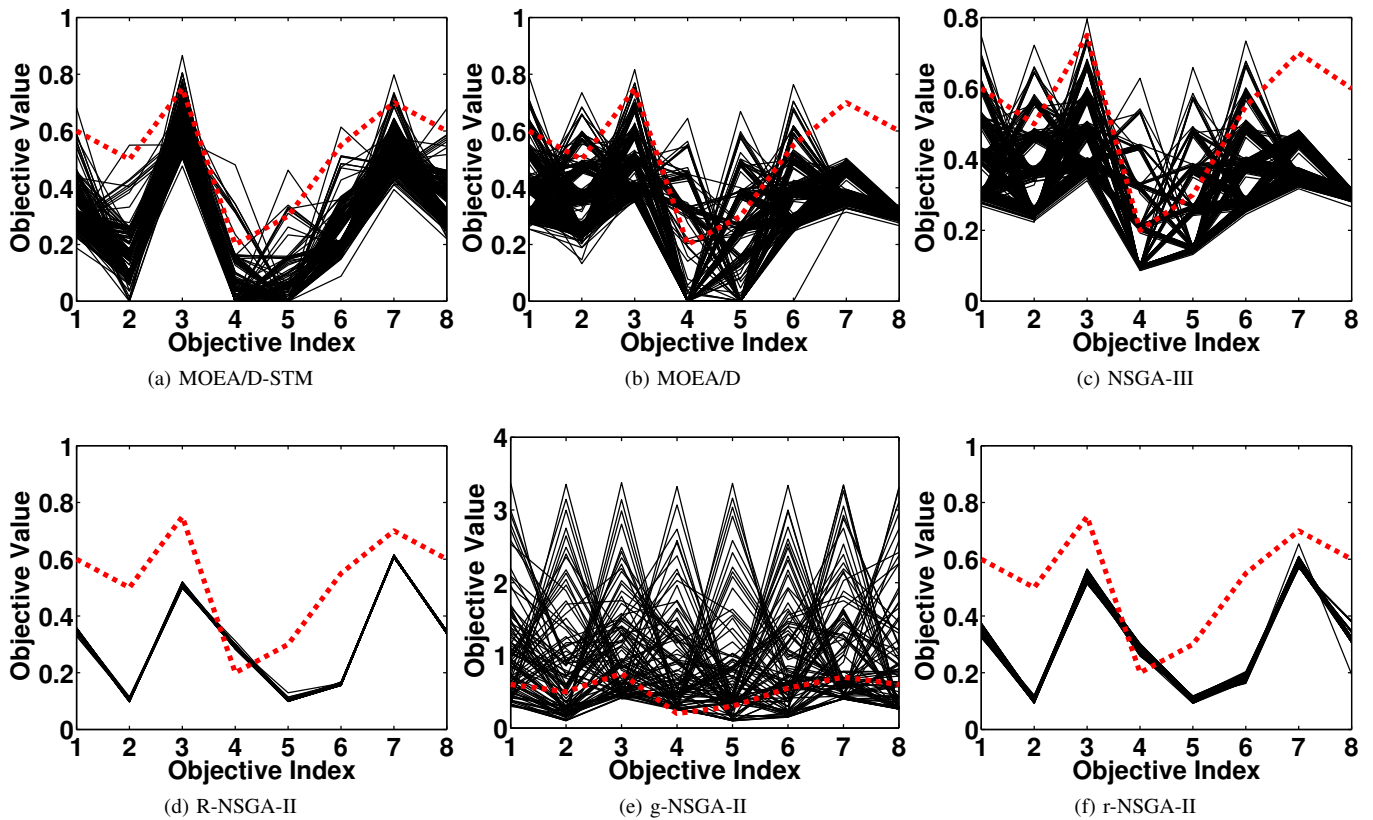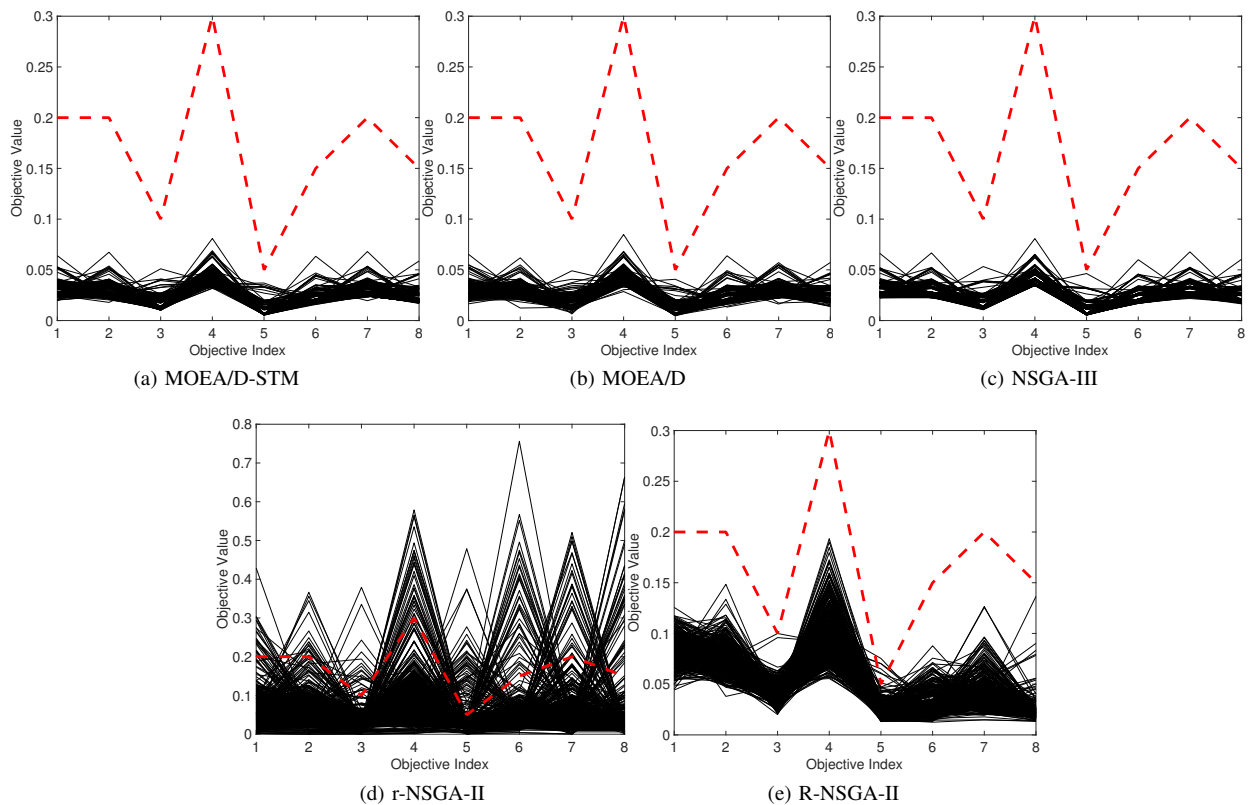
Fig. 33: Comparisons on 8-objective DTLZ4 where $\mathbf{z}^r = (0.6, 0.5, 0.75, 0.2, 0.3, 0.55, 0.7, 0.6)^T$.
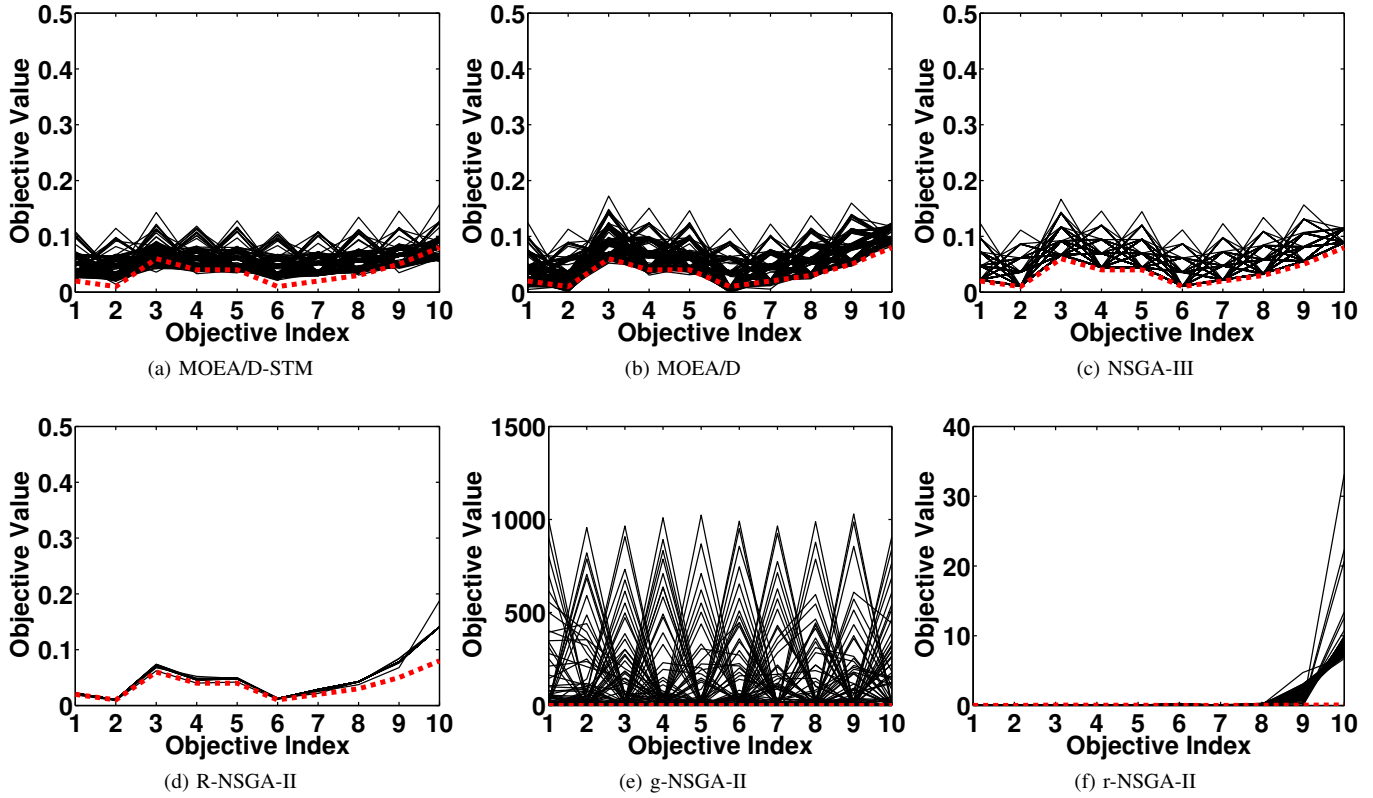
Fig. 34: Comparisons on 10-objective DTLZ1 where $\mathbf{z}^r = (0.02, 0.01, 0.06, 0.04, 0.04, 0.01, 0.02, 0.03, 0.05, 0.08)^T$.
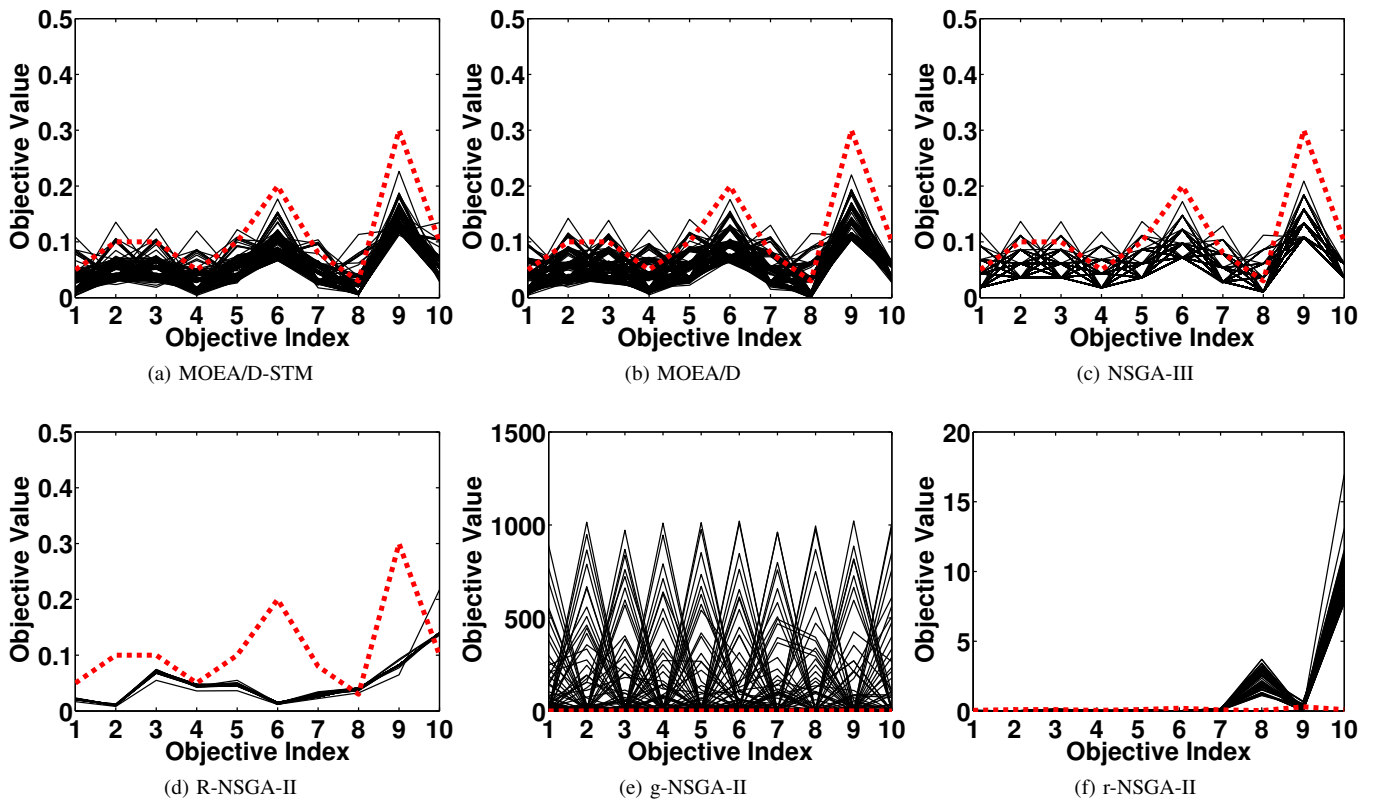
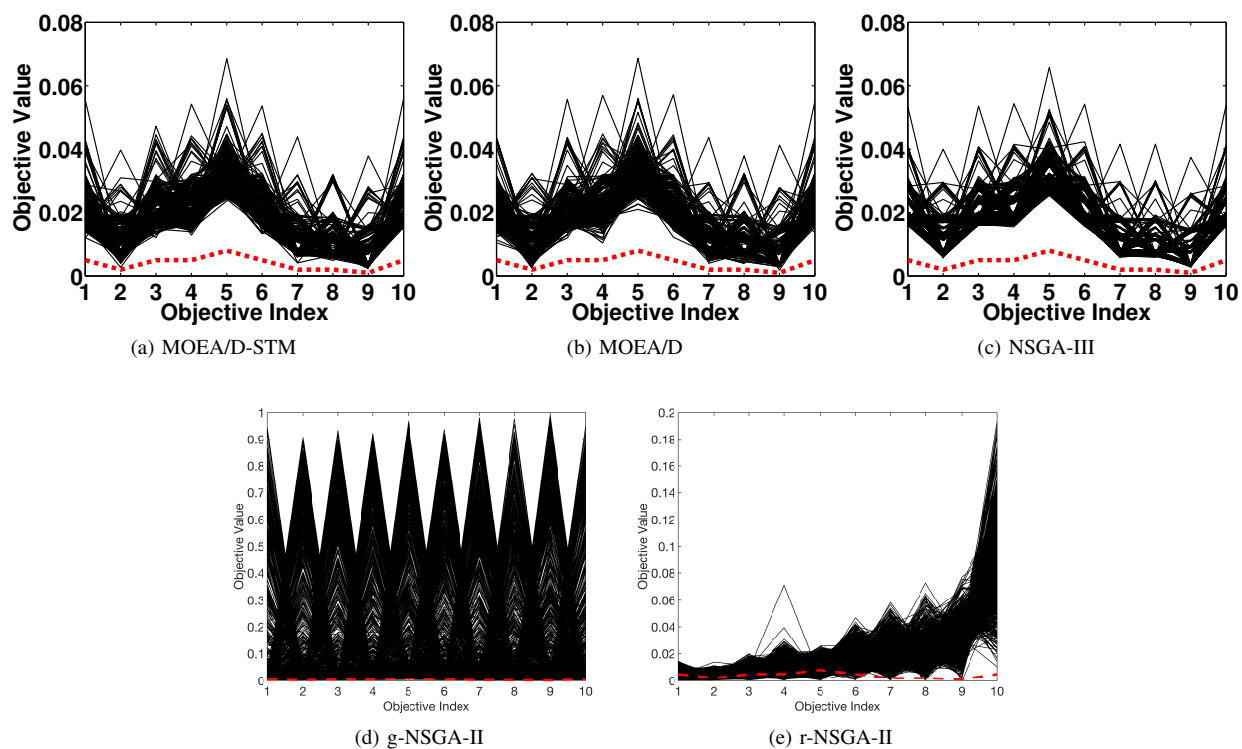Fig. 35: Comparisons on 10-objective DTLZ1 where $\mathbf{z}^r = (0.05, 0.1, 0.1, 0.05, 0.1, 0.2, 0.08, 0.03, 0.3, 0.1)^T$.

(a) MOEA/D-STM

(b) MOEA/D

(c) NSGA-III

(d) R-NSGA-II

(e) r-NSGA-II
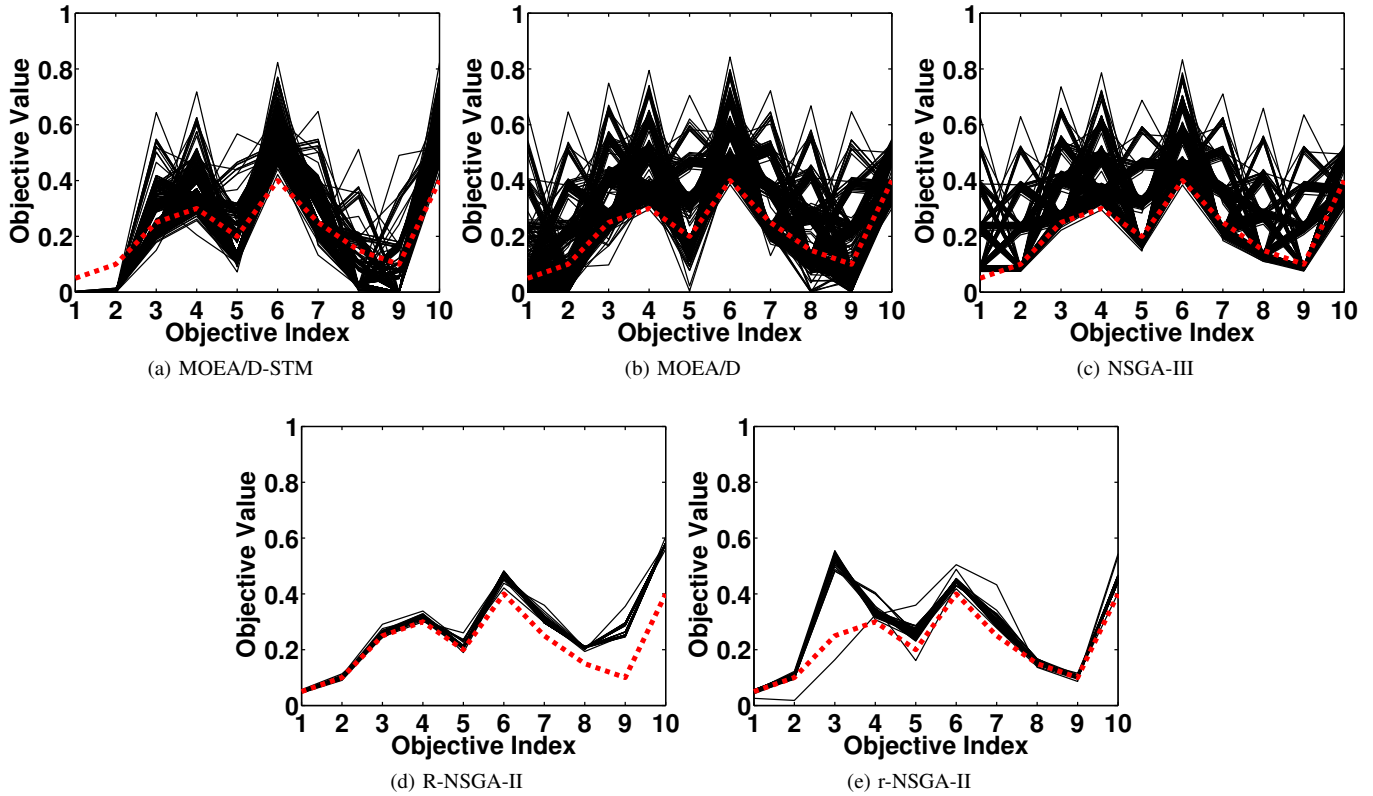
Fig. 36: Comparisons on 10-objective DTLZ2 where $\mathbf{z}^r = (0.05, 0.1, 0.25, 0.3, 0.2, 0.4, 0.25, 0.15, 0.1, 0.4)^T$.

(a) MOEA/D-STM

(b) MOEA/D

(c) NSGA-III

(d) R-NSGA-II

(e) NSGA-III
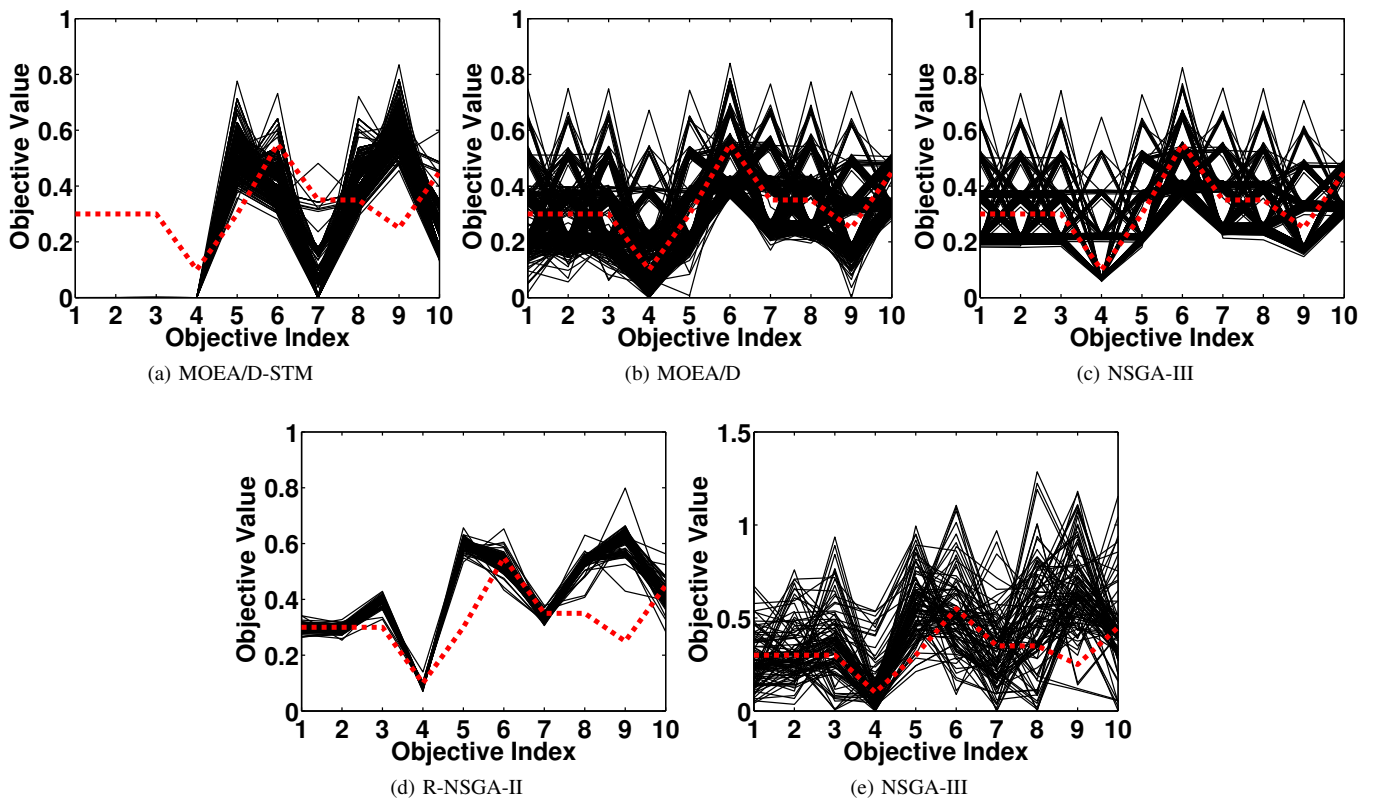
Fig. 37: Comparisons on 10-objective DTLZ2 where $\mathbf{z}^r = (0.3, 0.3, 0.3, 0.1, 0.3, 0.55, 0.35, 0.35, 0.25, 0.45)^T$.

(a) MOEA/D-STM

(b) MOEA/D

(c) NSGA-III

(d) R-NSGA-II

(e) r-NSGA-II
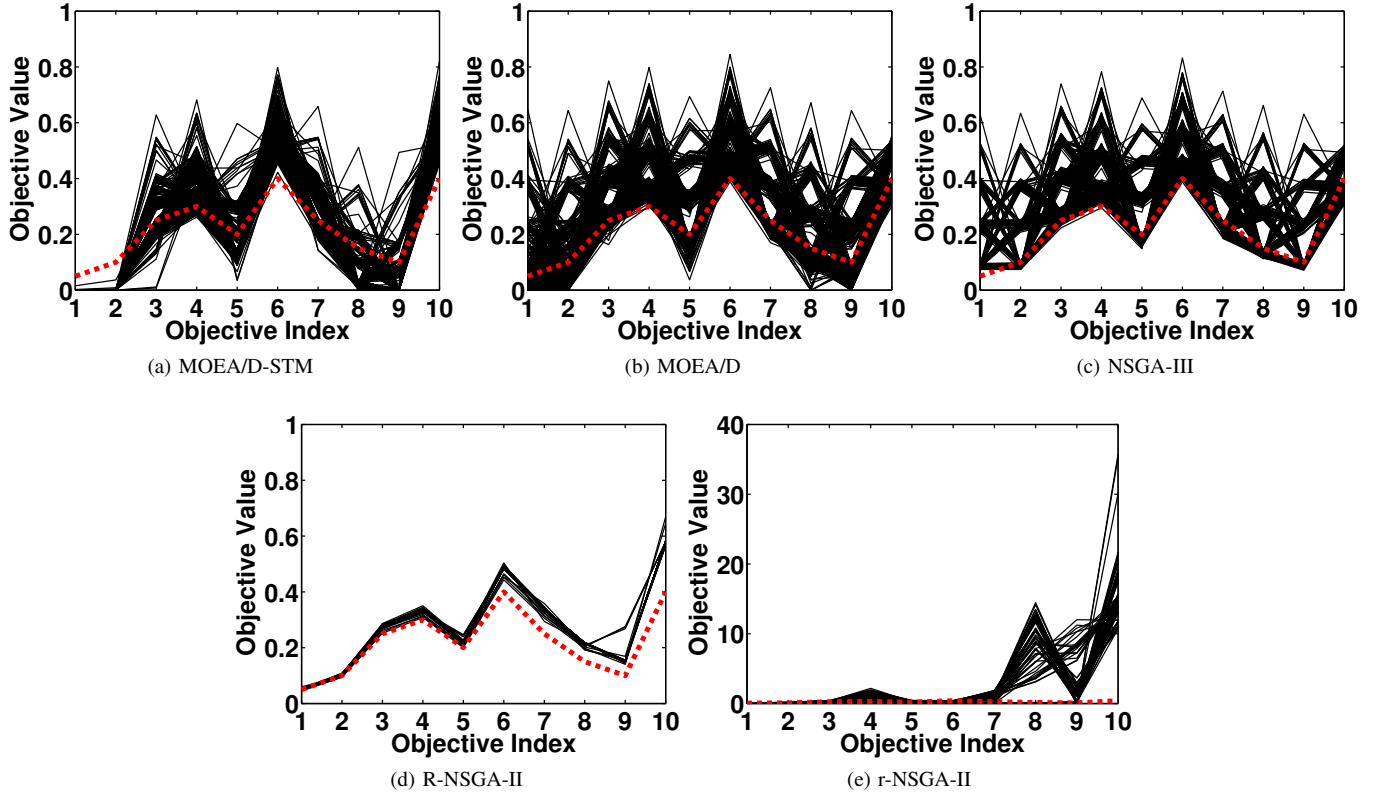
Fig. 38: Comparisons on 10-objective DTLZ3 where $\mathbf{z}^r = (0.05, 0.1, 0.25, 0.3, 0.2, 0.4, 0.25, 0.15, 0.1, 0.4)^T$.

(a) MOEA/D-STM

(b) MOEA/D

(c) NSGA-III

(d) R-NSGA-II

(e) r-NSGA-II
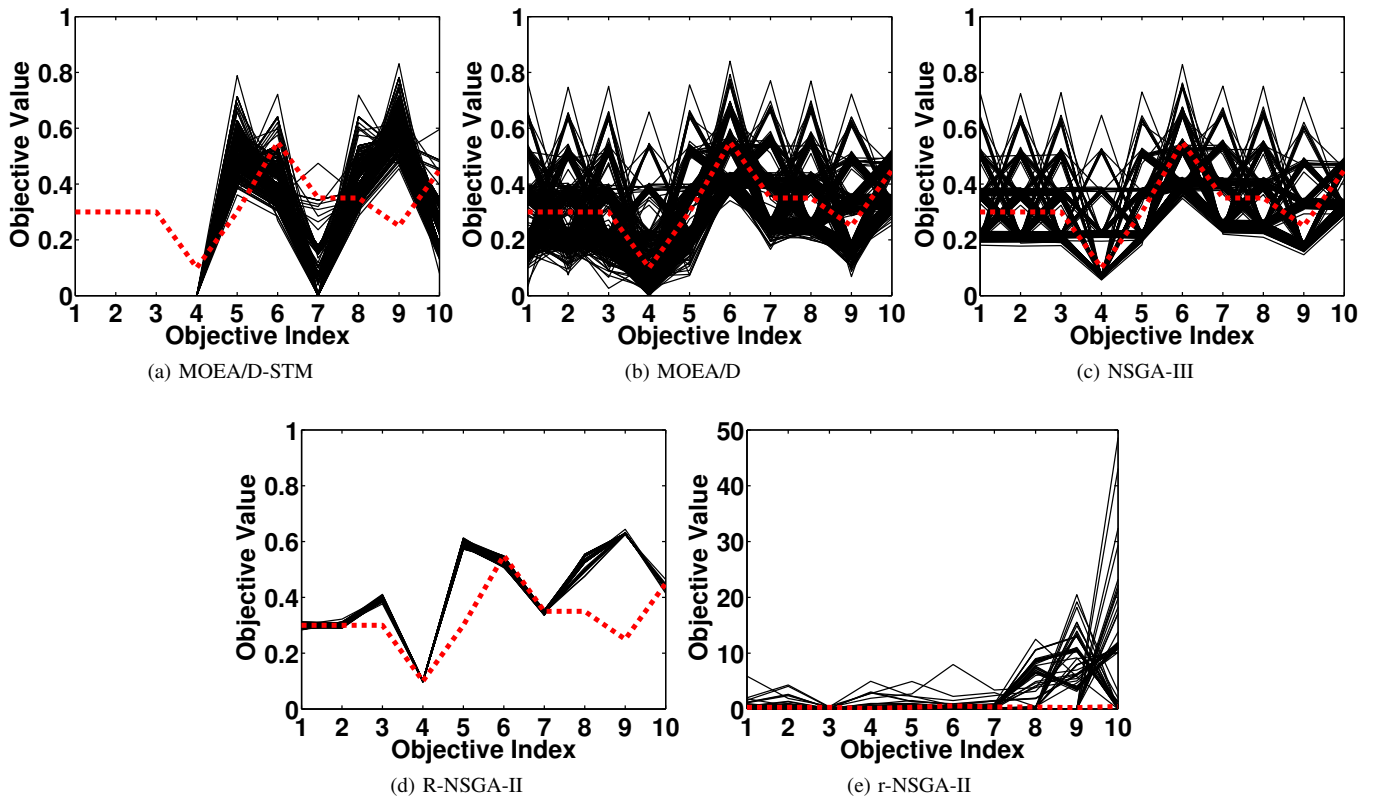
Fig. 39: Comparisons on 10-objective DTLZ3 where $\mathbf{z}^r = (0.3, 0.3, 0.3, 0.1, 0.3, 0.55, 0.35, 0.35, 0.25, 0.45)^T$.
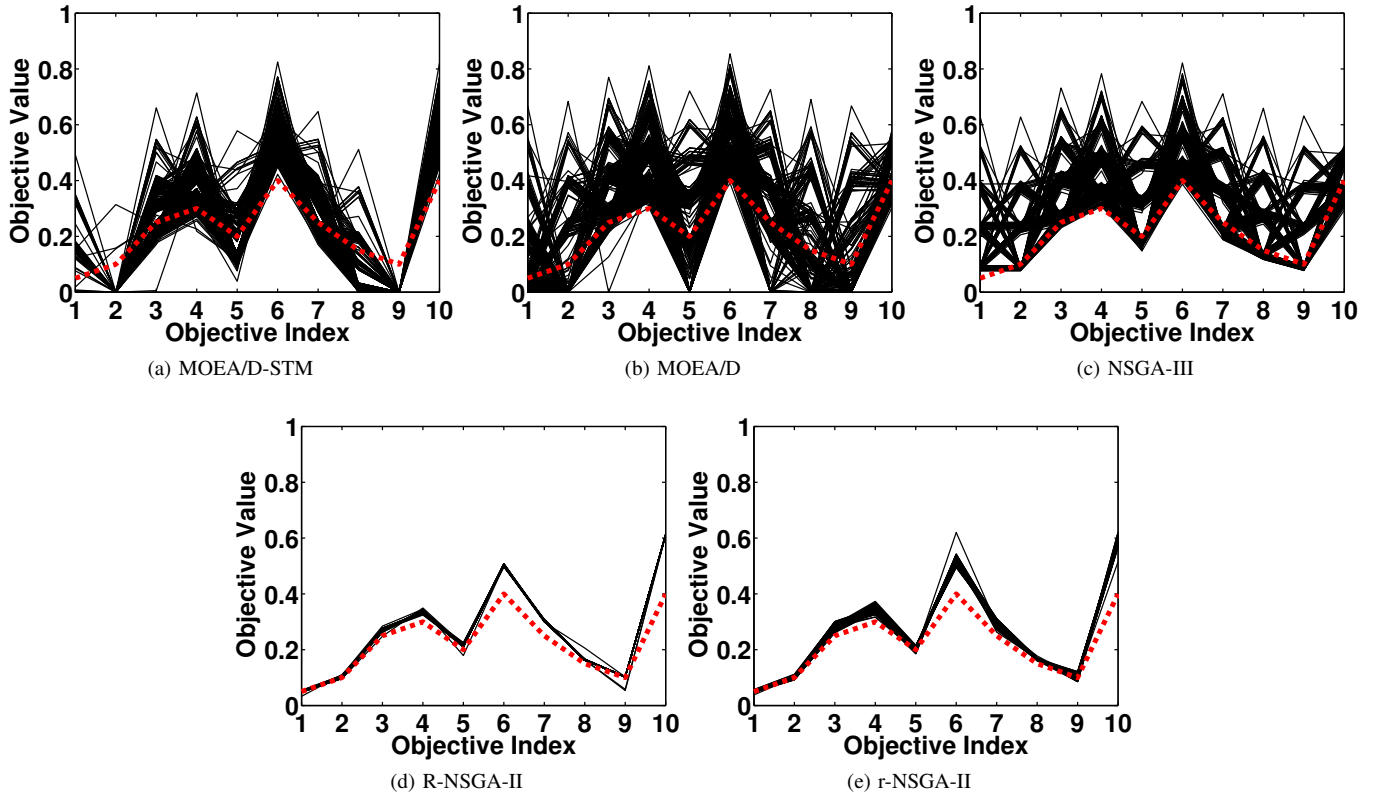
Fig. 40: Comparisons on 10-objective DTLZ4 where $\mathbf{z}^r = (0.05, 0.1, 0.25, 0.3, 0.2, 0.4, 0.25, 0.15, 0.1, 0.4)^T$.
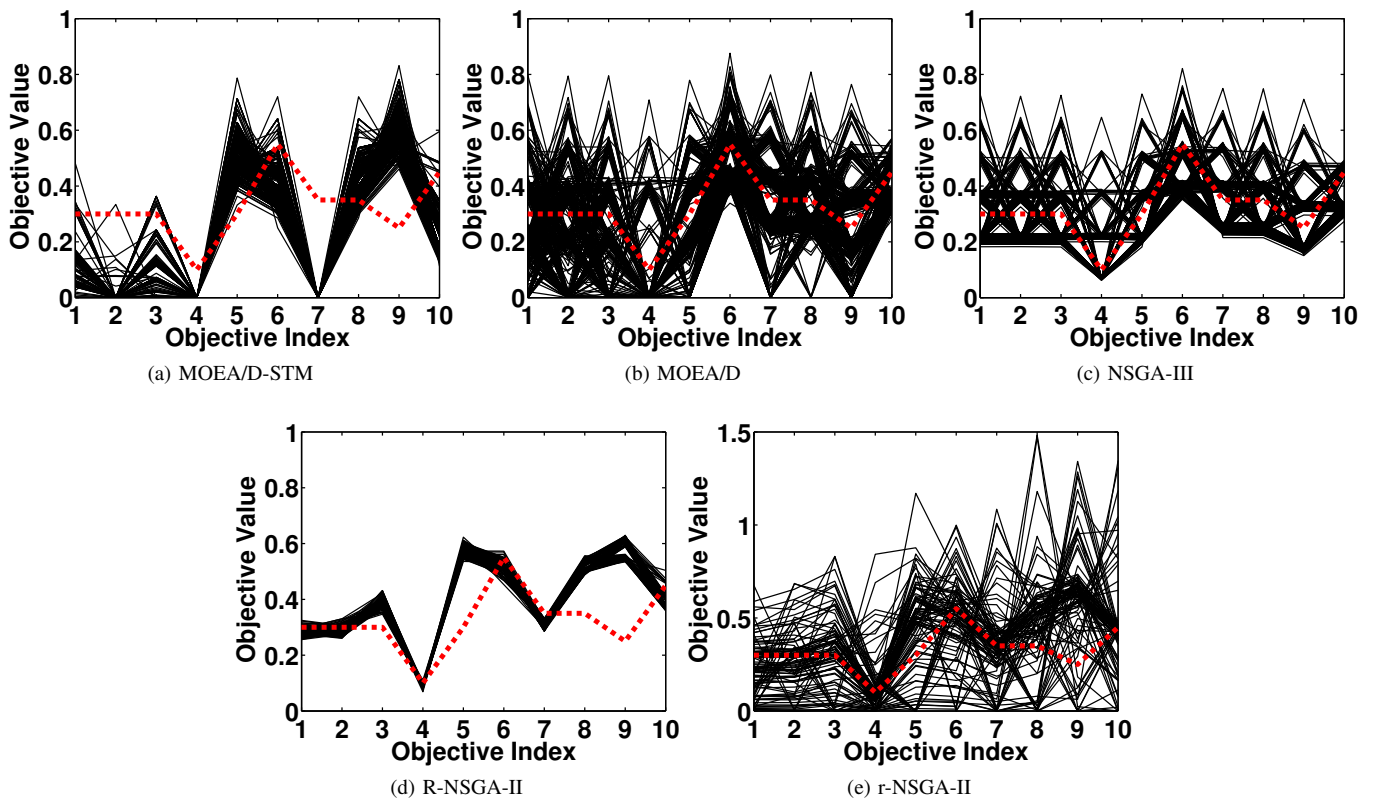
Fig. 41: Comparisons on 10-objective DTLZ4 where $\mathbf{z}^r = (0.3, 0.3, 0.3, 0.1, 0.3, 0.55, 0.35, 0.35, 0.25, 0.45)^T$.
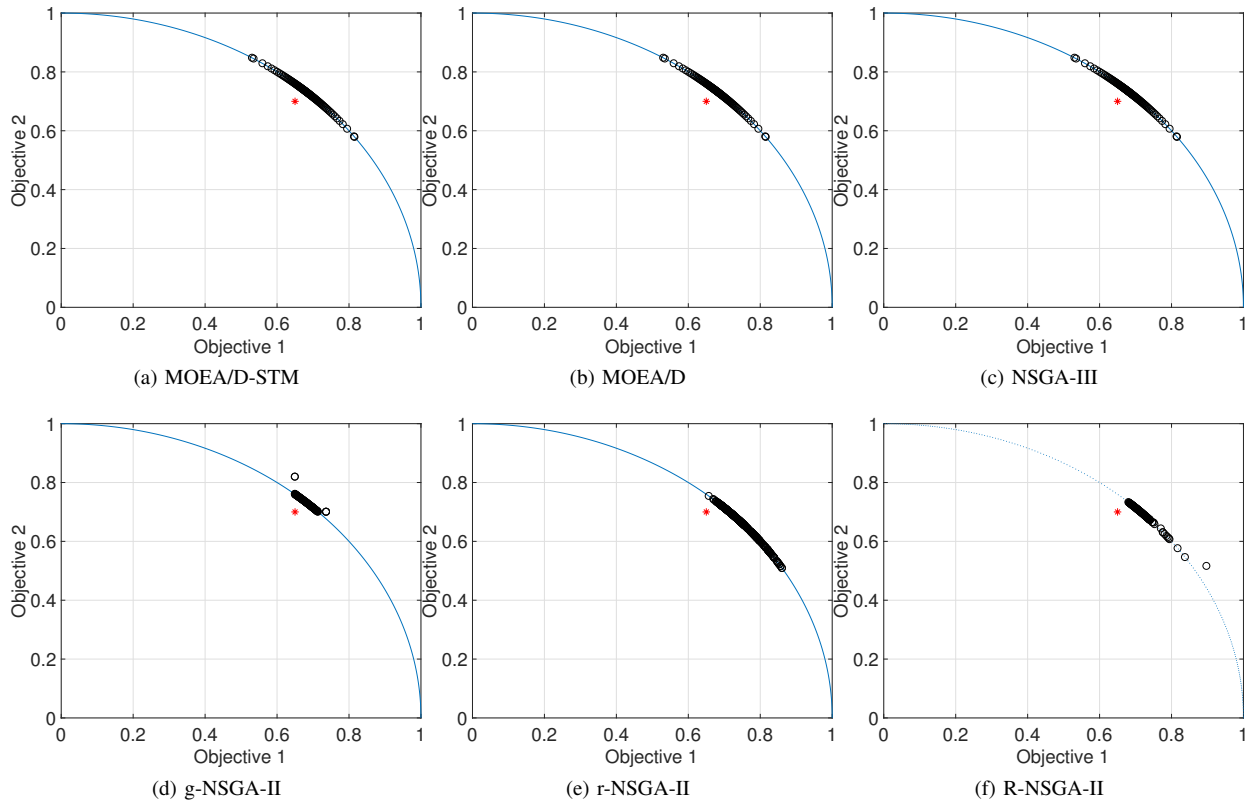
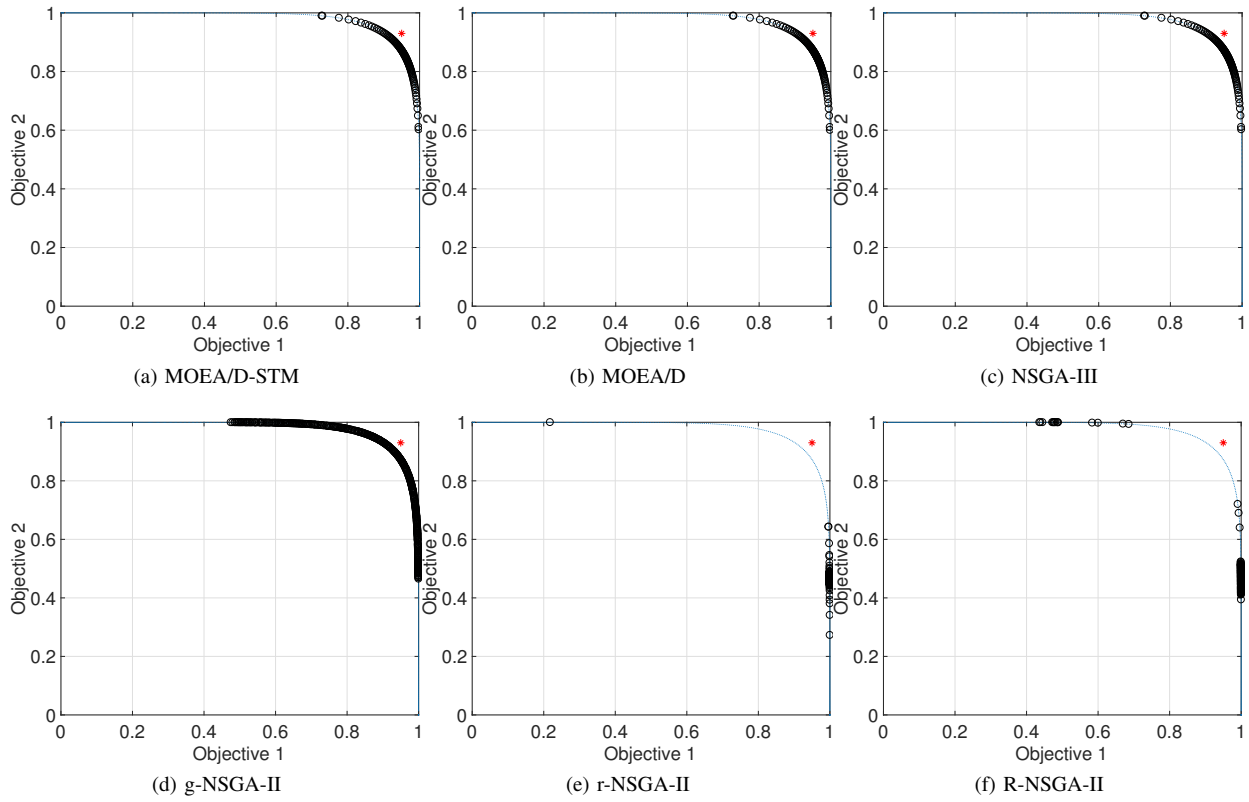Fig. 42: Comparisons on 2-objective WFG41 where $\mathbf{z}^r = (0.65, 0.7)^T$.
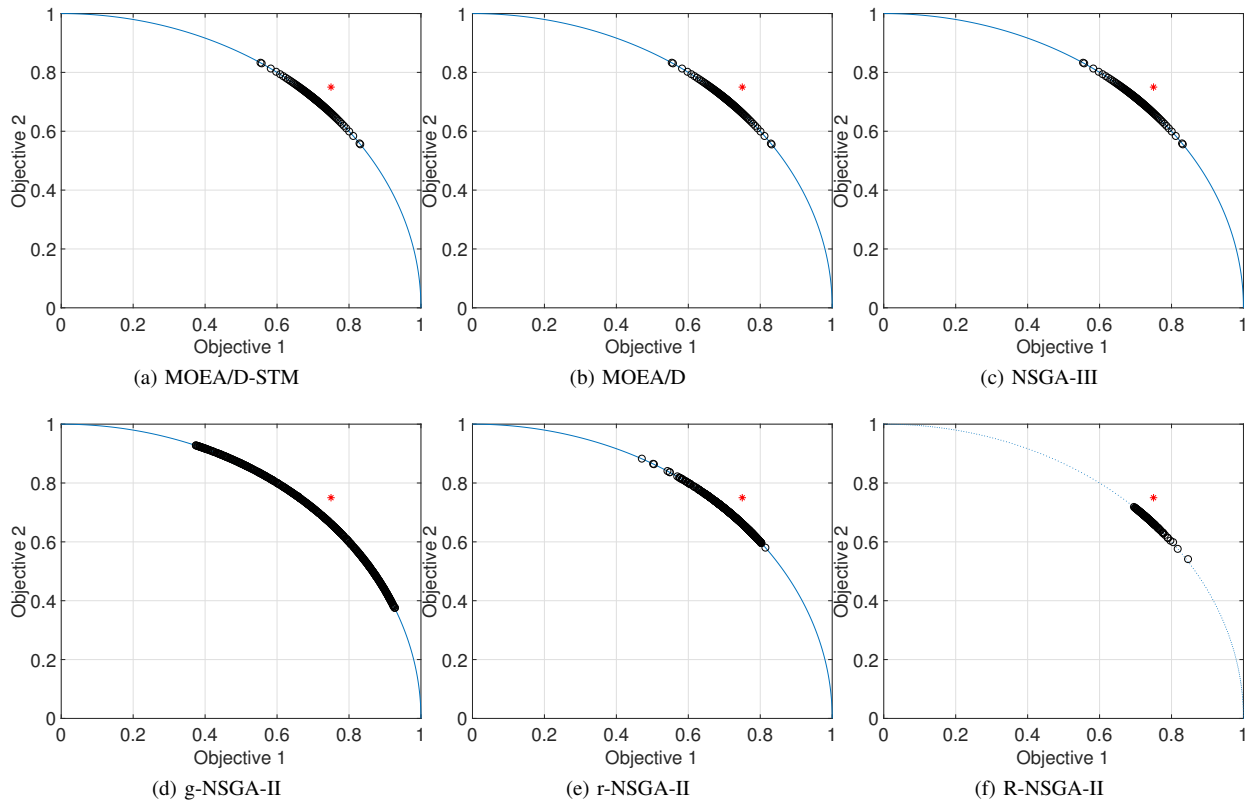
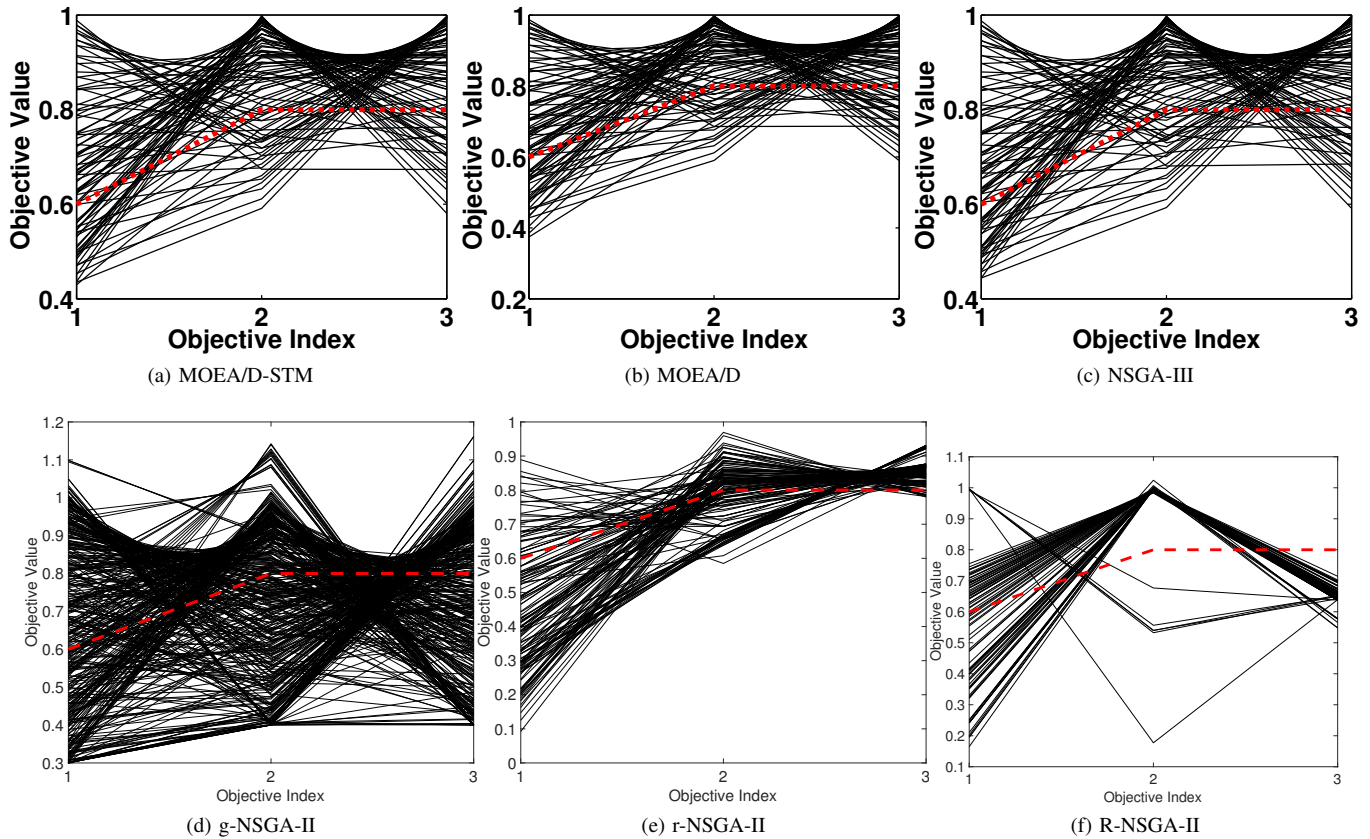Fig. 43: Comparisons on 2-objective WFG41 where $\mathbf{z}^r = (0.75, 0.75)^T$.
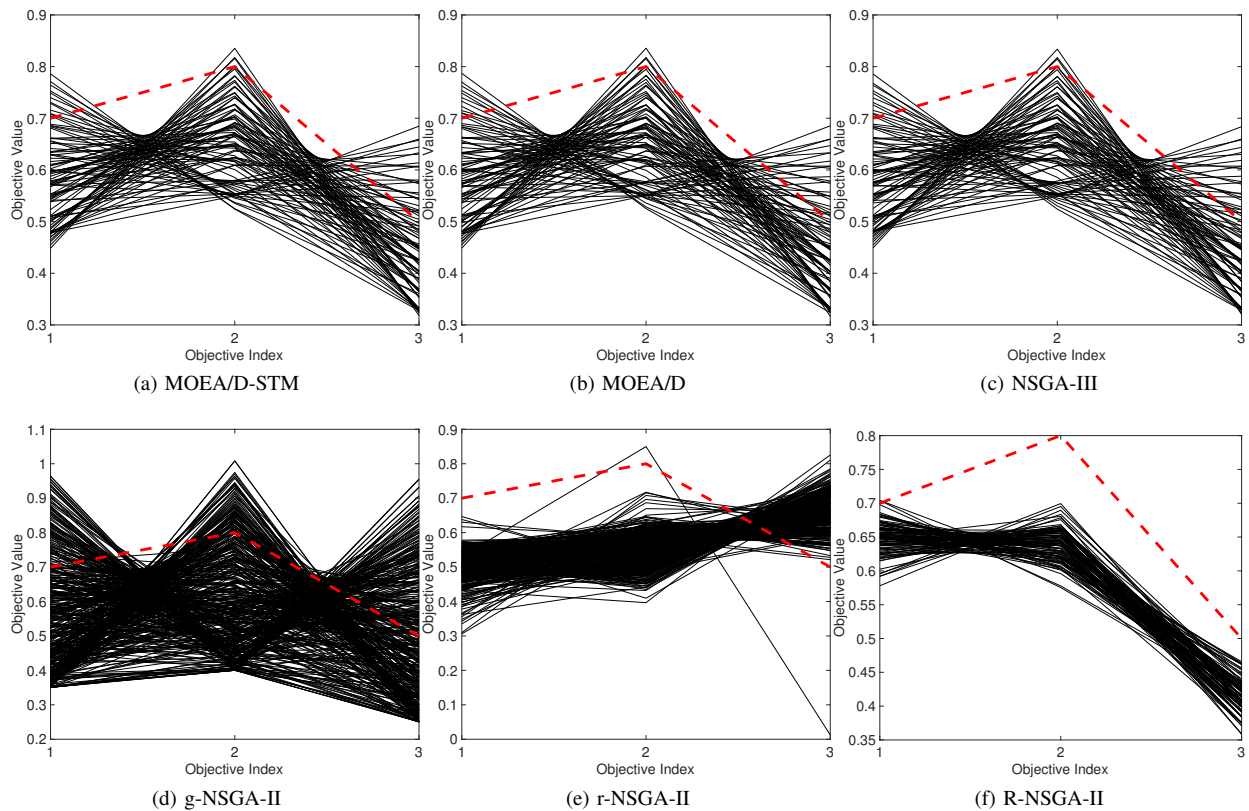
(a) MOEA/D-STM

(b) MOEA/D

(c) NSGA-III

(d) g-NSGA-II

(e) r-NSGA-II

(f) R-NSGA-II

Fig. 44: Comparisons on 3-objective WFG41 where $\mathbf{z}^r = (0.2, 0.5, 0.6)^T$.

(a) MOEA/D-STM

(b) MOEA/D

(c) NSGA-III

(d) g-NSGA-II

(e) r-NSGA-II

(f) R-NSGA-II

Fig. 45: Comparisons on 3-objective WFG41 where $\mathbf{z}^r = (0.7, 0.8, 0.5)^T$.

(a) MOEA/D-STM   (b) MOEA/D   (c) NSGA-III

(d) g-NSGA-II   (e) r-NSGA-II   (f) R-NSGA-II

Fig. 46: Comparisons on 5-objective WFG41 where $\mathbf{z}^r = (0.3, 0.1, 0.4, 0.2, 0.3)^T$.

(a) MOEA/D-STM   (b) MOEA/D   (c) NSGA-III

(d) g-NSGA-II   (e) r-NSGA-II   (f) R-NSGA-II
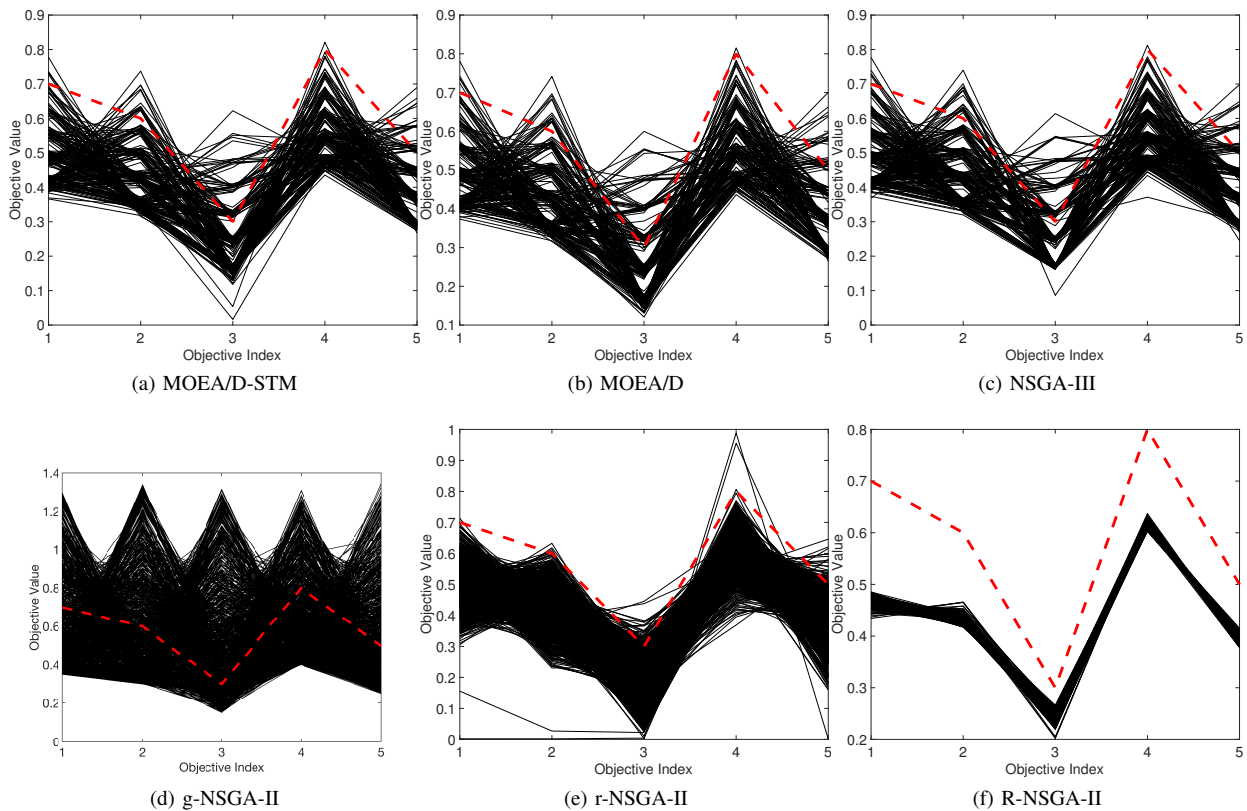
Fig. 47: Comparisons on 5-objective WFG41 where $\mathbf{z}^r = (0.7, 0.6, 0.3, 0.8, 0.5)^T$.
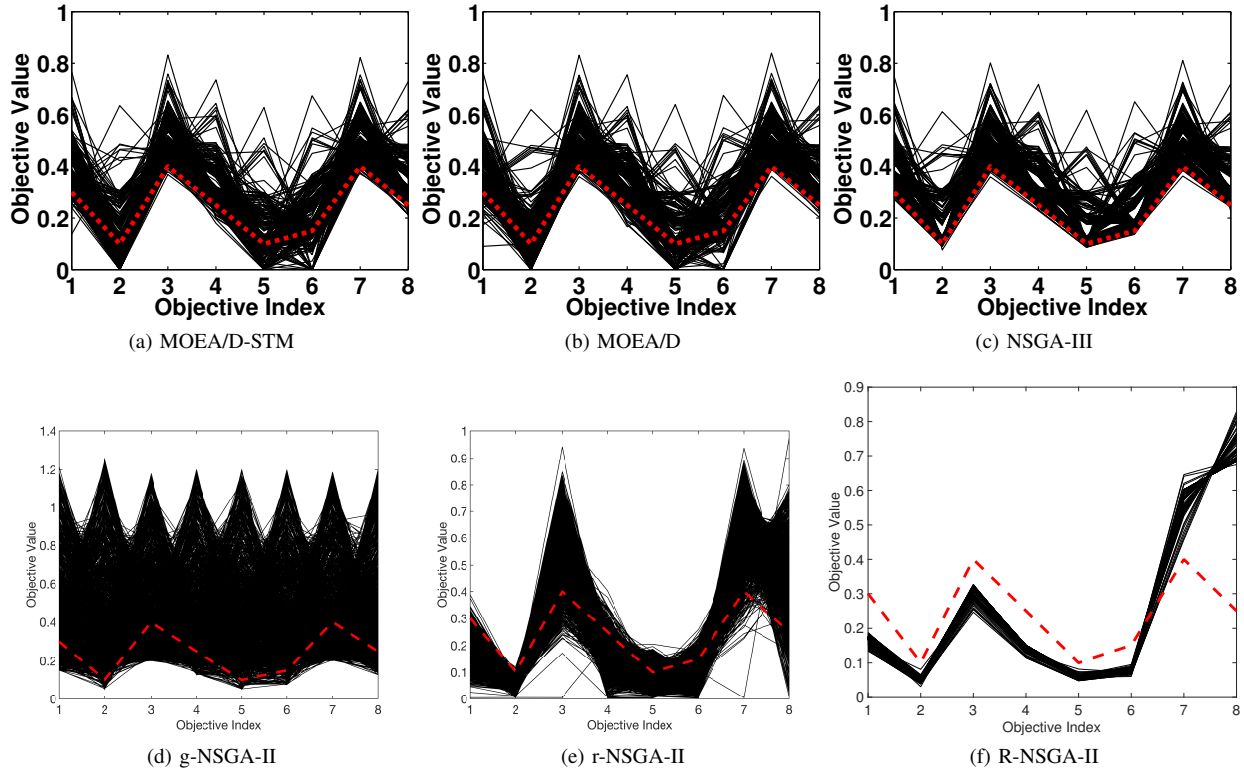
Fig. 48: Comparisons on 8-objective WFG41 where $\mathbf{z}^r = (0.3, 0.1, 0.4, 0.25, 0.1, 0.15, 0.4, 0.25)^T$.
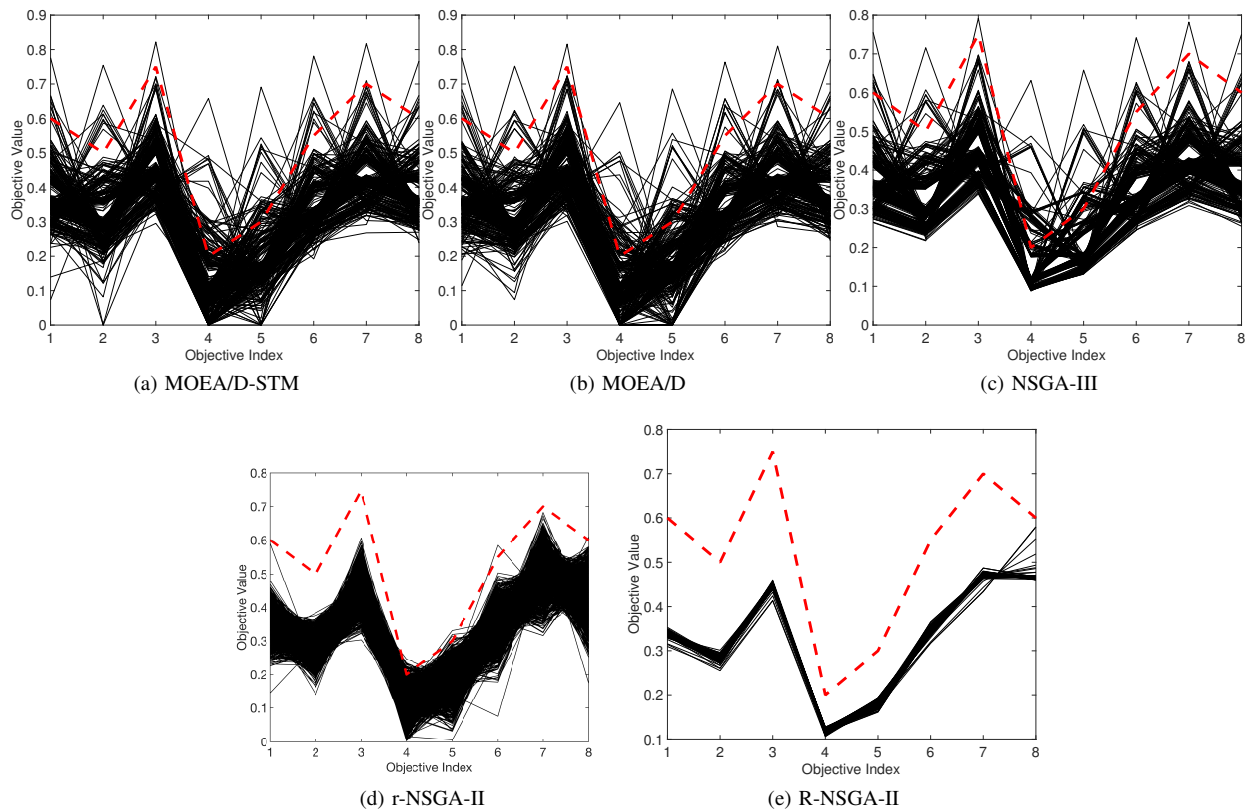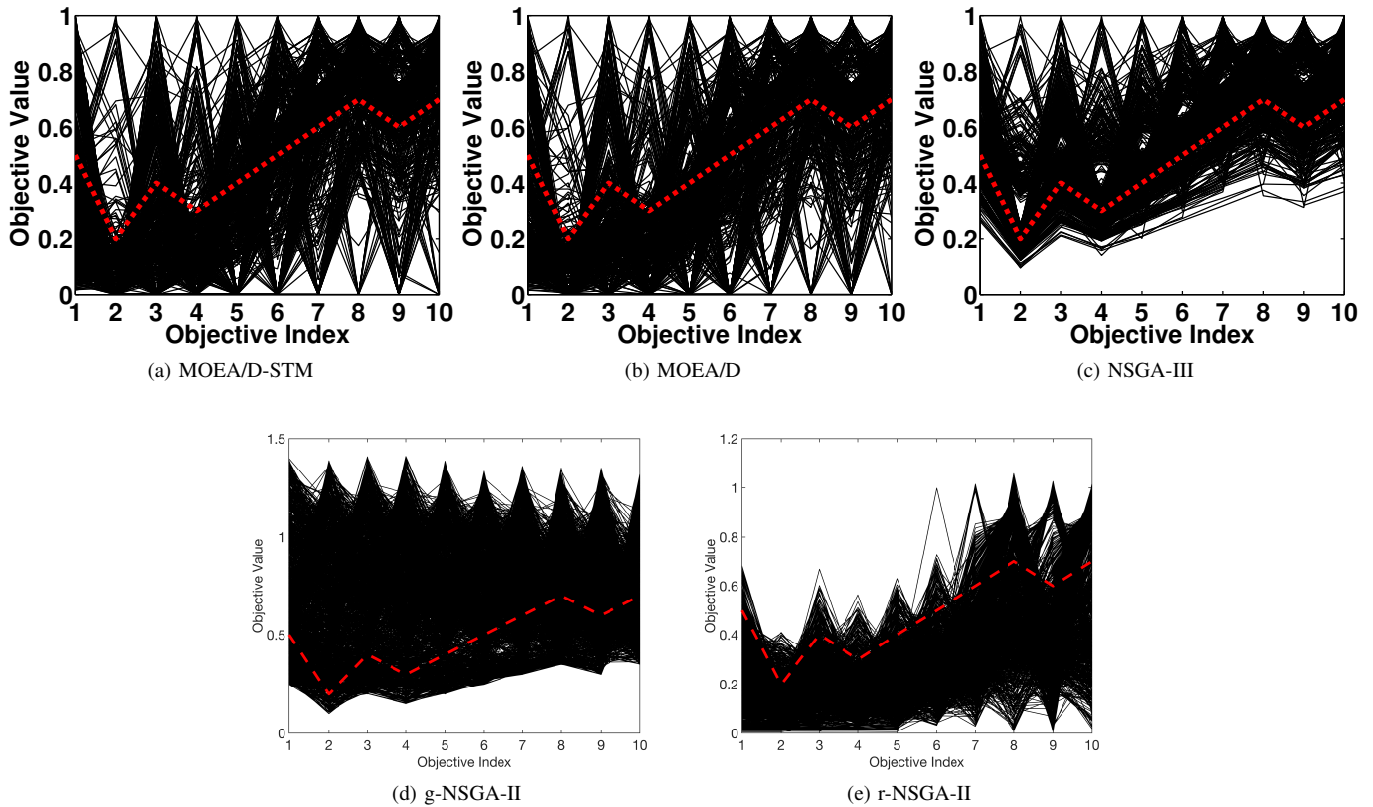

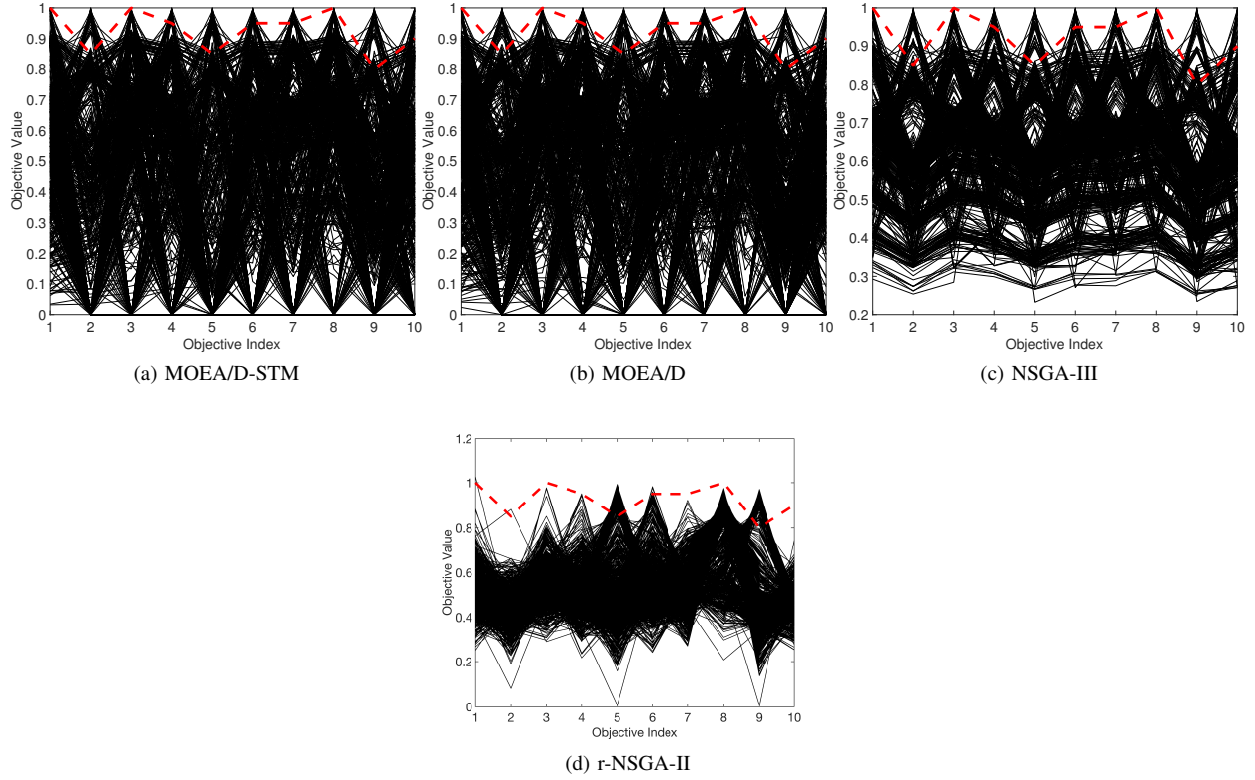Fig. 49: Comparisons on 8-objective WFG41 where $\mathbf{z}^r = (0.6, 0.5, 0.75, 0.2, 0.3, 0.55, 0.7, 0.6)^T$.
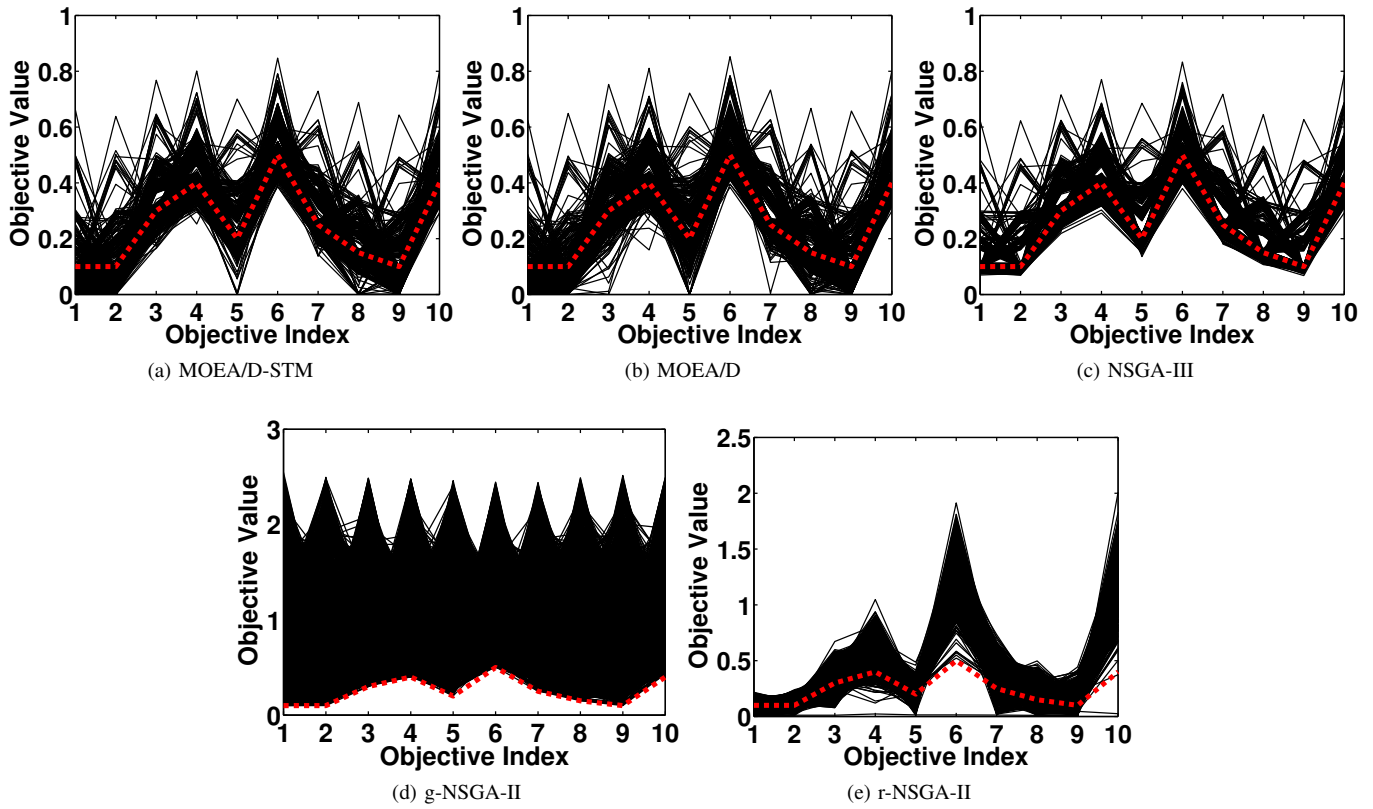
Fig. 50: Comparisons on 10-objective WFG41 where $\mathbf{z}^r = (0.1, 0.1, 0.3, 0.4, 0.2, 0.5, 0.25, 0.15, 0.1, 0.4)^T$.
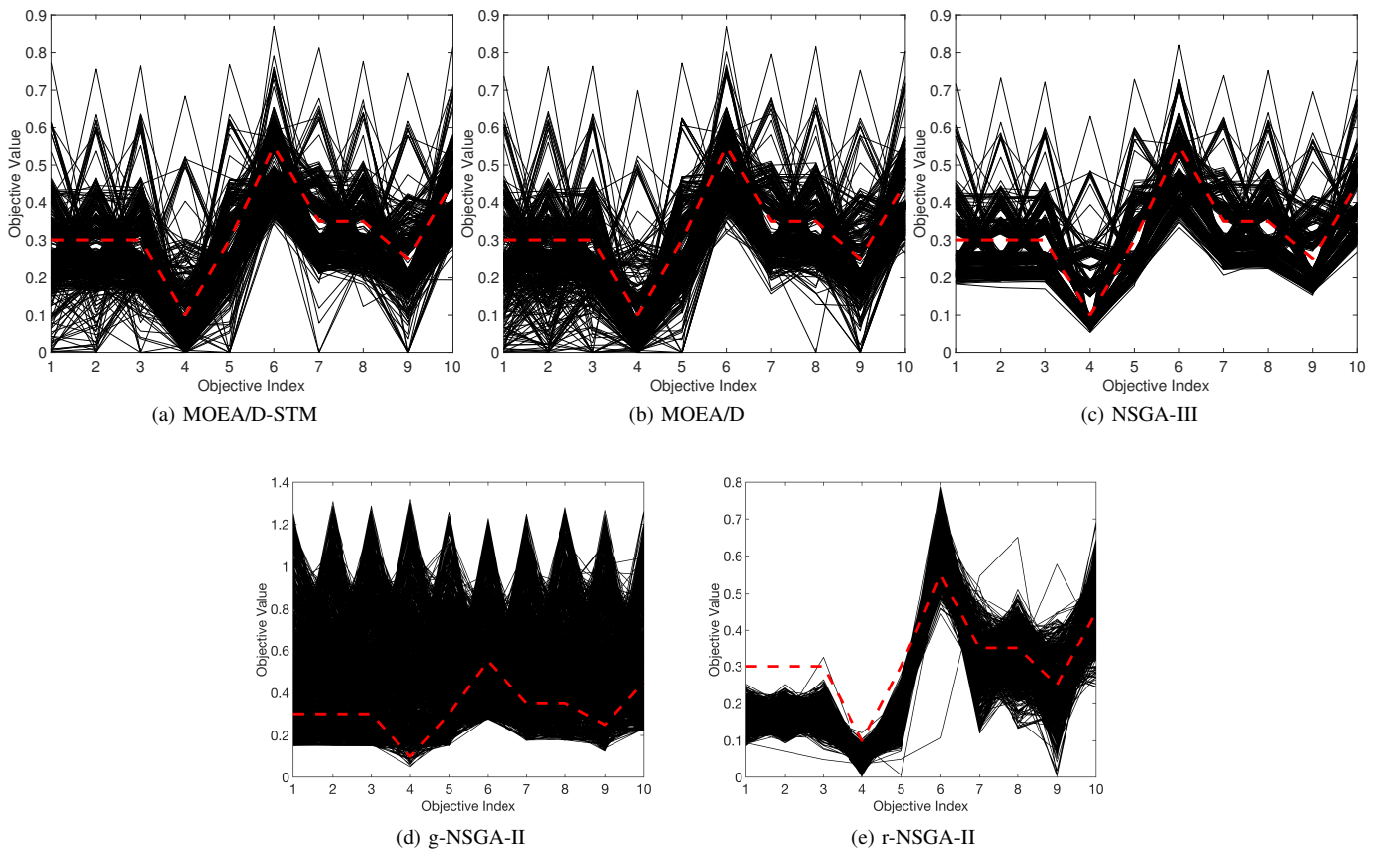
Fig. 51: Comparisons on 10-objective WFG41 where $\mathbf{z}^r = (0.3, 0.3, 0.3, 0.1, 0.3, 0.55, 0.35, 0.35, 0.25, 0.45)^T$.

(a) MOEA/D-STM

(b) MOEA/D

(c) NSGA-III

(d) g-NSGA-II

(e) r-NSGA-II

(f) R-NSGA-II
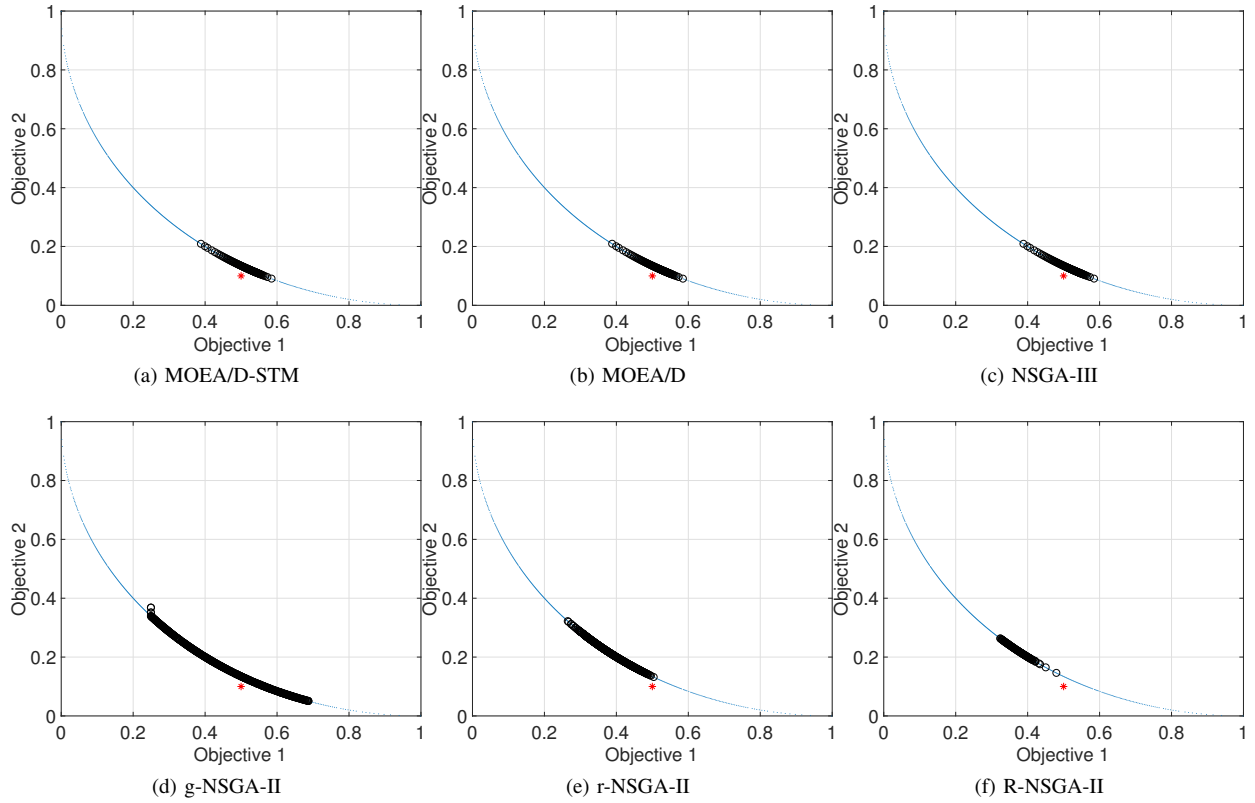
Fig. 52: Comparisons on 2-objective WFG42 where $\mathbf{z}^r = (0.5, 0.1)^T$.

(a) MOEA/D-STM

(b) MOEA/D
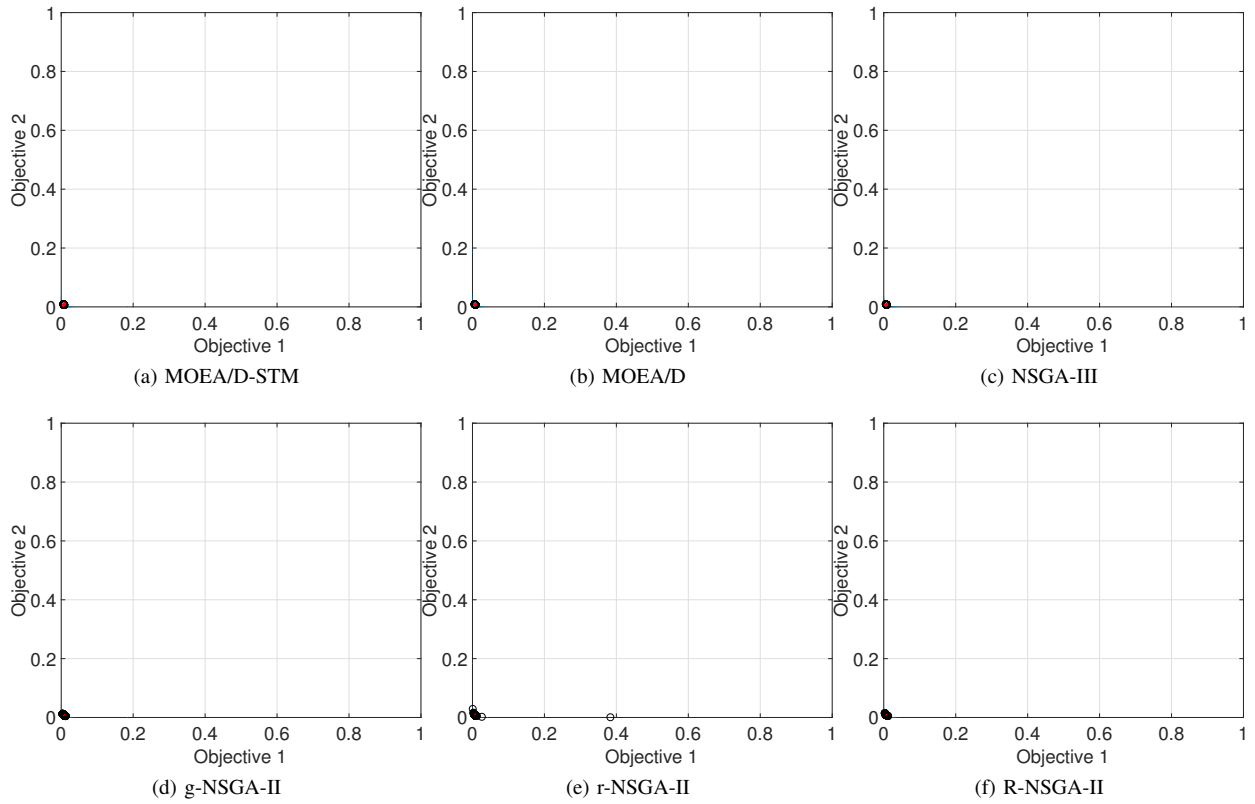
(c) NSGA-III

(d) g-NSGA-II

(e) r-NSGA-II

(f) R-NSGA-II
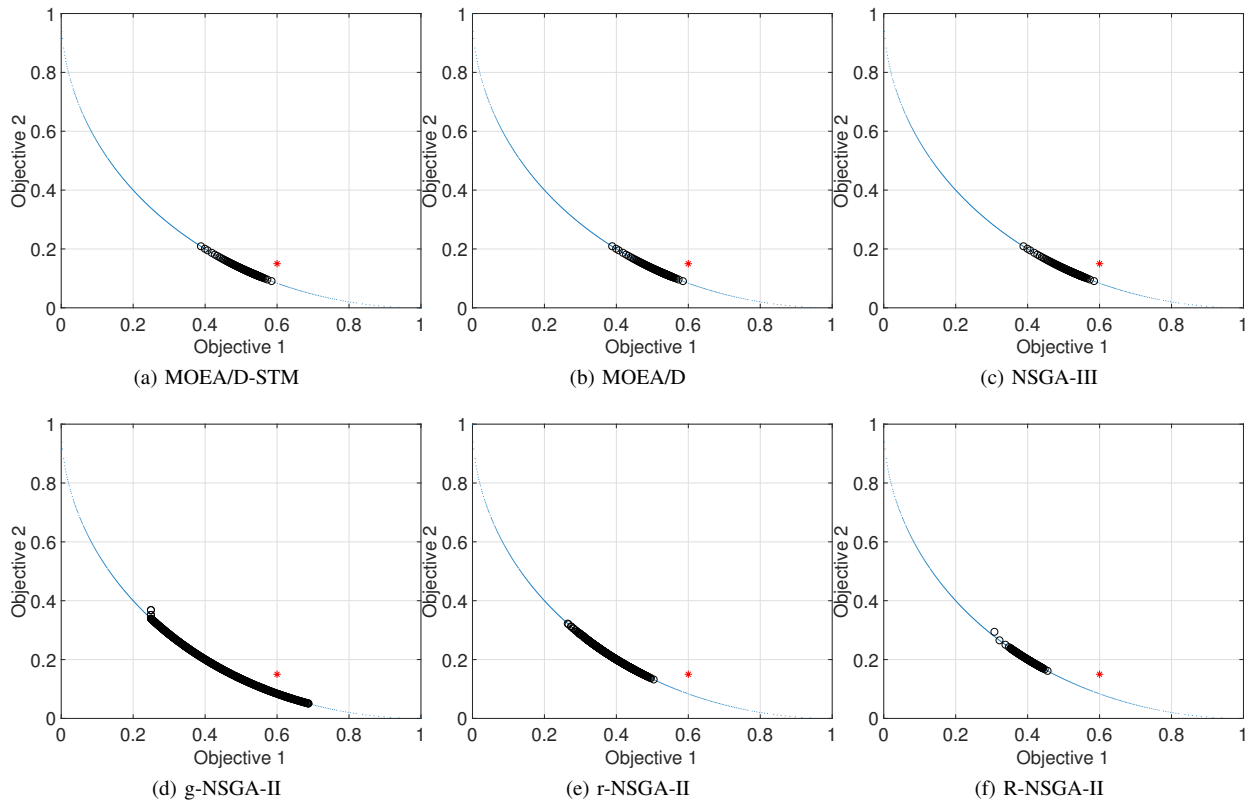
Fig. 53: Comparisons on 2-objective WFG42 where $\mathbf{z}^r = (0.6, 0.15)^T$.

Fig. 54: Comparisons on 3-objective WFG42 where $\mathbf{z}^r = (0.05, 0.05, 0.2)^T$.

Fig. 55: Comparisons on 3-objective WFG42 where $\mathbf{z}^r = (0.15, 0.15, 0.25)^T$.

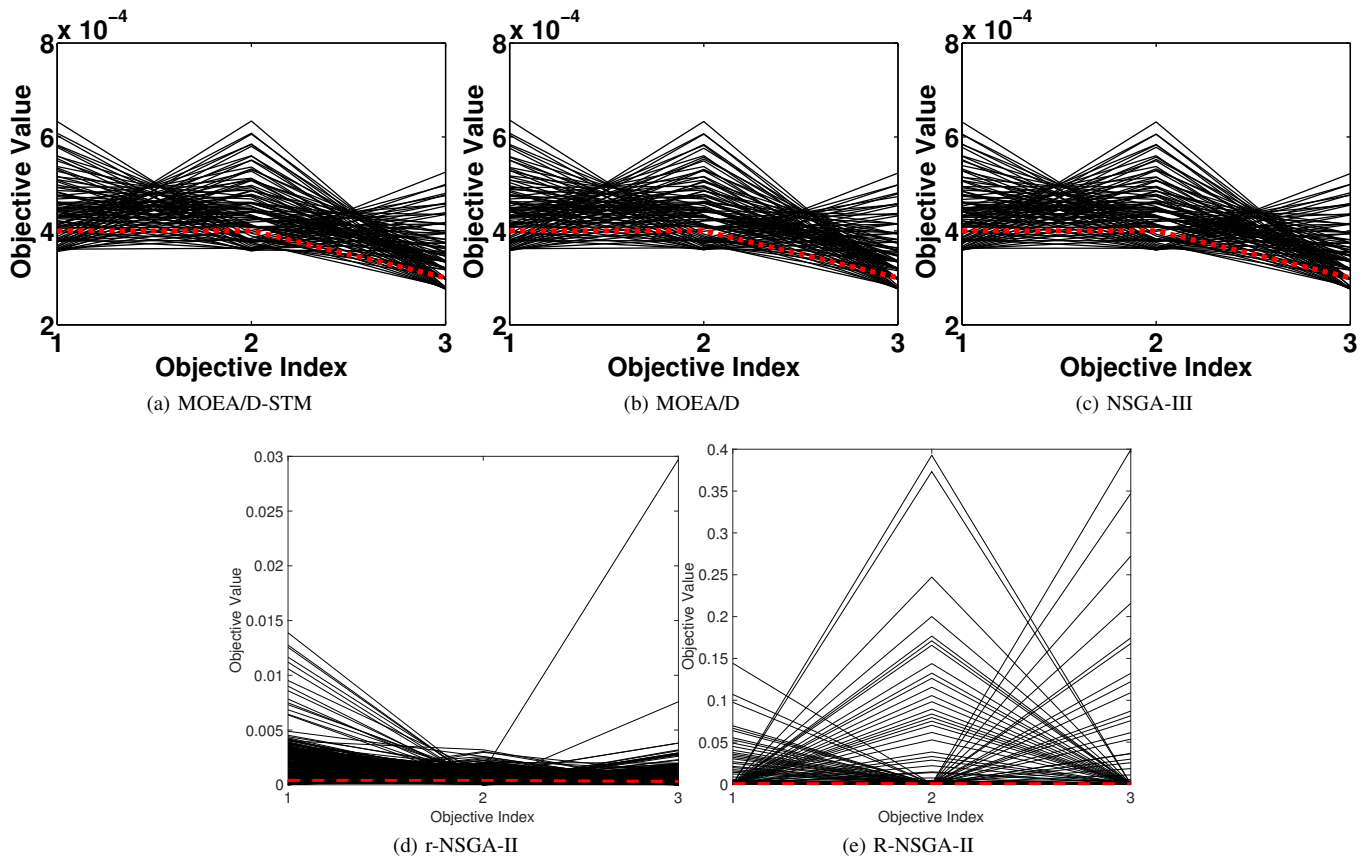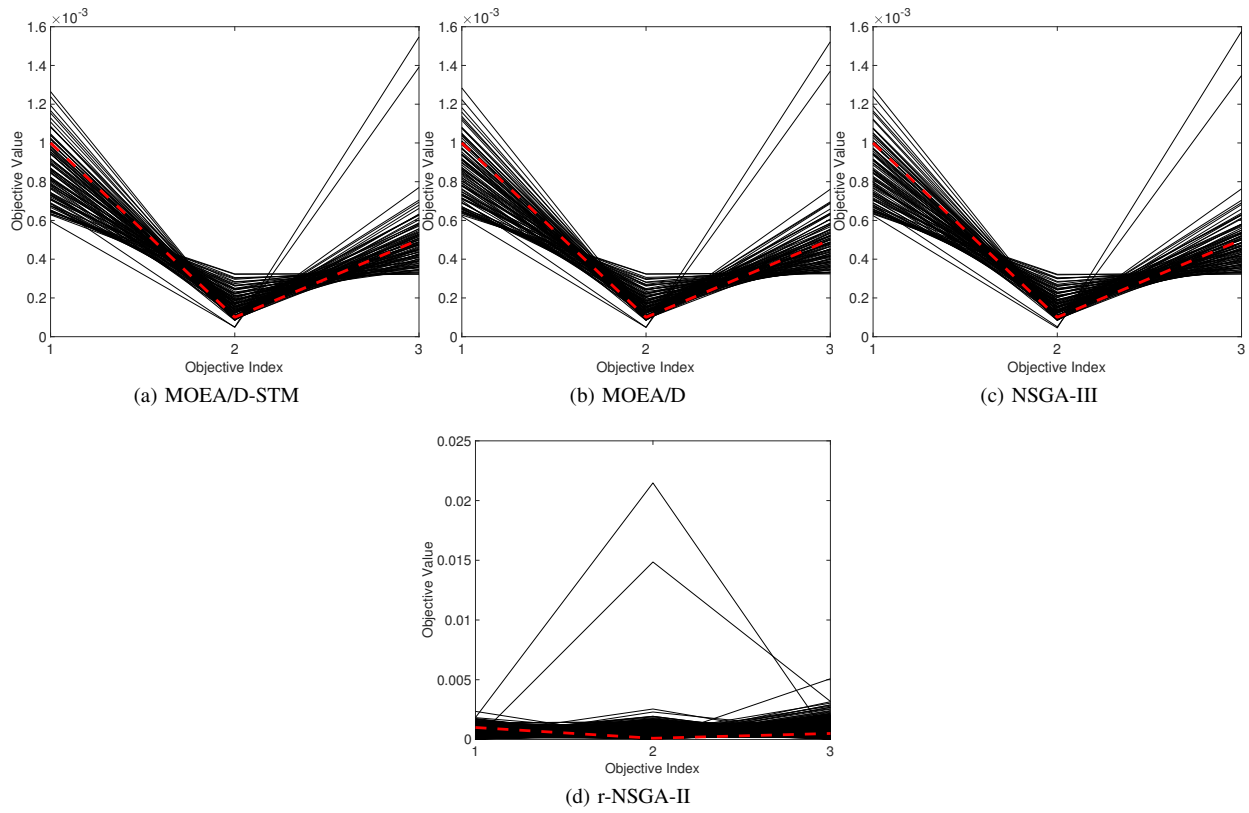Fig. 56: Comparisons on 5-objective WFG42 where $\mathbf{z}^r = (0.03, 0.04, 0.08, 0.04, 0.04)^T$.

Fig. 57: Comparisons on 5-objective WFG42 where $\mathbf{z}^r = (0.1, 0.05, 0.1, 0.05, 0.05)^T$.
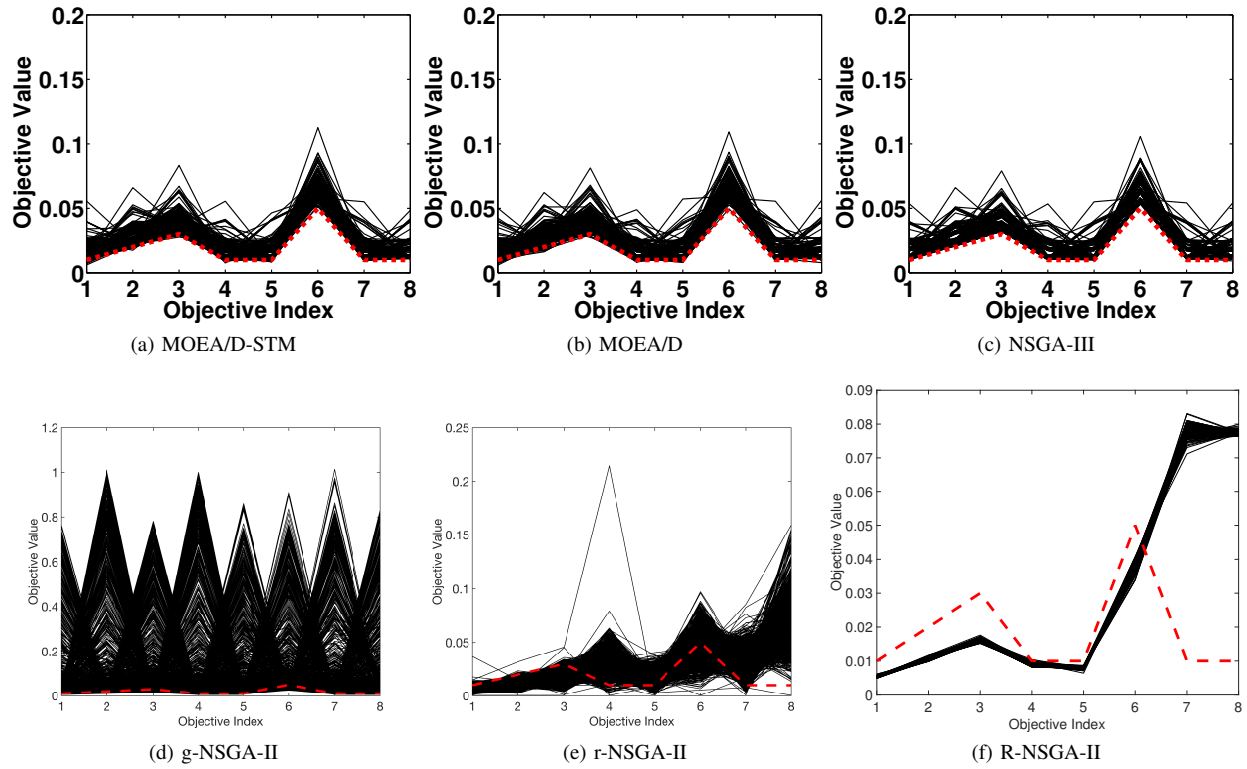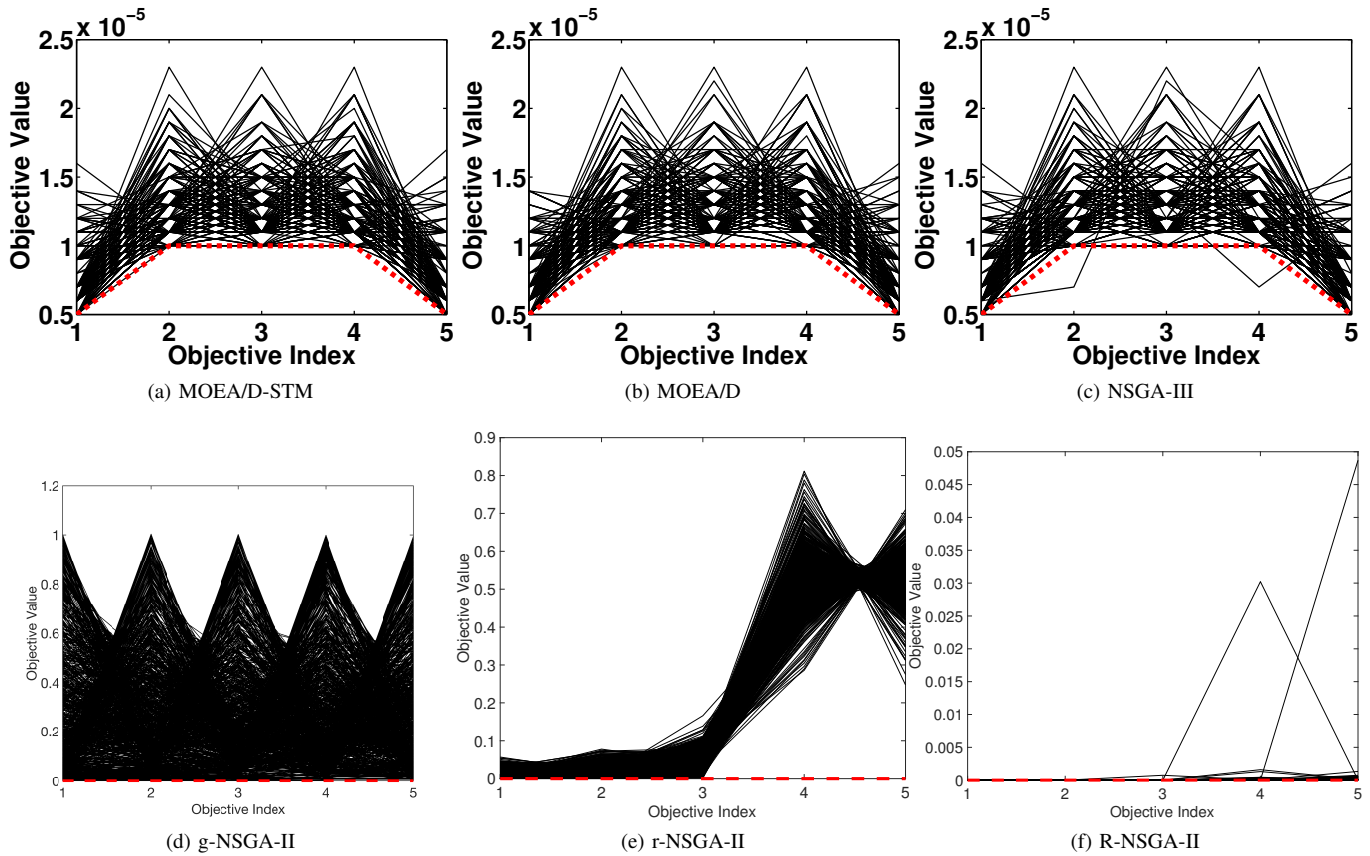
Fig. 58: Comparisons on 8-objective WFG42 where $\mathbf{z}^r = (0.01, 0.02, 0.03, 0.01, 0.01, 0.05, 0.01, 0.01)^T$.

Fig. 59: Comparisons on 8-objective WFG42 where $\mathbf{z}^r = (0.2, 0.2, 0.1, 0.3, 0.05, 0.15, 0.2, 0.15)^T$.

(a) MOEA/D-STM

(b) MOEA/D

(c) NSGA-III

(d) g-NSGA-II

(e) r-NSGA-II

Fig. 60: Comparisons on 10-objective WFG42 where $\mathbf{z}^r = (0.005, 0.002, 0.005, 0.005, 0.008, 0.005, 0.002, 0.002, 0.001, 0.005)^T$.

(a) MOEA/D-STM

(b) MOEA/D

(c) NSGA-III

(d) g-NSGA-II

(e) r-NSGA-II
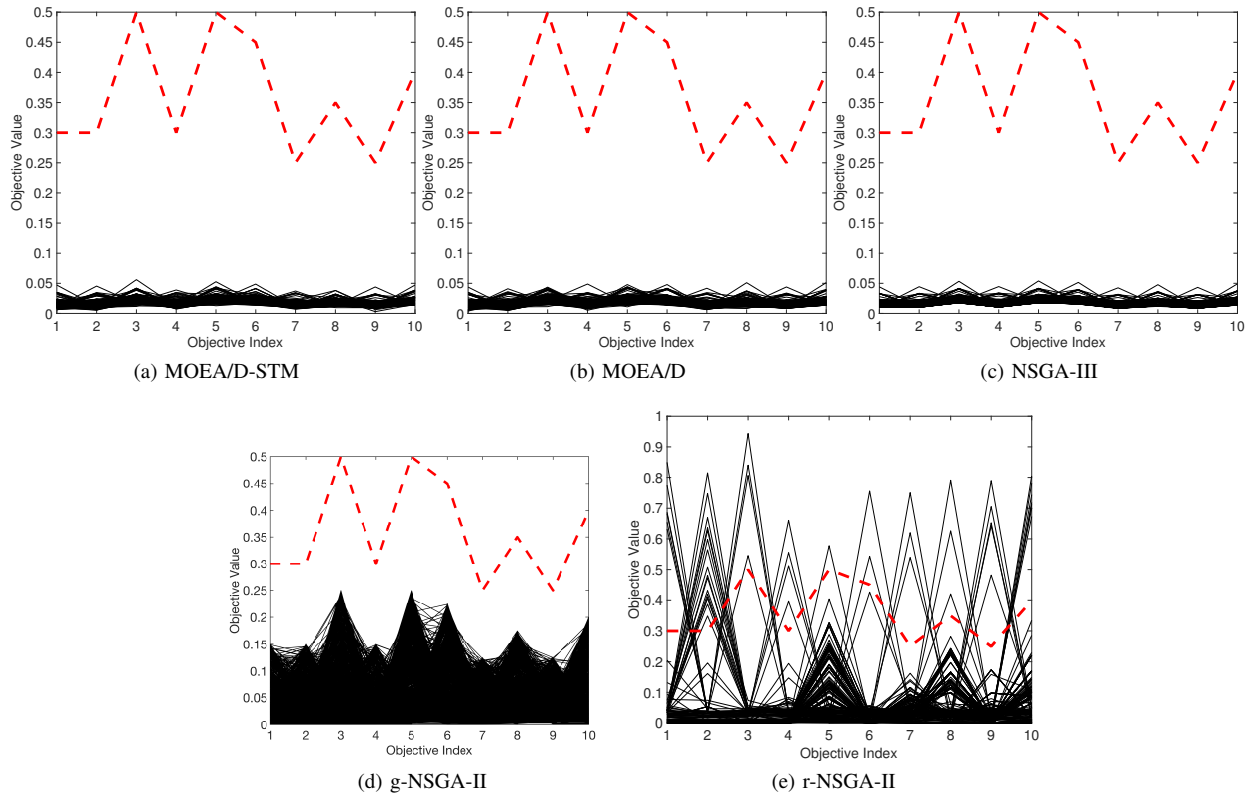
Fig. 61: Comparisons on 10-objective WFG42 where $\mathbf{z}^r = (0.3, 0.3, 0.5, 0.3, 0.5, 0.45, 0.25, 0.35, 0.25, 0.4)^T$.

(a) MOEA/D-STM

(b) MOEA/D

(c) NSGA-III

(d) g-NSGA-II

(e) r-NSGA-II

(f) R-NSGA-II
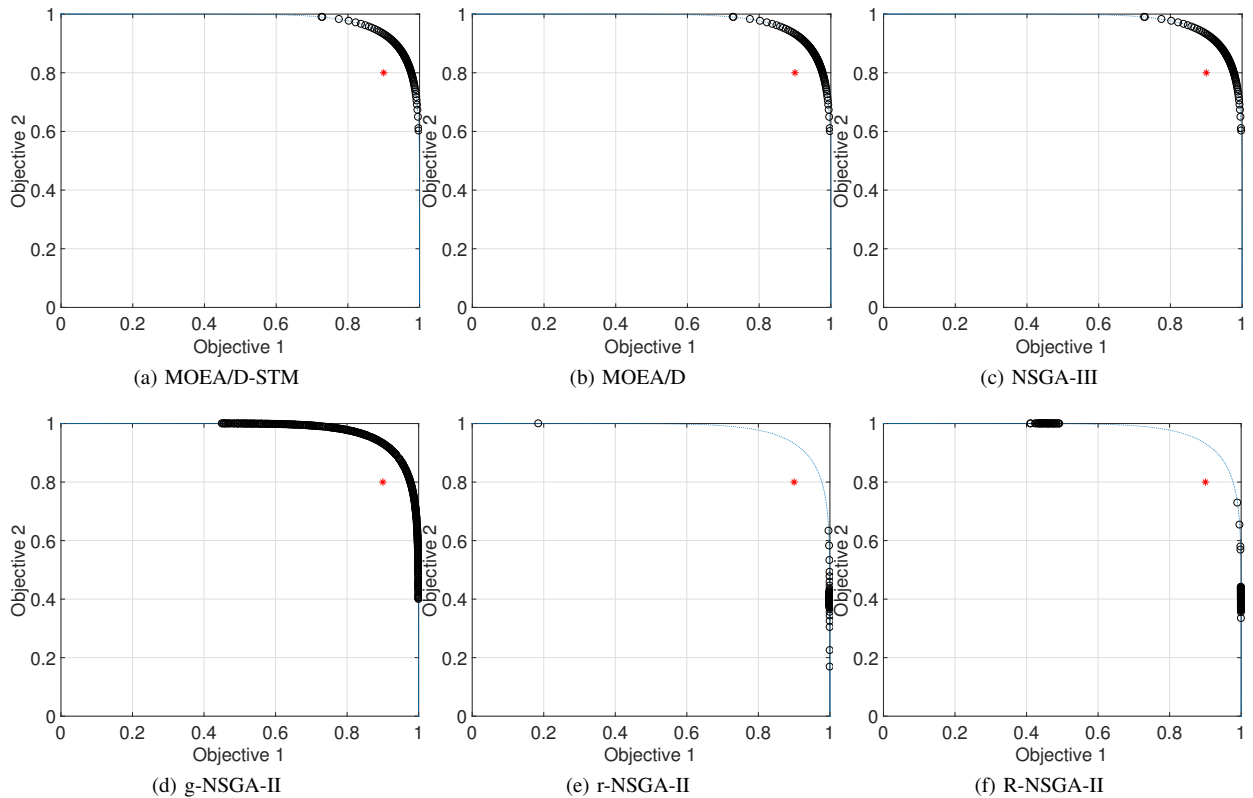
Fig. 62: Comparisons on 2-objective WFG43 where $\mathbf{z}^r = (0.9, 0.8)^T$.

Fig. 63: Comparisons on 2-objective WFG43 where $\mathbf{z}^r = (0.95, 0.93)^T$.

Fig. 64: Comparisons on 3-objective WFG43 where $\mathbf{z}^r = (0.6, 0.8, 0.8)^T$.

(a) MOEA/D-STM

(b) MOEA/D

(c) NSGA-III

(d) g-NSGA-II

(e) r-NSGA-II

(f) R-NSGA-II
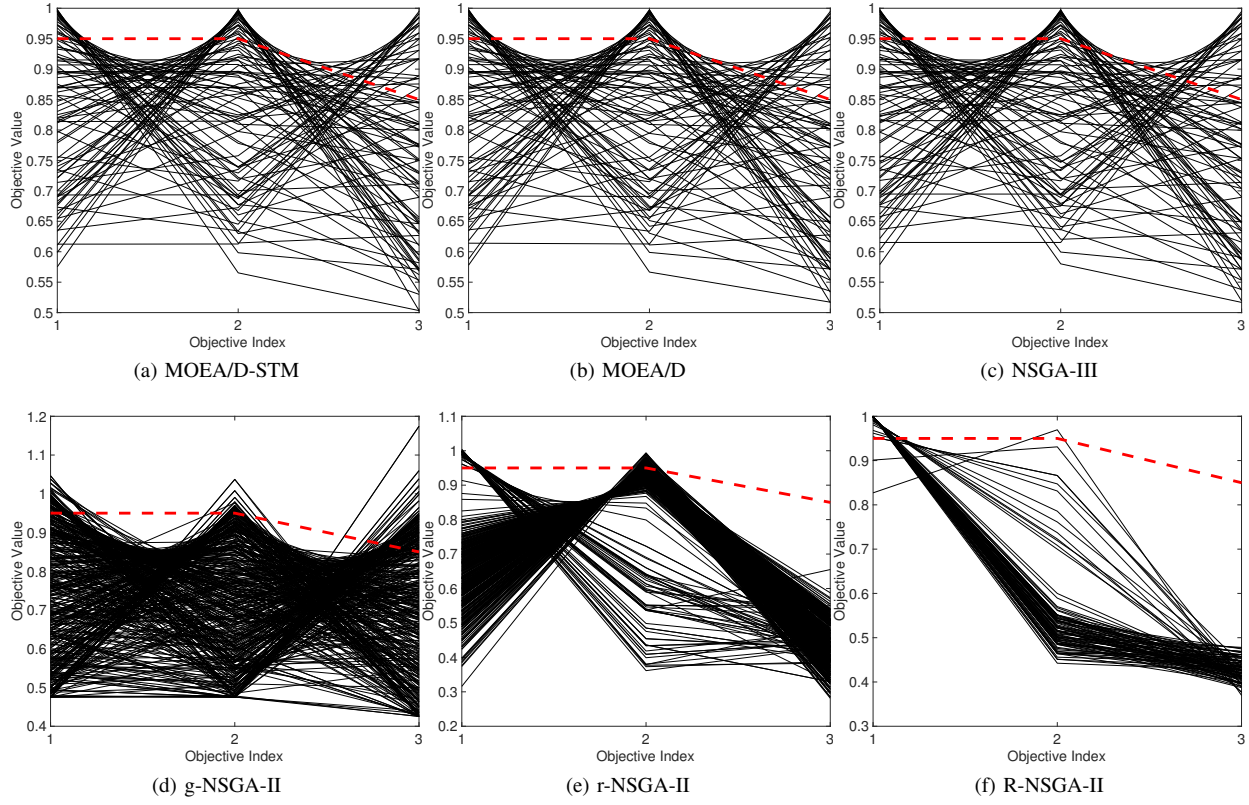
Fig. 65: Comparisons on 3-objective WFG43 where $\mathbf{z}^r = (0.95, 0.95, 0.85)^T$.

(a) MOEA/D-STM

(b) MOEA/D

(c) NSGA-III

(d) g-NSGA-II

(e) r-NSGA-II

(f) R-NSGA-II

Fig. 66: Comparisons on 5-objective WFG43 where $\mathbf{z}^r = (0.4, 0.4, 0.5, 0.4, 0.4)^T$.

(a) MOEA/D-STM

(b) MOEA/D

(c) NSGA-III

(d) g-NSGA-II

(e) r-NSGA-II

(f) R-NSGA-II
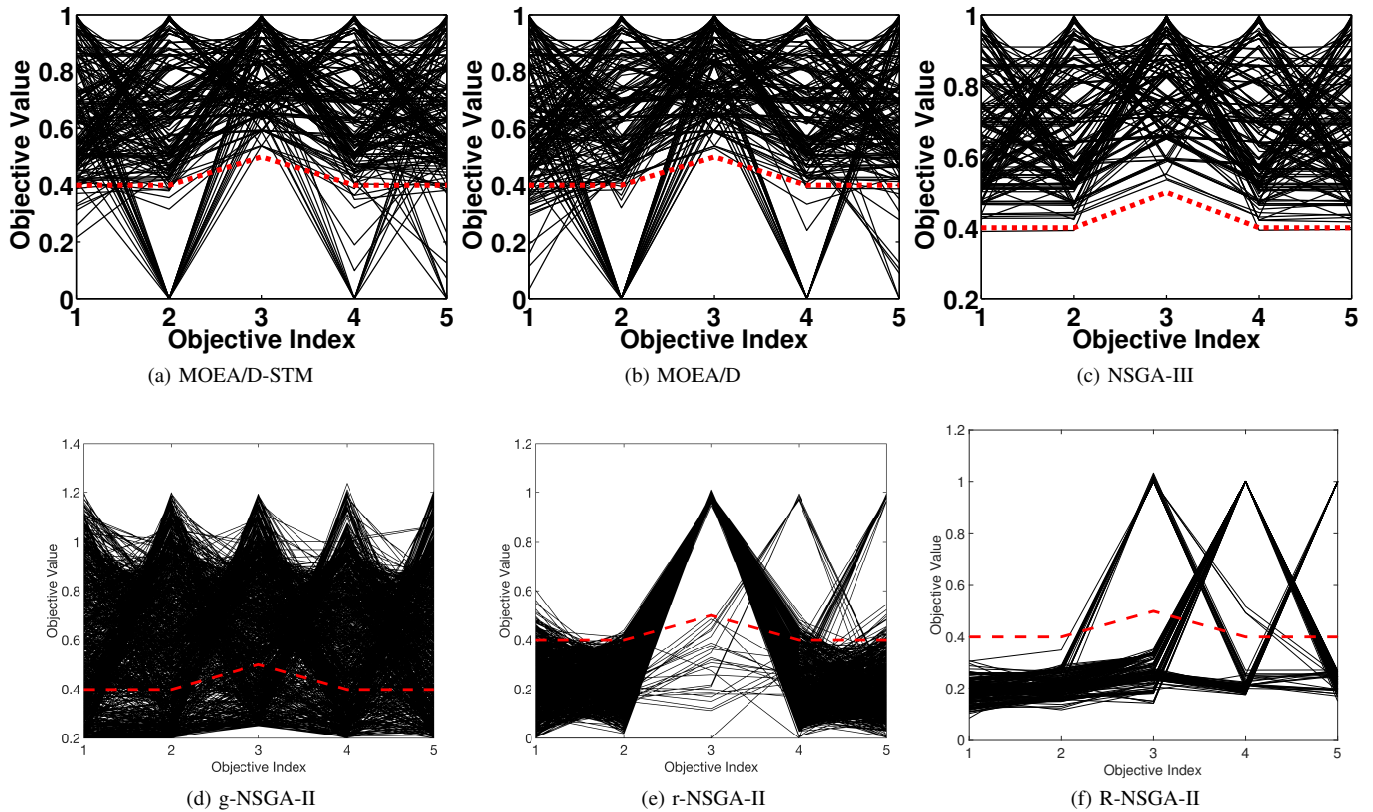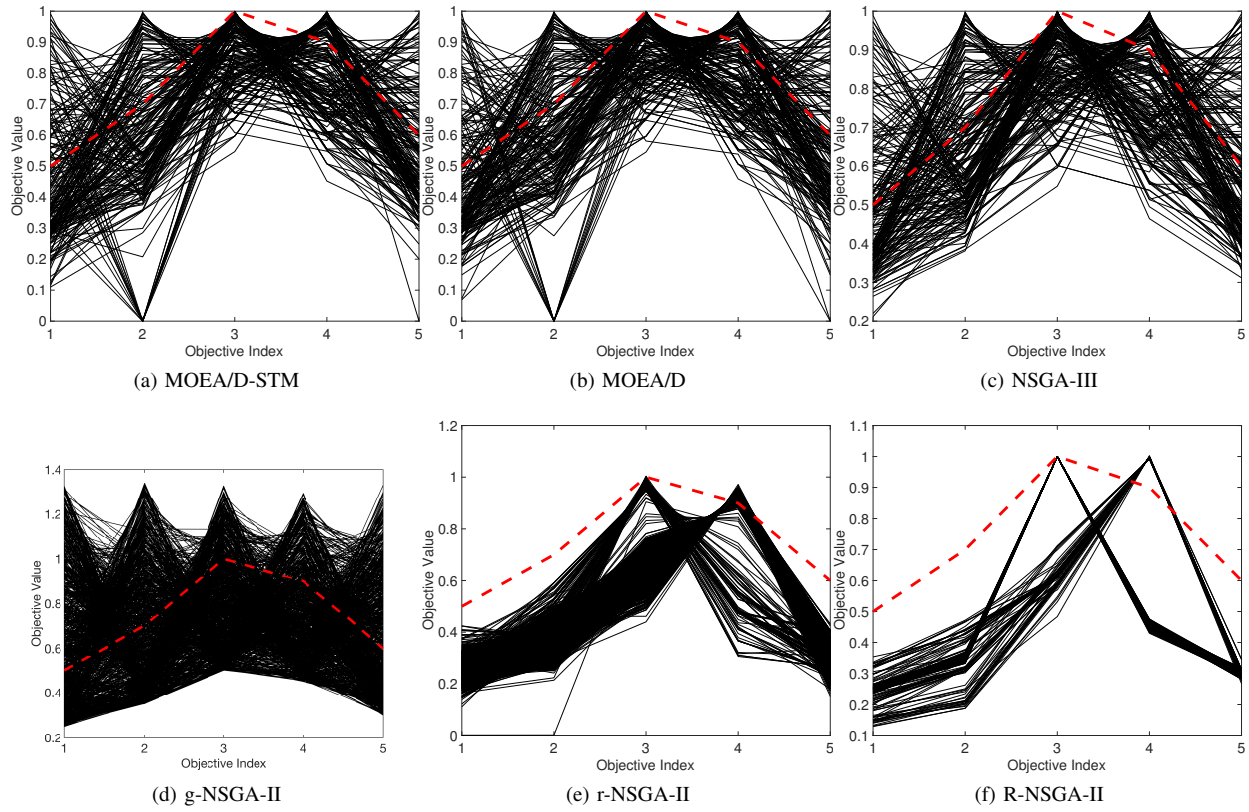
Fig. 67: Comparisons on 5-objective WFG43 where $\mathbf{z}^r = (0.5, 0.7, 1.0, 0.9, 0.6)^T$.

(a) MOEA/D-STM

(b) MOEA/D

(c) NSGA-III

(d) g-NSGA-II

(e) r-NSGA-II

(f) R-NSGA-II
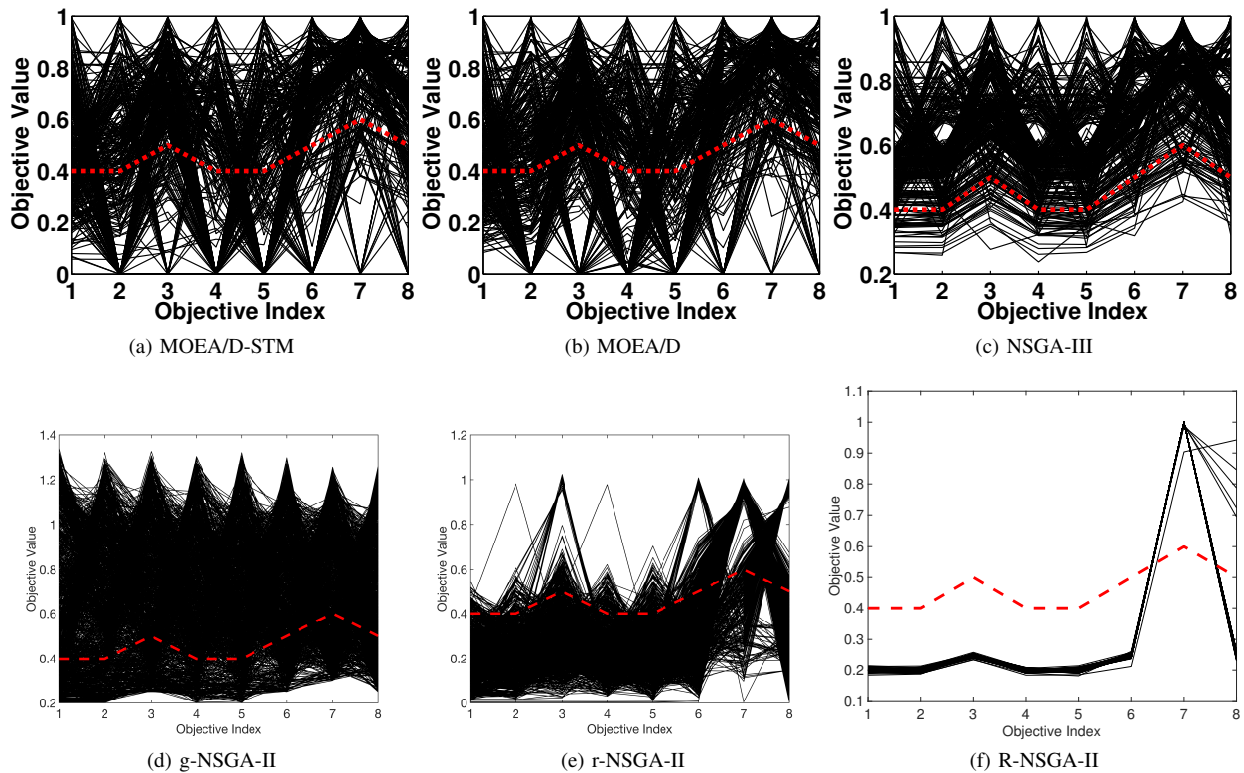
Fig. 68: Comparisons on 8-objective WFG43 where $\mathbf{z}^r = (0.4, 0.4, 0.5, 0.4, 0.4, 0.5, 0.6, 0.5)^T$.

(a) MOEA/D-STM

(b) MOEA/D

(c) NSGA-III

(d) r-NSGA-II

(e) R-NSGA-II
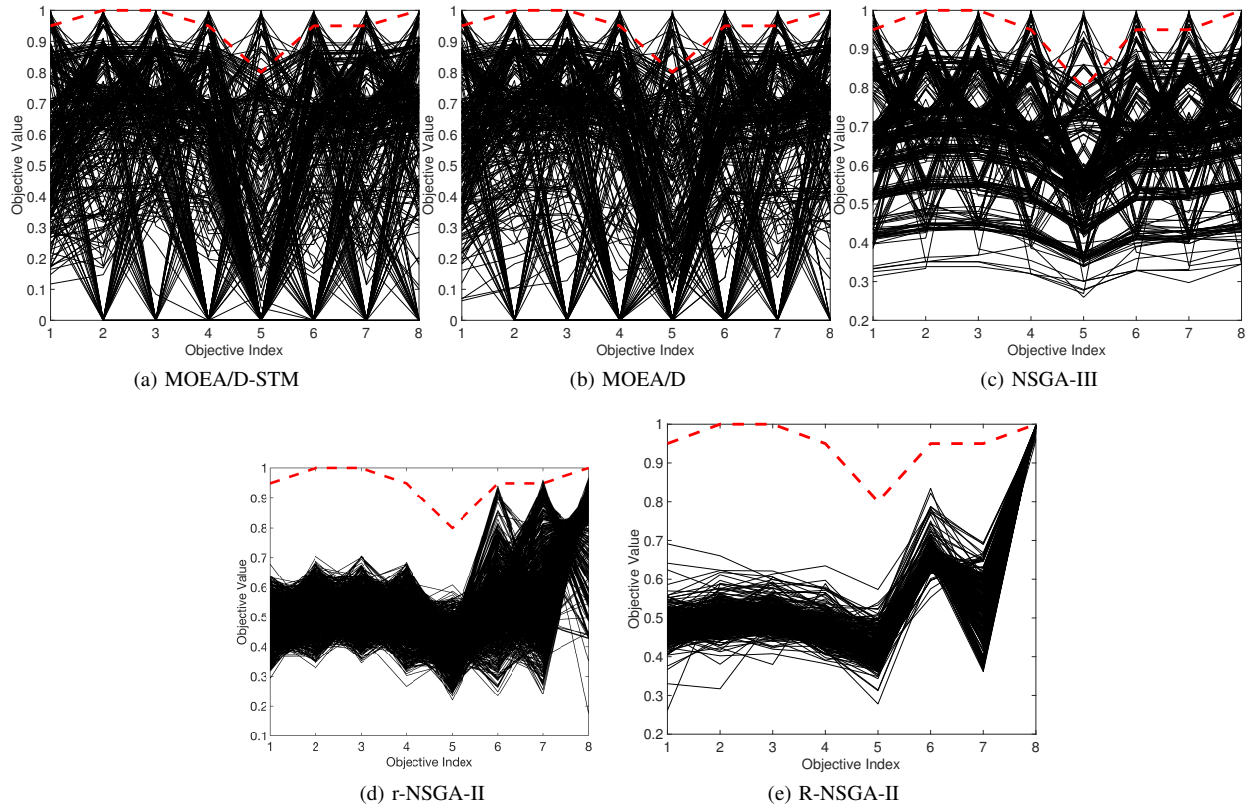
Fig. 69: Comparisons on 8-objective WFG43 where $\mathbf{z}^r = (0.95, 1.0, 1.0, 0.95, 0.8, 0.95, 0.95, 1.0)^T$.

(a) MOEA/D-STM

(b) MOEA/D

(c) NSGA-III

(d) g-NSGA-II

(e) r-NSGA-II

Fig. 70: Comparisons on 10-objective WFG43 where $\mathbf{z}^r = (0.5, 0.2, 0.4, 0.3, 0.4, 0.5, 0.6, 0.7, 0.6, 0.7)^T$.

(a) MOEA/D-STM

(b) MOEA/D

(c) NSGA-III

(d) r-NSGA-II

Fig. 71: Comparisons on 10-objective WFG43 where $\mathbf{z}^r = (1.0, 0.85, 1.0, 0.95, 0.85, 0.95, 0.95, 1.0, 0.8, 0.9)^T$.

(a) MOEA/D-STM

(b) MOEA/D

(c) NSGA-III

(d) g-NSGA-II

(e) r-NSGA-II

(f) R-NSGA-II
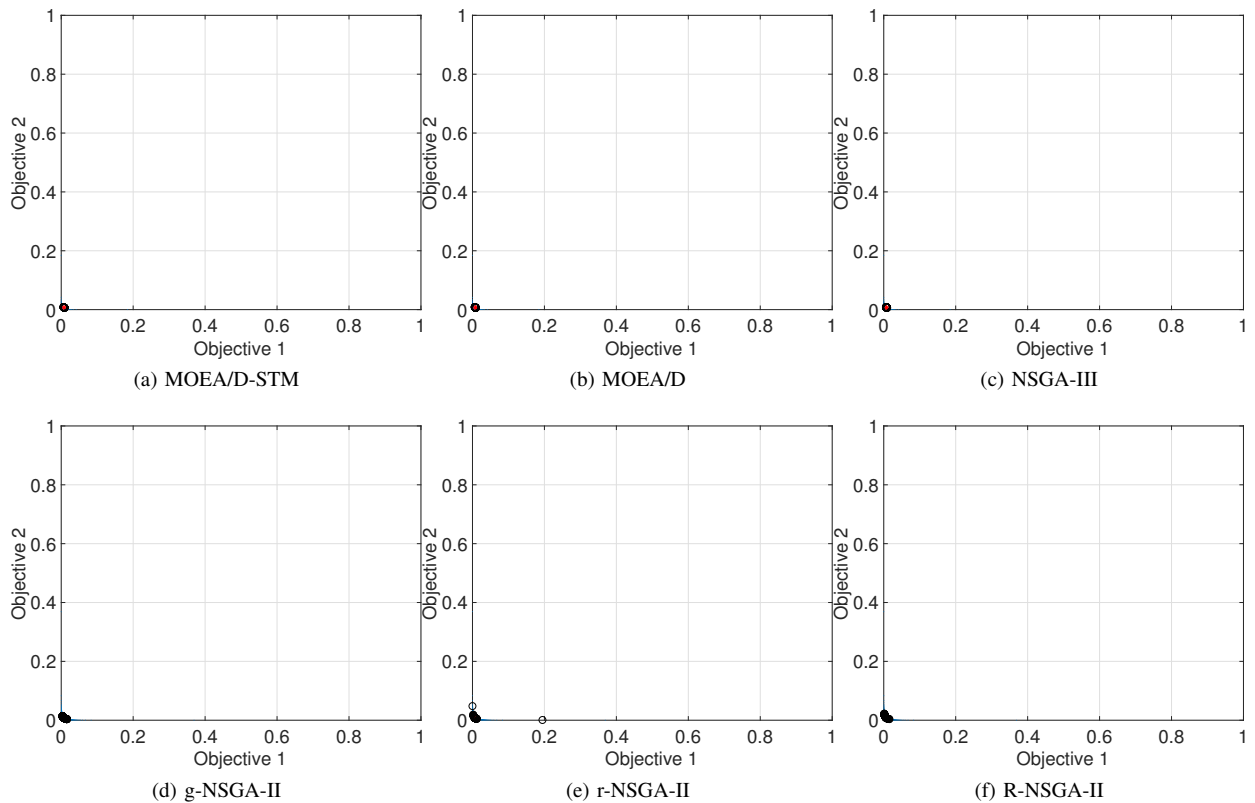
Fig. 72: Comparisons on 2-objective WFG44 where $\mathbf{z}^r = (0.008, 0.006)^T$.

Fig. 73: Comparisons on 2-objective WFG44 where $\mathbf{z}^r = (0.009, 0.008)^T$.

Fig. 74: Comparisons on 3-objective WFG44 where $\mathbf{z}^r = (0.0004, 0.0004, 0.0003)^T$.

(a) MOEA/D-STM

(b) MOEA/D

(c) NSGA-III

(d) r-NSGA-II

Fig. 75: Comparisons on 3-objective WFG44 where $\mathbf{z}^r = (0.001, 0.0001, 0.0005)^T$.

(a) MOEA/D-STM

(b) MOEA/D

(c) NSGA-III

(d) g-NSGA-II

(e) r-NSGA-II

(f) R-NSGA-II

Fig. 76: Comparisons on 5-objective WFG44 where $\mathbf{z}^r = (0.000005, 0.00001, 0.00001, 0.00001, 0.000005)^T$.

(a) MOEA/D-STM

(b) MOEA/D

(c) NSGA-III

(d) r-NSGA-II

(e) R-NSGA-II
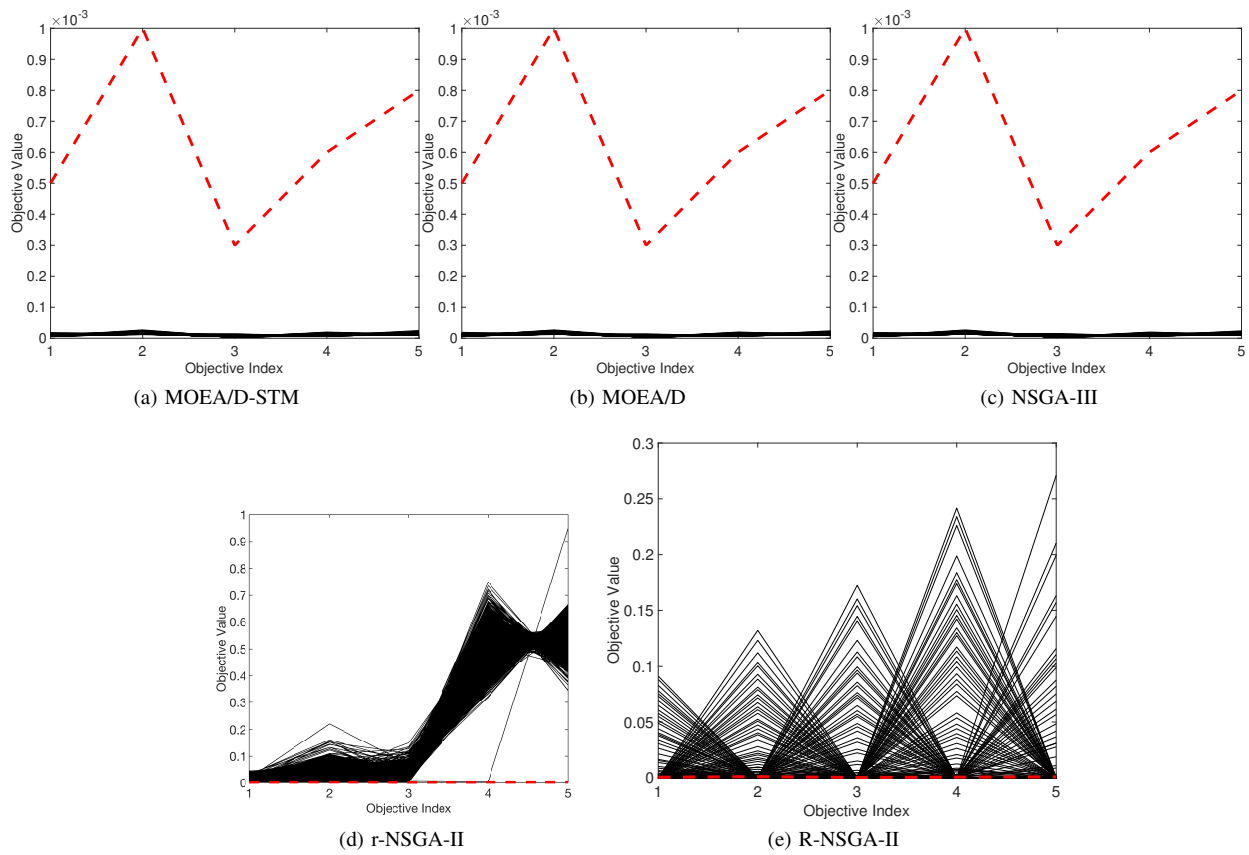
Fig. 77: Comparisons on 5-objective WFG44 where $\mathbf{z}^r = (0.0005, 0.001, 0.0003, 0.0006, 0.0008)^T$.

(a) MOEA/D-STM

(b) MOEA/D

(c) NSGA-III

(d) r-NSGA-II
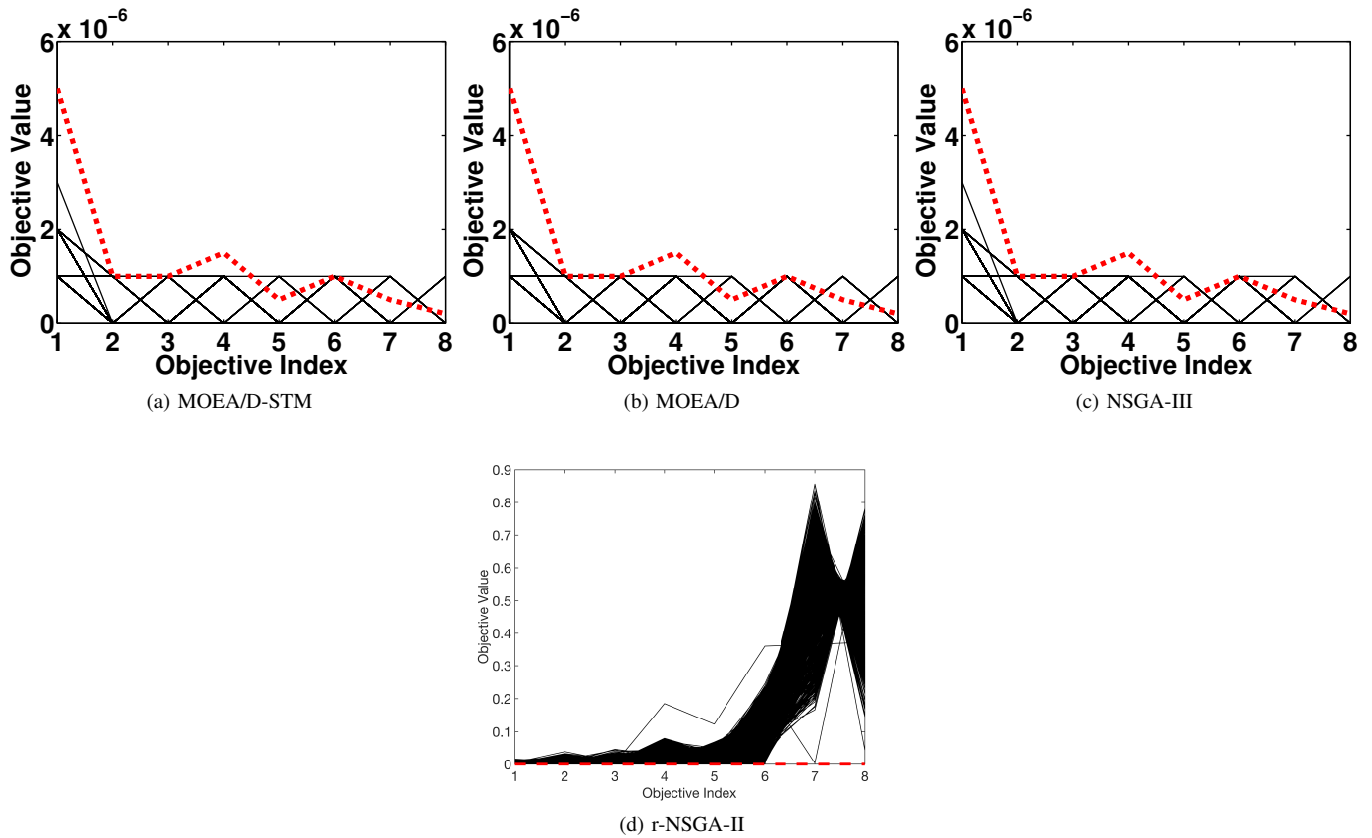
Fig. 78: Comparisons on 8-objective WFG44 where $\mathbf{z}^r = (0.000005, 0.000001, 0.000001, 0.0000015, 0.0000005, 0.000001, 0.0000005, 0.000$

(a) MOEA/D-STM

(b) MOEA/D

(c) NSGA-III
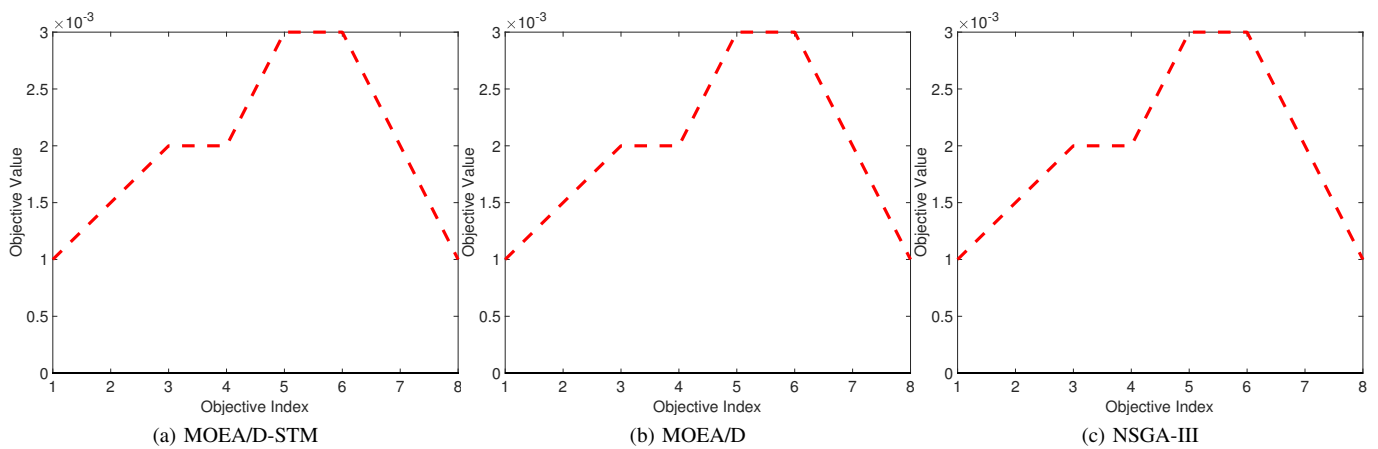
Fig. 79: Comparisons on 8-objective WFG44 where $\mathbf{z}^r = (0.001, 0.0015, 0.002, 0.002, 0.003, 0.003, 0.002, 0.001)^T$.
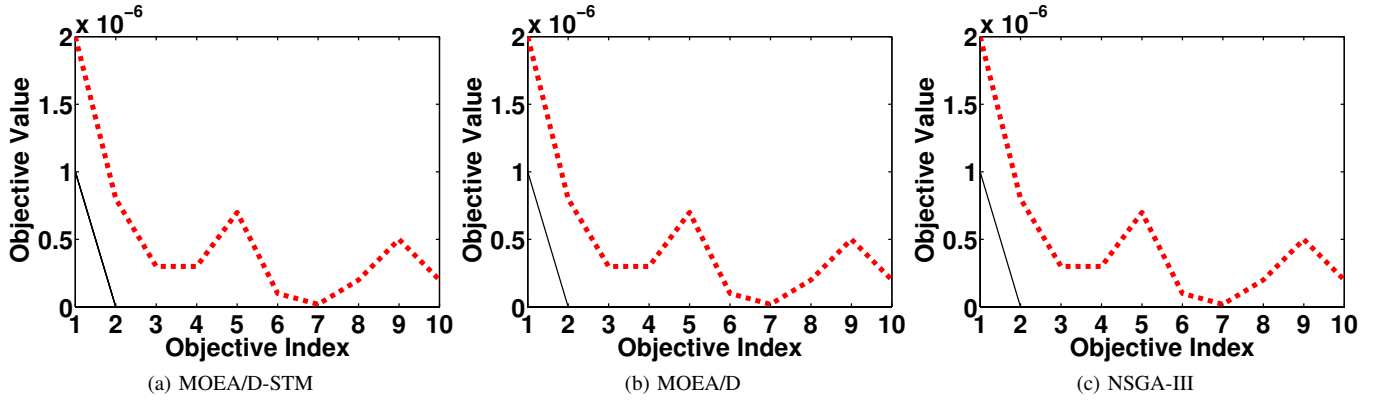
Fig. 80: Comparisons on 10-objective WFG44 where $\mathbf{z}^r = (0.000002, 0.0000008, 0.0000003, 0.0000003, 0.0000007, 0.0000001, 0.00000002$
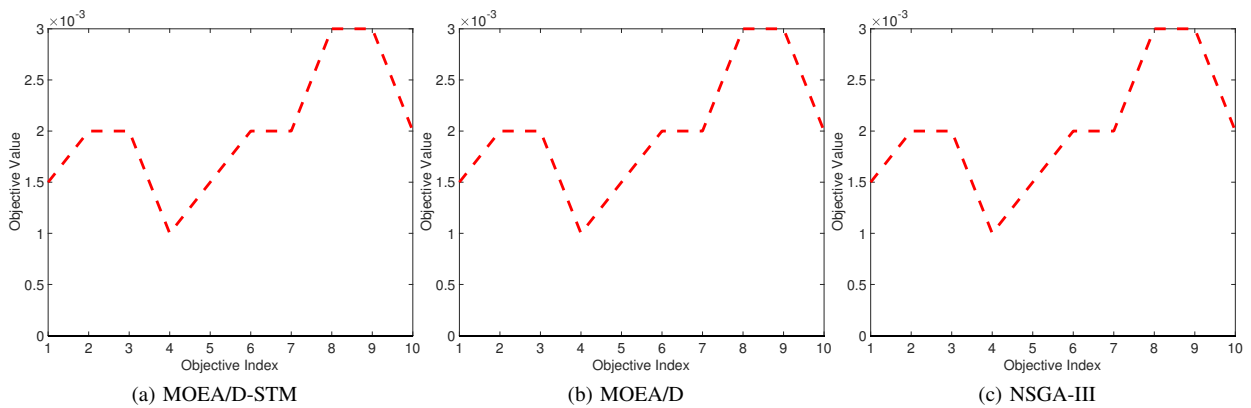
Fig. 81: Comparisons on 10-objective WFG44 where $\mathbf{z}^r = (0.0015, 0.002, 0.002, 0.001, 0.0015, 0.002, 0.002, 0.003, 0.003, 0.002)^T$.

(a) MOEA/D-STM

(b) MOEA/D

(c) NSGA-III

(d) g-NSGA-II

(e) r-NSGA-II

(f) R-NSGA-II
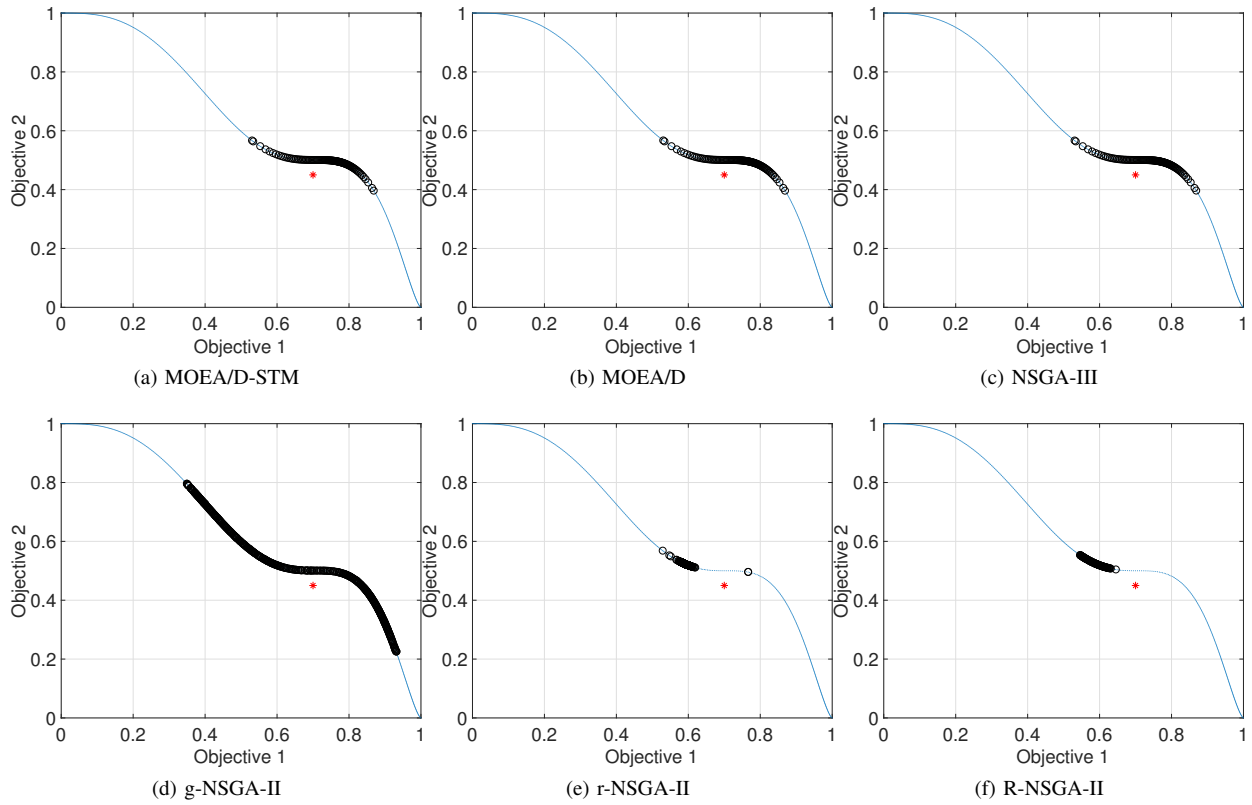
Fig. 82: Comparisons on 2-objective WFG45 where $\mathbf{z}^r = (0.7, 0.45)^T$.

(a) MOEA/D-STM

(b) MOEA/D

(c) NSGA-III

(d) g-NSGA-II

(e) r-NSGA-II

(f) R-NSGA-II
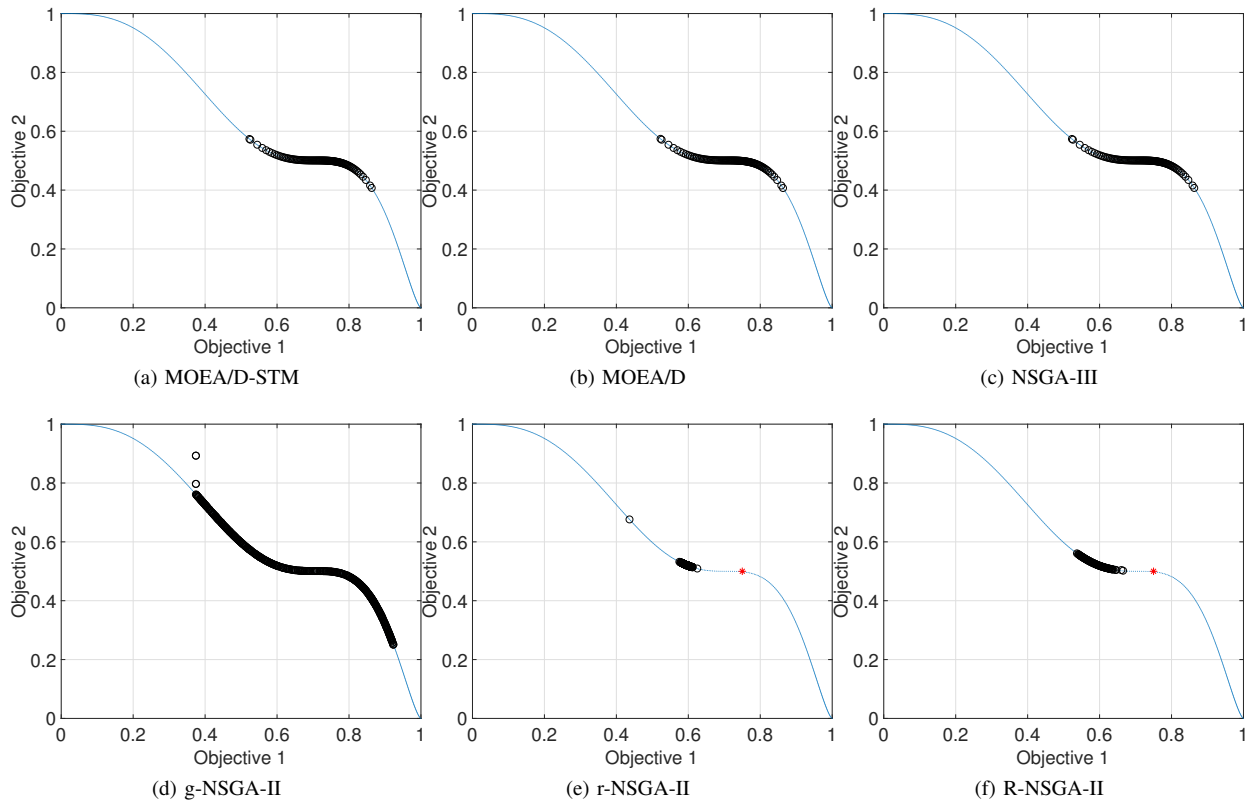
Fig. 83: Comparisons on 2-objective WFG45 where $\mathbf{z}^r = (0.75, 0.5)^T$.
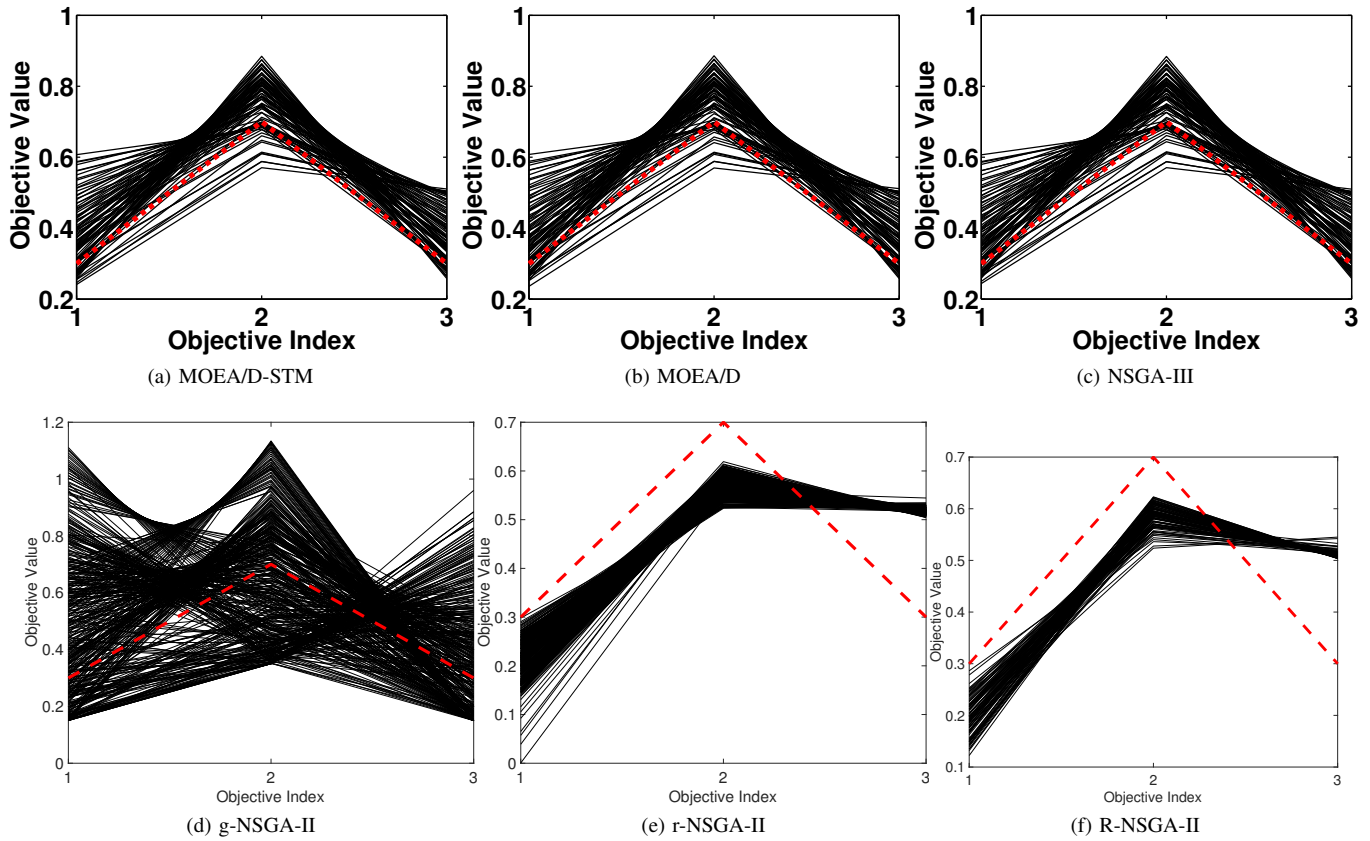
(a) MOEA/D-STM

(b) MOEA/D

(c) NSGA-III

(d) g-NSGA-II

(e) r-NSGA-II

(f) R-NSGA-II

Fig. 84: Comparisons on 3-objective WFG45 where $\mathbf{z}^r = (0.3, 0.7, 0.3)^T$.

(a) MOEA/D-STM

(b) MOEA/D

(c) NSGA-III

(d) g-NSGA-II

(e) r-NSGA-II

(f) R-NSGA-II

Fig. 85: Comparisons on 3-objective WFG45 where $\mathbf{z}^r = (0.5, 0.8, 0.5)^T$.

(a) MOEA/D-STM (b) MOEA/D (c) NSGA-III

(d) g-NSGA-II (e) r-NSGA-II (f) R-NSGA-II
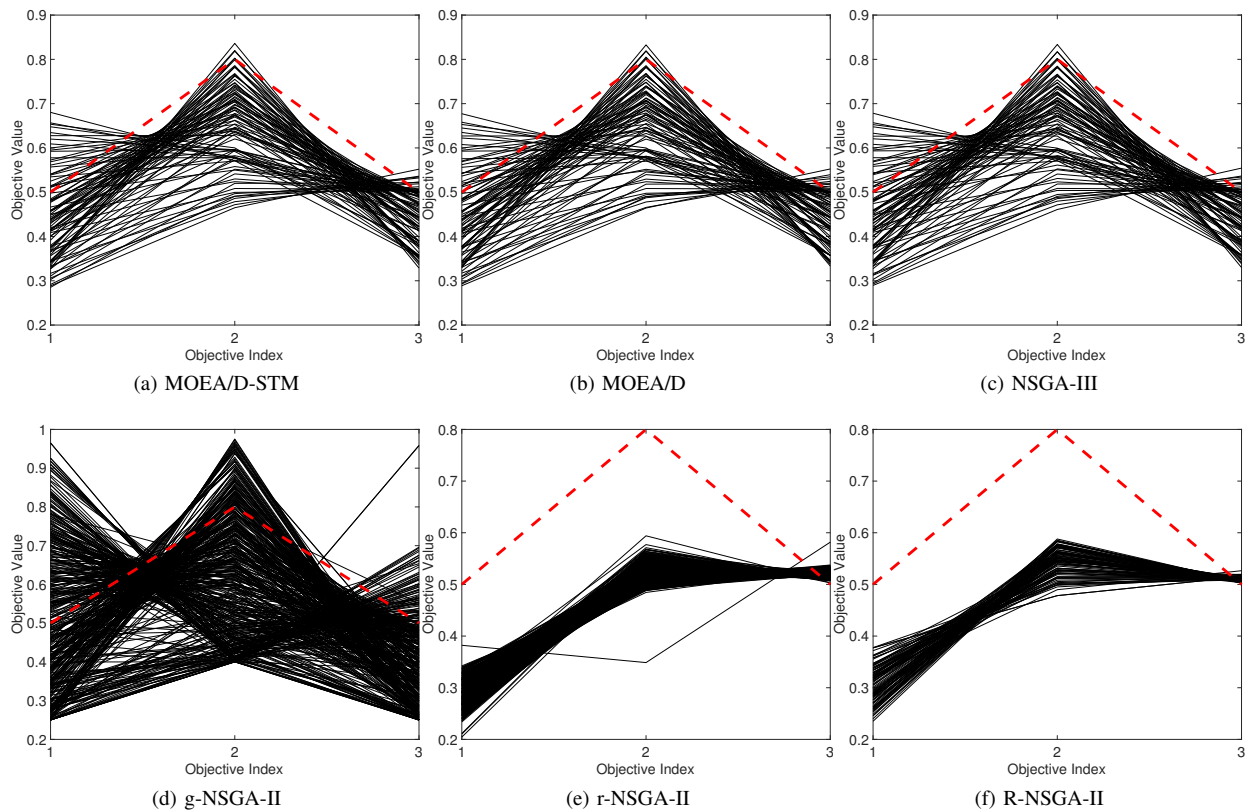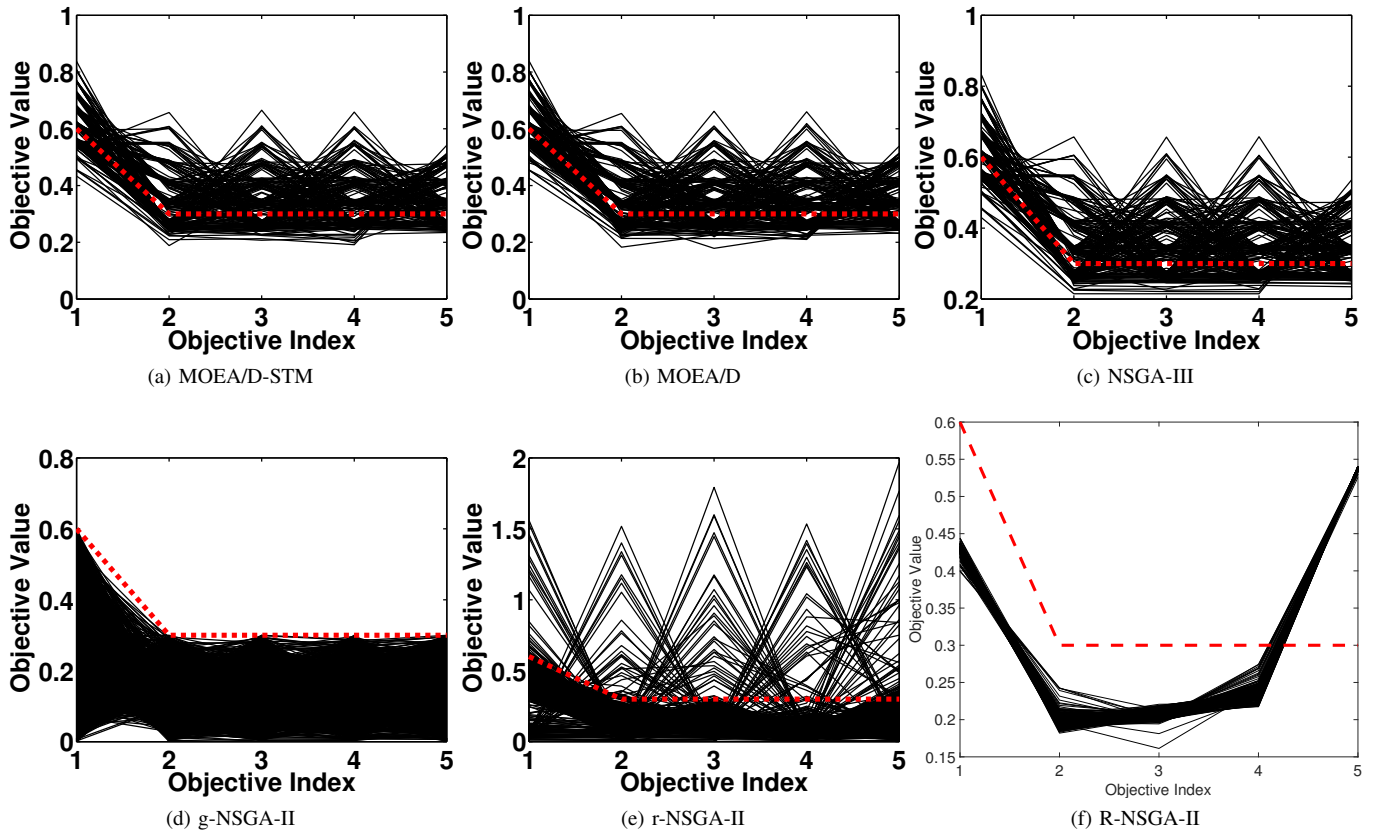
Fig. 86: Comparisons on 5-objective WFG45 where $\mathbf{z}^r = (0.6, 0.3, 0.3, 0.3, 0.3)^T$.

(a) MOEA/D-STM (b) MOEA/D (c) NSGA-III

(d) g-NSGA-II (e) r-NSGA-II (f) R-NSGA-II

Fig. 87: Comparisons on 5-objective WFG45 where $\mathbf{z}^r = (0.8, 0.5, 0.4, 0.5, 0.5)^T$.

(a) MOEA/D-STM

(b) MOEA/D

(c) NSGA-III

(d) g-NSGA-II

(e) r-NSGA-II

(f) R-NSGA-II
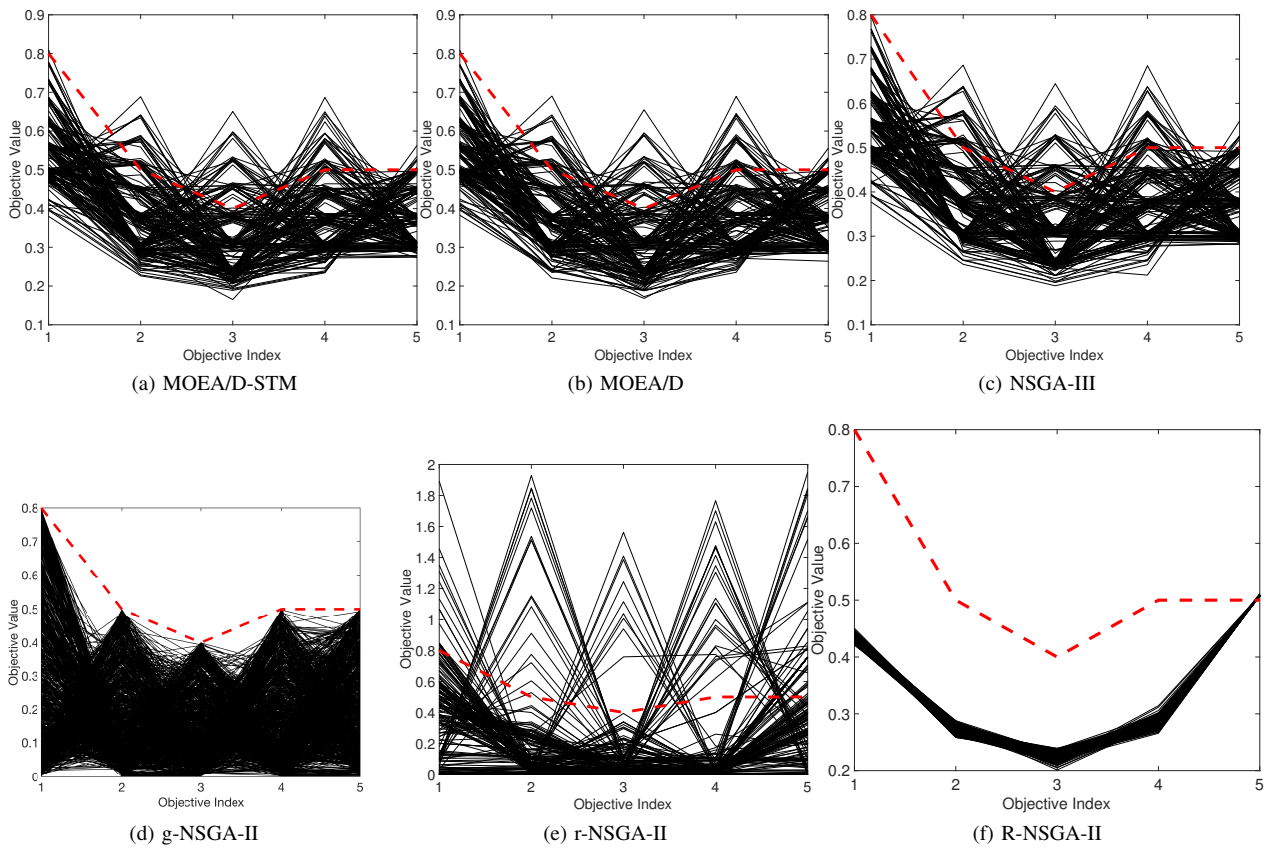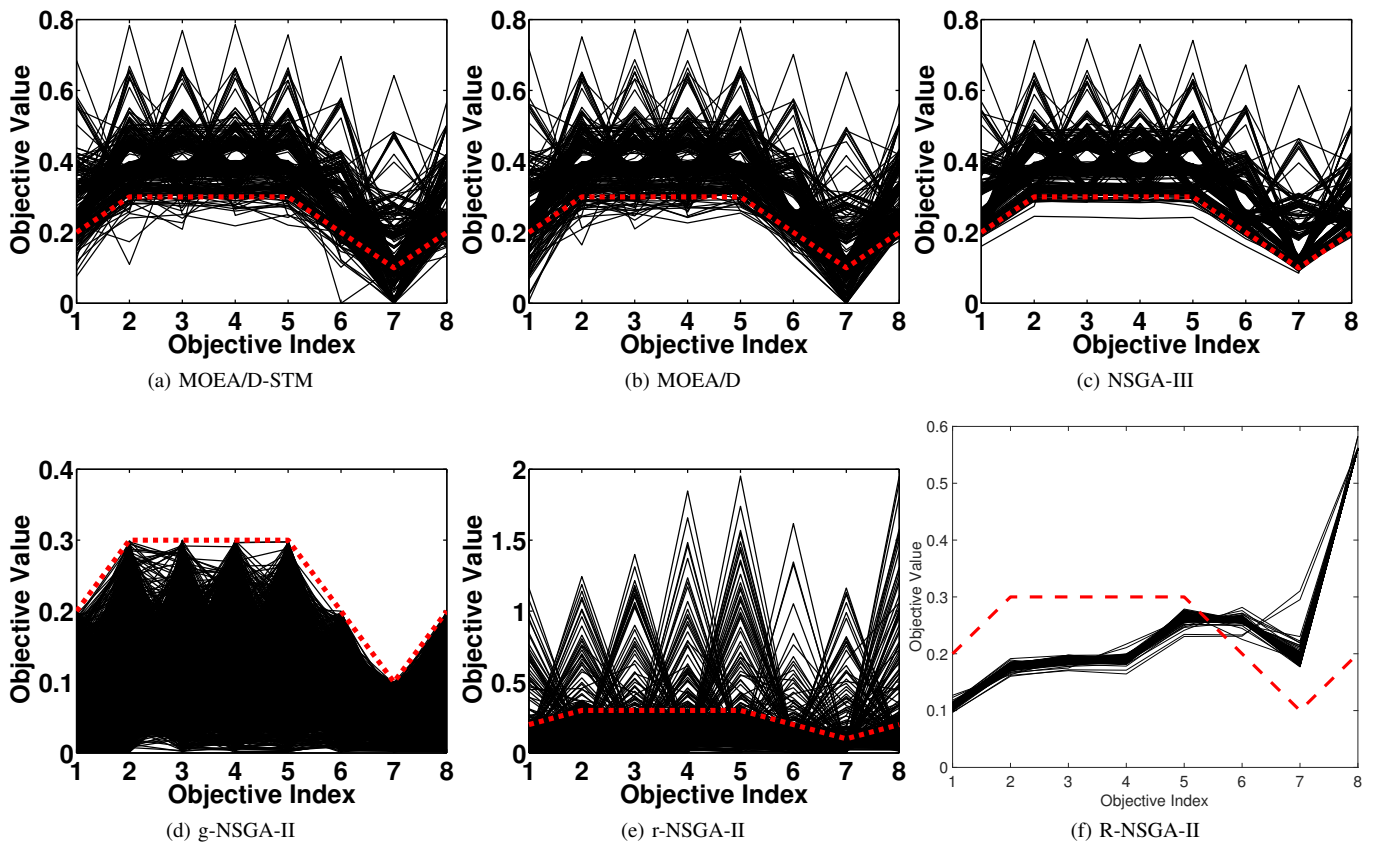
Fig. 88: Comparisons on 8-objective WFG45 where $\mathbf{z}^r = (0.2, 0.3, 0.3, 0.3, 0.3, 0.2, 0.1, 0.2)^T$.

(a) MOEA/D-STM

(b) MOEA/D

(c) NSGA-III

(d) r-NSGA-II

(e) R-NSGA-II
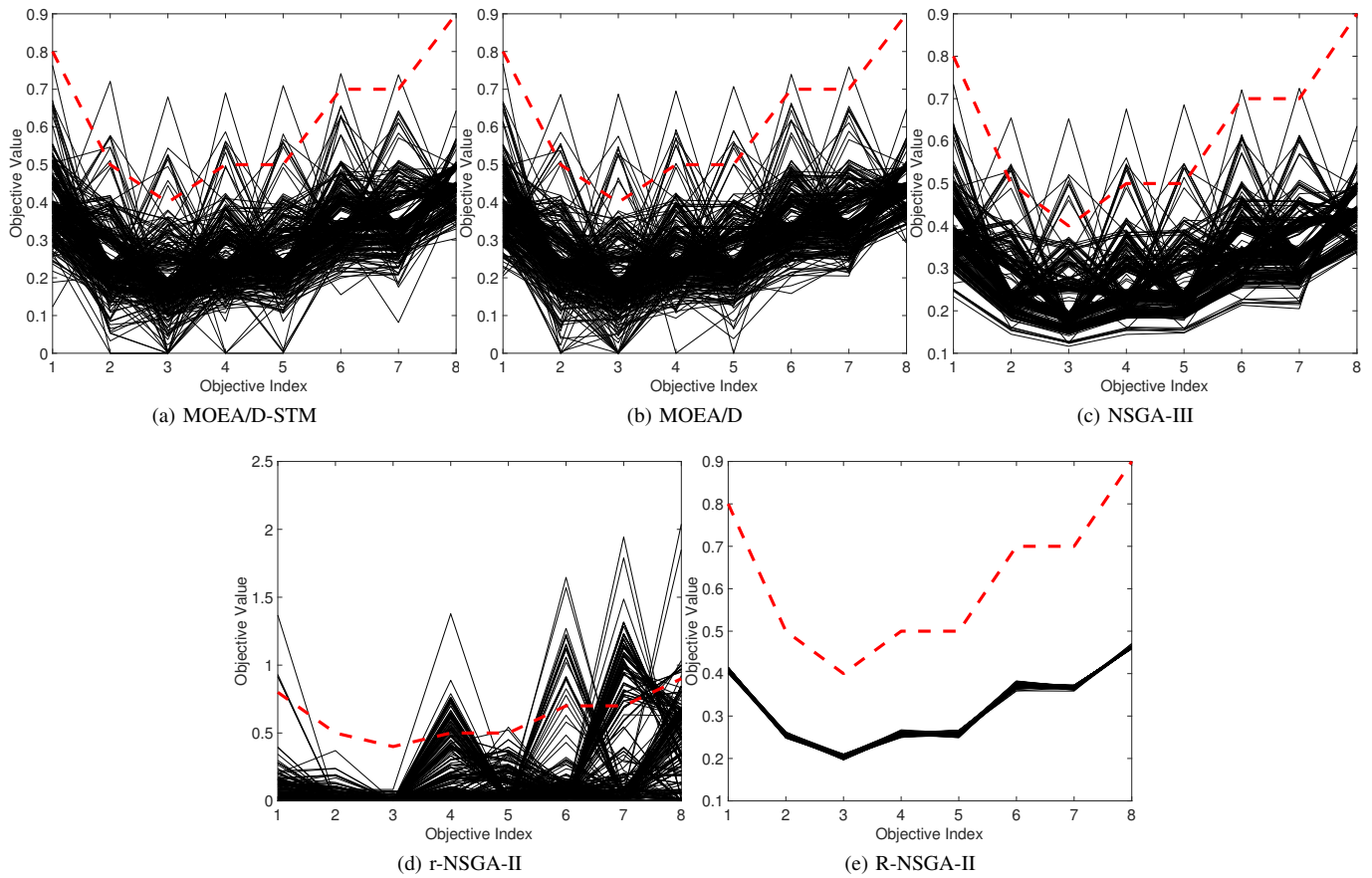
Fig. 89: Comparisons on 8-objective WFG45 where $\mathbf{z}^r = (0.8, 0.5, 0.4, 0.5, 0.5, 0.7, 0.7, 0.9)^T$.

(a) MOEA/D-STM

(b) MOEA/D

(c) NSGA-III

(d) g-NSGA-II

(e) r-NSGA-II
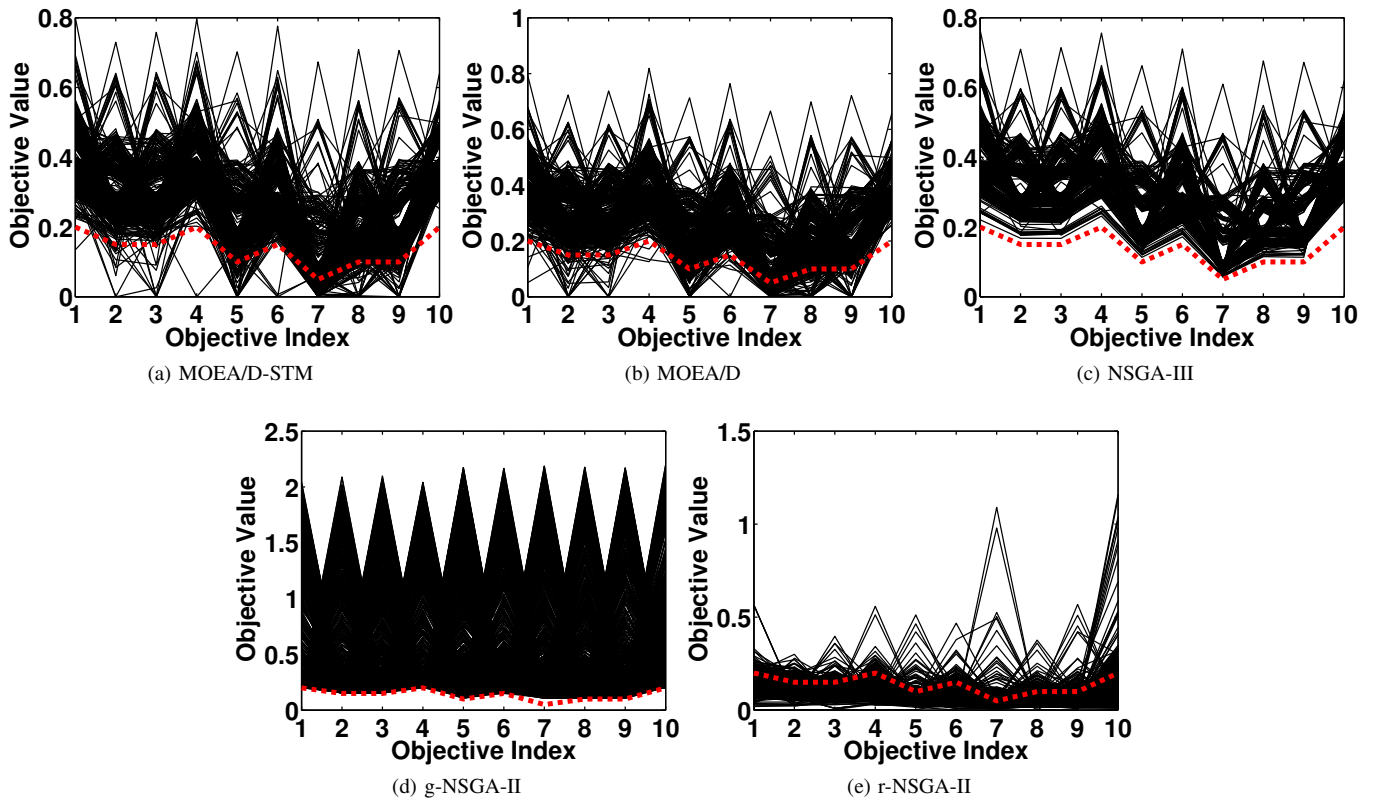
Fig. 90: Comparisons on 10-objective WFG45 where $\mathbf{z}^r = (0.2, 0.15, 0.15, 0.2, 0.1, 0.15, 0.05, 0.1, 0.1, 0.2)^T$.

(a) MOEA/D-STM

(b) MOEA/D

(c) NSGA-III

(d) r-NSGA-II
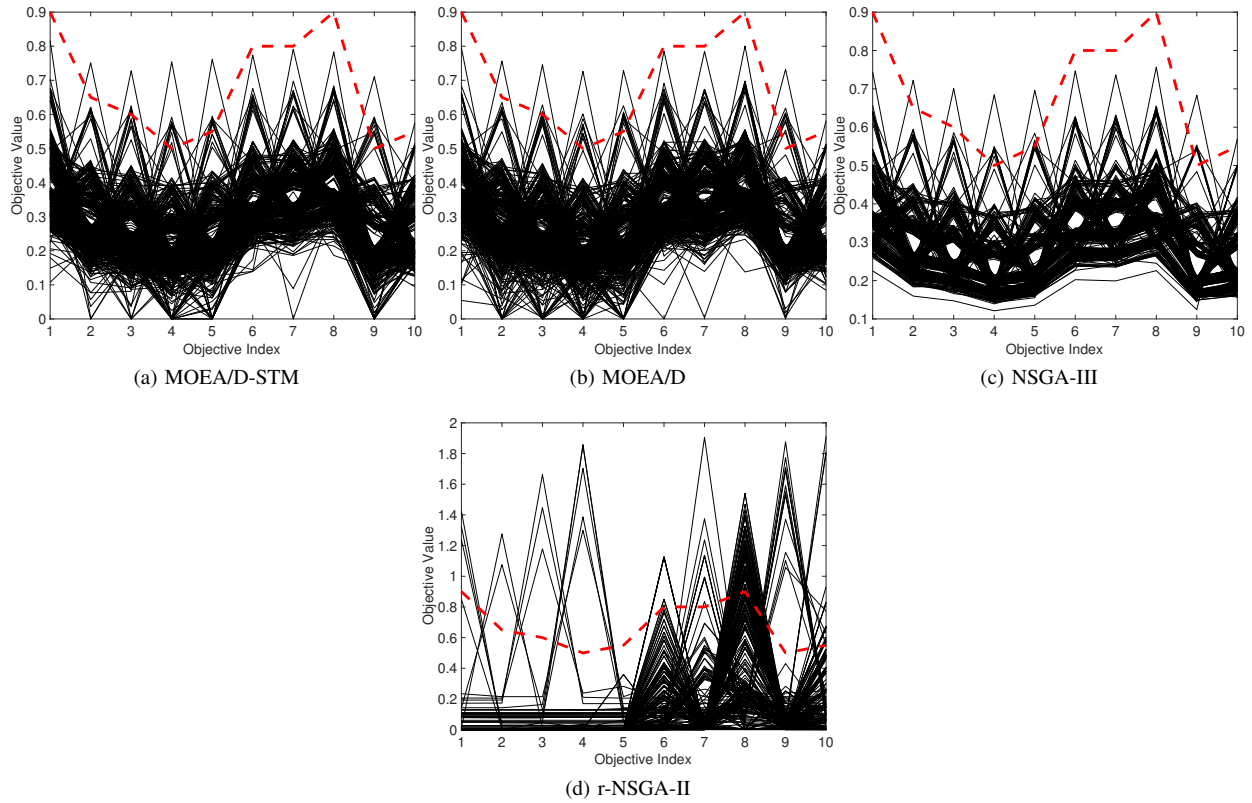
Fig. 91: Comparisons on 10-objective WFG45 where $\mathbf{z}^r = (0.9, 0.65, 0.6, 0.5, 0.55, 0.8, 0.8, 0.9, 0.5, 0.55)^T$.

(a) MOEA/D-STM

(b) MOEA/D

(c) NSGA-III

(d) g-NSGA-II

(e) r-NSGA-II

(f) R-NSGA-II
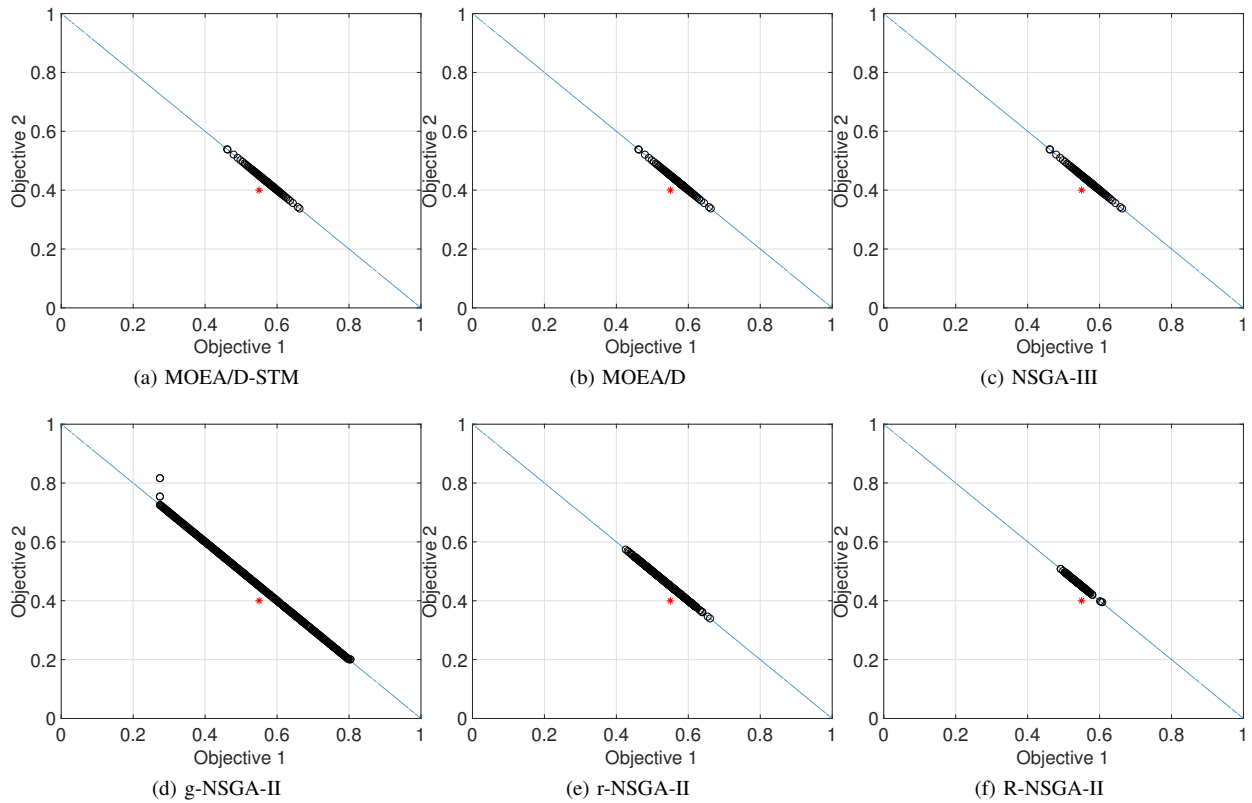
Fig. 92: Comparisons on 2-objective WFG46 where $\mathbf{z}^r = (0.55, 0.4)^T$.

(a) MOEA/D-STM   (b) MOEA/D   (c) NSGA-III

(d) g-NSGA-II   (e) r-NSGA-II   (f) R-NSGA-II
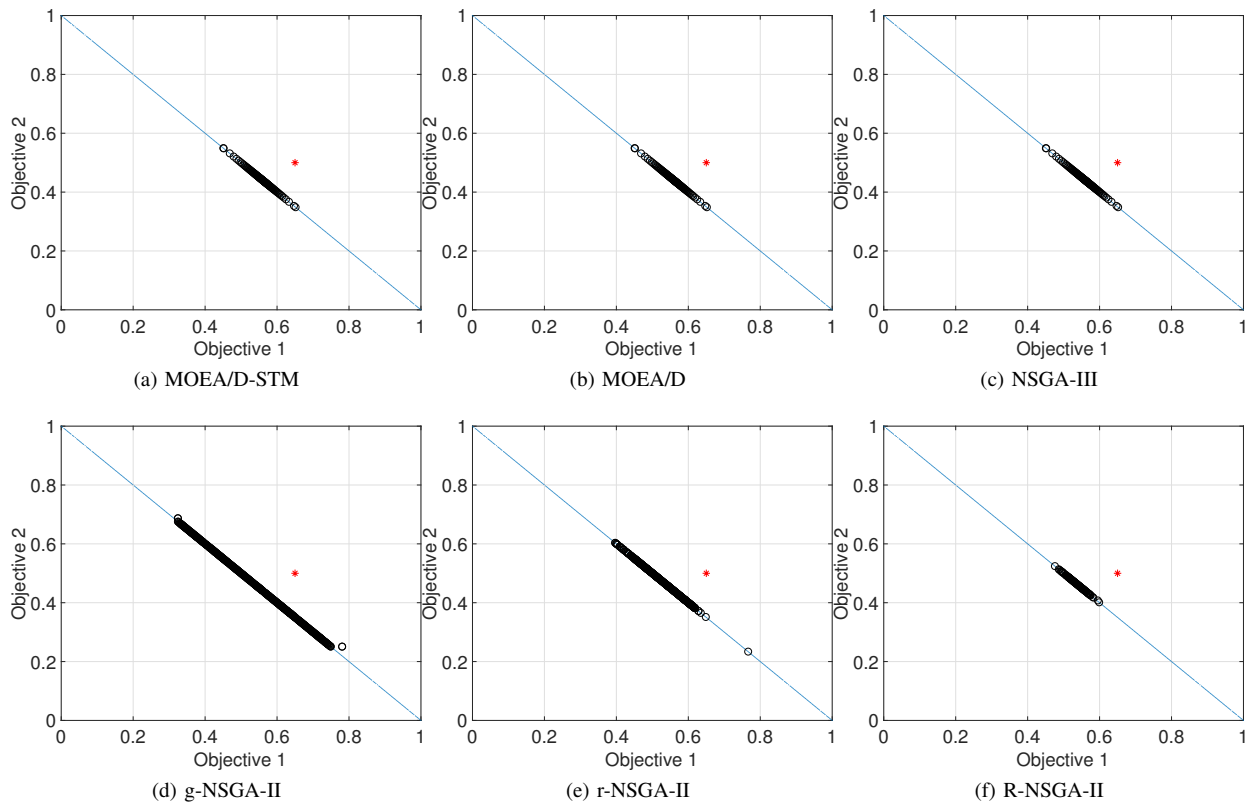
Fig. 93: Comparisons on 2-objective WFG46 where $\mathbf{z}^r = (0.65, 0.5)^T$.

(a) MOEA/D-STM   (b) MOEA/D   (c) NSGA-III

(d) g-NSGA-II   (e) r-NSGA-II   (f) R-NSGA-II
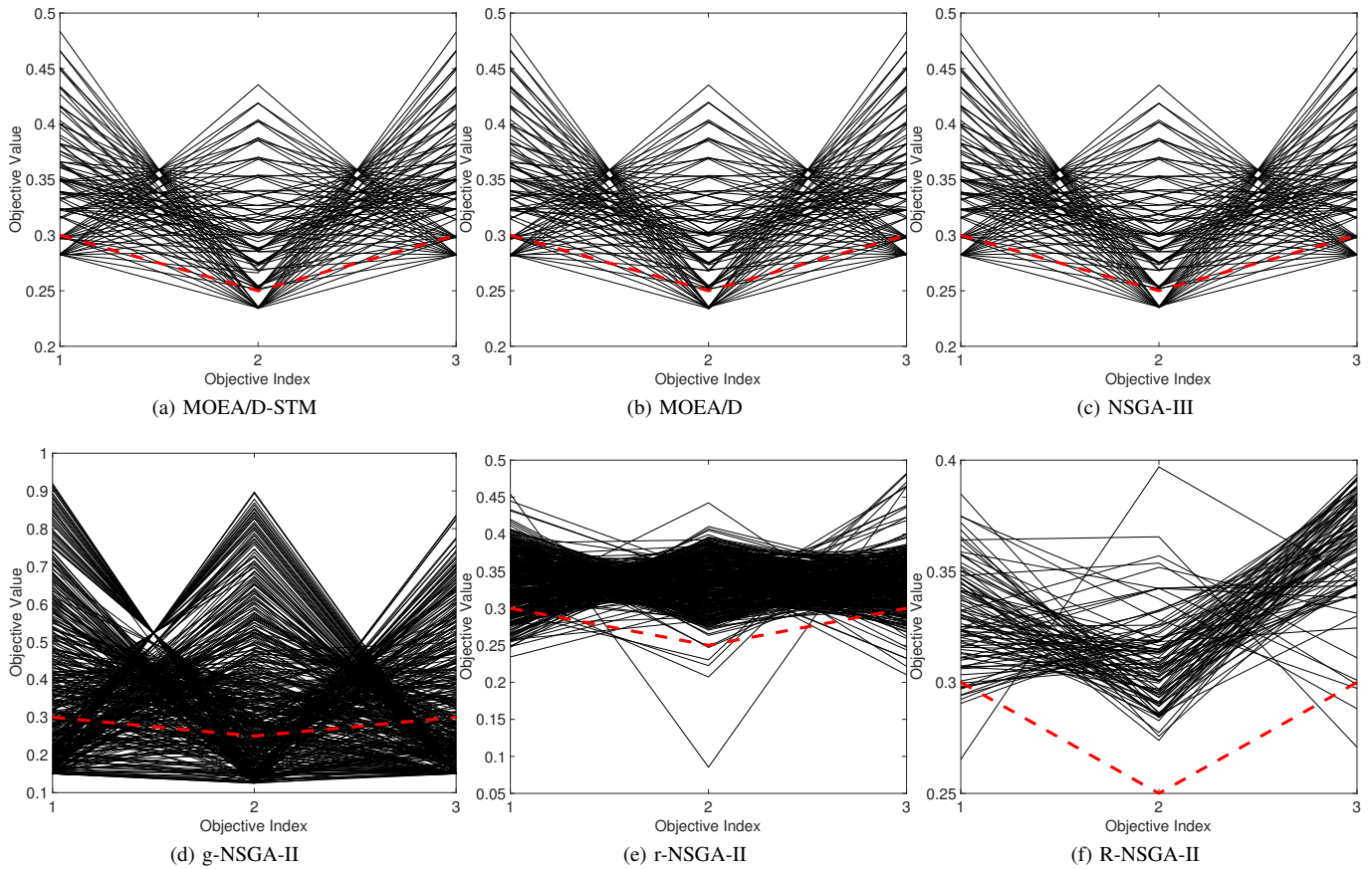
Fig. 94: Comparisons on 3-objective WFG46 where $\mathbf{z}^r = (0.3, 0.25, 0.3)^T$.

(a) MOEA/D-STM

(b) MOEA/D

(c) NSGA-III

(d) g-NSGA-II

(e) r-NSGA-II

(f) R-NSGA-II
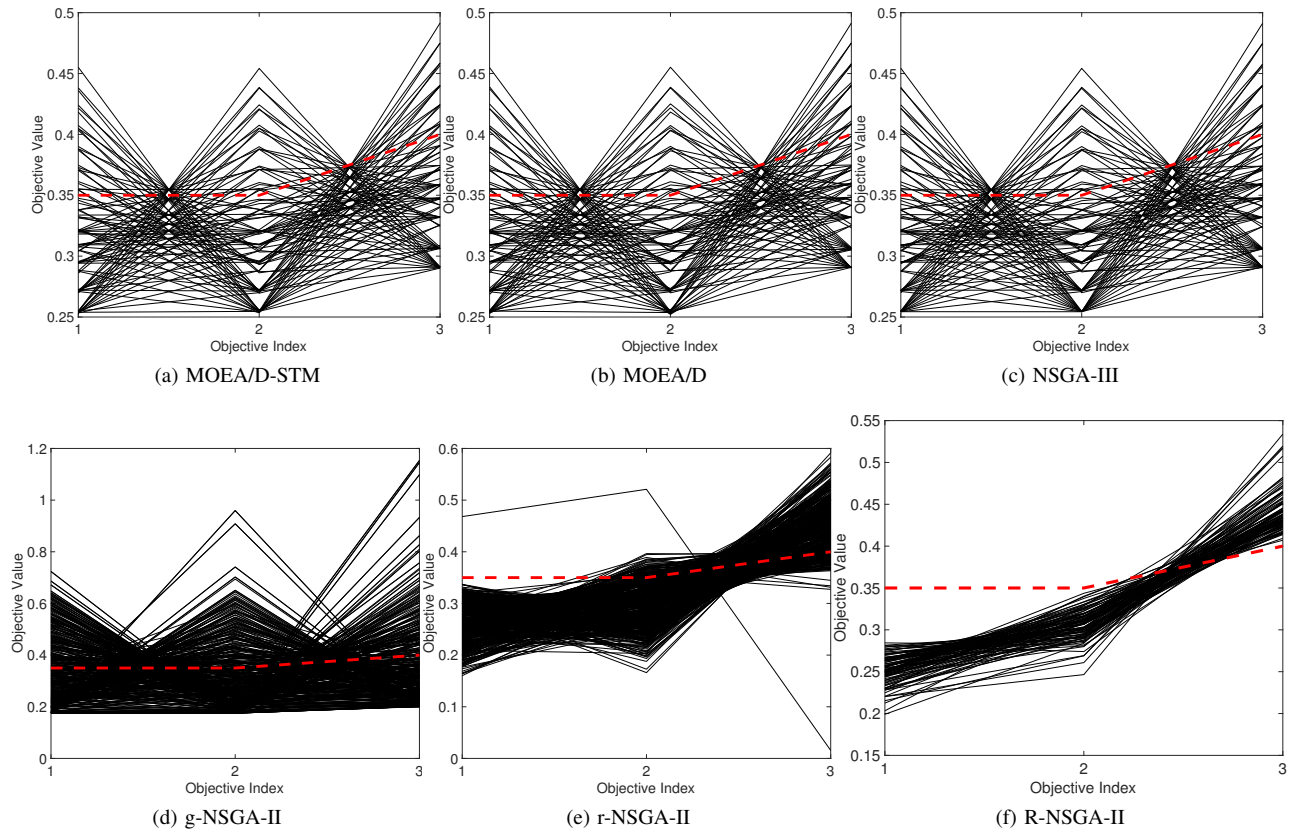
Fig. 95: Comparisons on 3-objective WFG46 where $\mathbf{z}^r = (0.35, 0.35, 0.4)^T$.

(a) MOEA/D-STM

(b) MOEA/D

(c) NSGA-III

(d) g-NSGA-II

(e) r-NSGA-II

(f) R-NSGA-II
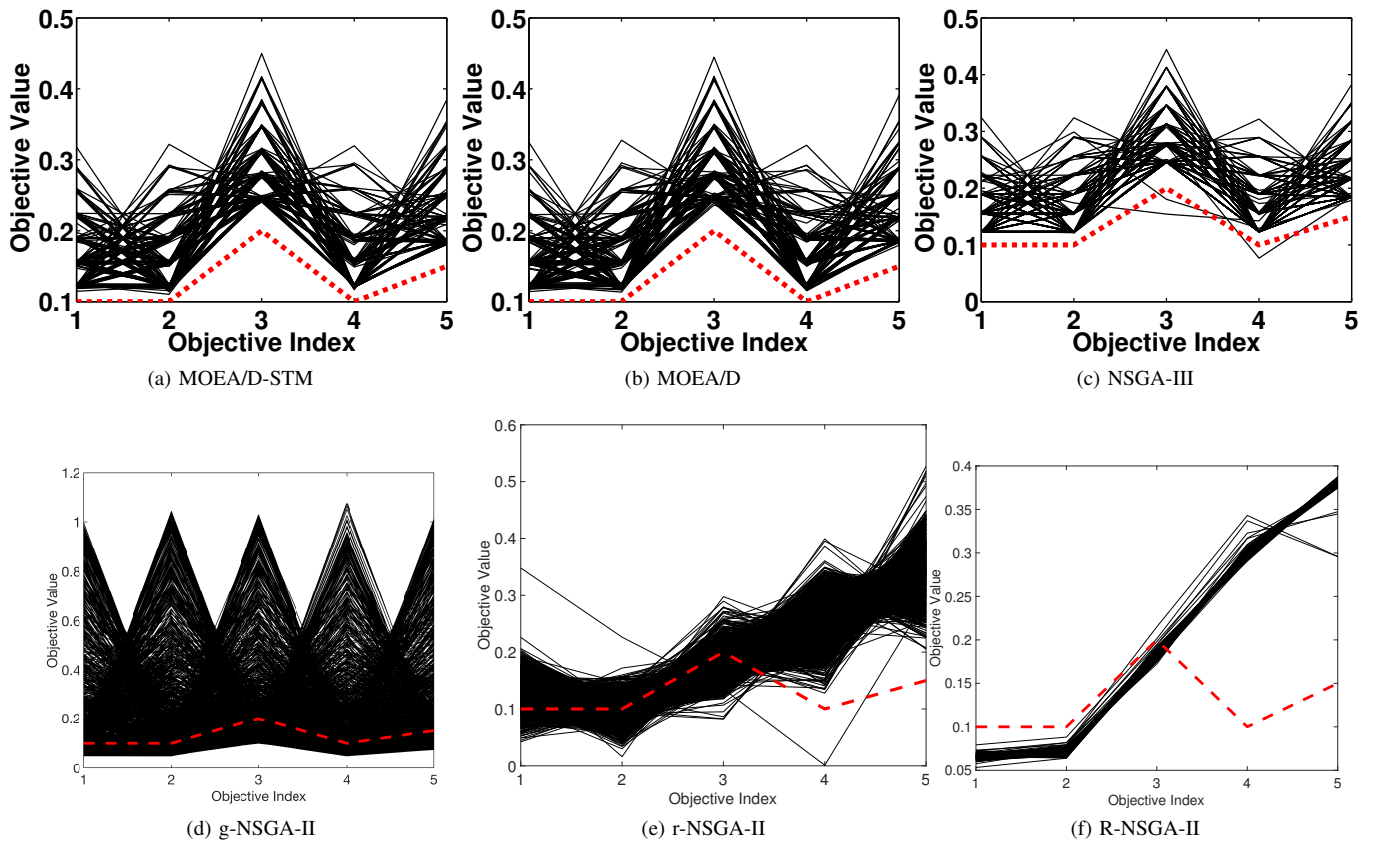
Fig. 96: Comparisons on 5-objective WFG46 where $\mathbf{z}^r = (0.1, 0.1, 0.2, 0.1, 0.15)^T$.
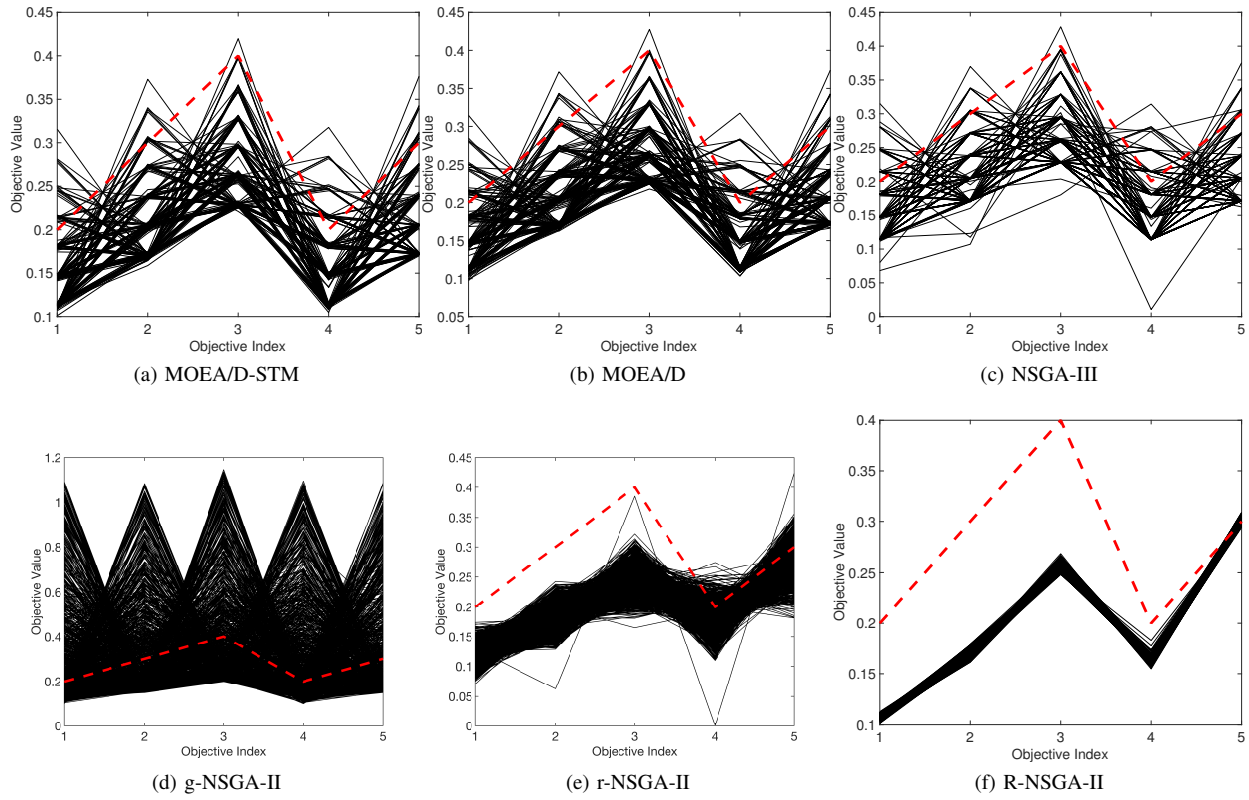
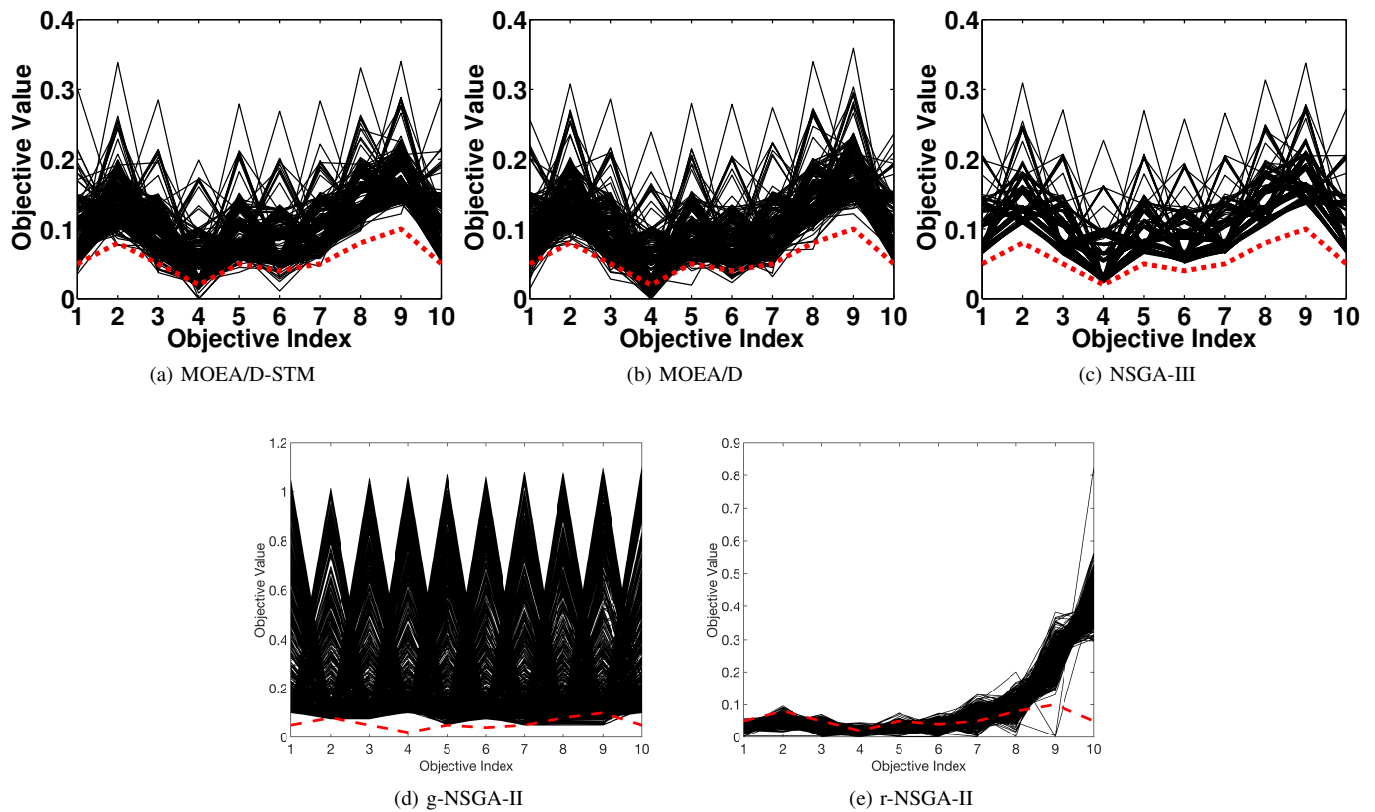Fig. 97: Comparisons on 5-objective WFG46 where $\mathbf{z}^r = (0.2, 0.3, 0.4, 0.2, 0.3)^T$.

(a) MOEA/D-STM
(b) MOEA/D
(c) NSGA-III
(d) g-NSGA-II
(e) r-NSGA-II
(f) R-NSGA-II
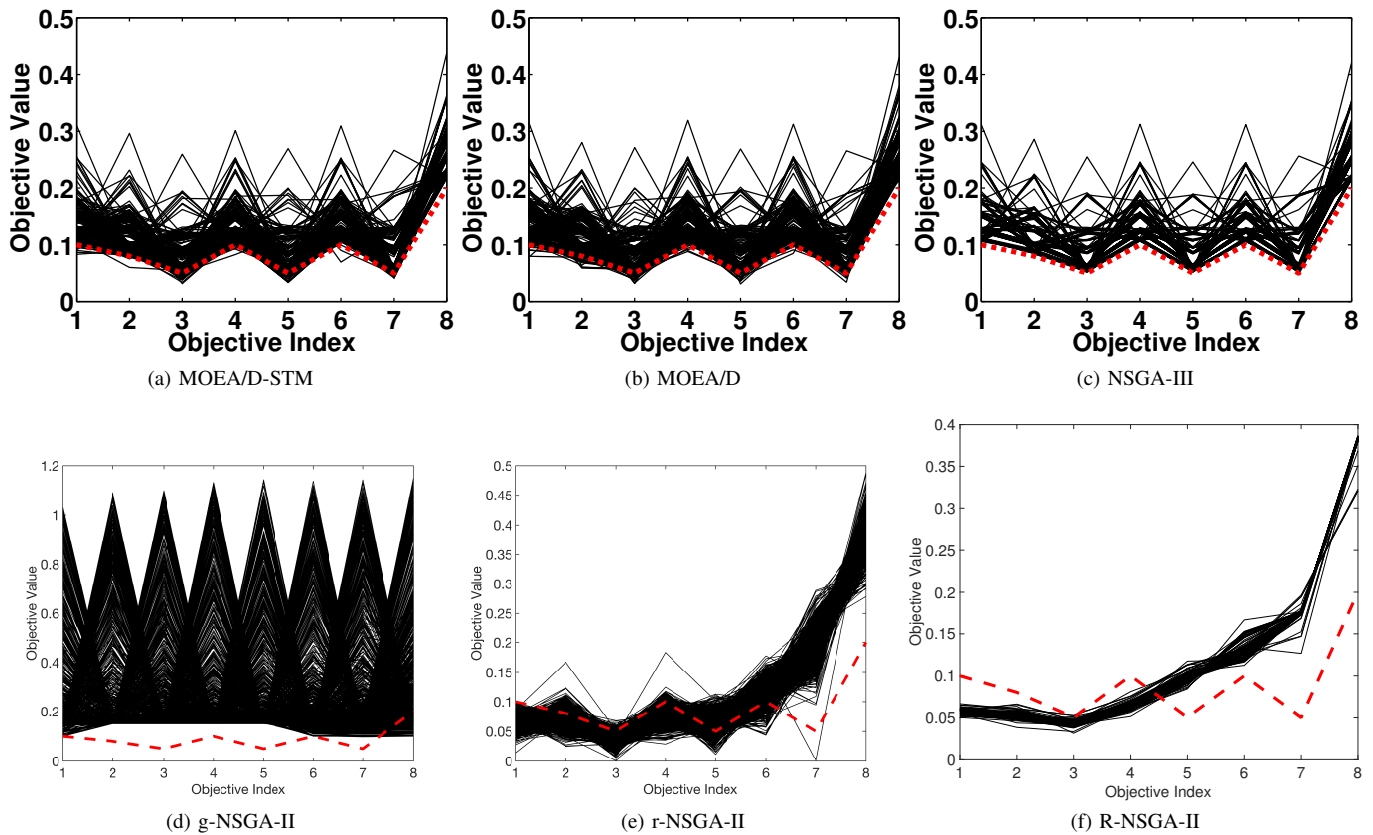
Fig. 98: Comparisons on 8-objective WFG46 where $\mathbf{z}^r = (0.1, 0.08, 0.05, 0.1, 0.05, 0.1, 0.05, 0.2)^T$.

(a) MOEA/D-STM
(b) MOEA/D
(c) NSGA-III
(d) g-NSGA-II
(e) r-NSGA-II
(f) R-NSGA-II

(a) MOEA/D-STM   (b) MOEA/D   (c) NSGA-III

(d) r-NSGA-II   (e) R-NSGA-II
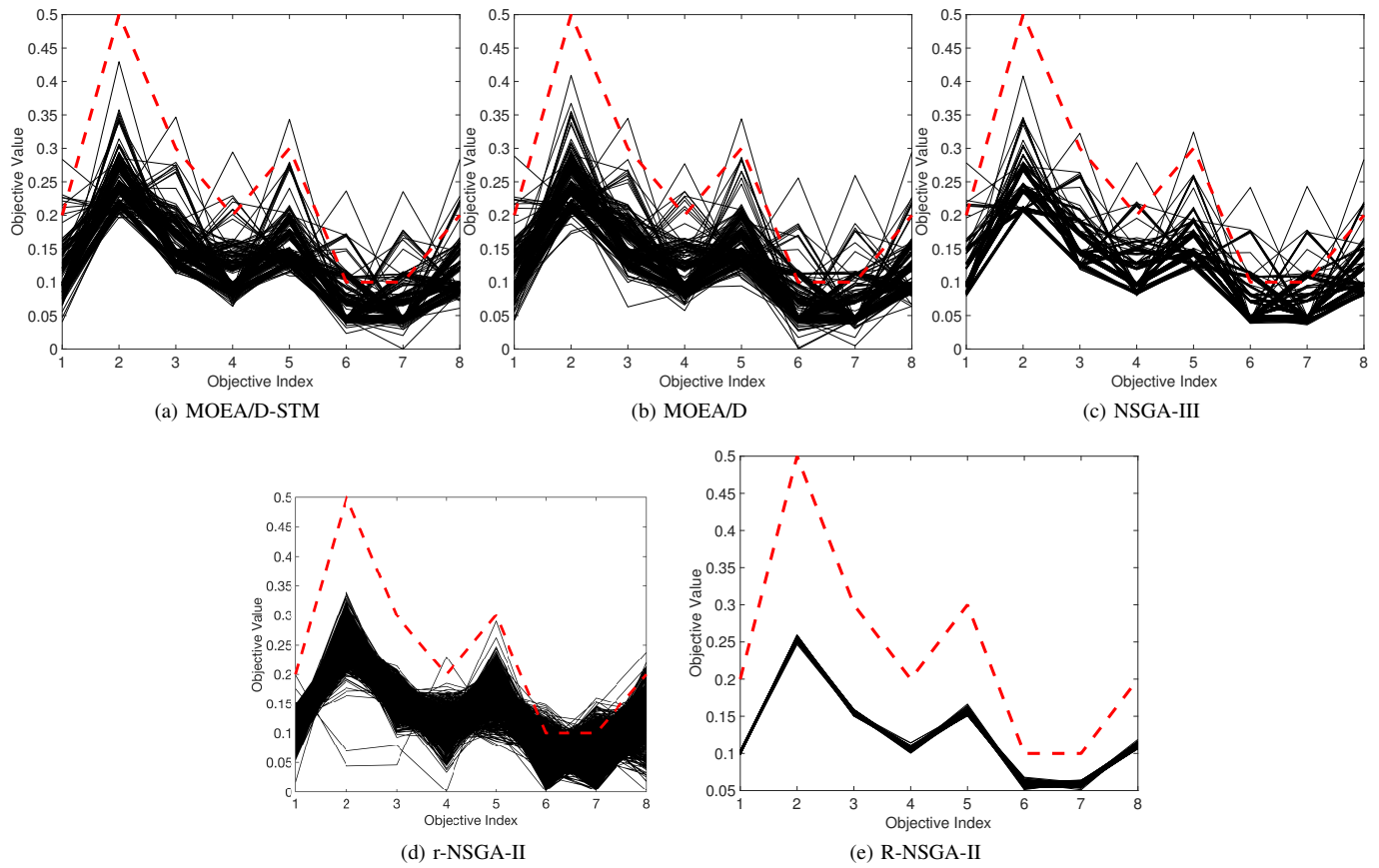
Fig. 99: Comparisons on 8-objective WFG46 where $\mathbf{z}^r = (0.2, 0.5, 0.3, 0.2, 0.3, 0.1, 0.1, 0.2)^T$.

(a) MOEA/D-STM   (b) MOEA/D   (c) NSGA-III

(d) g-NSGA-II   (e) r-NSGA-II

Fig. 100: Comparisons on 10-objective WFG46 where $\mathbf{z}^r = (0.05, 0.08, 0.05, 0.02, 0.05, 0.04, 0.05, 0.08, 0.1, 0.05)^T$.

(a) MOEA/D-STM

(b) MOEA/D

(c) NSGA-III

(d) r-NSGA-II
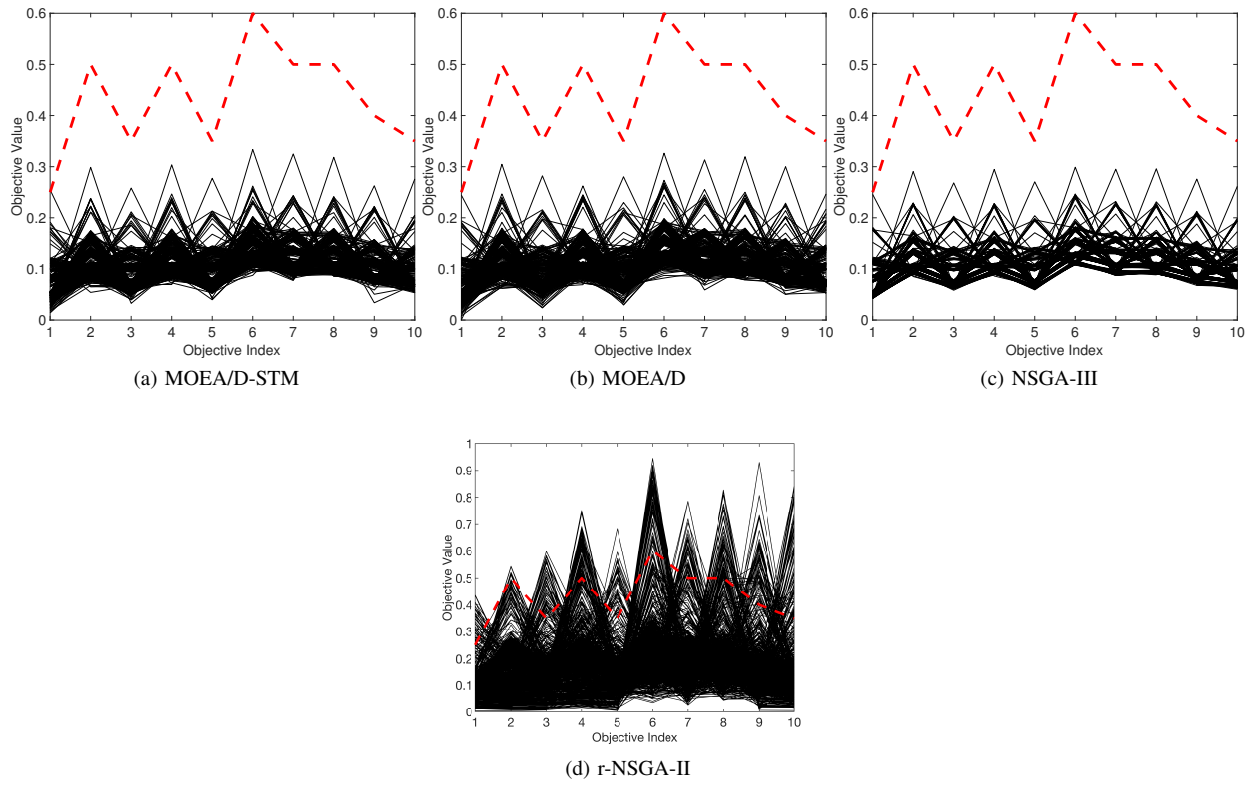
Fig. 101: Comparisons on 10-objective WFG46 where $\mathbf{z}^r = (0.25, 0.5, 0.35, 0.5, 0.35, 0.6, 0.5, 0.5, 0.4, 0.35)^T$.

(a) MOEA/D-STM

(b) MOEA/D

(c) NSGA-III

(d) g-NSGA-II

(e) r-NSGA-II

(f) R-NSGA-II
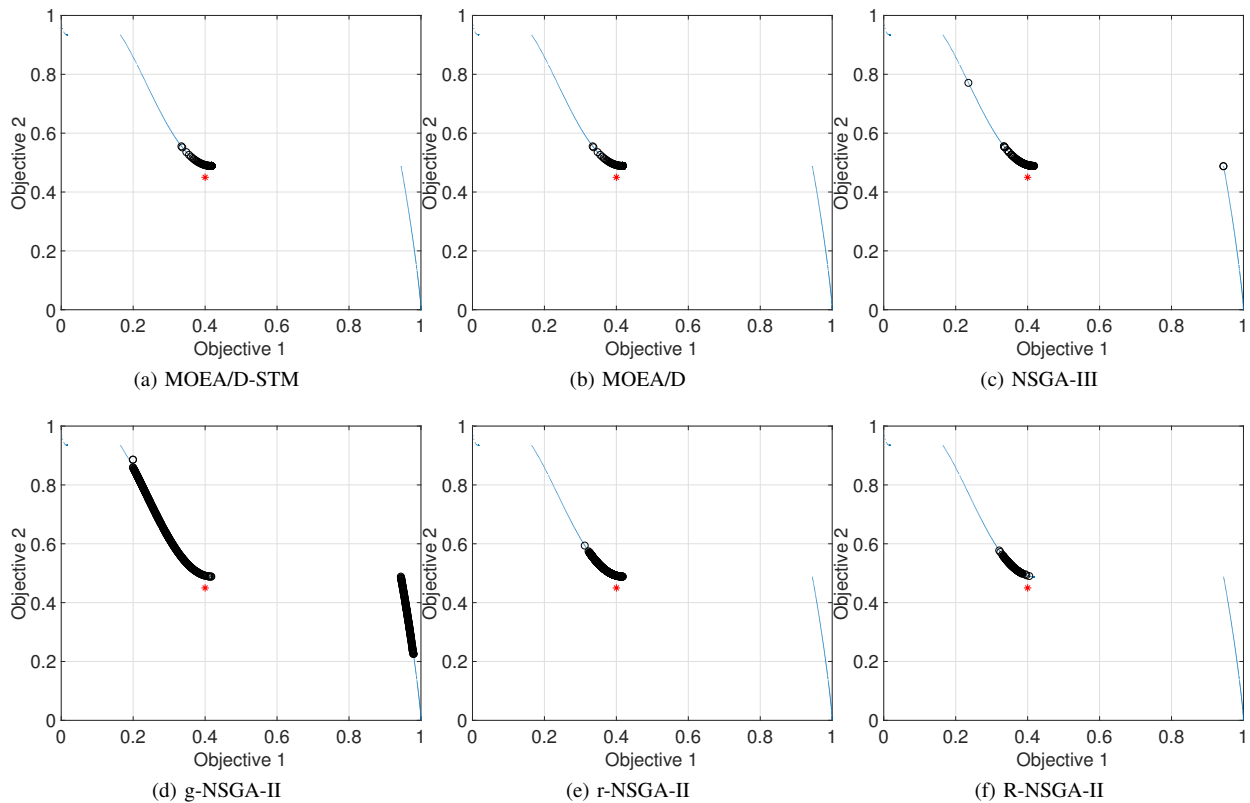
Fig. 102: Comparisons on 2-objective WFG47 where $\mathbf{z}^r = (0.4, 0.45)^T$.

(a) MOEA/D-STM

(b) MOEA/D

(c) NSGA-III

(d) g-NSGA-II

(e) r-NSGA-II

(f) R-NSGA-II
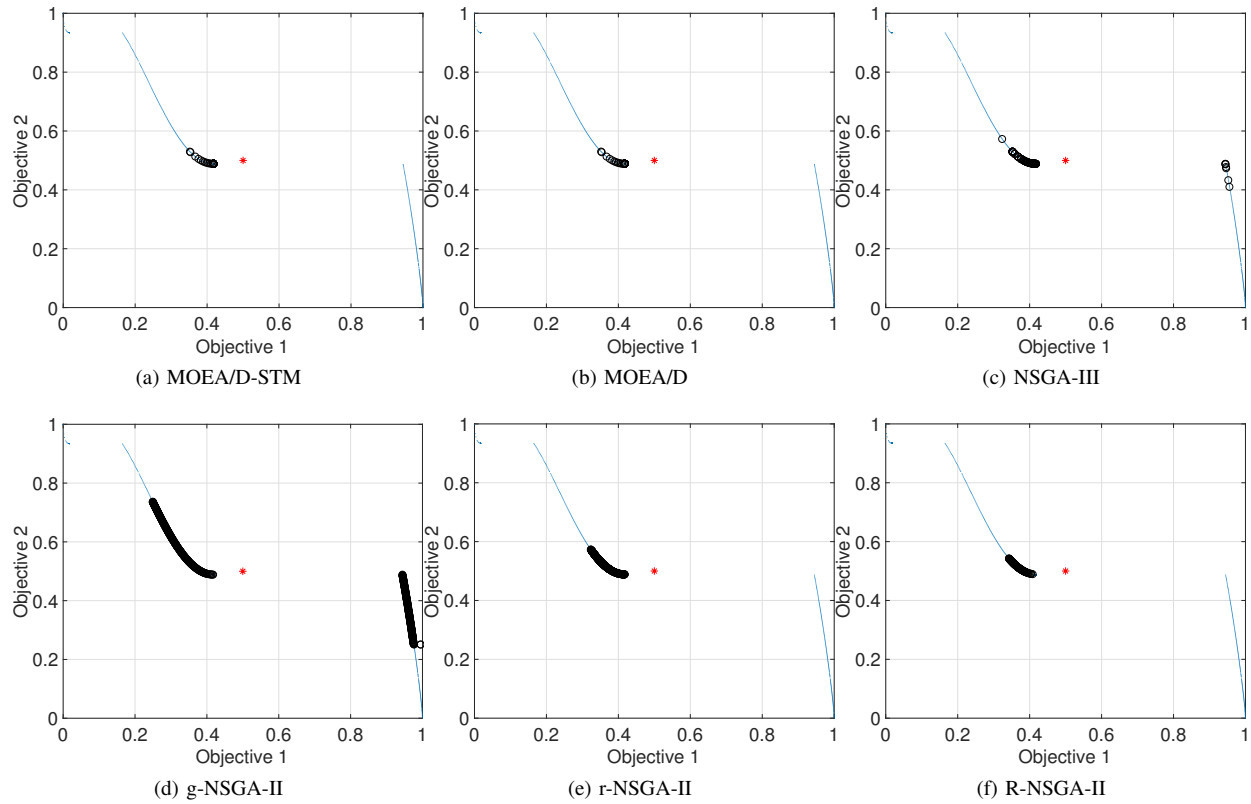
Fig. 103: Comparisons on 2-objective WFG47 where $\mathbf{z}^r = (0.5, 0.5)^T$.

REFERENCES

[1] I. Das and J. E. Dennis, "Normal-Boundary Intersection: A new method for generating the pareto surface in nonlinear multicriteria optimization problems," *SIAM Journal on Optimization*, vol. 8, pp. 631–657, 1998.

[2] J. J. Durillo, A. J. Nebro, C. A. C. Coello, J. García-Nieto, F. Luna, and E. Alba, "A study of multiobjective metaheuristics when solving parameter scalable problems," *IEEE Trans. Evolutionary Computation*, vol. 14, no. 4, pp. 618–635, 2010.

[3] K. Li, Q. Zhang, S. Kwong, M. Li, and R. Wang, "Stable matching based selection in evolutionary multiobjective optimization," *IEEE Trans. Evolutionary Computation*, vol. 18, no. 6, pp. 909–923, Dec. 2014.

[4] K. Deb and R. B. Agrawal, "Simulated binary crossover for continuous search space," *Complex Systems*, vol. 9, pp. 1–34, 1994.

[5] K. Deb and M. Goyal, "A combined genetic adaptive search (GeneAS) for engineering design," *Computer Science and Informatics*, vol. 26, pp. 30–45, 1996.

[6] E. Zitzler, K. Deb, and L. Thiele, "Comparison of multiobjective evolutionary algorithms: Empirical results," *Evolutionary Computation*, vol. 8, no. 2, pp. 173–195, 2000.

[7] K. Deb, L. Thiele, M. Laumanns, and E. Zitzler, "Scalable test problems for evolutionary multiobjective optimization," in *Evolutionary Multiobjective Optimization*, ser. Advanced Information and Knowledge Processing, A. Abraham, L. Jain, and R. Goldberg, Eds. Springer London, 2005, pp. 105–145.

[8] K. Li, K. Deb, Q. Zhang, and S. Kwong, "An evolutionary many-objective optimization algorithm based on dominance and decomposition," *IEEE Trans. Evolutionary Computation*, vol. 19, no. 5, pp. 694–716, 2015.

[9] K. Deb and H. Jain, "An evolutionary many-objective optimization algorithm using reference-point-based nondominated sorting approach, part I: solving problems with box constraints," *IEEE Trans. Evolutionary Computation*, vol. 18, no. 4, pp. 577–601, Aug. 2014.

[10] S. Huband, P. Hingston, L. Barone, and L. While, "A review of multiobjective test problems and a scalable test problem toolkit," *IEEE Trans. Evolutionary Computation*, vol. 10, no. 5, pp. 477–506, Oct. 2006.
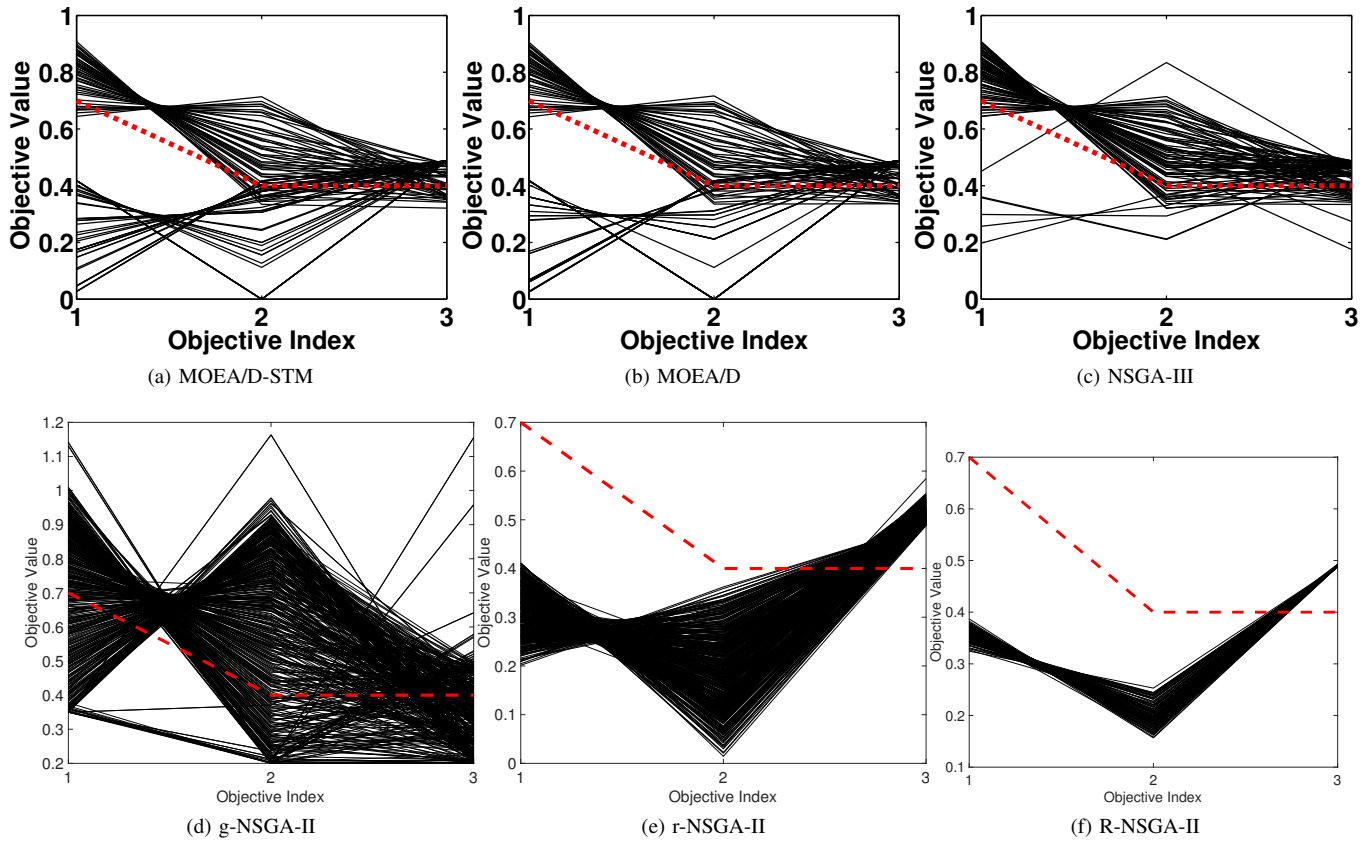
(a) MOEA/D-STM

(b) MOEA/D

(c) NSGA-III

(d) g-NSGA-II

(e) r-NSGA-II

(f) R-NSGA-II

Fig. 104: Comparisons on 3-objective WFG47 where $\mathbf{z}^r = (0.7, 0.4, 0.4)^T$.

(a) MOEA/D-STM

(b) MOEA/D

(c) NSGA-III

(d) g-NSGA-II

(e) r-NSGA-II

(f) R-NSGA-II
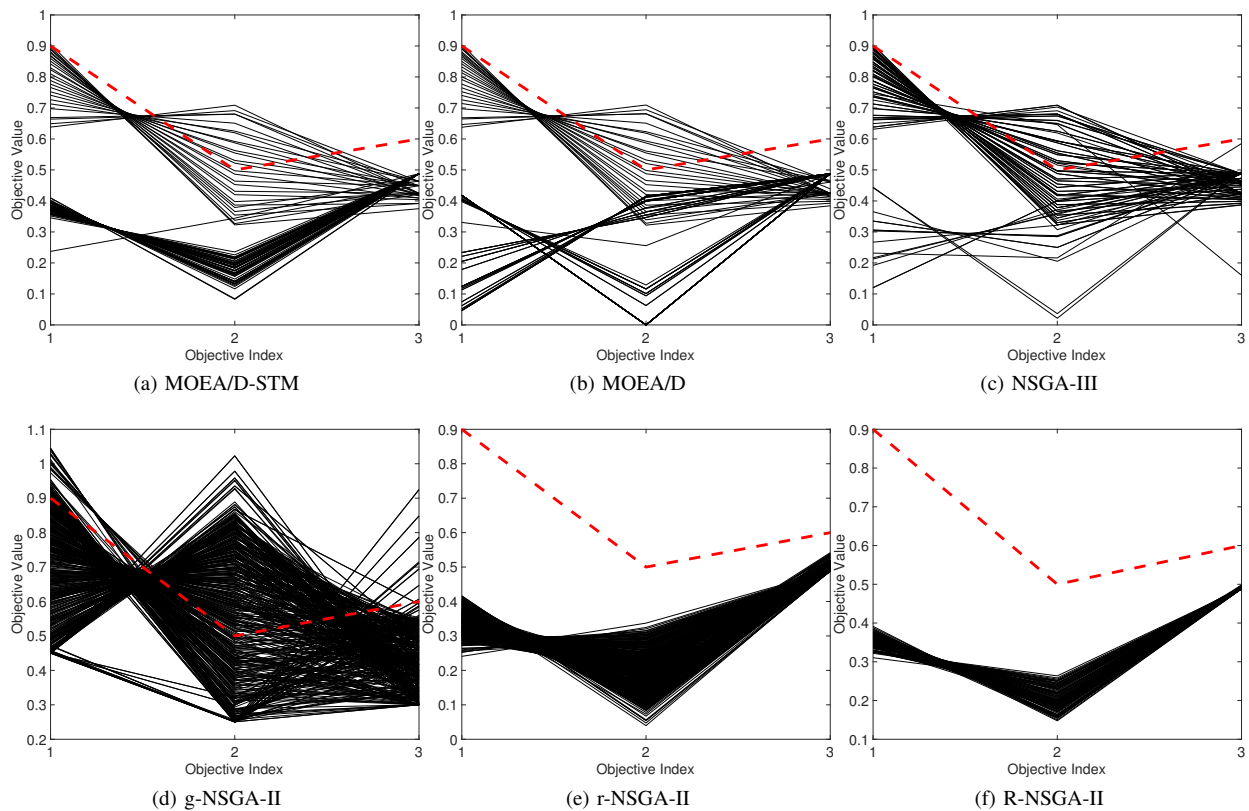
Fig. 105: Comparisons on 3-objective WFG47 where $\mathbf{z}^r = (0.9, 0.5, 0.6)^T$.

(a) MOEA/D-STM

(b) MOEA/D

(c) NSGA-III

(d) g-NSGA-II

(e) r-NSGA-II

(f) R-NSGA-II
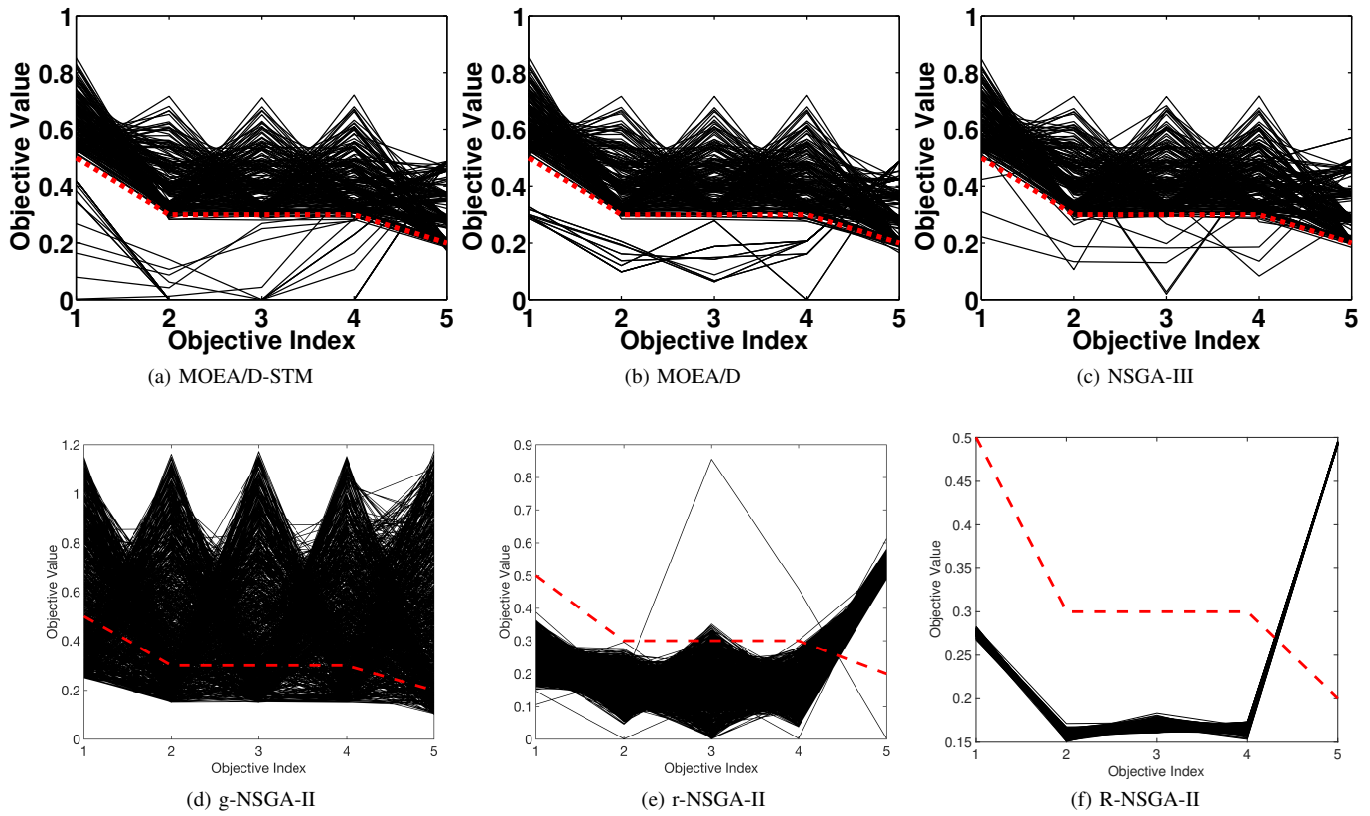
Fig. 106: Comparisons on 5-objective WFG47 where $\mathbf{z}^r = (0.5, 0.3, 0.3, 0.3, 0.2)^T$.

(a) MOEA/D-STM

(b) MOEA/D

(c) NSGA-III

(d) g-NSGA-II

(e) r-NSGA-II

(f) R-NSGA-II
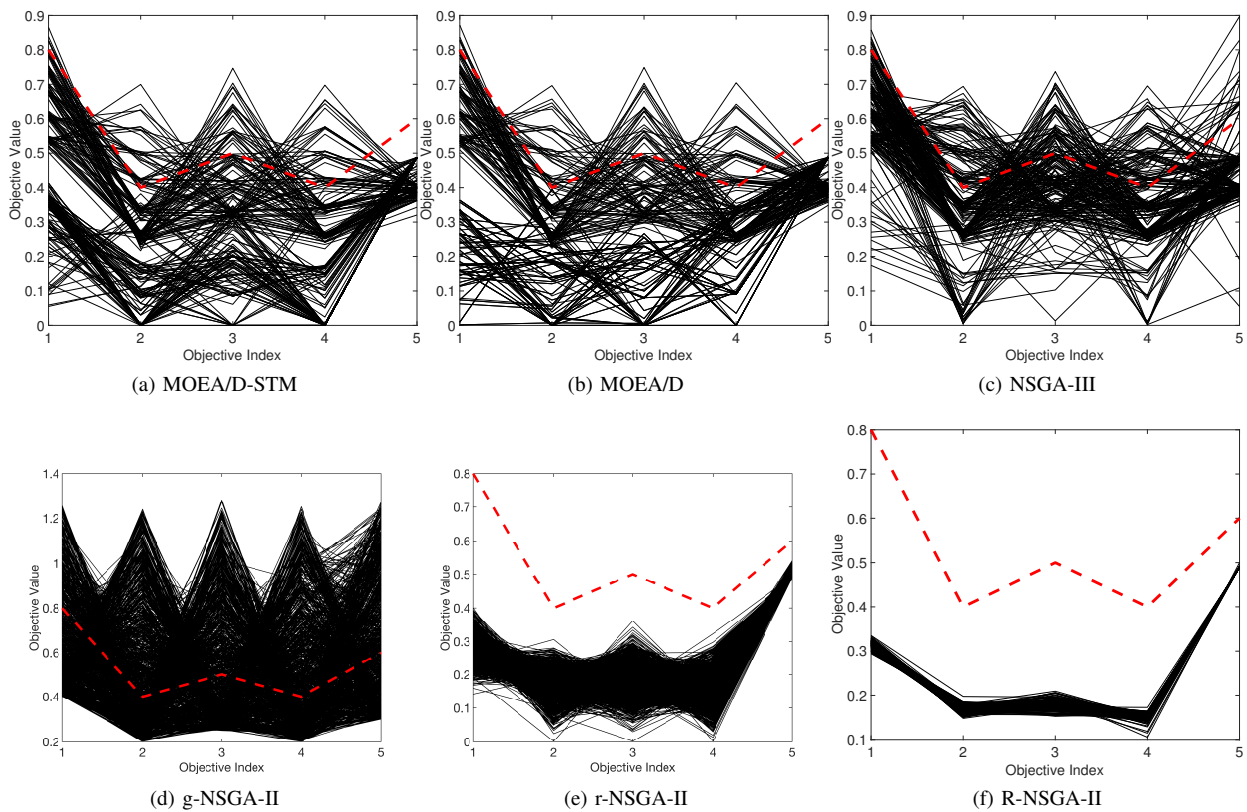
Fig. 107: Comparisons on 5-objective WFG47 where $\mathbf{z}^r = (0.8, 0.4, 0.5, 0.4, 0.6)^T$.

(a) MOEA/D-STM

(b) MOEA/D

(c) NSGA-III

(d) g-NSGA-II

(e) r-NSGA-II

(f) R-NSGA-II
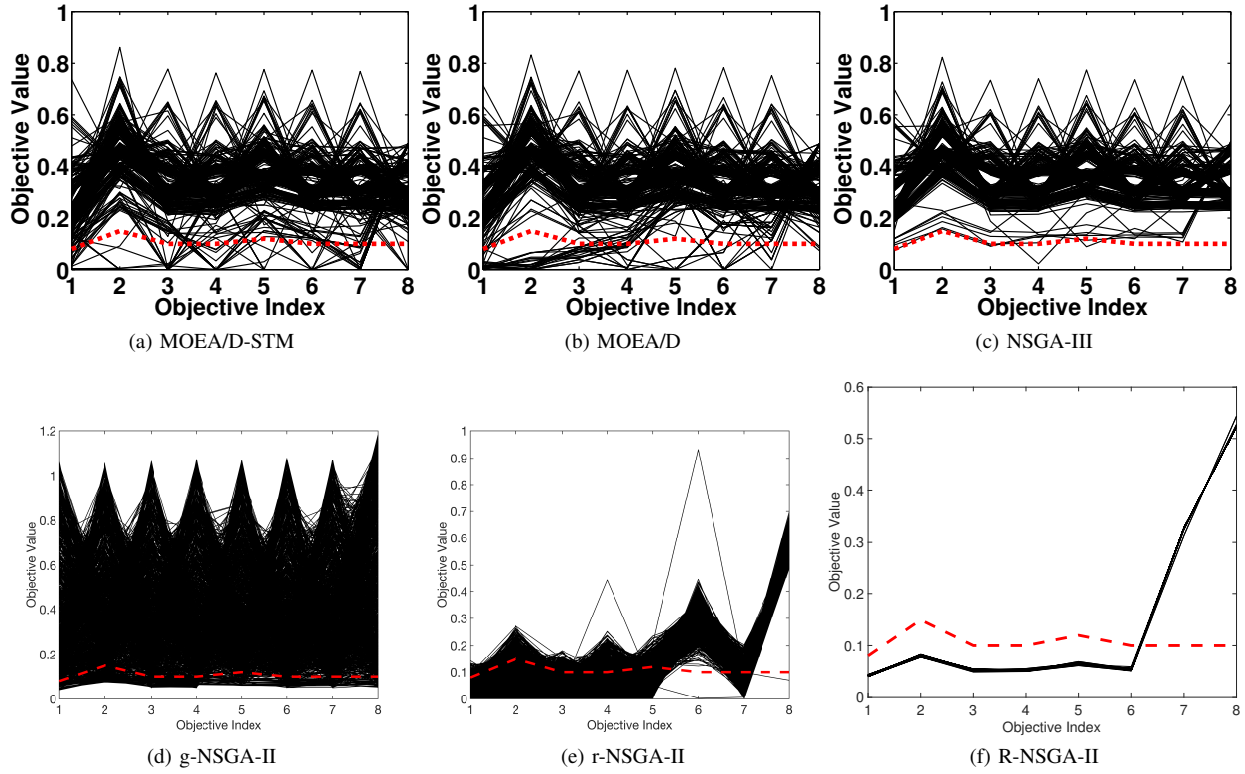
Fig. 108: Comparisons on 8-objective WFG47 where $\mathbf{z}^r = (0.08, 0.15, 0.1, 0.1, 0.12, 0.1, 0.1, 0.1)^T$.

(a) MOEA/D-STM

(b) MOEA/D

(c) NSGA-III

(d) r-NSGA-II

(e) R-NSGA-II
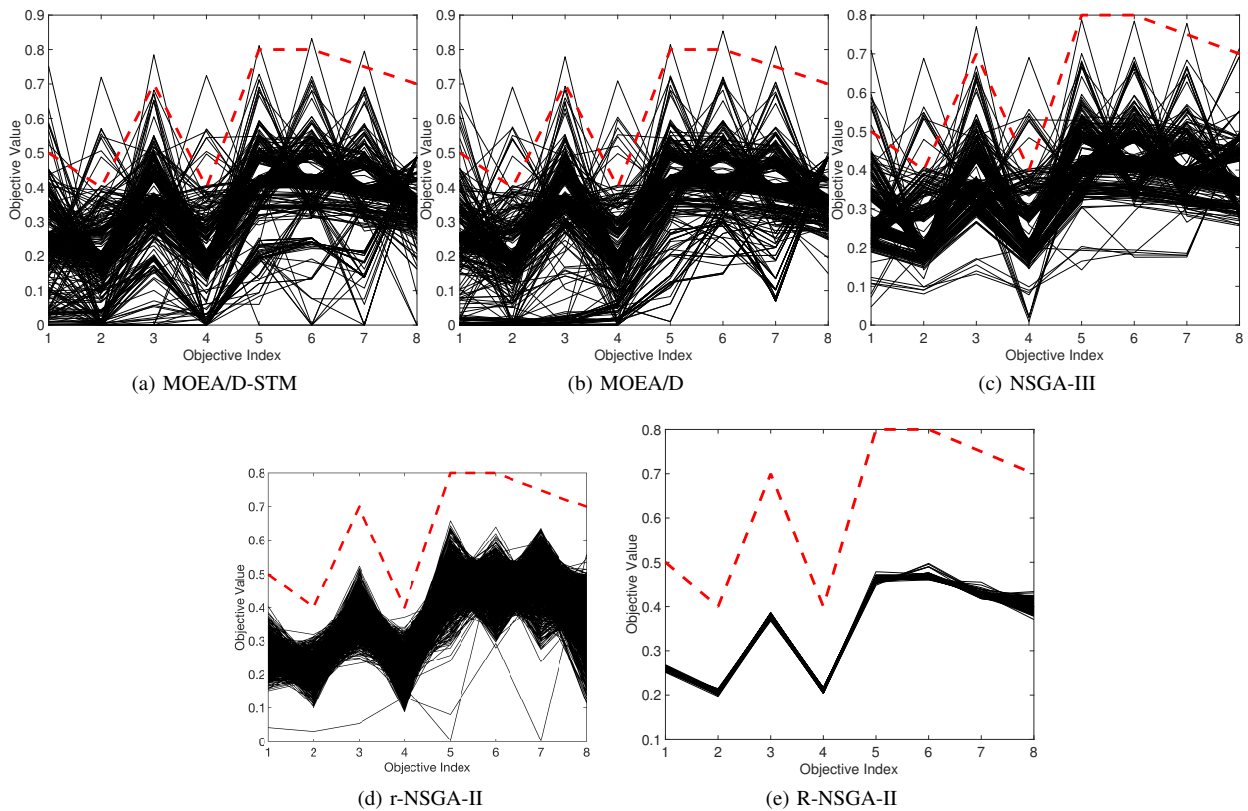
Fig. 109: Comparisons on 8-objective WFG47 where $\mathbf{z}^r = (0.5, 0.4, 0.7, 0.4, 0.8, 0.8, 0.75, 0.7)^T$.

(a) MOEA/D-STM　　　　　　　　(b) MOEA/D　　　　　　　　(c) NSGA-III

(d) g-NSGA-II　　　　　　　　(e) r-NSGA-II
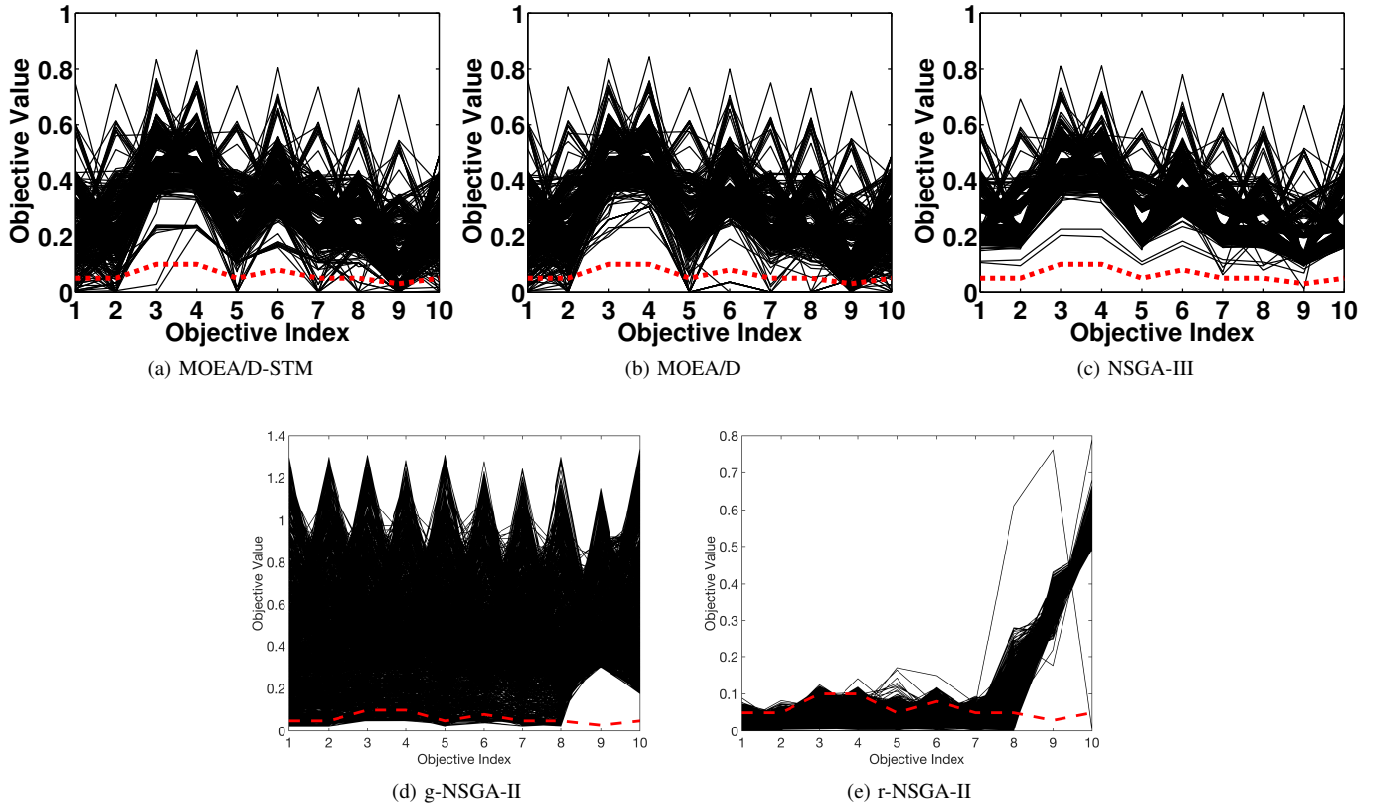
Fig. 110: Comparisons on 10-objective WFG47 where $\mathbf{z}^r = (0.05, 0.05, 0.1, 0.1, 0.05, 0.08, 0.05, 0.05, 0.03, 0.05)^T$.

(a) MOEA/D-STM　　　　　　　　(b) MOEA/D　　　　　　　　(c) NSGA-III

(d) r-NSGA-II
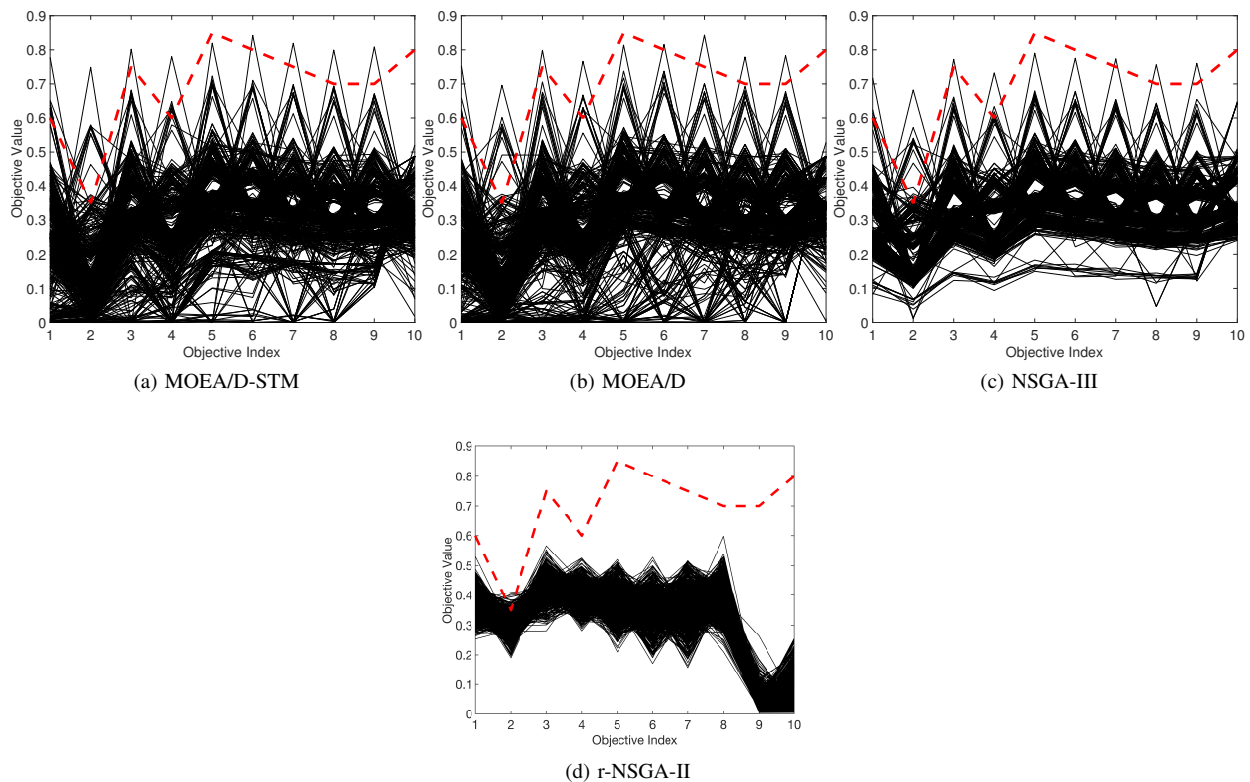
Fig. 111: Comparisons on 10-objective WFG47 where $\mathbf{z}^r = (0.6, 0.35, 0.75, 0.6, 0.85, 0.8, 0.75, 0.7, 0.7, 0.8)^T$.
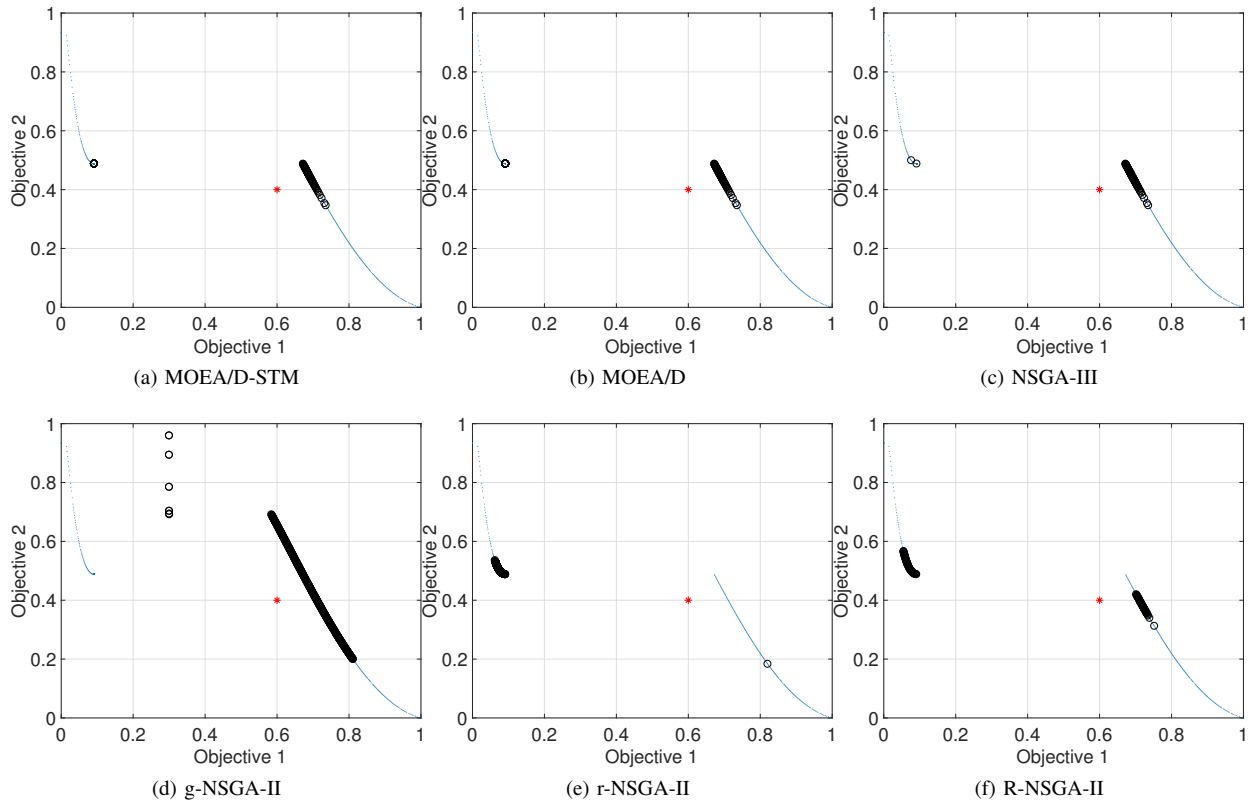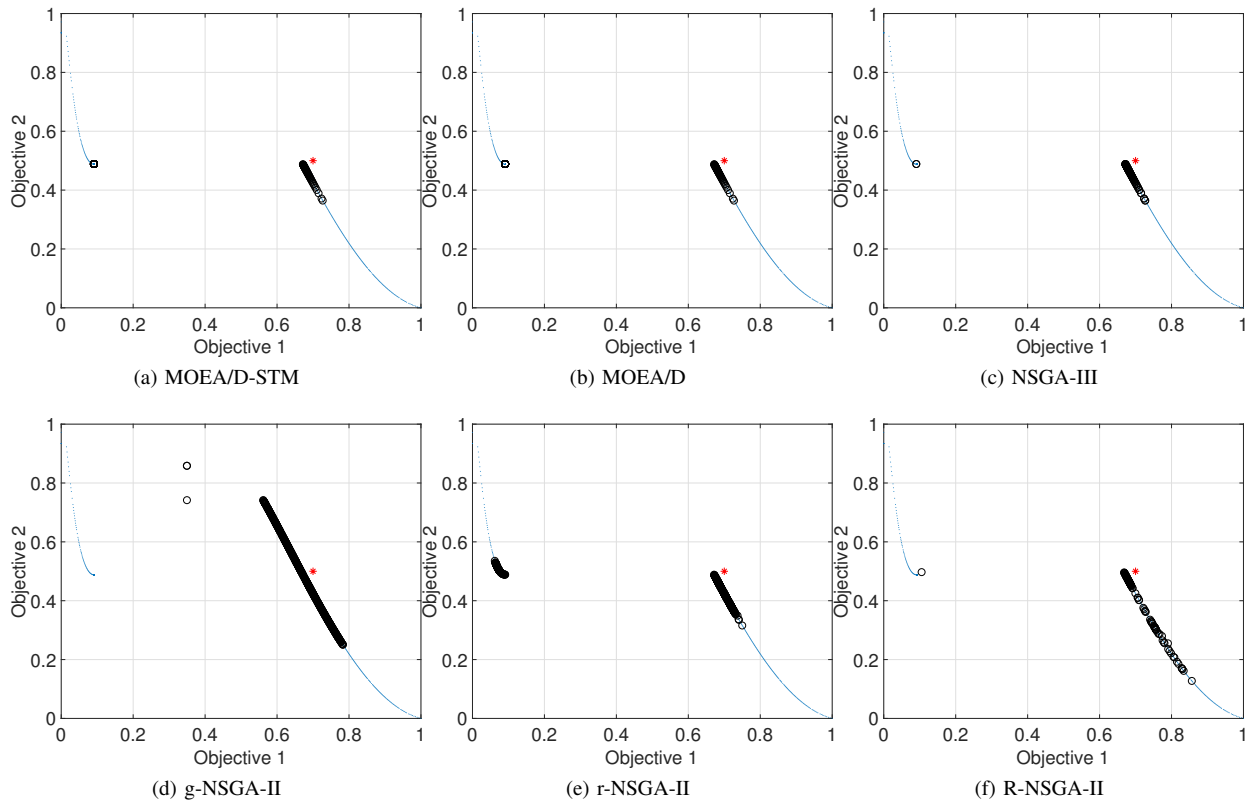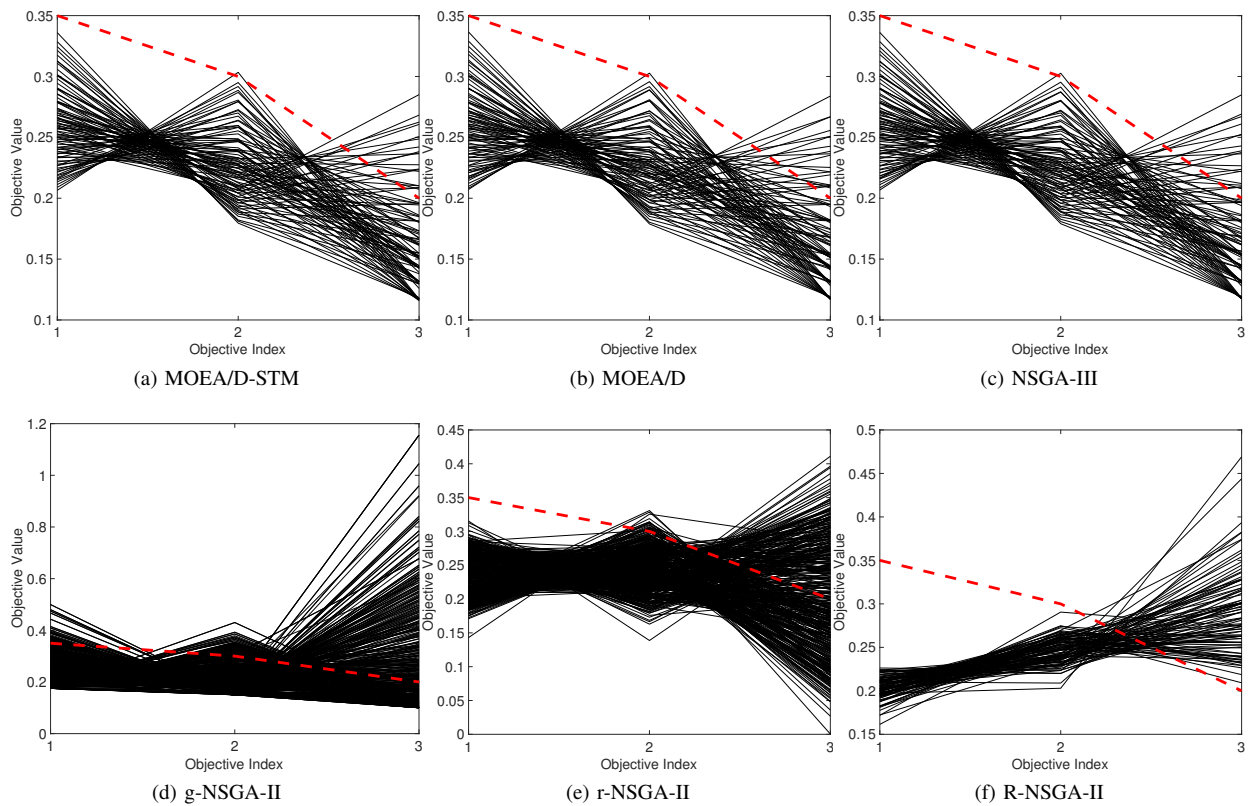
Fig. 112: Comparisons on 2-objective WFG48 where $\mathbf{z}^r = (0.6, 0.4)^T$.

Fig. 113: Comparisons on 2-objective WFG48 where $\mathbf{z}^r = (0.7, 0.5)^T$.

(a) MOEA/D-STM
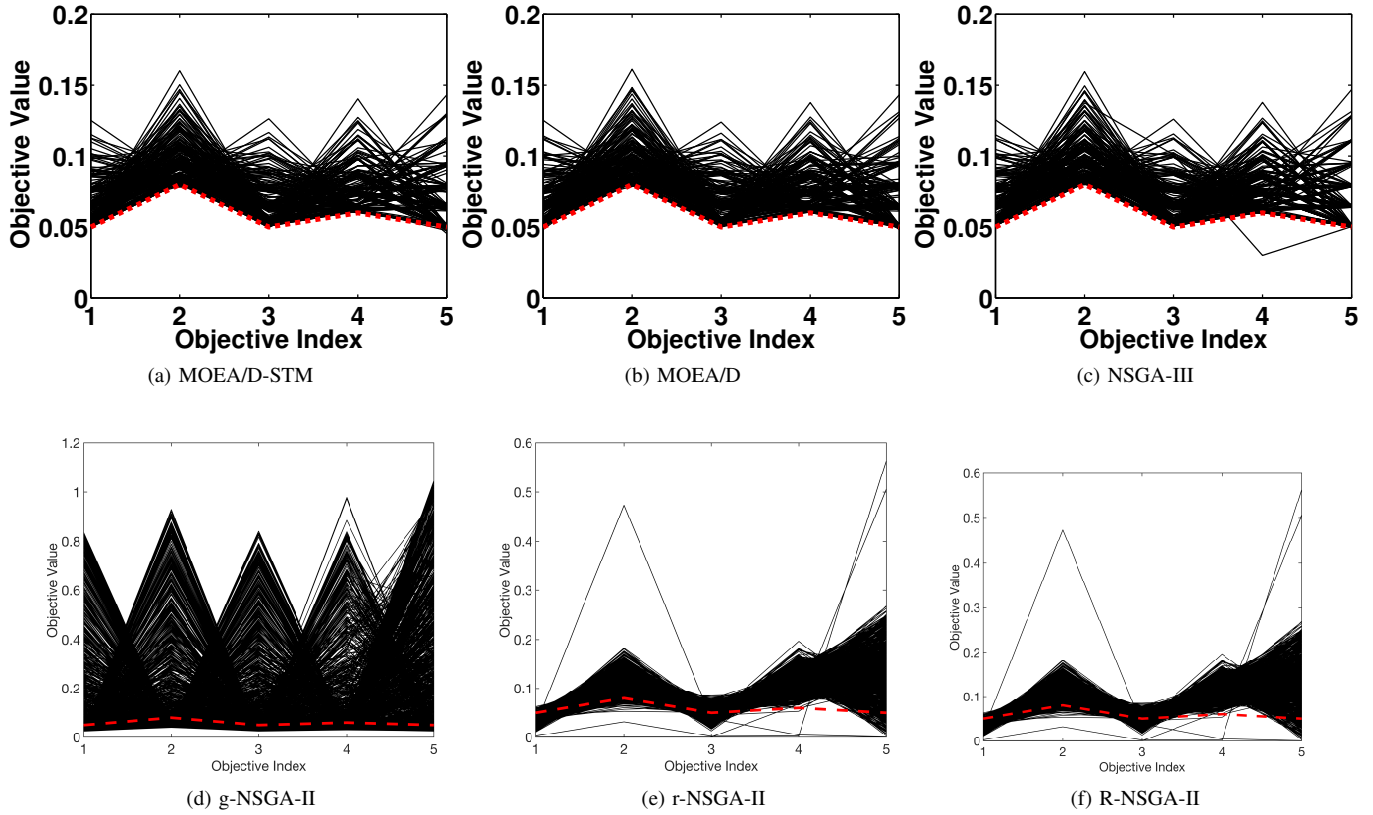
(b) MOEA/D

(c) NSGA-III

(d) g-NSGA-II

(e) r-NSGA-II

(f) R-NSGA-II
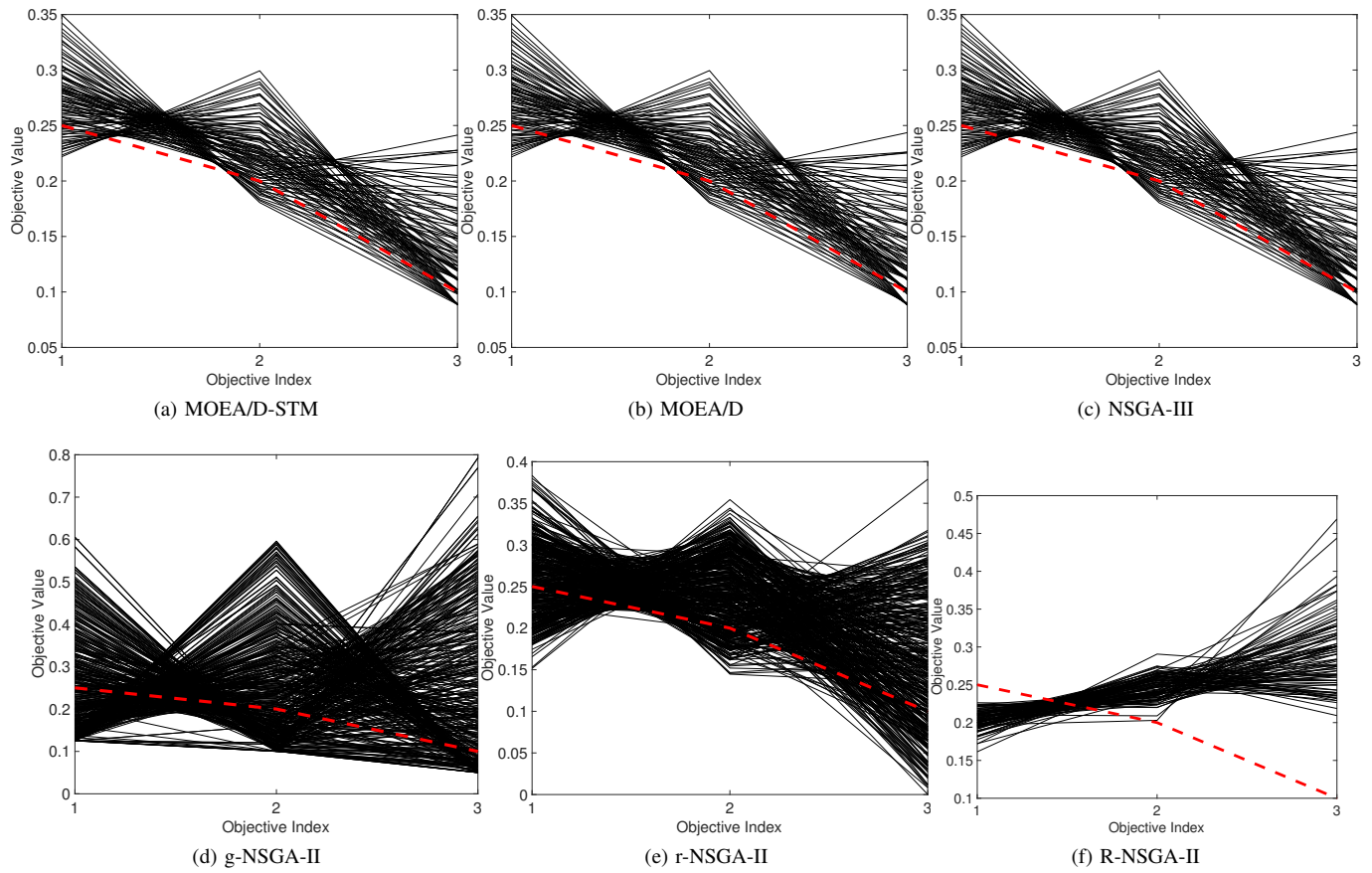
Fig. 114: Comparisons on 3-objective WFG48 where $\mathbf{z}^r = (0.25, 0.2, 0.1)^T$.

(a) MOEA/D-STM

(b) MOEA/D

(c) NSGA-III

(d) g-NSGA-II

(e) r-NSGA-II

(f) R-NSGA-II

Fig. 115: Comparisons on 3-objective WFG48 where $\mathbf{z}^r = (0.35, 0.3, 0.2)^T$.

Fig. 116: Comparisons on 5-objective WFG48 where $\mathbf{z}^r = (0.05, 0.08, 0.05, 0.06, 0.05)^T$.
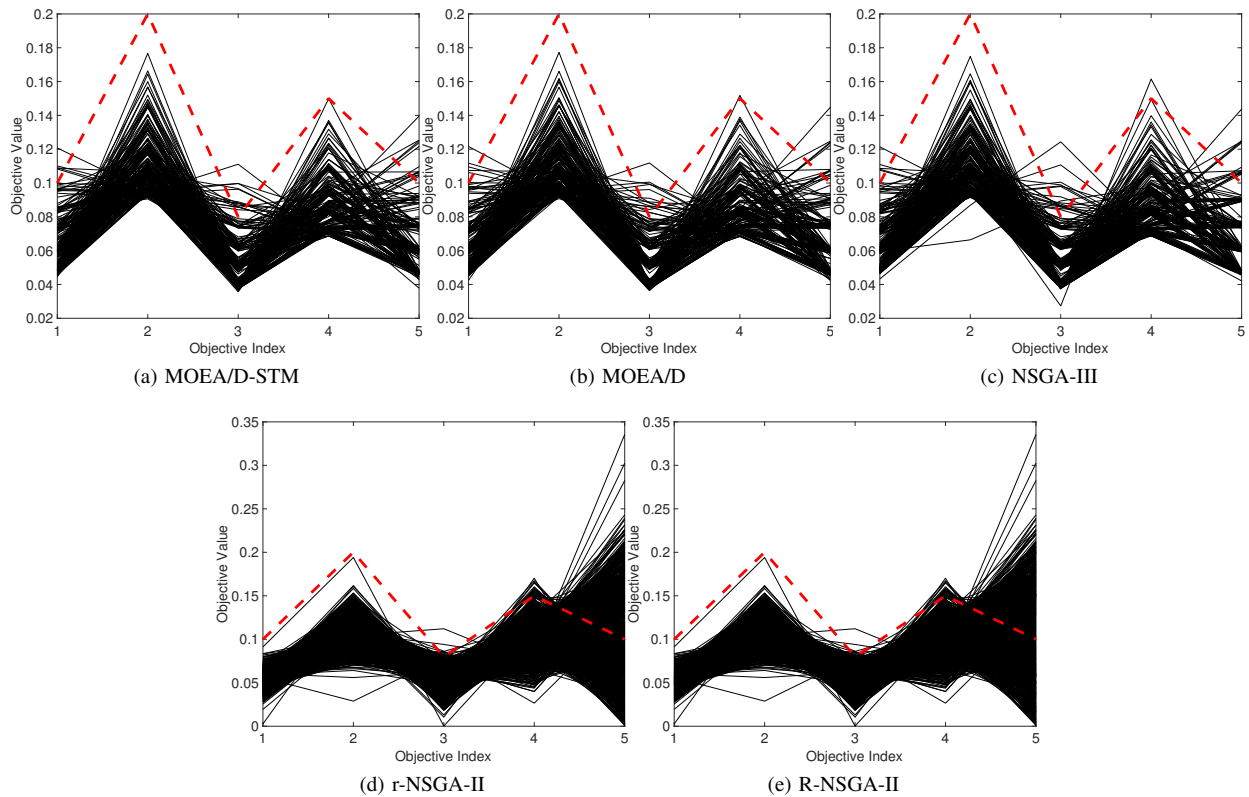

Fig. 117: Comparisons on 5-objective WFG48 where $\mathbf{z}^r = (0.1, 0.2, 0.08, 0.15, 0.1)^T$.
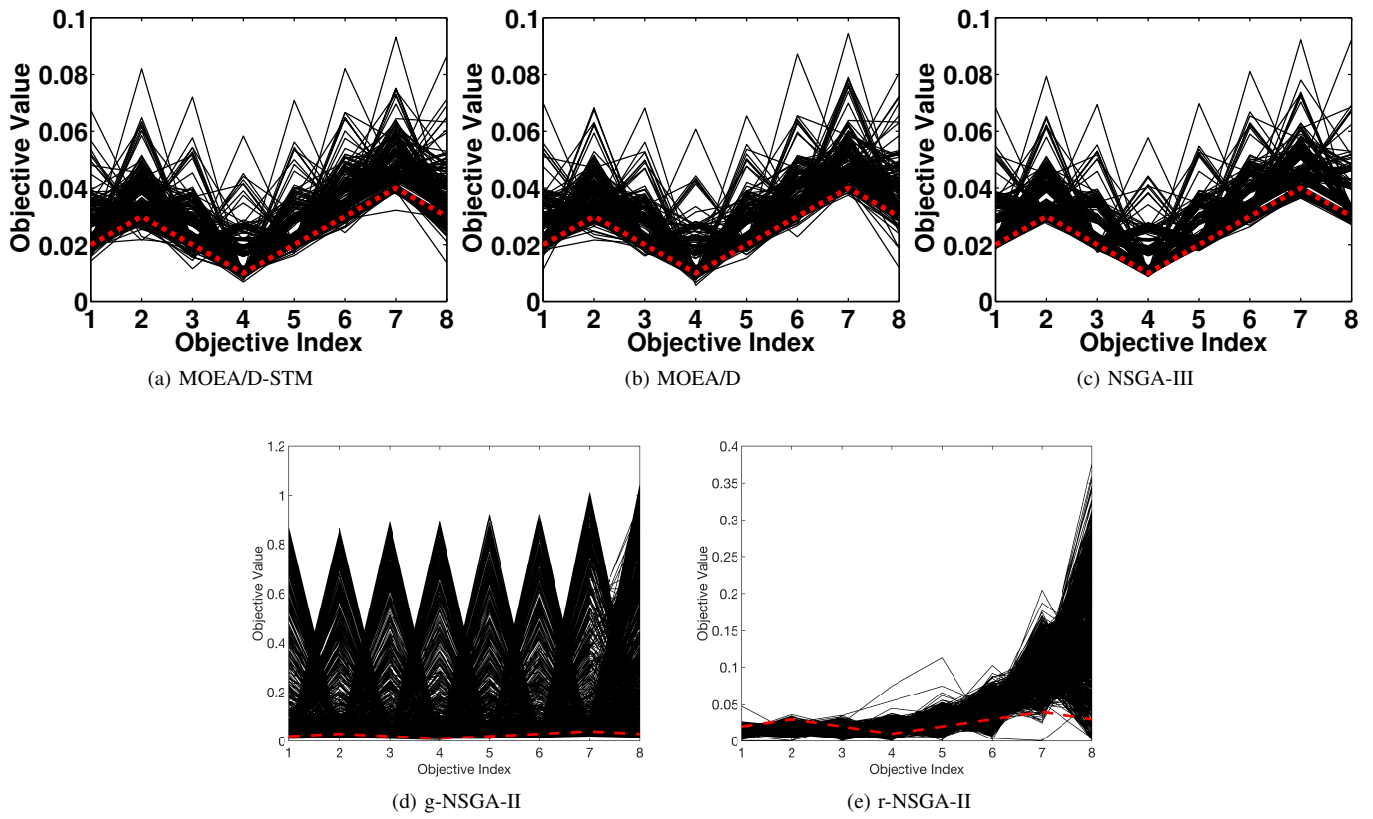
(a) MOEA/D-STM

(b) MOEA/D

(c) NSGA-III

(d) g-NSGA-II

(e) r-NSGA-II

Fig. 118: Comparisons on 8-objective WFG48 where $\mathbf{z}^r = (0.02, 0.03, 0.02, 0.01, 0.02, 0.03, 0.04, 0.03)^T$.

(a) MOEA/D-STM

(b) MOEA/D

(c) NSGA-III

(d) g-NSGA-II

(e) r-NSGA-II
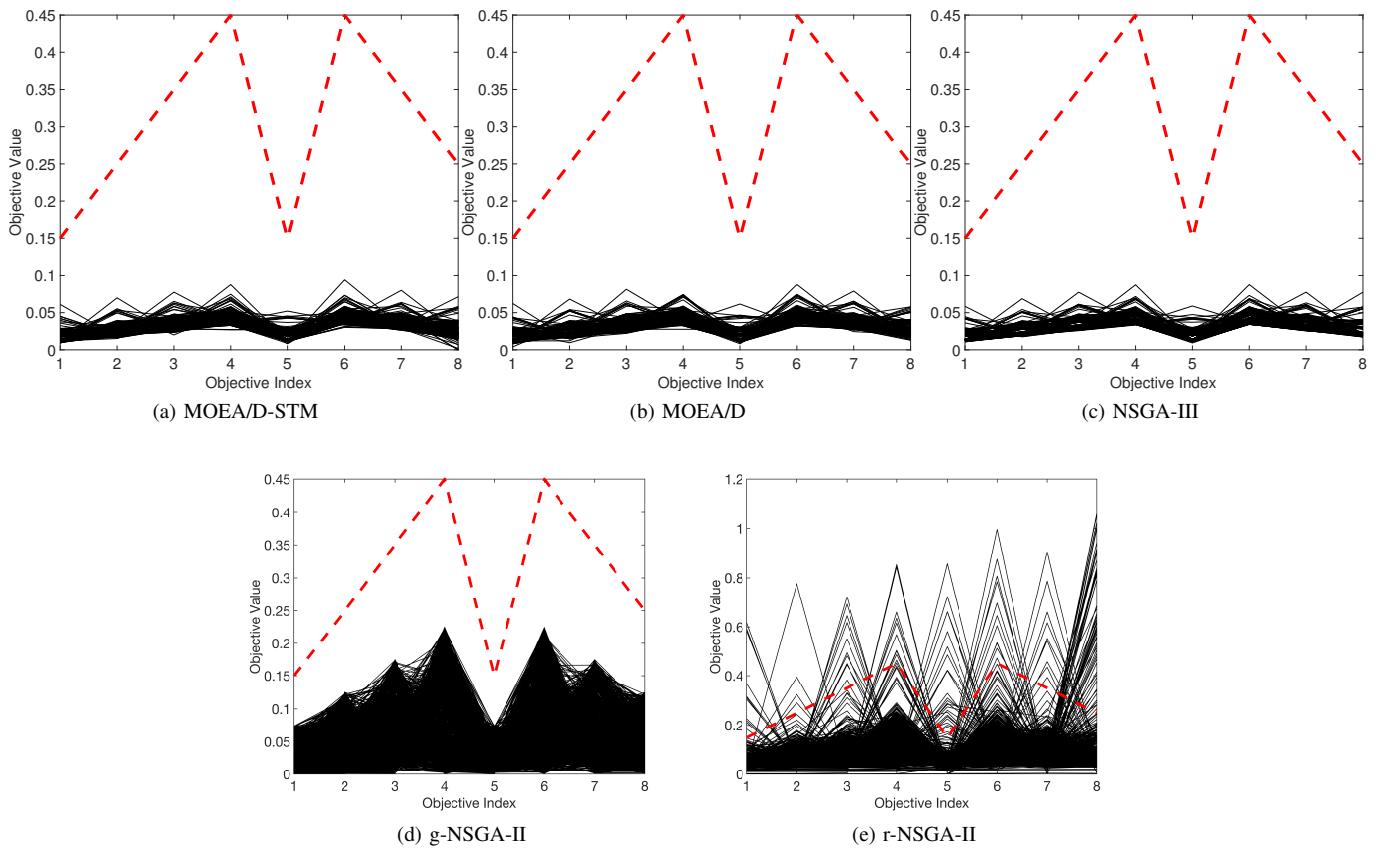
Fig. 119: Comparisons on 8-objective WFG48 where $\mathbf{z}^r = (0.15, 0.25, 0.35, 0.45, 0.15, 0.45, 0.35, 0.25)^T$.

(a) MOEA/D-STM

(b) MOEA/D

(c) NSGA-III

(d) r-NSGA-II

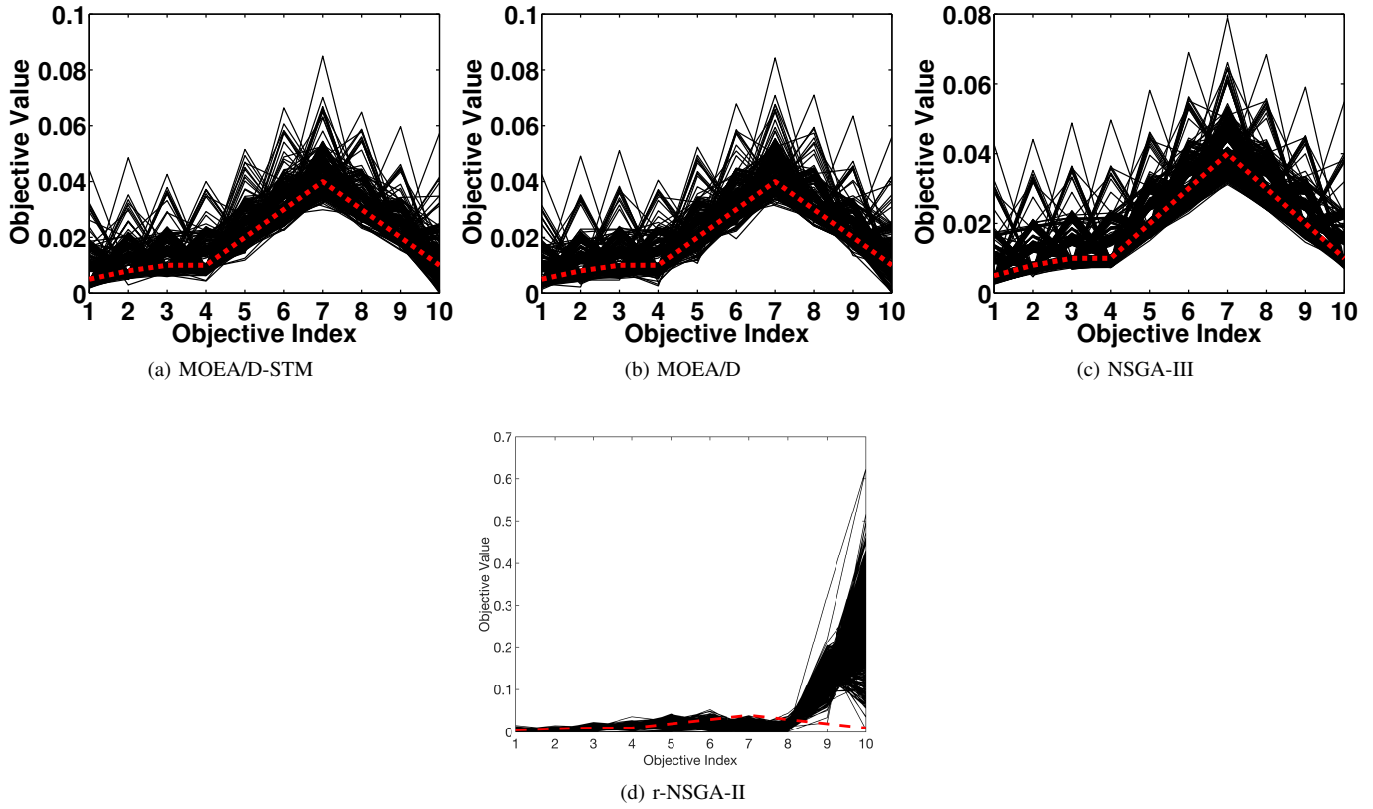Fig. 120: Comparisons on 10-objective WFG48 where $\mathbf{z}^r = (0.005, 0.008, 0.01, 0.01, 0.02, 0.03, 0.04, 0.03, 0.02, 0.01)^T$.

(a) MOEA/D-STM
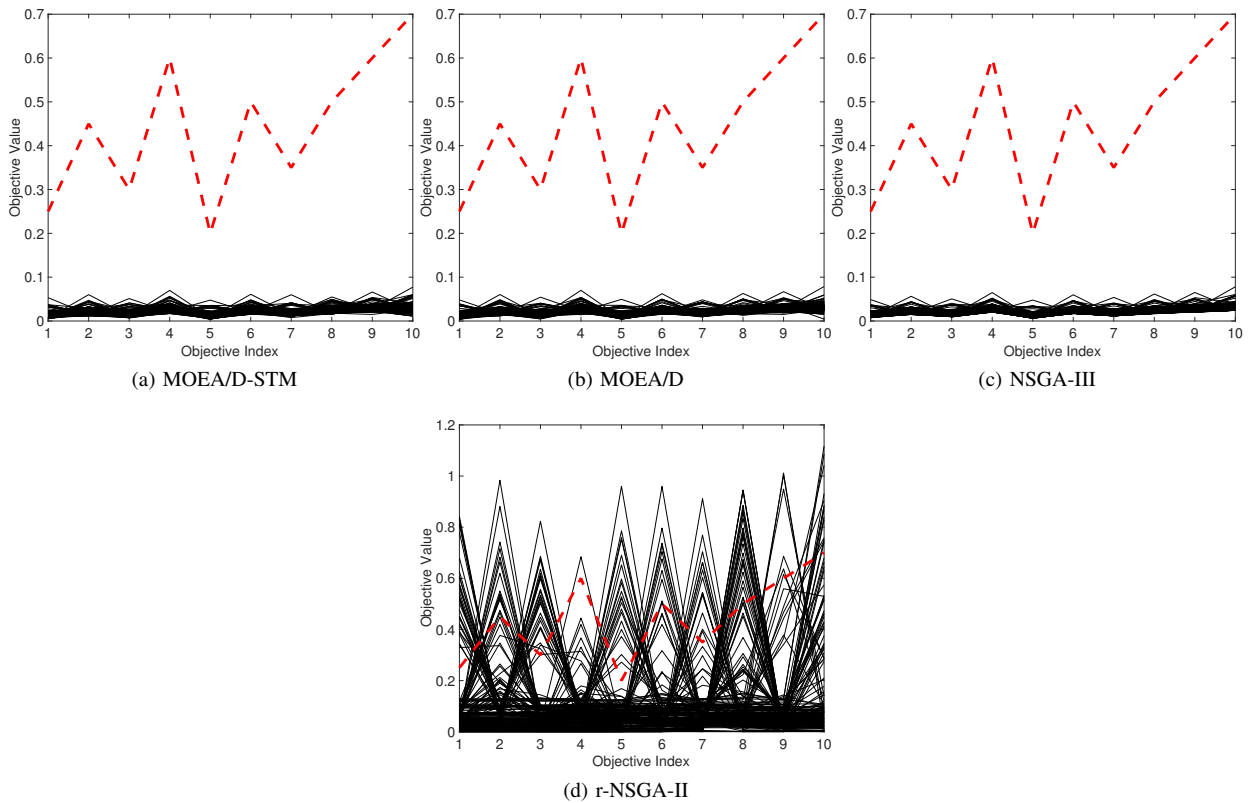
(b) MOEA/D

(c) NSGA-III

(d) r-NSGA-II

Fig. 121: Comparisons on 10-objective WFG48 where $\mathbf{z}^r = (0.25, 0.45, 0.3, 0.6, 0.2, 0.5, 0.35, 0.5, 0.6, 0.7)^T$.